A STUDY ON
UTILIZATION OF LD SLAG IN EROSION RESISTANT COATINGS AND POLYMER COMPOSITES

A THESIS SUBMITTED IN PARTIAL FULFILLMENT OF THE REQUIREMENTS FOR THE DEGREE OF

Doctor of Philosophy

in

Mechanical Engineering

By

PRAVAT RANJAN PATI

Roll No. 511 ME 122

Under the supervision of

Prof. Alok Satapathy

Associate Professor

Department of Mechanical Engineering

DEPARTMENT OF MECHANICAL ENGINEERING

National Institute of Technology

Rourkela (India)

September, 2015

Dedicated To
My Beloved
Family Members

National Institute of Technology
Rourkela

C E R T I F I C A T E

This is to certify that the thesis entitled ***A Study on Utilization of LD slag in Erosion Resistant Coatings and Polymer Composites*** submitted by **PRAVAT RANJAN PATI** to National Institute of Technology, Rourkela for the award of the degree of **Doctor of Philosophy** in *Mechanical Engineering*, is an authentic record of research work carried out by him under my guidance and supervision. The work incorporated in this thesis has not been, to the best of my knowledge, submitted to any other University or Institute for the award of a degree or diploma.

This work, in my opinion has reached the standard of fulfilling the requirements for the award of the degree of **Doctor of Philosophy** in accordance with the regulations of the Institute.

Date:

Place: Rourkela

Prof. Alok Satapathy
(Supervisor)
Associate Professor
Department of Mechanical Engineering
National Institute of Technology

ACKNOWLEDGEMENT

The research through my Ph.D. study would not have been complete without the help and support of many individuals who deserve my appreciation and special thanks.

I express my sincere regard and deepest gratitude to my guide and supervisor **Dr. Alok Satapathy**, Associate Professor, Department of Mechanical Engineering, NIT, Rourkela for his intellectual support, help, advice, encouragement and guidance during all stages of the work that made this dissertation possible. I would also like to express my sincere gratitude to the Head of the Department of Mechanical Engineering **Prof. S. S. Mahapatra** for his timely help during the entire course of my research work.

I thankfully appreciate the co-operation extended by the eminent scientists **Mr. Sisir Mantry** at the Institute of Minerals and Materials Technology, Bhubaneswar in carrying out the experimental work. I would specially like also to thank **Mrs. Susmita Satapathy** for her words of encouragement throughout the course of this work.

Very special thanks to my family members for their consistent support and faith shown upon me. Their love and patience made this work possible and their encouragement immensely helped me in my work for this thesis. I am also thankful to all those who have directly or indirectly helped during my research period.

I am extremely thankful to my research colleagues **Prasanta Kumar Padhi, Gaurav Gupta, Alok Agrawal, Debasmita Mishra, Madhusmita Sahu, Mimosha Dash and Somen Biswal** for helping me in every way they could and for making the past few years more delightful.

Finally, but most importantly, I am thankful to Almighty, my Lord for giving me the will power and strength to make it this far.

Date:

Place: Rourkela

Pravat Ranjan Pati
(Research Scholar)
Roll No. 511 ME 122

List of Figures

*****

List of Tables

*****

ABSTRACT

Although a variety of metal and ceramic powders are used as coating material and as reinforcing fillers in polymeric resins, the use of industrial wastes for this purpose has not been adequately explored. In view of this, the present investigation reports on the development and performance of new classes of plasma sprayed coatings and polymer composites using Linz-Donawitz slag (LDS) as the primary material. This LDS is a major solid waste generated in huge quantities during steel making and its chemical analysis suggests the presence of oxides of silicon, calcium and iron in it.

The research reported in this thesis broadly consists of two parts: The first part has provided the description of the materials used, the experimental details and the methods adopted for analysis of experimental results. This part has also presented various physical and mechanical characteristics of the plasma sprayed LDS based coatings and LDS filled epoxy and polypropylene composites. An assessment of LDS as a potential coating material and a particulate filler in polymers has been made by evaluating the physical and mechanical properties of these coatings and composites under controlled laboratory conditions. Effects of premixing of Al_2O_3 and TiO_2 powders on the physical and mechanical properties of LD slag coatings have also been reported. The second part of the thesis reports on the erosion wear characteristics of these coatings and composites. The wear response of LDS, 'LDS + Al_2O_3' and 'LDS + TiO_2' coatings have been discussed separately. Comparisons between the erosion characteristics of LD slag filled epoxy and polypropylene composites with and without glass fiber reinforcement have also been presented. Parametric analysis and wear response prediction has been made for all the coatings and composites under this study using statistical techniques namely Taguchi experimental design and artificial neural networks (ANN). Correlations have been developed to predict the wear rate for these coatings and composites under different test conditions.

This work suggests that LDS is eminently coatable and deposition of such coatings using plasma spraying route is possible. These coatings possess desirable characteristics such as good adhesion strength, hardness etc. This work further establishes that LD slag can also be used as a functional filler in both thermoset and thermoplastic polymers. These LD slag filled composites possess very low amount of porosity and improved micro-hardness. They also exhibit improved impact strength as compared to that of the neat polymers. The tensile and flexural strength of the composites are affected by the weight fraction of LDS in the composites. With improved hardness, these composites have the potential to be used in wear related applications.

Erosion wear characteristics of LDS coatings and LDS filled polymer composites have been successfully analyzed using Taguchi technique. Significant factors affecting the erosion rate of these coatings and composites are identified through successful implementation of this technique. Two predictive models; one based on artificial neural networks (ANN) approach and the other on Taguchi approach are proposed in this work. It is demonstrated that these models well reflect the effects of various factors on the wear loss and their predictive results are consistent with the experimental observations. Neural computation is successfully applied in this investigation to predict and simulate the wear response of these coatings and composites under various test conditions within and beyond the experimental domain. The predicted and the experimental values of erosion wear rate exhibit good agreement and validate the remarkable capability of a well-trained neural network for these kinds of processes.

*****

CONTENTS

*****

Chapter 1

Introduction

Chapter 1

INTRODUCTION

1.1 Background and Motivation

Significant quantities of sludge and slags are generated as waste materials or byproducts every day from iron and steel industries. They usually contain considerable quantities of valuable metals and materials. It is often possible to recover some values by physical or chemical mineral processing techniques such as crushing, grinding, classification, hydro-cyclone, magnetic separation, flotation, leaching or roasting. Transforming these solid wastes from one form to another to be reused either by the same production unit or by different industrial installations is very much essential not only for conserving metal and mineral resources but also for protecting the environment.

Linz-Donawitz (LD) slag is a major solid waste generated in huge quantities during steel making. It comes from slag formers such as burned lime/dolomite and from oxidising of silica, iron etc. while refining the iron into steel in the LD furnace. In large size steel plants, the amount of LD slag generated is huge and a sizable amount of it remains unutilized. Most of the steel plants dump this slag in open air and it occupies very large land space. It has been known since long that this slag contaminates the soil and owing to its very small size causes pollution in air as well. Therefore, exploring new avenues for its utilization and harmless disposal is the need of the hour. LD slag is presently being utilized in areas such as soil conditioners, fertilizers, recovery of metal values etc. Experiments have been conducted in the past using pulverized LD slag for growing vegetables like tomato, potato, onion, spinach and crops like wheat in the acidic soil [1]. Attempts are being made on the possibilities of recovering metal values from LD slag which is another exciting and challenging task as far as the materials recycle aspect is concerned. But its potential as a coating

material and as a reinforcing element in polymers has not been explored so far. In view of this, the present work attempts to explore the possibility of developing plasma sprayed LD slag coatings and LD slag filled polymer composites.

Plasma sprayed coatings find wide applications these days in the industrial work places ranging from textile industries to medical applications. In the automotive industries of many industrially advanced countries, these coatings are used to improve the wear resistance, thermal resistance and resistance to corrosion of machine components and structures. Plasma sprayed hard ceramic coatings are applied as protective layers on various engineering and structural components which are often used in situations where erosive wear occurs. Due to the operational requirements in dusty environments, the study of the erosion characteristics of these coatings becomes highly relevant. A full understanding of the effects of all operating and material variables on the wear rate is necessary in order to undertake appropriate steps in the design of components and in the choice of coating materials to reduce/control wear. The subject of erosion wear of plasma spray coatings has not received substantial research attention in the past although there is an increasing use of ceramic coatings in aerospace, transportation and process industries, where they can be subjected to multiple solid or liquid particle impact. Examples of such applications involving material loss by erosion wear are pipe lines carrying pulverized coal dust, helicopter rotor blades, compressor blades, high speed vehicles and aircrafts operating in desert environment etc. [2]. Despite its high significance, solid particle erosion behaviour of coatings has remained a less studied area. Hence, this aspect is taken up in the present investigation for a series of plasma sprayed LD slag based coatings.

Similarly, no research has so far been reported on the use of LD slag as a reinforcing filler material in polymer composites. Composites are engineering or naturally occurring materials made from two or more constituent materials with

significantly different physical or chemical properties, which remain separate and distinct at the macroscopic or microscopic scale within the finished structure. As matrix and reinforcements are the basic components of composites, the reinforcement materials play an important role in the formation of any composite material. This is so because when materials of varying specifications are imposed into a matrix, these materials significantly improve one or more operating properties of the newly formed composite [3].

Polymers and their composites form a very important class of tribo-engineering materials and are invariably used in mechanical components, where wear performance in non-lubricated condition is a key parameter for the material selection. Nowadays much attention is devoted towards the study of solid particle erosion behaviour of polymer composites due to extensive use of these materials in many mechanical and structural applications. Hence, erosion resistance of polymer composites has become an important material property, particularly in selection of alternative materials and therefore the study of solid particle erosion characteristics of the polymeric composites has become highly relevant. Investigations on the reinforcement of a number of conventional filler materials to improve erosion performance of polymers are being done these days. However, as already mentioned, use of LD slag for this purpose has not so far been explored.

Solid particle erosion (SPE) is a general term used to describe mechanical degradation (wear) of any material subjected to a stream of erodent particles impinging on its surface. The effects of solid particle erosion have been recognized by Wahl and Hartenstein [4] quite a long time back. Damage caused by erosion has been reported in several industries for a wide range of situations. Examples have been cited for transportation of airborne solids through pipes by Bitter [5], boiler tubes exposed to fly ash by Raask [6] and gas turbine blades by Hibbert and Roy [7]. Similar to other tribological processes, SPE is also a combined process: the mechanical load may be associated with secondary

thermal, chemical and physical reactions between the counterparts involved in the tribological system. Material removal due to solid particle erosion is a consequence of a series of essentially independent but similar impact events. Thus, the contact between the hard particles and the component surface is of a very short duration. During flight, a particle carries momentum and kinetic energy, which can be dissipated during impact, due to its interaction with a target surface. It is to be noted that solid particle erosion is different from the other forms of erosion like liquid impact erosion, slurry erosion, cavitation erosion etc. Moreover, erosion is completely different from the other closely related processes like sliding wear, abrasion, grinding and machining wherein the contact between the tool/abrasive and the work-piece/target is continuous.

Statistical methods have commonly been used for analysis, prediction and/or optimization of a number of engineering processes. Such methods enable the user to define and study the effect of every single condition possible in an experiment where numerous factors are involved. Solid particle erosion is a complex wear phenomenon in which a number of control factors collectively determine the performance output (i.e. the erosion rate) and there is enormous scope in it for implementation of appropriate statistical techniques for process optimization. But unfortunately, such studies have not been adequately reported so far. The present research work addresses to this aspect by adopting a statistical approach called Taguchi experimental design. This technique provides a simple, systematic and efficient methodology for the analysis of the control factors.

In the present research, a qualitative analysis of the experimental results with regard to erosion wear response of LD slag based coatings and composites has been presented. The analysis is aimed at identifying the operating variables/factors significantly influencing the erosion wear rate of coatings and composites. Like any experimental investigation, erosion trials also demand substantial amount of time, energy and materials. Hence, there is a need for a

prediction tool to supplement the experiments. In the present study, a model based on artificial neural networks (ANN) is implemented to predict the erosion rate of the coatings and composites subjected to different operating conditions. ANN is an information processing paradigm that is inspired by the way that biological nervous systems process information. It is composed of a large number of interconnected processing elements (neurons) working in unison [8, 9]. In other words, ANN represents a powerful tool for the identification of the relevant parameters and their interactions especially when relationships are very complex and highly non-linear [10]. Neural computation is used in the present work since solid particle erosion is a complex process that has many variables with multilateral interactions.

Against this background, the present research work is undertaken to study the processing, characterization and erosion wear analysis of LD slag based coatings and composites. The specific objectives of this work are clearly outlined in the next chapter.

1.2 Thesis Outline

The remainder of this thesis is organized as follows:

Chapter 2 Includes a literature review designed to provide a summary of the base of knowledge already available involving the issues of interest. It presents the research works on plasma spray coatings as well as particulate reinforced polymer composites reported by various investigators.

Chapter 3 Includes a description of the raw materials and the test procedures. It presents the details of development of coatings and fabrication of composites as well as the characterization of coatings and composites under investigation and also an explanation of the Taguchi experimental design and ANN.

Chapter 4 Presents the physical and mechanical properties of the coatings under this study.

Chapter 5 Includes the erosion wear characteristics of LDS, LDS-Al_2O_3 and LDS-TiO_2 coatings.

Chapter 6 Presents the physical and mechanical properties of the composites under this study.

Chapter 7 Includes the erosion wear characteristics of epoxy-LDS and polypropylene-LDS composites with and without glass fiber reinforcement.

Chapter 8 Provides summary of the findings of this research work, outlines specific conclusions drawn from both the experimental and analytical efforts and suggests ideas and directions for future research.

*****

Chapter 2

Literature Review

Chapter 2

LITERATURE REVIEW

In the current section, summary of the literature surveyed during the course of the research has been presented. This survey is expected to provide the background information and thus to select the objectives of the present investigation. This treatise embraces various aspects of plasma spray coatings and polymer composites with a special reference to their physical, mechanical and tribological characteristics. This chapter thus includes reviews of available research reports:

- Plasma Spray Coatings
- Wear Resistant Coatings
- Utilization of Industrial Wastes in Coatings
- Particulate filled Polymer Composites
- Fiber reinforced Polymer Composites
- Utilization of Industrial Wastes in Polymer Composites
- Wear and its Classification
- Erosion Wear Characteristics of Ceramic Coatings
- Erosion Wear Characteristics of Polymer Composites
- Implementation of Design-of-Experiments and Artificial Neural Networks in Wear Analysis

In the concluding section of this chapter, the summary of the literature review along with the knowledge gap in earlier investigations has been presented and the objectives of the present research have been outlined.

2.1 Plasma Spray Coatings

Plasma spray coating is a typical thermal spraying process that combines particle melting, quenching and consolidation in a single operation. The advantages of plasma spraying include formation of metallic/ceramic microstructures with fine, equi-axed grains without columnar defects, deposition of graded coatings with a wide compositional variability and application of high deposition rates during formation of thick coatings with only a modest investment in capital equipment [11-13]. Plasma-sprayed ceramic coatings have been widely adopted by many industries due to its flexibility, superior quality and high deposition rate. It has been able to process various low-grade-ore minerals to value-added products and deposit metals and ceramics, producing homogenous and functionally graded composite coatings with desired properties [14-18]. In spite of all these advantages, the high cost of spray-grade powders limits the adoption of this technique and therefore exploring newer and cheaper materials suitable for plasma spray coating has drawn a lot of research attention in recent time.

Plasma spray coating technique utilizes the exotic properties of the plasma medium to effect physical, chemical or metallurgical reactions to produce metallic and ceramic coatings for a variety of applications. It is an economical and effective surface modification method applied to various machine parts to reduce degradation. It is gaining importance in many critical areas of application due to the fact that it provides increased design flexibility and its high deposition rate, so that the parts made up from a combination of materials with widely differing physical and chemical properties could be employed [19, 20]. In plasma spraying, a coated layer is formed on a substrate surface by spraying melted powders on to the substrate at a high speed using a high-temperature plasma heat source. The microstructure and properties of plasma sprayed coatings depend on the design of the plasma torch, the operating parameters including torch input power, plasma forming gases and flow rates, spray distance, feedstock composition, feed rate and injection parameters etc. [21, 22].

Coatings through plasma spraying route are produced by introducing powder particles of the feedstock material into a plasma jet, which melts them and propels towards the substrate. The formation of a coating depends on the interaction between a droplet and the substrate or the previously deposited layers, i.e. spreading of a droplet, the formation of a splat (lamella) and its solidification. The difference in the degree of a splat flattening results in the difference in porosity and its shape as well as distribution and these factors could affect also the bonding between lamellae. A schematic diagram of plasma spray process is shown in Figure 2.1.

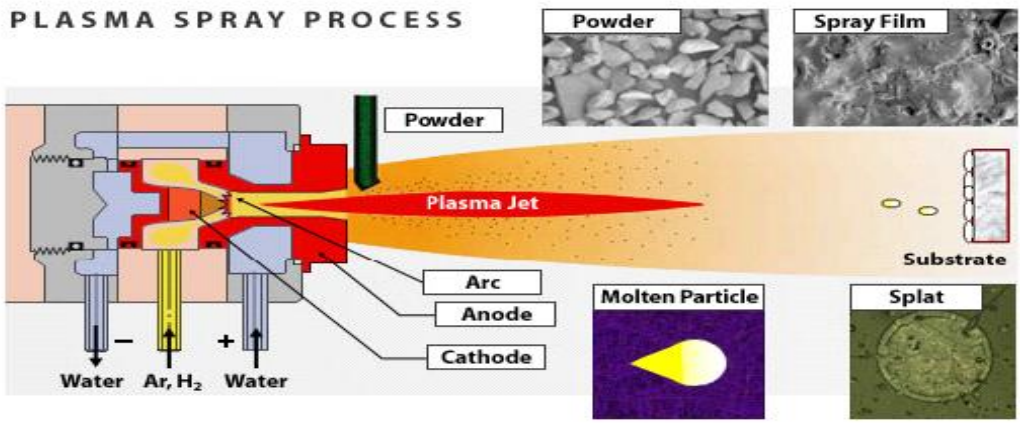

Figure 2.1 Conventional plasma spraying process

Plasma is considered to be the fourth state of matter, consisting of a mixture of electrons, ions and neutral particles, although overall it is electrically neutral. Most simply, plasma may be defined as nothing but a partially ionized state of gas. The degree of ionization of a plasma is the proportion of atoms that have lost (or gained) electrons and in the case of thermal plasmas, this is controlled mostly by temperature. Plasma technology involves the creation of a sustained electrical arc by the passage of electric current through a gas in a process referred to as electrical breakdown. Because of the electrical resistivity across the system, significant heat is generated, which strips away electrons from the gas molecules resulting in an ionized gas stream known as *plasma*. At about 2000^0C, gas molecules dissociate into the atomic state and when the temperature is raised to about 3000^0C, gas molecules lose electrons and become ionized. In

this state, gas has a liquid-like viscosity at atmospheric pressure and the free electric charges confer relatively high electrical conductivities that can approach those of metals [23]. A non-transferred DC arc plasma has been conventionally used for coating purposes and is most widely employed in the thermal spray industries. Such coatings have been commonly used for industrial parts as well as for structural applications in order to develop resistances to corrosion, oxidization, erosion and high temperature [21, 22, 24-27].

Plasma spray set-up:

A typical plasma spray set up essentially consists of a plasma spray gun/torch, a control console, a powder feeder, a power supply unit and a torch cooling system. An arc is created between tungsten tipped copper cathode and an annular copper anode (both water cooled). The plasma generating gas is forced to pass through the annular space between the electrodes. While passing through the arc, the gas undergoes ionization in the high temperature environment resulting plasma. The ionization is achieved by collisions of electrons of the arc with the neutral molecules of the gas. The plasma protrudes out of the electrode encasement in the form of a flame. The consumable material, in the powdered form, is poured into the flame in metered quantity. The powders melt immediately and absorb the momentum of the expanding gas and rush towards the target to form a thin deposited layer. The next layer deposits onto the first one immediately after the deposition of first layer and thus the coating builds up layer by layer [28-31]. The temperature in the plasma arc can be as high as $10{,}000^0$C. Elaborate cooling arrangement is required to protect the plasmatron (i.e., the plasma generator) from excessive heating.

A typical plasma spraying equipment consists of the following modules [32]:

1. Plasmatron: It is the device which houses the electrodes and in which the plasma reaction takes place. It has the shape of a gun and it is connected to the water cooled power supply cables, powder supply hose and gas supply hose.

2. Power supply unit: Normally plasma arc works in a low voltage (40-70 volts) and high current (300-1000 Amperes), DC ambient. The available power (AC, 3 phase, 440 V) must be transformed and rectified to suit the reactor. This is taken care of by the power supply unit.

3. Powder feeder: The powder is kept inside a hopper. A separate gas line directs the carrier gas which fluidizes the powder and carries it to the plasma arc. The flow rate of the powder can be controlled precisely.

4. Coolant water supply unit: It circulates water into the plasmatron, the power supply unit and the power cables. Units capable of supplying refrigerated water are also available.

5. Control unit: Important functions (current control, gas flow rate control etc.) are performed by the control unit. It also consists of the relays and solenoid valves and other interlocking arrangements essential for safe running of the equipment. For example, the arc can only be started if the coolant supply is on and water pressure and flow rate is adequate.

Process parameters in plasma spraying

In plasma spraying one has to deal with a lot of process parameters, which determine the degree of particle melting, adhesion strength and deposition efficiency of the powder [33]. An elaborate listing of these parameters and their effects are reported in the literature [34-36]. Some important parameters are arc power, plasma gas, carrier gas, mass flow rate of powder, torch to base distance, spraying angle, substrate cooling, powder related variables, preheating of the substrate, angle of powder injection etc.

The requirements for plasma spraying

1. *Roughness of the Substrate Surface***:** A rough surface provides a good coating adhesion and enough room for anchorage of the splats facilitating bonding through mechanical inter-locking.

2. *Cleanliness of the Substrates***:** The substrate to be sprayed on must be free from any dirt or grease or any other material that might prevent intimate contact of the splat and the substrate. For this purpose the substrate must be thoroughly cleaned (ultrasonically, if possible) with a solvent before spraying.

3. *Bond Coat:* Materials like ceramics cannot be sprayed directly onto metals, owing to a large difference between their thermal expansion coefficients (α). So bond coat is required for these types of coatings. For example, in wear related applications, an alumina and Ni-Al top and bond coats combination can be used [37]. In thermal barrier application, CoCrAlY or Ni-Al bond coat and zirconia top coat are popular [38].

4. *Cooling Water:* For cooling purpose, distilled water should be used, whenever possible. Normally a small volume of distilled water is re-circulated into the gun and it is cooled by an external water supply from a large tank. Sometime water from a large external tank is pumped directly into the gun [32].

2.2 Wear Resistant Coatings

A thorough study of the wear resistance of thermally sprayed coatings must involve plasma-sprayed ceramics because plasma sprayed coatings have been proved to be very useful in various tribological applications [39-41]. Much research related to the basic wear mechanisms of plasma sprayed oxide ceramics exists, since such coatings have been studied for a long time [42-45]. However, there exists a few works comparing them to the characteristics of other thermally sprayed coatings as well as to other industrially widespread wear resistant coatings, such as hard chrome electroplating and nickel electroless plating [46, 47]. Furthermore, to fully assess the industrial applicability of thermally sprayed coatings in general and of plasma sprayed oxides in particular, wear maps should be experimentally obtained, as it is currently being done for massive sintered ceramics [48-50].

Today a variety of materials, e.g., carbides, oxides, metallic etc. belonging to the above category are available commercially. The wear resistant coatings can accordingly be classified into the following categories: [29]

2.2.1 Carbide Coatings

Tungsten carbide (WC) is very popular for wear and corrosion applications [51] among the carbides. The WC powders are clad with a cobalt layer. During spraying, the cobalt layer undergoes melting and upon solidification form a metallic matrix in which the hard WC particles remain embedded. Spraying of WC-Co involves a close control of the process parameters such that only the cobalt phase melts without degrading the WC particles.

Other carbides like TiC, TaC and NbC are provided along with WC in the cermet to improve upon the oxidation resistance, hardness and hot strength. Similarly the binder phase is also modified by adding chromium and nickel with cobalt [29]. The wear mechanism of plasma sprayed WC-Co coatings depends on a number of factors, e.g., mechanical properties, cobalt content, experimental conditions, mating surfaces etc. The wear mode can be abrasive, adhesive or surface fatigue [52-56]. The coefficient of friction of WC-Co (in self-mated condition) increases with increasing cobalt content [55]. A WC-Co coating when tested at a temperature of 450^0 C exhibits signs of melting [57]. The wear resistance of these coatings also depends on porosity [53]. These pores can act as source from where the cracks may grow. Thermal diffusivity of the coatings is another important factor. In narrow contact regions, an excessive heat generation may occur owing to rubbing. If the thermal diffusivity of the coating is low, the heat cannot escape from a narrow region easily which results a rise in temperature and thus failure occurs owing to thermal stress [53, 57]. The wear mechanism of WC-Co nano-composite coating on mild steel substrates has been studied in details [58]. The wear rates of such coatings are found to be much greater than that of commercial WC-Co composite coating, presumably owing to an enhanced decomposition of nano-particles during spraying. Wear has been

found to occur by subsurface cracking along the preferred crack paths provided by the binder phase or failure at the inter-splat boundary.

A coating of Cr_3C_2 (with Ni-Cr alloy cladding) is known for its excellent sliding wear resistance and superior oxidation and erosion resistance, though its hardness is lower than that of WC [29]. After spraying in air, Cr_3C_2 loses carbon and transforms to Cr_7C_3. Such transformation generally improves hardness and erosion resistance of the coating [59]. The sliding wear behaviour of the Cr_3C_2-Ni-Cr composite against various metals and ceramics has been studied by several authors in the past [53, 56, 60]. It is felt that at lower load, the wear is owing to the detachment of splats from the surface. As the load increases melting, plastic deformation and shear failure come into play.

2.2.2 Oxide Coatings

Metallic coatings and metal containing carbide coatings sometime are not suitable in high temperature environment in both wear and corrosion applications. Often they fail owing to oxidation or decarburization. In such cases, the material of choice can be an oxide ceramic coating, e.g., Al_2O_3 and TiO_2 or their combinations. However, high wear resistances, chemical and thermal stability of these materials are counter-balanced by the disadvantages of low values of thermal expansion coefficient, thermal conductivity, mechanical strength, fracture toughness and somewhat weaker adhesion to substrate material. Therefore, to obtain a good quality coating it is essential to exercise proper choice of bond coat, spray parameters and reinforcing additives [29].

Alumina (Al_2O_3) Coatings**:** Alumina is obtained from a mineral called bauxite, which exists in nature as a number of hydrated phases, e.g., boehmite (γ-Al_2O_3, H_2O), hydragillate and diaspore (α-Al_2O_3. $3H_2O$). It also exists in several other metastable forms like β, δ, θ, η, κ and X [61]. α - Al_2O_3 is known to be a stable phase and it is available in nature in the form of corundum. In addition, α-Al_2O_3 can be extracted from the raw materials by fusing them.

The phase transformation during freezing of the plasma sprayed alumina droplets has been studied in details [62, 63]. From the molten particles, γ- Al_2O_3 tends to nucleate, since liquid to γ transformation involves a low interfacial energy. The phase finally formed upon cooling depends on the particle diameter. For particle diameter less than 10 μm, the metastable form is retained (γ, δ, β or θ). Plasma spraying of alumina particles having a mean diameter of 9 μm results in the development of the γ phase in the coating after cooling [64]. The α-form is found in the large diameter particles. In fact larger is the diameter, greater is the fraction of α-Al_2O_3 in the cooled solid. This form is desirable for its superior wear properties. On the other hand, if the aforesaid heat transfer is faster than the heat injection rate from the growing solidification front, equi-axed crystals are supposed to form. In reality, columnar crystals are generally found. There are several advantages of alumina as a structural material, e.g., availability, hardness, high melting point, resistance to wear and tear etc. It bonds well with the metallic substrates when applied as a coating on them.

Titania (TiO_2) Coating: Titania coating is known for its high hardness, density and adhesion strength [53, 56]. It has been used to combat abrasive, erosive and fretting wear either in essentially pure form or in association with other compounds [65, 66]. The mechanism of wear of TiO_2 at 450^0C under both lubricated and dry contact conditions has been studied in the past [56, 57]. It has been found to undergo a plastic smearing under lubricated contact, where as it fails owing to the surface fatigue in dry condition. TiO_2-stainless steel couples in various speed load conditions have also been investigated in details [67]. At a relatively low load, the failure is owing to the surface fatigue and adhesive wear, whereas at a high load the failure is attributed to the abrasion and delamination associated with a back and forth movement [68]. At low speed the transferred layer of steel oxidizes to form Fe_2O_3 and the wear progresses by the adhesion and surface fatigue. At a high speed, Fe_3O_4 forms instead of Fe_2O_3 [69]. The TiO_2 top layer also softens and melts owing to a steep rise in temperature, which helps in reducing the temperature subsequently [70]. The performance of the

plasma sprayed pure TiO_2 has been compared with those of Al_2O_3-40 wt% TiO_2 and pure Al_2O_3 under both dry and lubricated contact conditions [71]. TiO_2 owing to its relatively high porosity can provide good anchorage to the transferred film and also can hold the lubricants effectively [72].

2.2.3 Metallic Coatings

Metallic coatings can be easily applied by flame spraying or welding techniques making the process very economical. Metallic wear resistant materials are classified into three categories i.e. cobalt based alloys, nickel based alloys and iron based alloys.

The common alloying elements in a cobalt-based alloy are Cr, Mo, W and Si. The microstructure is constituted by dispersed carbides of M_7C_3 type in a cobalt rich FCC matrix. The carbides provide the necessary abrasion and corrosion resistance.

NiCoCrAlY is an example of plasma sprayable super alloy. It shows an excellent high temperature corrosion resistance and hence finds application in gas turbine blades. The compositional flexibility of such coatings permits tailoring of such coating composition for both property improvement and coating-substrate compatibility. In addition, it serves as a bond coat for zirconia based thermal barrier coatings [73, 74].

Iron based alloys are classified into pearlitic/austenitic/martensitic steels and high alloy irons. The principal alloying elements used are Mo, Ni, Cr and C. The softer materials, e.g., ferritic, are for rebuilding purpose. The harder materials, e.g., martensitic, on the other hand provide wear resistance. Such alloys do not possess much corrosion, oxidation or creep resistance [75-77]. Nickel aluminide is another example of coating material for wear purpose. The pre-alloyed Ni-Al powders, when sprayed, react exothermically to form nickel aluminide. This reaction improves the coating-substrate adhesion. In addition to wear application, it is also used as bond coat for ceramic materials [38].

2.2.4 Diamond Coatings

Thin diamond films for industrial applications are commonly produced by chemical vapour deposition (CVD), plasma assisted CVD, ion beam deposition and laser ablation technique [78, 79]. Such coatings are used in electronic devices and ultra wear resistant overlays. The limitation of the aforesaid methods is their slow deposition rates. However, the process is extremely sensitive to the process parameters. Deposition of diamond film is also possible using a oxy-acetylene torch [80]. One significant limitation of a diamond coating is that it cannot be rubbed against ferrous materials, owing to a phase transformation leading to the formation of other carbon allotropes [81]. Diamond films are tested for the sliding wear against abrasive papers, where wear progresses by micro-fracturing of protruding diamond grits. The processes continue till the surface becomes flat and thereafter wear progresses by an interfacial spalling. Therefore, the life of the coating is limited by its thickness [82].

2.3 Utilization of Industrial Wastes in Coatings

Ceramic coatings are applied in many industries to protect and improve the surface properties of metallic materials [83, 84]. The selection of these ceramic materials depends not only on their oxidation and corrosion resistance but also on their ability to operate under severe conditions, including high temperatures and abrasive environments. There are many techniques available for the deposition of ceramic coatings, such as atmospheric plasma spray (APS), chemical vapour deposition (CVD), physical vapour deposition (PVD) and dip-coating. Among these, APS is the most effective technique due to the high deposition efficiency that can be obtained. However, APS is an expensive technique because of the cost associated with the complex process for manufacturing spray-grade powders [85]. This high cost can be overcome using substitute powders that are inexpensive and readily available in industrial wastes.

As far as the field of ceramic coating is concerned, during last two decades, a large number of investigations have been carried out on processing of variety of plasma sprayed coatings for industrial applications [86]. A possibility that wastes from industries and low grade minerals could be used as coating materials had not received adequate research attention for quite a long time. Thus, the research history of coatings prepared from industrial wastes, both in the Indian and International context, has been very brief. Only very few researchers have explored the coating potential of various abundantly available industrial wastes such as red mud, fly ash, copper slag and low grade minerals like ilmenite.

Red mud emerges as a byproduct from the caustic leaching of bauxite during production of alumina by Bayer's process whose major constituents are SiO_2, Fe_2O_3, Al_2O_3, TiO_2, Na_2O and CaO. Successful deposition of red mud on metallic substrates by plasma spraying was first carried out by Mishra et al. in 2002 [87]. Subsequently they developed coatings of red mud premixed with different proportions of fly ash, carbon and aluminium powder on mild steel, copper and aluminium substrates and established the coatability of red mud by plasma spraying route [88]. Recently, Mishra et al. have reported the processing and characterization of fly ash-ilmenite coatings on metal substrates by the same atmospheric plasma spraying technique [89]. Sahu et al. [90] studied the processing, characterization and the erosion wear response of a new class of metal-ceramic composite coatings deposited on metal substrates by plasma spraying. Yilmaz et al. [91] have reported the applicability of fly ash as a coating onto the steel substrates by means of plasma spraying. They showed that the interface bond strength of coating increases by the addition of aluminum powder to fly ash prior to coating deposition. Krishna et al. [92] have also reported the coatability of fly ash on steel substrates, but by a different coating deposition technique called detonation spraying. This investigation showed that the resultant fly ash coatings were two to three times harder than the substrate material and exhibited a three-fold reduction in coefficient of friction under sliding wear conditions.

Exhaustive literature review suggests that way back, Ramesh et al. [93] developed nickel-fly ash composite coatings on mild steel substrates and studied the sliding wear characteristics. The coatings were produced by sediment electro-codeposition method, which however, is not a thermal spraying technique. According to this report, nickel-fly ash composite coatings possess better wear resistance than nickel coating and the percentage of fly ash in the composite coating influences the wear rate. Ramesh and Seshadri [94] have further studied and reported extensively on the mechanical characteristics and the fatigue behaviour of these nickel-fly ash coatings.

In 2000, Mishra et al. [95] attempted to develop coatings of fly ash by thermal spraying route. They produced fly ash coatings on copper and stainless steel substrates at various plasma torch input power ranging from 10 to 20 kW. Subsequently they sprayed mixtures of fly ash with 5 and 15 wt% aluminium powder onto the same metallic substrates. This study revealed that the coating quality and properties were improved with higher aluminium content in the feed material. Sidhu et al. [96] obtained fly ash coatings by shrouded plasma spray process on carbon steel and studied their sliding wear and oxidation behaviour. Muhammad et al. [97] reported the plasma spray deposition of fly ash onto mild steel substrates. Mantry et al. [98] reported the deposition of plasma-sprayed Cu Slag-Al composite coatings on mild steel substrates and also studied the erosion wear analysis of these coatings. They found that maximum erosion takes place at an angle of 60^0, showing the semi-ductile response of the metal-ceramic composite coating to solid particle erosion. Mantry et al. [99] have also studied the evaluation and characterization of plasma sprayed Cu slag-Al composite coatings on metal substrates.

With increased environmental threat, it has become necessary to find out alternative utilization of industrial wastes and to develop value added products using them. Though substantial development has taken place in the area of disposal and utilization of these wastes, a focused and systematic research on its coating potential has not been adequately done.

2.4 Particulate filled Polymer Composites

Composite is a synergistic combination of two or more micro-constituents that differ in physical form and chemical composition and are insoluble in each other. Composite materials have successfully substituted the traditional materials in several light weight and high strength applications. The reasons why composites are selected for such applications are mainly their high strength-to-weight ratio, high tensile strength at elevated temperatures, high creep resistance and high toughness. Typically, in a composite, the reinforcing materials are strong with low densities while the matrix is usually a ductile or tough material. If the composite is designed and fabricated correctly it combines the strength of the reinforcement with the toughness of the matrix to achieve a combination of desirable properties not available in any single conventional material. The strength of the composites depends primarily on the amount, arrangement and type of fiber and/or particle reinforcement in the resin.

Polymers are classified broadly into two groups: thermoplastics and thermosets. The most commonly adopted thermoplastics include polypropylene (PP), polyethylene and poly vinyl chloride (PVC); while phenolic resin, epoxy and polyester resins are some of the most used thermosetting polymer matrices. Particulate filled polymer composites are being used extensively in various fields due to their low production costs and the ease with which they can be formed into complex shapes. Besides, they behave isotropically and are not as sensitive as long fiber composites to the mismatch of thermal expansion between the matrix and the reinforcement [100, 101]. Generally, particulate fillers are used in polymers for a variety of reasons such as cost reduction, improved processing, density control, optical effects, thermal conductivity, modified electrical and magnetic properties, flame retardancy, improved hardness and wear resistance. Hard particulate fillers consisting of ceramic or metal particles and fiber-fillers made of glass are being used these days to improve the performance of polymer composites to a great extent [102]. Various kinds of polymers and polymer matrix composites reinforced with metal particles have a wide range of industrial

applications such as heaters, electrodes [103], composites with thermal durability at high temperature etc. [104]. Similarly, ceramic filled polymer composites have also been the subject of extensive research in last two decades. When silica particles are added into a polymer matrix, they play an important role in improving electrical, mechanical and thermal properties of the composites [105, 106]. The mechanical properties of particulate filled polymer composites depend strongly on the particle size, particle-matrix interface adhesion and particle loading. Sumita et al. [107] underlined the interest of replacing micro-scale silica by its nano-scale counterpart, since nano-scale silica particles possess superior mechanical properties. Smaller particle size yields higher fracture toughness also for calcium carbonate filled high density polyethylene (HDPE) [108]. Similarly, epoxy filled with smaller alumina tri-hydrate particles shows higher fracture toughness [109]. Thus, particle size is being reduced rapidly and many recent studies have focused on how single-particle size affects mechanical properties [110, 111].

Yamamoto et al. [112] reported that the structure and shape of silica particle have significant effects on the mechanical properties such as fatigue resistance, tensile and fracture properties. Nakamura et al. [113, 114] discussed the effects of size and shape of silica particles on the strength and fracture toughness based on particle-matrix adhesion. Usually the strength of a composite strongly depends on the stress transfer between the particles and the matrix [115]. For well-bonded particles, the applied stress can be effectively transferred to the particles from the matrix resulting in an improvement in the strength. However, for poorly bonded micro-particles, reduction in strength is found to have occurred. Nicolais and Nicodemo [116] studied the effect of particle shape on tensile properties of glassy thermoplastic composites. While most of these investigations have focused either on the particle shape or on particle size, the study made by Patnaik et al. [117] reported that the mechanical properties of polyester based hybrid composites are highly influenced also by the type and content of the filler materials. Padhi et al. [118] reported on processing,

characterization and wear analysis of short glass fiber-reinforced polypropylene composites filled with blast furnace slag particles. They also predicted and simulated the erosion wear behavior of these composites. Tagliavia et al. [119] reported analysis of flexural properties of composites filled with hollow particles. They studied the flexural properties of hollow-glass particle filled vinyl ester composites, which are used in marine applications. Weidenfeller et al. [120] made a detailed study on cooling behaviour of particle filled polypropylene composites during injection molding process. Hassan et al. [121] studied morphological and mechanical properties of carbonized waste maize stalk as reinforcement for eco-composites. Omar et al. [122] investigated on the particle size dependence on the static and dynamic compression properties of polypropylene/silica composites. Recently, Gupta and Satapathy [123] have reported the processing, characterization and wear analysis of borosilicate glass microsphere (BGM) filled epoxy composites.

Lauke and Fu [124] reported the theoretical modeling for the fracture toughness of particulate-polymer composites by considering a simple geometrical model of particle-particle interaction in a regular particle arrangement. They also discussed the influence of structural properties such as particle volume fraction and matrix mechanical properties on fracture toughness. Jerabek et al. [125] studied filler/matrix-debonding and micro-mechanisms of deformation in particulate filled polypropylene composites under tension. In their approach, they introduced a novel method for the detection of debonding using volume strain measurements, which takes into account the dilatational and deviatoric behaviour of the neat matrix polymer and the composite. Bishay et al. [126] studied electrical, mechanical and thermal properties of polyvinyl chloride (PVC) composites filled with aluminum powder. Agrawal and Satapathy [127] developed a heat conduction model and investigated on thermal conductivity enhancement of AlN/epoxy composites. They further investigated thermal and dielectric properties of epoxy and polypropylene reinforced with micro-sized AlN particles [128].

2.5 Fiber Reinforced Polymer Composites

Fiber reinforced polymer (FRP) composites are now-a-days experiencing significant growth in composite industries. Today, fiber composites are routinely used in diverse applications such as automobiles, aircrafts, space vehicles, off-shore structures, containers and piping, sporting goods, electronics and appliances. They offer outstanding mechanical properties, unique flexibility in design capability and ease of fabrication. Additional advantages include light weight, corrosion and impact resistance and excellent fatigue strength.

Because of the tremendous strength-to-weight properties and impressive design flexibility, the FRP composites find their popularity in the transportation industry also. Many researchers have studied and reported the physico-mechanical properties as well as tribological aspects of varieties of fiber reinforced polymer composites. Recently, Khalil et al. [129] made a detail review on natural fiber reinforced poly vinyl chloride (PVC) composites. In their study, the authors discussed the reinforcing effects, plasticization effects along with modification by coupling agents on the composite properties and applications. Abdulmajeeda et al. [130] studied the effect of high fiber fraction on some mechanical properties of unidirectional glass fiber reinforced composites. Garoushi et al. [131] investigated the reinforcing effect of short E-glass fiber fillers on mechanical properties of dental composite with inter-penetrating polymer network (IPN)-polymer matrix. The significant use of short fiber fillers with IPN-polymer matrix yielded improved mechanical performance compared to those of conventional restorative composites. Karsli and Aytac [132] studied tensile and thermo-mechanical properties of short carbon fiber reinforced polyamide-6 (PA6) composites.

Multi-fiber composites, in which two or more types of fibers are used to reinforce a common matrix, are developed now-a-days to achieve tailored material properties. Whilst possessing overall excellent mechanical properties, the relatively low ratio of compressive-to-tensile strength for carbon fiber [133-

135] may be a disadvantage for the use of carbon fiber reinforced polymer (CFRP) composites when utilized as structural members subjected to compressive and/or flexural loading. Although glass fibers possess lower tensile strength in comparison even to low strength carbon fiber [136, 137], their strain-to-failure is higher due to the lower modulus. Thus, it is possible to incorporate high elongation fibers e.g. glass into low elongation fibers e.g. carbon to improve the failure strains [138]. High elongation fibers enhance the strain levels required to propagate cracks through the composites and hence behave like crack arrestors on a micro-mechanical level [139]. A study on the flexural strength of epoxy composites reinforced by S-2 glass and T700S carbon fibers in an intra-ply configuration has been presented by Dong and Davies [140]. Encinas et al. [141] focused their work on the creation of wettable glass fiber reinforced epoxy and polyester composites, thus improving their adhesion performance. Sridhar et al. [142] studied the optimal design of customized hip prosthesis using carbon fiber reinforced poly-ether-ether-ketone matrix lay-up. Kumar et al. [143] developed continuous fiber reinforced functionally graded composites (FGCs) using quartz fabric reinforcement for thermo-structural aerospace applications. Avci et al. [144] studied the fracture characteristics of glass fiber reinforced polymer composites. Shamsuddoha et al. [145] made a review on the use of fiber-reinforced polymer composites for in-air, underground and underwater pipeline repairs. The use of fiber reinforced composites has already been proven effective for the construction and retrofit of filled and hollow in-air, marine and underground cylindrical elements [146]. Ramesh et al. [147] made a comparative evaluation of hybrid glass fiber-sisal/jute reinforced epoxy composites.

Multi-fiber composites may be produced in many different arrangements; however, research into the mechanical properties of such composites has mostly been limited to configurations in which fibers have been intimately mixed within the matrix or arranged in a purposeful manner. When considering the mechanical properties, a general rule-of-mixture approach may be utilized which quantifies a material property with respect to the volume concentration of its constituents.

Many researchers have however noted the existence of a hybrid effect in which the material property as predicted by the rule-of-mixture differs to that observed in reality. A positive or negative hybrid effect can be defined as a positive or negative deviation of a certain mechanical property from the rule-of-mixture behaviour respectively [148].

A fiber reinforced composite is not simply a mass of fibers dispersed within a polymer. It consists of fibers embedded in or bonded to a polymer matrix with distinct interfaces between the two constituent phases. The fibers are usually of high strength and modulus. While the fibers serve as the principal load carrying members, the matrix also bears a part of the applied load. The matrix also serves to protect the fibers from environmental damage before, during and after composite processing. In a composite, both fibers and matrix largely retain their identities and yet result in many properties that cannot be achieved with either of the constituents acting alone. A wide variety of fibers are available for use in composites. The most commonly used fibers are various types of carbon, glass and aramid fibers. Besides, natural fibers such as: jute, sisal and ceramic fibers like alumina, silicon carbide, mullite and silicon nitride are also used in composite making. The unique combinations of properties available in these fibers provide the outstanding functional and structural characteristics such as: high specific strength and specific stiffness to the fiber reinforced composites.

A key feature of fiber composites that makes them so promising as engineering materials is the opportunity to tailor the materials properties through the control of fiber and matrix combinations and the selection of processing techniques. In principle, an infinite range of composite types exists, from randomly oriented chopped fiber based materials at the low property end to continuous, unidirectional fiber composites at the high performance end. A judicious selection of matrix and the reinforcing phase can lead to a composite with a combination of strength and modulus comparable to or even better than those of conventional metallic materials [149]. The physical and mechanical

characteristics can further be modified by adding a solid filler phase to the matrix body during the composite preparation.

Recently, it has been observed that by incorporating filler particles into the matrix of fiber reinforced composites, synergistic effects may be achieved in the form of higher modulus and reduced material costs, yet accompanied with decreased strength and impact toughness [150, 151]. Such multi-component composites consisting of a matrix phase reinforced with a fiber and filled with particulate matters are termed as hybrid composites. Garcia at al. [152] were the first to suggest this kind of composite technique for improving the matrix-dominated properties of continuous fiber reinforced composites. Liau et al. [153] found a significant improvement in impact energy of hybrid composites incorporating either particulates or ceramic whiskers. Attempts to understand the modifications in the physical, mechanical and tribological behaviour of such hybrid composites have been made by a few researchers [154, 155] in the past.

2.6 Utilization of Industrial Wastes in Polymer Composites

Although lot of work have been done on particulate filled polymer composites, reports on the use of industrial solid wastes as particulate fillers have been rare. Only a few studies on use of industrial wastes like red mud, fly ash, copper slag etc. in polymer composites have been reported so far. However, owing to the high cost of conventional fillers, this is emerging as a subject of extensive research in recent years. Utilization of fly ash as a filler in polymer composites has received increased attention recently, particularly for high volume applications for effective disposal of the material and reducing the overall cost of the composites. Fly ash is a waste material, obtained in huge quantities from thermal power plant as by-product of the burning of pulverized coal. A microscopic view would reveal that the particles are essentially spherical. Fly ash has been used as spherical filler for the production of lightweight high strength concrete [156]. Chaowasakoo and Sombatsompop [157] studied the mechanical and morphological properties of fly ash/epoxy composites using

conventional thermal and microwave curing methods. Raja et al. [158] described the mechanical behaviour of fly ash impregnated E-glass fiber reinforced polymer composites. Findings on epoxy composites filled with fly ash have also been reported by Srivastava and Pawar [159]. Gu et al. [160] investigated the effect of porosity on the damping properties of modified epoxy composites filled with fly ash. Patnaik et al. [161, 162] studied erosion wear response of the glass-fiber reinforced fly ash filled polyester composites using Taguchi's design-of-experiment method. Patnaik et al. [163] further investigated the parametric appraisal of the dry sliding wear response for a set of new composites consisting of polyester as the matrix, flakes of pine-bark as the fibrous reinforcing component and the kiln-dust of a cement plant as the filler. Asaad and Tawfik [164] described that due to the economical and environmental concern, polymer mortar and polymeric composites are prepared by mixing recycled polystyrene waste and cement dust waste as fillers. Mahapatra [165] describes the development of a multiphase hybrid composite consisting of polyester reinforced with E-glass fiber and solid industrial wastes. Siddhartha et al. [166] studied the wear characteristics of a cement by-pass dust (CBPD) reinforced epoxy-based functionally graded composite. Gangil et al. [167] utilized particulate-filled CBPD and short kevlar fiber to produce homogenous and functionally graded vinyl ester composites.

Similarly, production of alumina from bauxite by the Bayer's process is associated with the generation of red mud as the major waste material in alumina industries. Attempts have been made over the years to study the usage of red mud as a partial substitute of clay in ceramic products like bricks, tiles etc. [168]. A recent experimental study by Mahata et al. [169] confirmed formation of aluminium titanate-mullite composite from red mud rich in titanium. Zhang et al. [170] studied the mechanical and thermal properties of the red mud/polypropylene (PP) composites. Akinci et al. [171] investigated the use of red mud as a filler material in a polypropylene matrix composite. Bhat et al. [172] had taken up a research work with an objective to explore the use of red

mud as a reinforcing material in the polymer matrix as a low cost option. Saradava et al. [173] have reported on the processing and evaluation of mechanical properties of red mud filled coir fiber reinforced polymer composites.

Similarly, copper slag is another solid waste that is generated in copper extraction industries during matte smelting and refining of copper [174]. Biswas and Satapathy [175] made the first attempt to use copper slag in polymers. In their study, using copper slag as a filler in glass-epoxy composites, the hardness, tensile modulus, flexural and impact strength are found to be increased. They also developed a new class of hybrid glass-epoxy composites using red mud as filler material and studied the erosion wear behavior of these composites [176]. Later, Biswas et al. [177] studied the effect of red mud and copper slag particles on physical and mechanical properties of bamboo-fiber-reinforced epoxy composites. Recently, Padhi and Satapathy [178-181] have reported on the processing and characterization of polymer composites filled with blast furnace slag, a solid waste generated during iron making.

2.7 Wear and its Classification

Wear is the process occurring at the interfaces between interacting bodies and is usually hidden from investigators by the wearing components. However, this obstacle has been gradually overcome by scientists, revealing an intricate world of various wear modes and mechanisms. The widest definition of wear, which has been recognized for at least 50 years, includes the loss of material from a surface, transfer of material from one surface to another or movement of material within a single surface [182]. Although a narrower definition of wear has been proposed as ‘progressive loss of substances from the operating surface of a body occurring as a result of relative motion at the surface’ [183], the wide range of engineering applications of concern to the tribologists is served better by a broader definition. A simple and useful statement is that wear is ‘damage to a solid surface, generally involving progressive loss of material, due to relative

motion between that surface and a contacting substance or substances' [184]. This includes:

1. Degradation by the displacement of material within the surface (leading to changes in surface topography without loss of material), as well as the more usual case of material removal,
2. The wear processes common in machines in which one surface slides or rolls against another, either with or without the presence of a deliberately applied lubricant, and
3. The more specialized types of wear which occur when the surface is abraded by hard particles moving across it, or is eroded by solid particles or liquid drops striking it or by the collapse of cavitation bubbles in a liquid.

This definition, quite deliberately tells nothing about the mechanisms by which the degradation takes place. These may be purely mechanical, for example involving plastic deformation or brittle fracture or they may involve significant chemical aspects, like oxidation of a metal or hydration of a ceramic; in many practical cases, both chemical and mechanical processes play a role [185].

A fundamental scheme to classify wear was first outlined by Burwell and Strang [186]. Later, Burwell [187] modified the classification to include five distinct types of wear, namely:

1. Abrasive wear: Abrasive wear or abrasion is generally defined as the wear that is caused by the displacement of material from a solid surface due to hard particles sliding along the surface and cutting grooves on the softer surfaces. It accounts for most failures in practice. This hard material may originate from one of the two surfaces, rubbing against each other. In sliding mechanisms, abrasion can arise from the existing asperities on one surface (if it is harder than the other), from the generation of wear fragments which are repeatedly deformed and hence get work hardened or oxidized until they become harder

than either or both of the sliding surfaces or from the adventitious entry of hard particles, such as dirt from outside the system.

2. Adhesive wear: Adhesive wear can be defined as wear due to localized bonding between contacting solid surfaces leading to material transfer between the two surfaces or the loss from either surface. For adhesive wear to occur it is necessary for the surfaces to be in intimate contact with each other. Surfaces, which are held apart by lubricating films, oxide films etc. reduce the tendency for adhesion to occur.

3. Surface fatigue: Wear of a solid surface can also be caused by fracture arising from material fatigue. The term 'fatigue' is broadly applied to the failure phenomenon where a solid is subjected to cyclic loading involving tension and compression above a certain critical stress. Repeated loading causes the generation of micro-cracks, usually below the surface, at the site of a pre-existing point of weakness. On subsequent loading and unloading, the micro-crack propagates. Once the crack reaches the critical size, it changes its direction to emerge at the surface and thus flat sheet like particles is detached during wearing. The number of stress cycles required to cause such failure decreases as the corresponding magnitude of stress increases. Vibration is a common cause of fatigue wear.

4. Corrosive wear: Most metals are thermodynamically unstable in air and react with oxygen to form an oxide, which usually develop layer or scales on the surface of metals or alloys when their interfacial bonds are poor. Corrosion wear is the gradual eating away or deterioration of unprotected metal surfaces by the effects of the atmosphere, acids, gases, alkalis etc. This type of wear creates pits and perforations and may eventually dissolve metal parts.

5. Erosive wear: In tribology, erosive wear can be defined as the progressive loss of original material from a solid surface due to mechanical interaction between the surface and impinging particles. Erosive wear is caused by the

impact of particles of solid or liquid against the surface of an object. It occurs in a wide variety of machinery and typical examples are the damage to gas turbine blades when an aircraft flies through dust clouds and the wear of pump impellers in mineral slurry processing systems. In common with other forms of wear, mechanical strength does not guarantee wear resistance and a detailed study of material characteristics is required for wear minimization. The properties of the eroding particle are also significant and are increasingly being recognized as a relevant parameter in the control of this type of wear. Erosive wear involves several wear mechanisms which are largely controlled by the particle material, the angle of impingement, the impact velocity and the particle size. Where liquid particles are the erodent, abrasion does not take place and the wear mechanisms involved are the result of repetitive stresses on impact. The term 'erosive wear' refers to an unspecified number of wear mechanisms which occur when relatively small particles impact against mechanical components. This definition is empirical by nature and relates more to practical considerations than to any fundamental understanding of wear.

Mechanism of erosive wear

Wear due to erosion is caused by the impact of particles of solid or liquid against the surface of an object. It occurs in a wide variety of machinery and typical examples are the damage to gas turbine blades when an aircraft flies through dusty clouds and wear of pump impellers in mineral slurry processing systems. In common with other forms of wear, mechanical strength does not guarantee wear resistance and therefore a detailed study of material characteristics is necessary for wear minimization. The properties of the eroding particles are also significant and are increasingly being recognized as a relevant parameter in the control of this type of wear. The term 'erosive wear' refers to an unspecified number of wear mechanisms which occur when relatively small particles impact against mechanical components. The mechanisms of erosive wear are schematically shown in Figure 2.2.

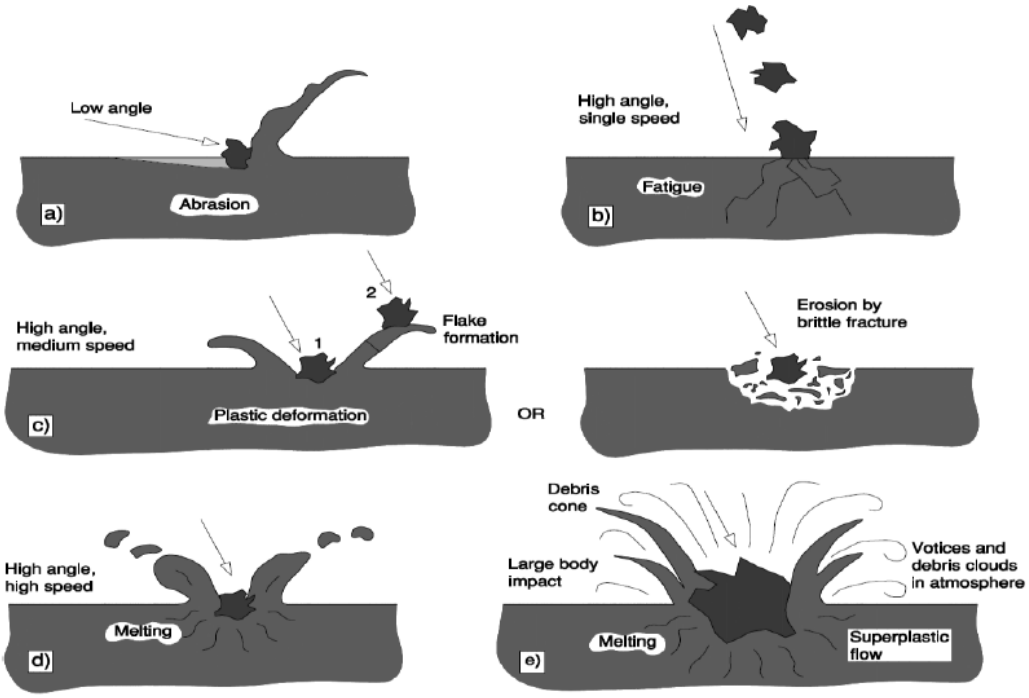

Fig. 2.2 Schematic illustrations of erosion wear mechanism

The impact speed of the particle has a very strong effect on the wear rate. If the speed is very low, then stresses at impact are insufficient for plastic deformation to occur and wear proceeds by surface fatigue. When the speed is increased to around 20 m/s, it is possible for the eroded material to deform plastically on particle impact. In this regime, which is quite common for many engineering components, wear may occur by repetitive plastic deformation. If the eroding particles are blunt or spherical then thin plates of worn material form on the worn surface as a result of plastic deformation. If the particles are sharp, then cutting or brittle fragmentation is more likely to happen. Brittle materials, on the other hand, wear by sub-surface cracking. At very high particle speeds melting of the impacted surface might even occur.

2.8 Erosion Wear Characteristics of Ceramic Coatings

Erosion of materials by solid particle impact is a complex wear phenomenon where the material is removed as a result of brittle fracture or plastic deformation [188-190]. Plasma sprayed coatings are used now a days as erosion resistant coatings in a wide variety of applications [191-193, 25]. Extensive research shows that the deposition parameters like energy input to the plasma and the powder properties affect the porosity, splat size, phase composition, coating hardness etc. [194-201]. These in turn, have an influence on the erosion wear resistance of the coatings. Quantitative studies of the combined erosive effect of repeated impacts are very useful in predicting component lifetimes, in comparing the performance of materials and also in understanding the underlying damage mechanisms involved.

Kulu et al. [202-205] have carried out significant research in the field of erosion resistant coatings and have reported that under extreme conditions, solid particle erosion (SPE) is a serious problem for many industrial equipment. Response of a material to SPE is a complex function of the physical properties of the target, the impacting particles and the erosive environment [206]. Many erosion mechanisms have been proposed in the past and have been supported by the experimental data from erosion tests. Various models for the erosion of bulk metals, glass and ceramics have also been proposed [207] usually considering different combinations of micro-cutting, plastic deformation, melting, fatigue and fracture mechanisms [208]. According to Finnie and McFadden [209], there are four principal factors that influence the erosion behaviour of a material: the erodent velocity and size, the impact angle and the properties of the eroded material.

Few reports are available in the existing literature on erosion behaviour of alumina coatings. The resistance to erosion of such coatings depends upon inter-splat cohesion, shape, size and hardness of erodent particles, particle velocity, angle of impact and the presence of cracks and pores [197, 210-213]. The slurry

and particle erosion response of flame sprayed alumina coatings has also been reported in the literature [70]. It is seen that high particle velocity enhances the erosion rate and it reaches a maximum for an impact angle of 90^0. The loss of material is by the progressive removal of splats and can be attributed to the presence of defects and pores in the inter-splat regions within the coating. Similar observations have also been reported for the plasma sprayed alumina coatings subjected to an erosive wear caused by the SiO_2 particles [214].

Branco et al. [215] examined the room temperature solid particle erosion of zirconia and alumina based ceramic coatings with different levels of porosity and varying microstructure and mechanical properties. The erosion tests were carried out by a stream of alumina particles with an average size of 50 μm at a velocity of 70 m/s, carried by an air jet with impingement angle of 90^0. The results of this study indicated that there is a strong relationship between the erosion rate and the coating porosity. Similarly, Mishra et al. [216] investigated the erosion characteristics of plasma sprayed alumina-titania coatings deposited on mild steel substrates. This study revealed that premixing of titania in alumina significantly improves the resistance of the coating to solid particle erosion.

Ercenk et al. [217] studied the effects of impingement angle and SiC reinforcement on the erosion wear behaviour of basalt based glass and glass-ceramic coatings. Erosion tests were realized by using corundum media at the different impingement angles and velocities. The test results showed that the addition of SiC in the basalt based coatings resulted in enhancement of erosive wear resistance. Krishnamurthy et al. [218] examined the solid particle erosion behaviour of plasma sprayed alumina and calcia-stabilized zirconia coatings on Al-6061 substrate. Satapathy [88] carried out an extensive research on erosion wear behaviour of plasma sprayed red mud coatings under different test conditions. This study revealed that impact velocity and the impingement angle are the significant factors that influence the erosion rate of the coatings to a great extent. Subsequently, Sahu et al. [219] performed tribo-performance analysis of

plasma sprayed fly ash-aluminum coatings using experimental design and artificial neural network. Recently, Gupta and Satapathy [220, 221] have reported extensively on solid particle erosion response of plasma sprayed glass microsphere coatings under different operating conditions.

Several erosion models were developed by many researchers to provide a quick answer to design engineers in the absence of a comprehensive practical approach for prediction of erosion response. One of the early prediction correlations is that developed by Finnie [222] expressing the rate of erosion in terms of particle mass and impact velocity. In that correlation, the rate of erosion was proportional to the square of the impact velocity. Nesic [223] found that Finnie's model over-predicts the erosion rate and presented another formula in terms of a critical velocity rather than the impact velocity. The erosion model suggested by Bitter [5, 224] assumed that the erosion occurred in two main mechanisms; the first was caused by repeated deformation during collisions that eventually results in the breaking loose of a piece of material while the second was caused by the cutting action of the free-moving particles. Glaeser and Dow [225] suggested another two-stage mechanism for explaining different aspects of the erosion process for ductile materials. In the first stage, the particles indent the target surface, causing chips to be removed and some material to be extruded to form vulnerable hillocks around the scar. The second stage was the one in which the particles break up on impact causing fragments to be projected radially to produce a secondary damage. Some other erosion models were also suggested by Laitone [226], Salama and Venkatesh [227], Bourgoyne [228], Chase et al. [229], McLaury [230], Svedeman and Arnold [231] and Jordan [232].

Different models have also been proposed that allow estimation of the stresses that a moving particle will impose on a target during erosion [233]. It has been experimentally observed by many investigators that during the impact, the target can be locally scratched, extruded, melted and/or cracked in different ways [234-236]. The imposed surface damage will vary with the target material, erodent

particle, impact angle, erosion time, particle velocity etc. [234, 237]. Over the years, solid particle erosion of metals and coatings has been reviewed time to time by Kosel [238], Engel [239], Preece and Macmillan [240], Hutchings [241], Finnie et al. [242], Ruff and Wiederhom [243], Shewmon and Sundararajan [244], Sundararajan [245], Levy [246] and many others [247-257, 25].

It is well known that resistance of engineering components encountering the attack of erosive environments during operation can be improved by applying hard ceramic coatings on their surfaces. Alonso et al. [258] experimented with the production of plasma sprayed erosion-resistant coatings on carbon-fiber-epoxy composites and studied their erosion behaviour. Tabakoff and Shanov [259] designed a high temperature erosion test facility to obtain erosion data in the range of operating temperatures experienced in compressors and turbines. In addition to the high temperatures, this facility properly simulates all the erosion parameters important from the aerodynamics point of view.

2.9 Erosion Wear Characteristics of Polymer Composites

Various applications of polymers and their composites in erosive wear situations are reported by Pool et al. [3], Kulkarni and Kishore [260] and Aglan and Chenock [261] in the literature. But solid particle erosion (SPE) of polymers and their composites has not been investigated to the same extent as for metals or ceramics. However, Tewari et al. [262] have evaluated the resistance of various types of polymers and their composites to SPE. It is widely recognized that polymers and their composites have poor erosion resistance. Their erosion rates are considerably higher than metals. In some cases that the erosion rates of polymer composites are even higher than that of neat polymers as reported by Häger et al. [263]. Tilly and Sage [264] have investigated the influence of velocity, impact angle, particle size and weight of impacted abrasives on nylon, carbon-fiber-reinforced nylon, epoxy resin, polypropylene and glass-fiber-reinforced plastic.

It has been reported in the literature that polymers and their related composites are extensively used in erosive wear situations. Consequently, many researchers have investigated the solid particle erosion behaviour of various polymers and their composites. Polymers that have been reported in the literature include polystyrene [265], polypropylene [266, 267], nylon [268], polyethylene [269], ultra high molecular weight polyethylene [270], poly-ether-ether-ketone [271], polycarbonate and poly-methyl-meth-acrylate [272], epoxy [264], bismileimide [273], elastomers [274, 275] and rubber [276]. Barkoula and Karger-Kocsis [185] have also presented a detailed review on important variables in erosion process and their effects on different classes of polymers and composites. Miyazaki and Takeda [277] studied the effect of matrix materials, reinforcement fibers, fiber matrix interface strength, impact angle and particle velocity on the solid particle erosion behaviour of fiber reinforced plastics (FRP). They observed that the erosion rate of a FRP decreases with the increase of the interface strength between matrix material and fibers. Miyazaki and Hamao [278] further carried out another similar study on the erosion behaviour of short fiber reinforced thermoplastic resins with special attention focussed on an incubation period of erosion.

Harsha et al. [279] reported the influence of impingement angles and impact velocities on SPE of various poly-aryl-ether-ketones and their composites with short fiber reinforcement. In another investigation, Barkoula and Karger-Kocsis [280] studied the effects of fiber content and relative fiber orientation on the SPE of glass fiber/polypropylene composites. Tewari et al. [281] studied the influence of impingement angle and fiber orientation and concluded that unidirectional carbon and glass fiber reinforced epoxy composites showed semi-ductile erosion behaviour with the maximum erosion rate occurring at 60° impingement angle. In another study, Arjula and Harsha [282] have discussed the usefulness of the erosion efficiency parameter to identify various wear mechanisms. Few publications by Patnaik et al. [283-288] on erosion wear characteristics of glass-polyester composites filled with different particulate

fillers suggest that in such hybrid composites, the rate of material loss due to SPE reduce significantly with the addition of hard particulate fillers into the matrix. They have also reviewed extensively on erosion wear characteristics of fiber and particulate filled polymer composites [289]. Panda et al. [290] studied the erosive wear analysis of glass fiber-epoxy reinforced AlN hybrid composites and more recently, Kaundal [291] made a critical review on role of process variables on the SPE of polymer composites. Bagci and Imrek [292] studied solid particle erosion behaviour of a new composite material formed by adding boric acid particles to glass fibers and epoxy resin. Friction and wear behaviour of the polyimide composites at elevated temperature under sliding and erosive conditions have been investigated by Zhao et al. [293]. Zhang et al. [294] investigated on the erosion characteristics of molded carbon fiber composites by sand erosion test using silica particles. Padhi and Satapathy [179, 180] have also reported on the erosion behaviour of blast furnace slag filled epoxy composites with and without glass fiber reinforcement. Recently, Gupta and Satapathy [123] have studied the erosion wear response of borosilicate glass microsphere filled epoxy composites under different test conditions. Mohapatra et al. [295] reported the processing and erosion response of a multiphase composite consisting of epoxy resin reinforced with E-glass fiber and TiC particles. They further investigated the solid particle erosion behaviour of glass-epoxy composites filled with TiC derived from ilmenite [296].

Tsuda et al. [297] studied sand erosion behaviour and wear mechanism of various types of glass fiber reinforced plastics. Rajesh et al. [298] selected a series of polyamides for investigating the effects of chemical structure and hence, mechanical properties on erosive wear behaviour by impinging silica sand particles at various angles and doses. Biswas and Satapathy [176] developed a mathematical model for estimating erosion damage caused by solid particle impact on red mud filled glass fiber reinforced epoxy matrix composites and also found a correlation derived from the results of Taguchi experimental design.

In a study by Srivastava and Pawar [159], experiments were carried out to study the effects of fly ash filler, impingement angle and particle velocity on the solid particle erosion behaviour of E-glass fiber reinforced epoxy composites. The result showed semi-ductile erosion behaviour with maximum erosion rate at 60^0 impingement angle. Yang and Nayeb-Hashemi [299] investigated the effects of solid particle erosion on the strength and fatigue properties of E-glass/epoxy composites. Harsha and Jha [300] studied the erosion resistances of neat epoxy, unidirectional glass fiber reinforced epoxy and unidirectional carbon fiber reinforced epoxy as well as bidirectional E-glass woven reinforced epoxy composites. It was found that bidirectional glass fiber reinforced epoxy composites exhibited higher erosion resistance than their unidirectional fiber reinforced counterparts.

2.10 Implementation of Design-of-Experiments and Artificial Neural Networks in Wear Analysis

Wear processes in composites and coatings are complex phenomena involving a number of operating variables and it is essential to understand how the wear characteristics are affected by different operating conditions. Although many researchers have reported on properties, performance and wear characteristics of materials, the significance of different process parameters and their relative influence on wear rate has not adequately been studied yet. Selecting the correct operating conditions is always a major concern as traditional experimental design would require many experimental runs to achieve a satisfactory result. In any experimental research, since test procedures are generally expensive and time consuming, the need to satisfy the design objectives with the minimum possible number of tests is clearly an important requirement. However, it does not provide optimal testing parameters for a particular situation. Thus, several mathematical models based on statistical regression techniques have been constructed to select the proper testing conditions [301-306]. In this context, Taguchi method suggested by Taguchi and Konishi [307, 308] provides the designer with a systematic and efficient approach for experimentation to

determine near optimum settings of design parameters in terms of performance, time and cost. This method involves laying out the test conditions using specially constructed tables known as 'orthogonal arrays'.

Design-of-experiments (DOE) is an effective method for conducting experiments to improve the performance output by finding optimum test conditions. This also provides a better understanding of physical mechanisms involved in a complex phenomenon like a wear process or a spraying process. Pierlot et al. [309] have given an exhaustive review on the implementation of DOE methodology useful for thermal spray coatings and associated processes of post spray treatment. This report highlights four different DOE approaches namely Hadamard or Plackett-Burman matrices [310, 311], two-level full factorial designs [312-316], two-level fractional factorial designs [317] and response of surface methodology. These designs enable to find out a polynomial regression equation which expresses the influences of process parameters on the response. The number of runs required for full factorial design increases geometrically whereas fractional factorial design is efficient and significantly reduces the time. This method is popular because of its simplicity, but this very simplicity has led to unreliable results and inadequate conclusions. The fractional design might not contain the best design point. Moreover, the traditional multi-factorial experimental design is the 'change-one-factor-at-a time' method. Under this method only one factor is varied, while all the other factors are kept fixed at a specific set of conditions.

To overcome these problems, Taguchi and Konishi [307] advocated the use of orthogonal arrays and Taguchi [308] devised a new experimental design that applied signal-to-noise ratio with orthogonal arrays to the robust design of products and processes. In this procedure, the effect of a factor is measured by average results and therefore, the experimental results can be reproducible. This inexpensive and easy-to-operate experimental strategy based on Taguchi's parameter design has been adopted to study the effect of various parameters and

their interactions in a number of engineering processes [318-323]. Phadke [318], Wu and Moore [319] and others [320-323] have applied this method to design various products and process parameters. Mahapatra and Patnaik [324-327] have made optimization of parameter combinations in wire electrical discharge machining using this method. Patnaik et al. [162, 283-289, 328] have also successfully employed this in erosion wear analysis of polymer composites. Rubio et al. [329] reported the use of Taguchi's method in order to identify the best drilling setup of glass reinforced polyamide. Ramesh and Suresha [330] optimized the tribological parameters in abrasive wear of carbon-epoxy hybrid composites using Taguchi's orthogonal array. Vankanti and Ganta [331] optimized the process parameters namely, cutting speed, feed, point angle and chisel edge width in drilling of glass fiber reinforced polymer composites. Recently, Gupta and Satapathy [123] have reported the erosion wear behaviour of borosilicate glass microspheres filled epoxy composites using Taguchi method. Sahu et al. [219] have also made the tribo-performance analysis of fly-ash-aluminium coatings using Taguchi's experimental design.

Artificial Neural Network (ANN) is a technique inspired by the network of biological neurons and has already been used to solve a wide variety of problems in tribology. It was developed to simulate the strong learning, clustering and reasoning capacity of biological neurons. Using a well-trained ANN model, one can estimate predictive performance, pattern association and pattern classification. As already mentioned, the erosion process is a complicated phenomenon lacking adequate mathematical description and therefore, in this analysis, an integrated method has been proposed that combines Taguchi's design approach with the ANN for parametric analysis and prediction of wear performance. This proposed approach not only yields sufficient understanding of the effects of process parameters, but also produces an optimal parameter setting to ensure that the materials exhibit the best wear performance characteristics. The details of this ANN approach have been well documented by Kartalopoulos [332]. Zhang and Friedrich [333] also made a detailed review on application of

ANN to polymer composites whereas Kadi [324] made a review on modeling aspect of mechanical behaviour of fiber-reinforced polymer composites. While Jiang et al. [335] have made a prediction on wear properties of composites, Gyurova et al. [336] have developed a model on the sliding wear and friction properties of polyphenylene sulfide composites using artificial neural networks. ANN has been suitably applied on wear analysis of different materials like polyamide 66 by Abdelbary et al. [337], TiO_2 reinforced polyester composites by Satapathy et al. [338] and pine wood dust filled epoxy composites by Kranthi and Satapathy [339], while Gyurova [340] made a detailed study on preliminary investigation of neural network techniques for prediction of tribological properties. Padhi and Satapathy [178, 179] have studied the wear analysis of blast furnace slag filled epoxy and PP composites using Taguchi model and ANN. Recently, Gupta and Satapathy [220] have evaluated the wear response of plasma sprayed coatings of glass microspheres premixed with Al_2O_3 particles using this technique. Many other researchers [180, 181, 221, 341-344] have also used ANN for wear rate prediction of a wide variety of homogeneous and heterogeneous material systems under different test conditions.

2.11 Knowledge Gap in Earlier Investigations

The literature survey presented above reveals the following knowledge gap in earlier investigations that has helped to set the objectives of this research work:

- Few works have been carried out in the recent past on plasma sprayed coatings using industrial wastes like red mud, fly ash and copper slag etc., but use of LD slag as a potential material for wear resistant coatings has not been explored so far.

- Though much work has been reported on various wear characteristics of metals, alloys and homogeneous materials, comparatively less has been reported on the erosive wear performance of ceramic coatings and also no study is available particularly on coatings of LD slag.

- LD slag finds very limited utilization in areas like road base and sub base, recovery of metal values, fertilizer and soil conditioners, but no work attempt has so far been made for exploring its application as a filler material in polymer matrix composites.

- Tribological studies reported in the past have been mostly focused on conventional engineering materials like metals and alloys and research reports on wear behaviour of polymer composites have been relatively less.

- A possibility that the pre-mixing of some other conventional ceramics with LD slag prior to coating could provide an improvement in its wear resistance capability has not been studied so far and there is inadequate data available about phenomena behind the modified wear behaviour of such coatings.

- Studies carried out worldwide on wear behaviour of plasma sprayed coatings and composites have largely been experimental and use of statistical techniques and predictive tools in analysing the wear characteristics is rare.

- Taguchi method, in spite of being a simple, efficient and systematic approach to optimize designs for performance, quality and cost, is used only in a limited number of applications worldwide. Its implementation in parametric appraisal of wear processes has hardly been reported. Besides, there are only a few reports available on implementation of neural computation for analysis and prediction of tribo-performance of coatings and composites.

Against this background, the present research work is undertaken to explore the possibility of developing plasma sprayed LD slag coatings and LD slag filled

polymer composites. This work also includes a study on the erosion wear response of these coatings and composites under varying test conditions.

2.12 Objectives of the Present Research

The specific objectives of the present work are outlined as follows:

1. To explore the possible use of LD slag (LDS), an industrial waste, as a material for developing plasma sprayed coatings on aluminium substrate.
2. Fabrication of a new class of composites with different polymeric matrices (Epoxy and Polypropylene) filled with micro-sized LDS particles with and without glass fiber reinforcement.
3. Physical, mechanical and micro-structural characterization of these coatings and composites.
4. Experimental studies on erosion wear response of the prepared coatings and composites.
5. Study on the effect of premixing of Al_2O_3/TiO_2 with LDS on the coating characteristics and erosion response.
6. Parametric appraisal of the erosion wear process using Taguchi's experimental design. Development of predictive equations in terms of the operating variables for estimation of erosion rate.
7. Implementation of an artificial neural network (ANN) based prediction model for estimation of erosion rates under different test conditions within and beyond the experimental limits.

Chapter Summary

This chapter has provided

- An exhaustive review of research works on various aspects of plasma sprayed coatings and polymer composites with emphasis on their erosion characteristics reported by previous investigators
- The knowledge gap in earlier investigations
- The objectives of the present research work

The next chapter describes the materials and methods used for the deposition of coatings, fabrication of the composites and the experimental planning. It also provides introductory descriptions of the Taguchi method and neural computation.

*****

Chapter 3

Materials and Methods

Chapter 3

MATERIALS AND METHODS

This chapter describes the materials and methods used for the processing of the coatings and composites under this investigation. It presents the details of the characterization and erosion tests which the coating and composite samples have been subjected to during the course of this work. The methodology to analyze and predict the tribo-performance of these coatings and composites which is based on Taguchi experimental design integrated with artificial neural networks is also described in this part of the thesis.

3.1 Materials

3.1.1 Linz-Donawitz slag (LDS): *As the coating and filler material*

This research is aimed at using an industrial waste like LD slag in the development of wear resistant coatings and polymer composites. LDS collected from Rourkela Steel Plant, located in the eastern part of India is the primary material to be used in the present research. These slag particles are sieved to obtain an average particle size in the range of 90-100 µm. LDS is a major solid waste generated in huge quantities during steel making. It comes from slag formers such as burned lime/dolomite and from oxidising of silica, iron etc. while refining the iron into steel in the LD furnace. It is mainly composed of silicon oxide, calcium oxide and iron oxide. The approximate chemical composition of LD slag is given in Table 3.1 and a pictorial view of the LDS used in the present work is shown in Figure 3.1.

Table 3.1 Chemical composition of LD slag

Constituents	SiO_2	Al_2O_3	Fe_2O_3	CaO	MnO	MgO
Content (wt%)	12.16	1.22	26.30	47.88	0.28	0.82

Figure 3.1 LD slag used in the present work

3.1.2 Aluminium Oxide (Al_2O_3): *LDS to be premixed with Al_2O_3*

Aluminium oxide (Al_2O_3), an inorganic material and commonly referred to as alumina, can exist in several crystalline phases which all revert to the most stable hexagonal alpha phase at elevated temperatures. Alumina is the most cost effective and widely used material in the family of engineering ceramics. It is hard, wear resistant, has excellent dielectric properties, resistance to strong acid and alkali attack at elevated temperatures, high strength and stiffness. With an excellent combination of properties and a reasonable price, it is no surprise that fine grain technical grade Al_2O_3 has a very wide range of applications.

3.1.3 Titanium Dioxide (TiO_2): *LDS to be premixed with TiO_2*

Titanium dioxide (TiO_2) powders with average particle size of 90-100 µm are supplied by Qualikems Ltd. It is the naturally occurring oxide form of titanium and occurs in nature as rutile, anatase or brookite. It is mainly sourced from ilmenite ore. This is the most widespread form of titanium dioxide bearing ore around the world. Rutile is the next most abundant form of titanium dioxide ore. The metastable anatase and brookite phases convert to rutile upon heating. Table 3.2 provides some of the important properties of titanium dioxide and aluminium oxide. Rutile TiO_2 has been used for this study.

Table 3.2 Properties of Al_2O_3 and TiO_2

Characteristic Property	Values		
	Al_2O_3	TiO_2	
Density	3.89	4.19	g/cm^3
Compressive strength	710	680	MPa
Micro-hardness	6.82	6.13	GPa
Thermal conductivity	35	11.7	W/m-K
Coefficient of thermal expansion	8.1	8.6	$ppm/^0C$

3.1.4 Matrix Material

Matrix materials taken for fabrication of composites can be of different types like metal, ceramic and polymer. Among them, polymers are the most commonly used matrices because of cost efficiency, ease of fabricating complex parts with less tooling cost and they also have excellent room temperature properties when compared to metal and ceramic matrices. Polymer matrices can be either thermoplastic or thermoset. Thermoset matrices are formed due to an irreversible chemical transformation of the resin into an amorphous cross-linked polymer matrix. Due to huge molecular structures, thermoset resins provide good electrical and thermal insulation. They have low viscosity, which allow proper fiber wet out, excellent thermal stability and better creep resistance. Normally, these resins can be formulated to give a wide range of properties upon the requirement [345].

In the present work, one thermoset polymer (epoxy) and one thermoplastic (polypropylene) have been used as matrix materials which are reinforced with LDS in different proportions.

Matrix Material-1 (Epoxy)

The most commonly used thermoset resins are epoxy, polyester, vinyl ester and phenolics. Among them, the epoxy resins are being widely used for many advanced composites due to their excellent adhesion to wide variety of fibers, superior mechanical and electrical properties and good performance at elevated temperatures. In addition to that they have low shrinkage upon curing and good

chemical resistance. Due to several advantages over other thermoset polymers as mentioned above, epoxy (LY 556), chemically belonging to the epoxide family is used as the matrix material in the present work. Its common name is *Bisphenol-A-Diglycidyl-Ether*. Its molecular chain structure is shown in Figure 3.2. Epoxy provides a solvent free room temperature curing system when it is combined with the hardener tri-ethylene-tetramine (TETA) which is an aliphatic primary amine with commercial designation HY 951 (Figure 3.3). The LY 556 epoxy resin and the corresponding hardener HY 951 are procured from Ciba Geigy India Ltd. Table 3.3 provides some of the important properties of epoxy.

Table 3.3 Some important properties of epoxy

Characteristic Property	**Values**	
Density	1.1	g/cm^3
Compressive strength	90	MPa
Tensile strength	58	MPa
Micro-hardness	0.085	GPa
Thermal conductivity	0.363	W/m-K
Glass transition temperature	104	^0C
Coefficient of thermal expansion	62.83	$ppm/^0C$
Electrical conductivity	0.105×10^{-16}	S/cm
Volume resistivity	10^{15}	ohm-cm
Dielectric constant	3.98	at 1MHz

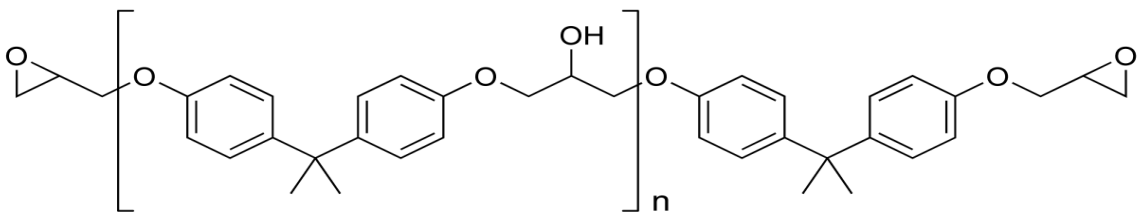

Figure 3.2 Unmodified epoxy resin chain
('**n**' denotes number of polymerized unit)

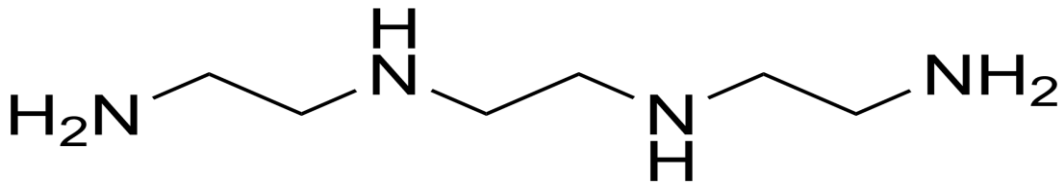

Figure 3.3 Tri-ethylene-tetramine (hardener used for epoxy matrix)

Matrix Material-2 (Polypropylene)

One of the most widely used thermoplastic polymers, polypropylene (PP), is another matrix material used for the present investigation. Polypropylene of homo-polymer M110 grade shown in Figure 3.4 is chosen whose molecular formula is $(C_3H_6)_n$, where n is the number of polymerized unit (Figure 3.5). It is used for its good mechanical performance, aesthetics, resistance to chemicals, cost effectiveness and thermal stability and recyclability. Table 3.4 provides some important properties of PP taken for this investigation.

Figure 3.4 Polypropylene of grade homo-polymer M110

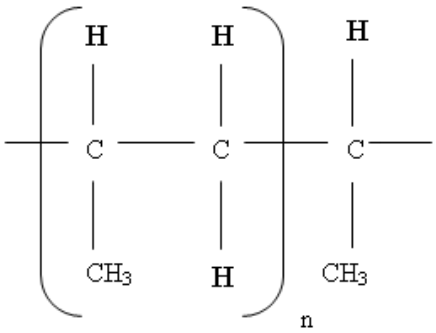

Figure 3.5 Polypropylene Chain (n is the number of polymerized unit)

Table 3.4 Properties of homo-polymer M110 polypropylene

Characteristic Property	**Values**	
Density	0.92	g/cm^3
Compressive strength	82	MPa
Tensile strength	41	MPa
Micro-hardness	0.057	GPa
Thermal conductivity	0.1	W/m-K
Glass transition temperature	-14.93	^0C
Coefficient of thermal expansion	31.144	$ppm/^0C$
Electrical conductivity	2.3	S/cm

3.1.5 Fiber Material: *Short glass fiber to be used in composite making*

Fiber is the reinforcing phase of a composite material. Normally two types of fibers are employed in composite making: synthetic and natural fibers. Some commonly used synthetic fibers are glass, carbon and aramid etc. Among them, glass fibers are the most commonly used fibers for engineering composites. Hence, glass fiber is chosen as the reinforcing fiber material in this work. It is commercially available in abundance with good mechanical properties; thus, is widely used in composite structures. Based upon different applications, glass fibers (silica-oxygen network) are classified into E glass, C glass and S glass fibers. E glass is used as an insulator and mostly used in electrical industry, hence got the name 'E' before the word 'glass'. E-glass also has good mechanical properties in addition to low cost and ease of usability. The letter 'S' in S-glass stands for structural applications. S-glass has got a different chemical formulation and although it has higher strength-to-weight ratio and higher elongation strain percentage, it is quite expensive. C-glass fibers are advantageous in resisting chemical corrosion.

Glass fibers are available in different forms like continuous, chopped and woven fabrics. In the present work, short E-glass fibers (supplied by Saint Gobain Ltd. India) have been used as the reinforcing material in the composites. The major constituents of E-glass are silicon oxide (54 wt %), calcium oxide (17 wt%), aluminum oxide (15 wt%), boron oxide (8 wt%) and magnesium oxide

(4.5wt%). E-glass fiber has an elastic modulus of 72.5 GPa and possesses a density of 2.59 g/cc. The pictorial view of short glass fibers used for composite fabrication in this study is given in Figure 3.6.

Figure 3.6 Short E-glass fiber used in the present work

3.2 Deposition of the Coatings

3.2.1 Preparation of Substrates

Commercially available Al 6061 aluminium plates are chosen as the substrates and these are cut into rectangular pieces of dimension 120 × 60 × 4 mm^3. The elemental composition of this Al 6061 aluminium is Al 98%, Fe 0.7%, Si 0.4-0.8%, Cr 0.04-0.35%, Mg 0.8-1.2%, Ti 0.15%, Cu 0.15-0.4%, Mn 0.15% and Zn 0.25%. The specimens are grit blasted at a pressure of 3 kg/cm^2 using alumina grits have size of around 60 μm size. During grit blasting, the average stand-off distance is kept constant at about 150 mm and the average roughness of the substrates obtained is 6.0-8.0 μm. The grit blasted specimens are cleaned in an ultrasonic cleaning unit and the weight of each cleaned specimen is taken by using a precision electronic balance with ± 0.1 mg accuracy. Spraying onto these specimens is carried out immediately after weighing. LDS and Al_2O_3 powders are thoroughly mixed in four different ratios (0, 10, 20 and 30% Al_2O_3) by weight. Mixtures of LDS and TiO_2 powder (again in same four different ratios by weight) are also prepared in similar manner and are used as the feed stock

materials in the present work (Table 3.5). The mixing is done in a rotary vibration mill and the mixtures are then dried prior to spraying.

Table 3.5 Mixtures used for coating deposition

S. No.	Coating Materials	Mixture Composition
1	LDS	LDS 100 wt %
2	LDS + Al_2O_3	LDS 90 wt %, Al_2O_3 10 wt %
3	LDS + Al_2O_3	LDS 80 wt %, Al_2O_3 20 wt %
4	LDS + Al_2O_3	LDS 70 wt %, Al_2O_3 30 wt %
5	LDS + TiO_2	LDS 90 wt %, TiO_2 10 wt %
6	LDS + TiO_2	LDS 80 wt %, TiO_2 20 wt %
7	LDS + TiO_2	LDS 70 wt %, TiO_2 30 wt %

[*]LDS: Linz-Donawitz slag

3.2.2 Plasma Spraying

Plasma spraying is one of the most widely used thermal spraying technique which finds a lot of applications due to its versatility of spraying a wide range of materials from metallic to non-metallic. It is most suitable for spraying of high melting point materials like refractory ceramics material, cermets etc. In this work, the coating deposition is done by plasma spraying route using a 80 kW atmospheric plasma spray system (APS) working in the non-transferred arc mode (Figure 3.7) supplied by Metallizing Equipment Co. Pvt. Ltd. at the Institute of Minerals and Materials Technology, Bhubaneswar, India. The plasma input power is varied from 10 to 24 kW by controlling plasma arc voltage and the arc current. Grit blasted aluminium substrates are fixed on the substrate holder and deposition of coating is carried out at a constant powder feed rate of 25 g/min. Al_2O_3 and TiO_2 particles are mixed to LDS particles prior to coating deposition. This is done in a mixing chamber (Figure 3.8) to ensure uniform distribution. The general arrangement of the plasma spraying equipment and schematic diagram of the spraying process are shown in Figures 3.9 and 3.10 respectively. The equipment consists of different units namely a plasma torch, a six axis robot, a mass flow controller, a robot controller, the control

console, powder feeders, the power supply unit, the torch cooling system, hoses, cables, gas cylinders and accessories.

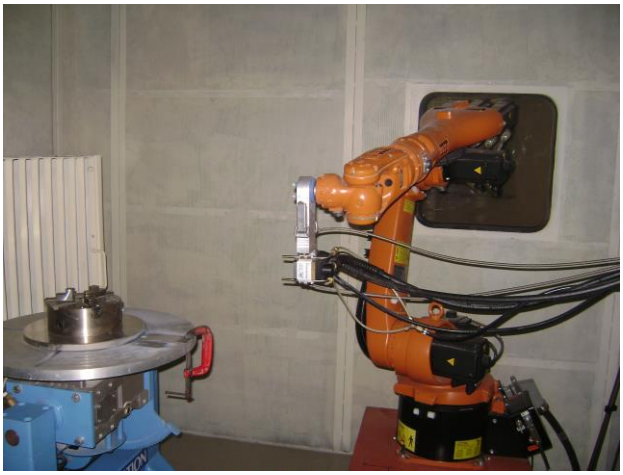

Figure 3.7 Plasma Spray Set-up

Figure 3.8 Mixing chamber in which premixing of Al_2O_3/TiO_2 with LD slag is done

Argon is used as the primary plasmagen gas and helium as the secondary gas. The powders are deposited at constant spraying angle of 90^0. The powder feeding is external to the gun. The operating parameters during coating deposition process are listed in Table 3.6 below. The schematic sketch of a plasma sprayed coating showing the substrate, coating and the interfacial boundary is given in Figure 3.11. The pictorial view of some typical coating samples made for this study is also given in the Figure 3.12.

Table 3.6 Operating parameters during coating deposition

Operating Parameters	**Values**
Plasma Arc Current (amp)	**250-450**
Arc Voltage (volt)	**30, 40, 50, 60, 70**
Torch Input Power (kW)	**10, 13, 16, 20, 22, 24**
Plasma Gas (Argon) Flow Rate (lpm)	**20**
Secondary Gas (He) Flow Rate (lpm)	**2**
Carrier Gas (Argon) Flow Rate (lpm)	**7**
Powder Feed Rate (g/min)	**25**
Torch to Base Distance TBD (mm)	**100**

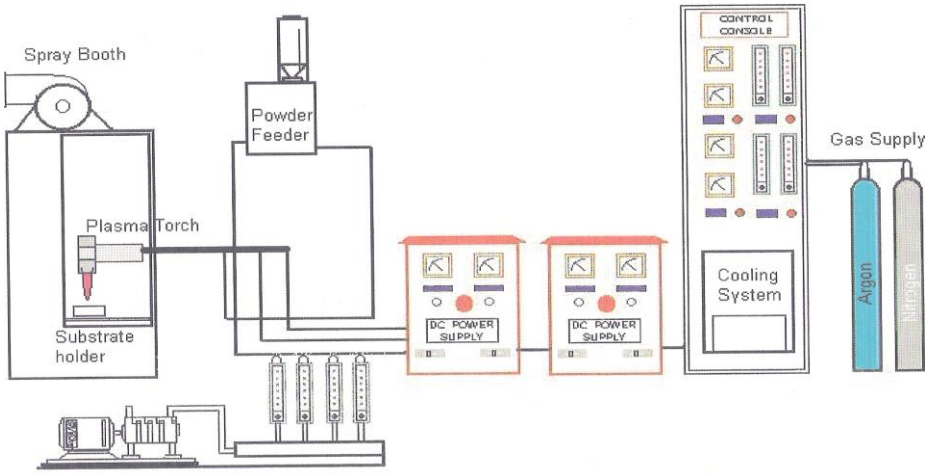

Figure 3.9 General arrangement of the plasma spraying equipment

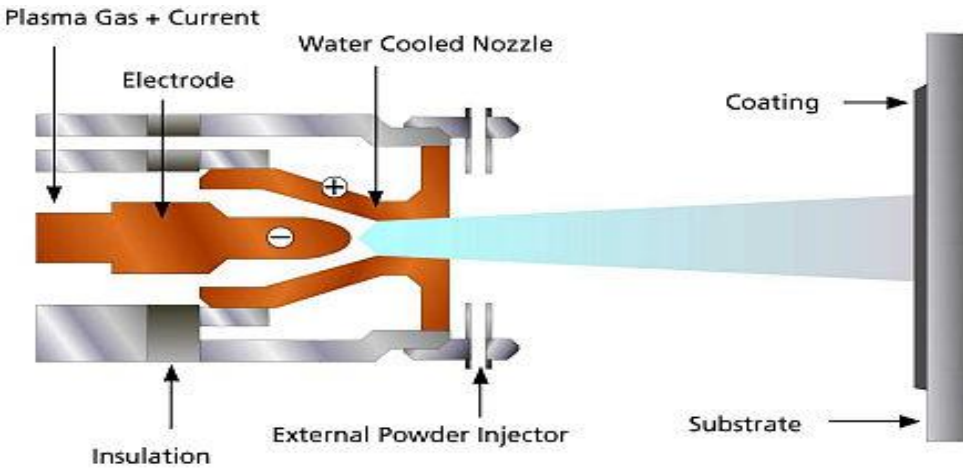

Figure 3.10 Schematic diagram of the plasma spraying process

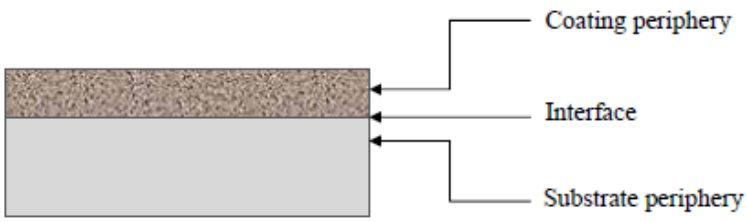

Figure 3.11 Schematic view of the plasma sprayed coatings

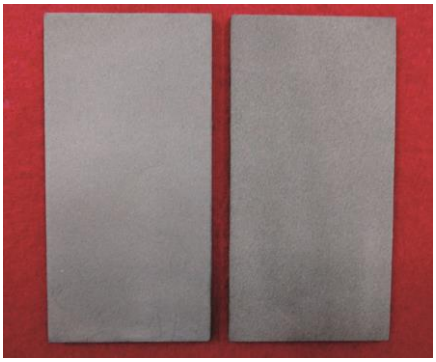

LDS Coating

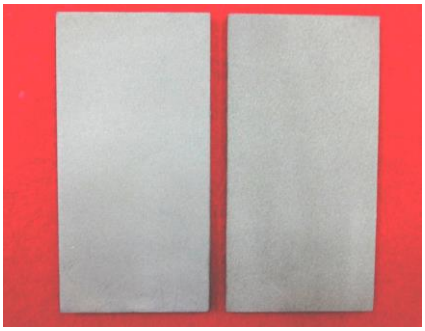

LDS+Al_2O_3 Coating

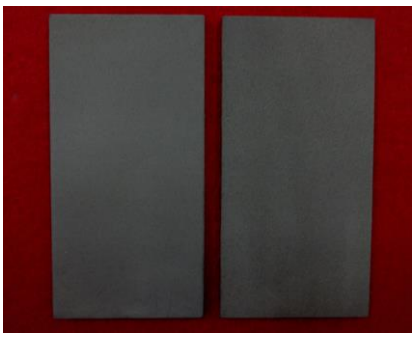

LDS+TiO_2 Coating

Figure 3.12 Pictorial view of plasma sprayed coating samples

3.3 Composite Fabrication

3.3.1 Epoxy composites fabricated by hand lay-up technique

Set 1 *Epoxy-LDS Composites*

Composite samples of various compositions are prepared by hand lay-up technique. Hand lay-up technique is the oldest and simplest technique for composite fabrication. The epoxy-LDS composites are prepared in the following steps (i) Uncured epoxy (LY556) and its corresponding hardener (HY 951) are mixed in a ratio of 10:1 by weight as per recommendation. (ii) Micro-sized LDS particles are mixed with the epoxy in different proportions. (iii) The uniformly mixed dough (epoxy filled with LDS) is then slowly decanted into the glass molds so as to get both cylindrical type specimens (diameter 10 mm and length 50 mm) and rectangular slab specimens (length 200 mm, width 200 mm and thickness 3 mm), coated beforehand with wax and a uniform thin film of silicone-releasing agent. (iv) The castings are then left at room temperature for about 24 hours and then the glass molds are broken and the samples are released. From the composite slabs, rectangular/square/dog-bone shaped specimens are

cut for different characterization tests. Composite samples of five different compositions (Set 1) with varying LDS content (Table 3.7) are made.

Set 2 *Epoxy-LDS-SGF Composites*

Further, a set of hybrid composites consisting of epoxy resin, LDS and short glass fibers (SGF) are prepared following the same procedure as that for Set-1 composites. Here, thorough mixing of short glass fibers (20 wt%) into the dough (epoxy filled with LDS) is done prior to casting of the composites in glass molds. The composites are thus cast by conventional hand-lay-up technique so as to obtain both cylindrical type specimens (diameter 10mm and length 50 mm) and rectangular slab specimens (length 200 mm, width 200 mm, thickness 3 mm). After proper curing, the samples are cut using a diamond cutter. The compositions of these composites (Set-2) are given in Table 3.7.

A schematic representation of LDS filled epoxy composite is shown in Figure 3.13. It also presents a pictorial view of some of these composite samples prepared through this hand-layup technique.

Table 3.7 Epoxy composites filled with LD slag with and without SGF

	Composition
Set-1	Epoxy + 0 wt% LDS
	Epoxy + 7.5 wt% LDS
	Epoxy + 15 wt% LDS
	Epoxy + 22.5 wt% LDS
	Epoxy + 30 wt% LDS
Set-2	Epoxy + 20 wt% SGF + 0 wt% LDS
	Epoxy + 20 wt% SGF + 7.5 wt% LDS
	Epoxy + 20 wt% SGF + 15 wt% LDS
	Epoxy + 20 wt% SGF + 22.5 wt% LDS

**LDS: Linz-Donawitz slag, SGF: Short Glass Fiber*

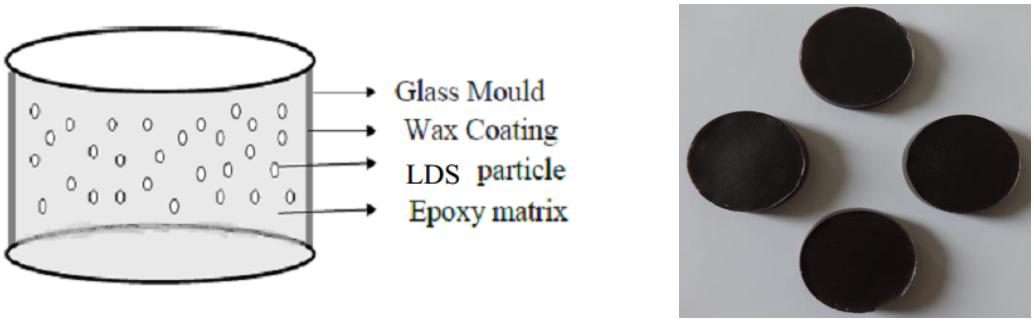

Figure 3.13 Schematic of hand lay-up set up and fabricated samples

3.3.2 Polypropylene composites fabricated through injection molding route

Set 3 *PP-LDS Composites*

An injection molding machine *Texair-40T*, shown in Figure 3.14, is used in the present work for fabrication of PP composite samples. Polypropylene granules mixed with different proportions of LDS particles (90-100 micron) are heated to a temperature of 80°C in the preheater for three hours. Since polypropylene is hydrophobic (maximum absorption capacity is 0.01%) in nature, moisture will be on the surface only and during preheating process, this moisture on the surface gets evaporated. Polymeric raw materials are fed into the barrel through the hopper and this process is called screw refilling. After screw refilling process, plunger moves linearly backwards to maintain set back pressure in the barrel. Entire injection system is then moved towards mold cavity by means of guide ways as the injection nozzle is fed into the inlet of mold. Screw plunger in the barrel moves forward and pushes the material through three heaters (which are maintained at a temperature 225, 230 and 235^{0}C respectively in the mold cavity). Mold cavity is completely filled with PP-LDS mix (semi-solid state). 40 Ton of clamping force is applied and is held for some time till it completely solidifies. Mold is provided with water cooling system. It is opened and samples are ejected from mold by ejection pin. The above steps can also be done by setting machine in automatic mode or semiautomatic mode. Barrel is not to be emptied when heaters are on. As overheating of PP causes evaporation, temperature is maintained below 250^{0}C. Oiling is done before starting the machine. Injection pressure is set at 900 kg/cm^2 and the stroke length at 50 mm length. Nozzle temperature is set to 50% of heaters' temperature. Main

parameters during the injection molding process are given in Table 3.8. The PP-LDS composites are thus fabricated and their compositions are listed in Table 3.9.

Figure 3.14 Injection molding machine

Table 3.8 Main parameters during the injection molding

1.	Clamping force	40 Ton
2.	Nozzle holding force	3 Ton
3.	Ejection force	3 Ton
4.	Mold open stroke	250 mm
5.	Screw diameter	32 mm
6.	Max. screw speed	200 RPM
7.	Screw stroke	140-150 mm
8.	Stroke volume	112-135 cm^3
9.	Injection pressure	550-660 bar
10.	Injection rate	75-90 g/sec
11.	Heating capacity	5.2 kW
12.	Electrical system	10.7 kW
13.	Maximum hydraulic system pressure	105 bar
14.	Oil tank capacity	140 litres
15.	Cooling time	2-4 min
16.	Cycle time	8 min
17.	Melting temperature of composite(Unreinforced)	170-190 ^0C
18.	Melting temperature of composite (Reinforced)	210-230 ^0C
19.	Mold temperature	30-40 ^0C
20.	Back pressure	50 bar
21.	The mixing quality	95-98 %

Table 3.9 PP composites filled with LD slag with and without SGF

	Composition
Set 3	PP + 0 wt% LDS
	PP + 7.5 wt% LDS
	PP + 15 wt% LDS
	PP + 22.5 wt% LDS
	PP + 30 wt% LDS
Set 4	PP + 20 wt% SGF + 0 wt% LDS
	PP + 20 wt% SGF + 7.5 wt% LDS
	PP + 20 wt% SGF + 15 wt% LDS
	PP + 20 wt% SGF + 22.5 wt% LDS

**LDS: Linz-Donawitz slag, PP: Polypropylene, SGF: Short Glass Fiber*

***Set 4** PP-LDS-SGF Composites*

Further, another set of PP composites with similar LDS content but with an additional reinforcement of short glass fibers (SGF) are also prepared following the injection molding process described above. These PP-LDS-SGF composites have fixed SGF loading of 20 wt% and are designated as Set-4 composites (Table 3.9) in the present work.

After proper curing, specimens of suitable dimensions are cut for various characterization and wear tests.

3.4 Coating Characterization

3.4.1 Coating Thickness

Thicknesses of LDS coatings on different substrates are measured on the coated cross-sections of the samples, using an Elcometer 456 thickness gauge (Figure 3.15). Readings are taken at five to six different points on each coated specimen and the average value is reported as the mean coating thickness.

3.4.2 Coating Adhesion Strength

To evaluate the coating adhesion strength, a horizontal table model universal testing machine PC-2000 Electronic Tenso-meter (Figure 3.16) is used. The test is conducted by the pull-out method in which two cylindrical specimens are

taken. The face of one of the cylinders is plasma spray coated with the material under investigation. This coated face is glued with a resin (epoxy 900 C) to the face of the other uncoated cylindrical specimen. This uncoated face is to be grit blasted prior to the gluing. The assembly of the two cylinders is then subjected to gradual tensile load. The tensile strength i.e. the coating adhesion strength is calculated from the division of the maximum load applied at the rupture (i.e. failure occurs only at the coating-substrate interface) by the cross sectional area of the cylindrical specimen considered. The tensile loading arrangement during the pull out test is shown schematically in Figure 3.17. The test is performed as per ASTM C-633.

3.4.3 Coating Porosity

Measurement of porosity or the void fraction in the coating is done using the image analysis technique. The polished top coats are kept under a microscope (Neomate) equipped with a CCD camera (JVC, TK 870E). This system is used to obtain a digitized image of the object. The digitized image is transmitted to a computer equipped with VOIS image analysis software. The total area captured by the objective of the microscope or a fraction thereof can be accurately measured by the software. Hence the total area and the area covered by the pores are separately measured and the porosity of the surface under examination is determined.

Figure 3.15 Elcometer 456 thickness gauge

Figure 3.16 PC-2000 Electronic Tenso-meter (Horizontal table model)

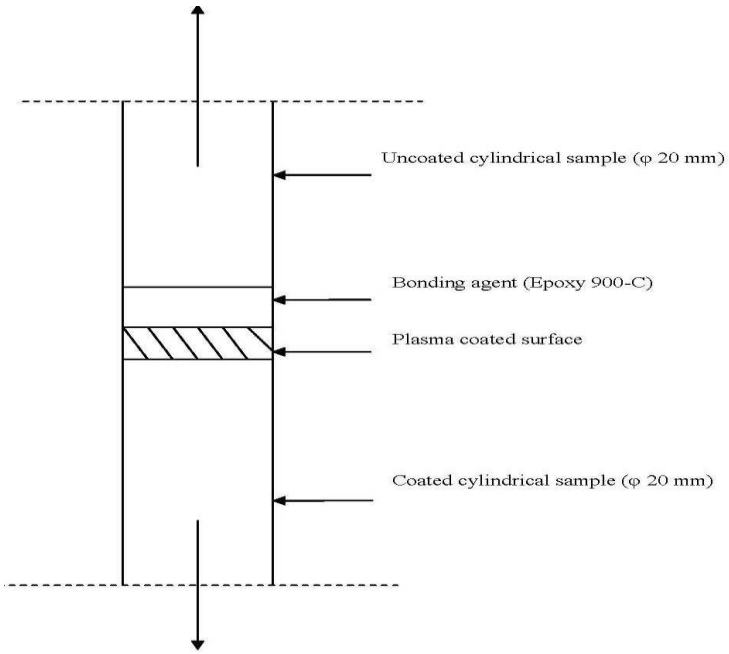

Figure 3.17 Loading pattern during coating pull out test

3.4.4 Coating Deposition Efficiency

Deposition efficiency is defined as the ratio of the weight of coating deposited on the substrate to the weight of the expended feedstock. For various torch input power levels, the coating is deposited onto different rectangular specimens (which are previously weighed, numbered and noted) for a time period of one

minute. The specimens are made of materials same as that of the substrates chosen for this work. After the spraying, the coated samples are weighed again and the difference of the weights of the coated and uncoated samples is calculated and is denoted as Gc. As mentioned previously, the weight of the coating material fed at a constant rate of 25 g/min for the entire duration of spraying is the weight of the expended feed stock denoted by Gp. Finally, the efficiencies of coating deposition for different substrates at different torch input power are found using the following equation [346]:

$$\eta_{deposition} = (Gc / Gp) \times 100 \ \% \quad \textbf{(3.1)}$$

3.4.5 Scanning Electron Microscopy

The surfaces of the coating and composite specimens are examined directly by scanning electron microscope JEOL JSM-6480LV (Figure 3.18). The specimens are cleaned thoroughly with acetone before being observed under SEM. Then the samples are mounted on stubs and the eroded and uneroded surfaces are examined. To enhance the conductivity of the samples, a thin film (100 Å thickness) of platinum is coated onto them in JEOL sputter ion coater before the photomicrographs are taken.

3.4.6 X-Ray Diffraction (XRD) Studies

The raw LD slag and the coatings are examined for the identification of the crystalline phases with a Philips X-Ray Diffractometer, shown in Figure 3.19. The X-ray diffractograms are taken using Cu Kα radiation.

3.4.7 Micro-hardness

Micro-hardness measurement is done using a Leitz micro-hardness tester (Figure 3.20). A diamond indenter, in the form of a right pyramid with a square base and an angle 136^0 between opposite faces, is forced into the material under a load *F*. The two diagonals *X* and *Y* of the indentation left on the surface of the material after removal of the load are measured and their arithmetic mean *L* is calculated.

In the present study, the load considered F = 0.5 N and Vickers hardness number is calculated using the following equation [347]:

$$H_v = 0.1889\frac{F}{L^2} \; and \; L = \frac{X+Y}{2} \tag{3.2}$$

Here, F is the applied load (N), L is the diagonal of square impression (mm), X is the horizontal length (mm) and Y is the vertical length (mm). About six to seven readings are taken for each sample on different optically distinguishable points and the average value is reported as the mean coating hardness. It is then converted and expressed in terms of SI units (GPa). This technique is used for the assessment of the hardness of both the coating and the composite samples under this investigation.

3.5 Composite Characterization

3.5.1 Density and Volume Fraction of Void

The theoretical density of composite materials in terms of weight fraction can easily be obtained as for the following equations given by Agarwal and Broutman [348]:

$$\rho_{ct} = \frac{1}{(W_f/\rho_f) + (W_m/\rho_m)} \tag{3.3}$$

where W and ρ represent the weight fraction and density respectively. The suffix f, m and ct stand for the fiber, matrix and the composite materials respectively.

The composites under this investigation consists of three components namely matrix, fiber and particulate filler. Hence the modified form of the expression for the density of the composite can be written as

$$\rho_{ct} = \frac{1}{(W_f/\rho_f) + (W_m/\rho_m) + (W_p/\rho_p)} \tag{3.4}$$

The actual density (ρ_{ce}) of the composite, however, can be determined experimentally by simple water immersion technique. The volume fraction of voids (V_v) in the composites is calculated using the following equation:

$$V_v = \frac{\rho_{ct} - \rho_{ce}}{\rho_{ct}} \quad \textbf{(3.5)}$$

3.5.2 Tensile and Flexural Strength

The dog-bone type specimens with end tabs are commonly used for tensile test. ASTM-D3039-76 standard test method is employed for tensile test of composite specimens. The test is performed using the universal testing machine (UTM) Instron 1195 (Figure 3.21) at a cross-head speed of 10 mm per minute. Each test is repeated three times on different composite specimens of same composition and the average of the three results is recorded as the mean value of the tensile strength. The pictorial view of the composite specimens and the loading arrangement for tensile test are shown in Figures 3.22 (a) and 3.22 (b) respectively.

The short beam shear (SBS) tests are performed on the composite samples at room temperature to evaluate the value of flexural strength. It is a 3-point bend test, which generally promotes failure by inter-laminar shear. The SBS test is conducted as per standard ASTM: D5379/D5379M using the same UTM. The dimension of each specimen is 60 × 10 × 3 mm^3. Span length of 40 mm and the cross-head speed of 10 mm/min are maintained. The pictorial view of the composite specimens and the loading arrangement for the 3 point bend test are shown in Figures 3.23 (a) and 3.23 (b) respectively. The flexural strength (*F.S*) of any composite specimen is determined using the following equation:

$$F \cdot S = \frac{3Pl}{2bt^2} \quad \textbf{(3.6)}$$

Where, l is the span length of the sample, P is the load applied; b and t are the width and thickness of the specimen respectively.

Figure 3.18 Scanning electron microscope

Figure 3.19 X-ray diffractometer

3.5.4 Impact Strength

The pendulum impact testing machine confirming to ASTM: D256 ascertains the notch impact strength of the material by shattering the specimen with a pendulum hammer, measuring the spent energy and relating it to the cross section of the specimen. The machine is adjusted such that the blade on the free-hanging pendulum just barely contracts the specimen (zero position). The specimens are clamped in a square support and are struck at their central point by a hemispherical bolt of diameter 5 mm.

Figure 3.20 Leitz micro-hardness tester

Figure 3.21 Instron 1195 universal testing machine

Figure 3.22 (a) Composite samples for tensile test

Figure 3.22 (b) Loading arrangement for tensile test

Figure 3.23 (a) Composite samples for flexural test

Figure 3.23 (b) Loading arrangement for flexural test

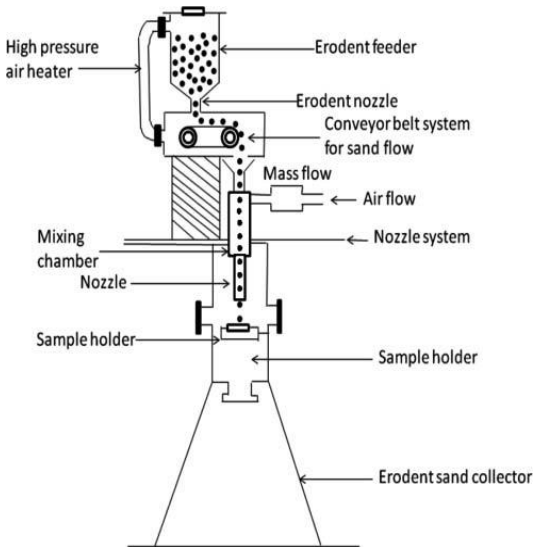

Figure 3.24 (a) Schematic diagram of erosion test rig

Figure 3.24 (b) Solid particle erosion test set-up

3.6 Erosion Wear Test

The set up for the solid particle erosion wear test used in this study is capable of creating reproducible erosive situations for assessing erosion wear resistance of the prepared coating and composite samples. This air jet type erosion test rig evaluates the erosion resistance of materials utilizing a repeated impact erosion approach. The pictorial view and the schematic diagram of the erosion test rig are given in Figures 3.24 (a) and 3.24 (b) respectively. The test is conducted following the test standards prescribed by ASTM G76 at the Institute of Minerals and Materials Technology, Bhubaneswar. The test rig consists of an air compressor, an air drying unit, a conveyor belt-type particle feeder and an air-particle mixing chamber and an accelerating chamber. In the present study, dry silica sand particles of different sizes ranging from 50 μm to 400 μm are used as erodent. The dried and compressed air is mixed with the erodent which is fed constantly by a conveyor belt feeder into the mixing chamber and then is accelerated by passing the mixture through a convergent nozzle of 5 mm internal diameter. The erodent particles impact the specimen which can be held at different angles with respect to the direction of erodent flow using different sample holders. The velocity of the eroding particles is determined using the standard double disc method [349]. The apparatus is equipped with a heater which can regulate and maintain the erodent temperature at any pre-determined fixed value (in the range 20^0C to 100^0C) during an erosion trial. The samples are cleaned in acetone, dried and weighed before and after the erosion trials using a precision electronic balance with an accuracy of ± 0.1 mg. The weight loss is recorded for subsequent calculation of erosion rate. The process is repeated till the erosion rate attains a constant value called *steady state erosion rate*. The erosion rate is defined as the ratio of this weight loss to the weight of the erodent particles causing the loss.

3.7 Process Optimization and Taguchi Method

Statistical methods are commonly used in engineering and related studies to improve the quality of a product or a process. Such methods enable the user to define and study the effect of every single condition possible in an experiment where numerous factors are involved. Solid particle erosion is such a process in

which a number of control factors collectively determine the performance output, i.e., the erosion rate. In this context, Taguchi experimental design happens to be a powerful analysis tool for modeling and analyzing the influence of control factors on the performance output. This method achieves the integration of design of experiments (DOE) with the parametric optimization of the process yielding the desired results. The orthogonal array (OA) indicates a set of well-balanced (minimum test runs) experiments. Taguchi's method uses a statistical measure of performance called signal-to-noise ratio (S/N), which is the logarithmic function of desired output to serve as objective functions for optimization. The ratio depends on the qualitative characteristics/attributes of the product/process variables to be optimized. The three categories of S/N ratios normally used are smaller-the-better (SB), higher-the-better (HB) and nominal-the-best (NB) as given by the Eqs. 3.7, 3.8 and 3.9 respectively. In the present study, the S/N ratio for minimum erosion rate falling under smaller-the-better norm can be calculated as logarithmic transformation of the loss function by using Eq. 3.7.

Smaller the better characteristics $$\frac{S}{N} = -10\log\frac{1}{n}\left(\sum y^2\right) \quad \textbf{(3.7)}$$

Higher the better characteristics $$\frac{S}{N} = -10\log\frac{1}{n}\left(\sum\frac{1}{y^2}\right) \quad \textbf{(3.8)}$$

Nominal the best characteristics $$\frac{S}{N} = -10\log\frac{1}{n}\left(\sum\frac{\bar{Y}}{S_Y^2}\right) \quad \textbf{(3.9)}$$

The most important stage in the design-of-experiments (DOE) lies in the proper selection of the control factors. Therefore, a large number of factors are initially included so that non-significant variables can be identified at the earliest opportunity. In Taguchi's experimental design, some selected parameters influencing the performance output are considered in determining the

experimental schedule as per the prescribed orthogonal arrays. The control factors and their selected levels considered for wear test of the LDS based coatings and the composites are listed in Tables 3.10 and 3.11 respectively. Correspondingly an L_{16} and an L_{25} orthogonal array are taken for the erosion wear experiments of these coating and composite samples respectively.

Table 3.10 Control factors and their selected levels for coating

Control Factor	Level				
	1	2	3	4	Units
A:Impact velocity	32	40	48	56	m/sec
B:Impingement angle	30	45	60	90	degree
C:Erodent size	100	200	300	400	µm
D:Erodent temperature	30	40	50	60	^{0}C
E:Al_2O_3/TiO_2 content	0	10	20	30	wt%

Table 3.11 Control factors and their selected levels for composite

Control Factor	Level					
	1	2	3	4	5	Units
A:Impact velocity	32	40	48	56	64	m/sec
B:Impingement angle	30	45	60	75	90	degree
C: LDS content	0	7.5	15	22.5	30	wt%
D:Erodent size	50	100	150	200	250	µm
E:Erodent temperature	30	40	50	60	70	^{0}C

3.8 Artificial Neural Network

Erosion wear process is considered as a non-linear problem with respect to its variables: either materials or operating conditions. As already mentioned, to obtain minimum wear rate, appropriate combinations of operating parameters have to be planned so as to study their interrelated effects and to predict the wear response under different operational conditions. To this end, a systematic analysis using another novel technique namely artificial neural network (ANN) is implemented in this work. ANN is a technique inspired by the biological neural system and has already been used to solve a wide variety of problems in

diverse fields [181, 333, 334, 350]. It was developed to simulate the strong learning, clustering and reasoning capacity of biological neurons. With a strong learning capability and use of parallel computation and non-linear mapping, neural networks can be successfully applied for identifying several non-linear systems and control problems. The multiple layered ANN is the most extensively applied neural network for various engineering materials, but is seldom utilized in research in the field of wear-resistant polymeric composites [301]. The back propagation ANN can be used to train such multiple layered feed-forward networks with differential transfer functions to develop a functional model. Using a well-trained ANN model, one can estimate predictive performance, pattern association and pattern classification. As aforementioned, the erosion process is a complicated phenomenon lacking adequate mathematical description and therefore, a powerful method that combines the ANN technique and the Taguchi‘s design is proposed in this study for better analysis and prediction of erosion performance of coatings and composites. This proposed approach not only yields a sufficient understanding of the effects of process parameters, but also produces an optimal parameter setting to ensure that the coatings and composites exhibit the best performance characteristics.

ANN is a technique that involves database training to predict input-output evolutions. Basically this method is suitable for some complex, nonlinear and multi-dimensional problems because it is able to imitate the learning capability of human beings. This means that the network can learn directly from the examples without any prior formulae about the nature of the problem and generalize by itself some knowledge, which could be applied for new cases. A neural network is a system composed of many cross-linked simple processing units called ‘neurons’. The network generally consists of three parts connected in series: input layer, hidden layer and output layer. Experimental result sets are used to train the ANN in order to understand the input-output correlations. The database is divided into three categories, namely: (i) a validation category, which is required to define the ANN architecture and adjust the number of neurons for

each layer. (ii) a training category, which is exclusively used to adjust the network weights and (iii) a test category, which corresponds to the set that validates the results of the training protocol. The coarse information is accepted by the input layer and processed in the hidden layer. Finally the results are exported via the output layer [351]. The details of this methodology are described by Rajasekaran and Pai [352].

Chapter Summary

This chapter has provided:

- The descriptions of materials used in the experiments
- The details of deposition and characterization of the coatings
- The details of fabrication and characterization of the composites
- The description of solid particle erosion wear test
- An explanation of the Taguchi experimental design and neural network analysis

The next chapter presents the physical, mechanical and micro-structural characterization of the plasma sprayed coatings under this study.

*****

Chapter 4

Coating Characterization

Chapter 4

COATING CHARACTERIZATION

This chapter reports on the characteristics of different coatings considered in this study. Plasma sprayed coatings of raw LD slag (LDS), LDS pre-mixed with Al_2O_3 and with TiO_2 in different weight proportions are deposited on aluminium substrate using an 80 kW atmospheric plasma spray system. Spraying is done at different input powers to the plasma torch in the range from 10-24 kW. Characterization of the coatings in regard to their physical and mechanical properties is done. The results of various characterization tests are presented and discussed in this chapter.

4.1 Characterization of Coating Material

4.1.1 Particle Size Analysis and Powder Morphology of Raw LD slag

The particle size distribution of raw LDS powder (after sieving and before plasma spraying) is characterized using LASER particle size analyzer of Malvern Instruments make. Figure 4.1 shows the particle size distribution of LD slag used in this research. It can be seen that, majority of particles are in the range of 90-100 μm. SEM micrograph of raw LDS in feedstock prior to coating is shown in Figure 4.2. It is observed that the particles are of varied sizes and are irregular in shape.

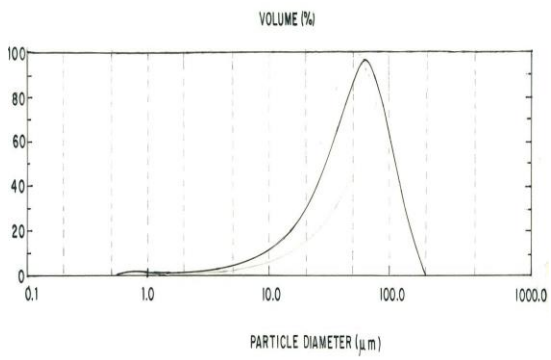

Figure 4.1 Particle size analysis of raw LDS

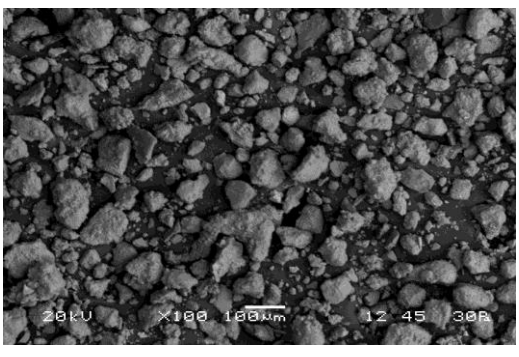

Figure 4.2 SEM micrograph of raw LDS powder prior to coating

4.2 Characterization of Coatings

4.2.1 Coating Thickness

To ensure the deposition of coating on the aluminium substrates taken, coating thickness is measured on the polished cross-sections of the samples, using an Elcometer 456 thickness gauge. The measured thickness values for 'LDS + Al_2O_3' and 'LDS + TiO_2' coatings deposited at different power levels are presented in Figures 4.3 and 4.4 respectively. Each data point on the curves is the average of at least five to six readings taken on different locations on each specimen. It is evident from these curves that with increase in torch input power the thickness of the coating increases irrespective of the coating material. It is further noted that during the deposition in the input power range of 13-20 kW, the increase in coating thickness is significant.

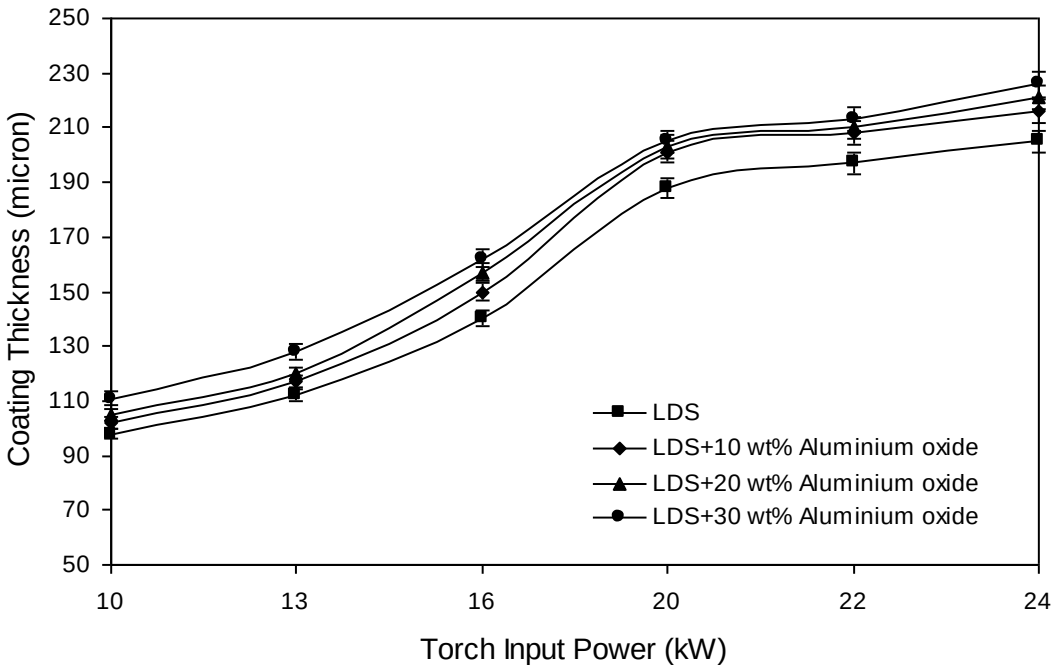

Figure 4.3 Variation of coating thickness for LDS and 'LDS + Al_2O_3' mix with torch input power on aluminium substrate

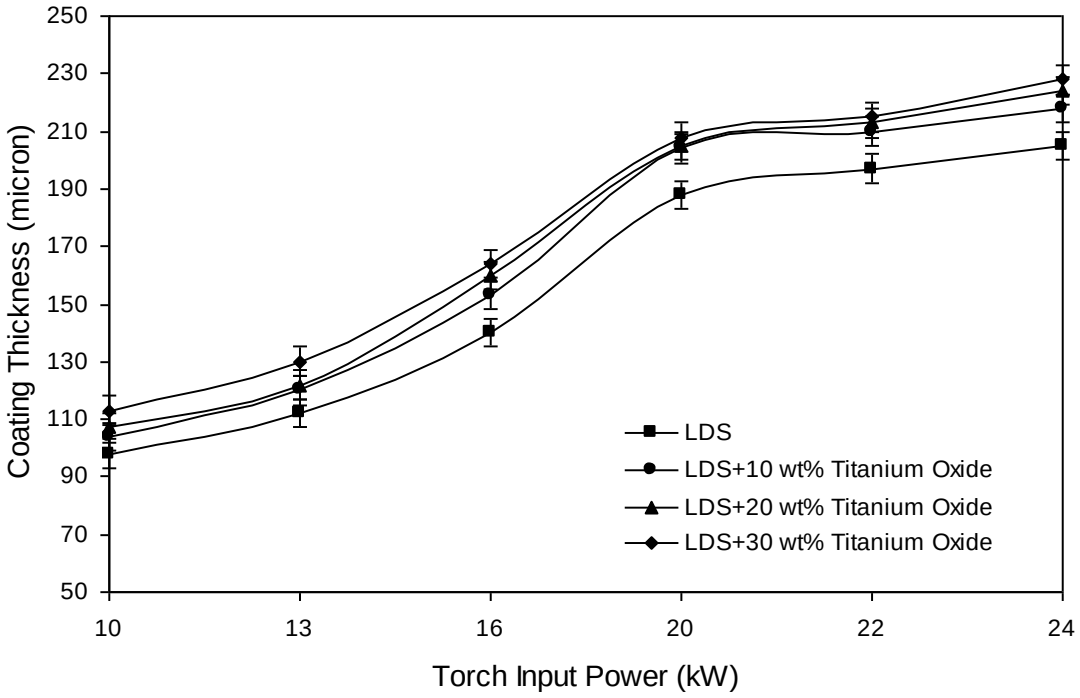

Figure 4.4 Variation of coating thickness for LDS and 'LDS + TiO_2' mix with torch input power on aluminium substrate

In case of deposition of raw LDS, the coating thickness is found to be varying in the range of 98 μm to 205 μm as the torch input power is increased from 10 to 24 kW. The thicknesses of the coatings made from LDS mixed with different proportions of Al_2O_3 are found to be varying in the range of 98 μm to 226 μm with the increase in torch input power. The feed material with 30 wt% Al_2O_3 powder resulted in thicker coatings, with a maximum thickness of 226 μm at 24 kW power level on aluminium substrate. Similarly, in case of LDS and TiO_2 mixture the coating thickness is varying in the range of 98 μm to 228 μm with the increase in torch input power level. The feed material with 30 wt% of TiO_2 powder gives thicker coatings, with maximum thickness of 228 μm at the 24 kW power level on aluminium substrate. It is known that for oxide coatings developed by atmospheric plasma spraying (APS) technique, particle deposition is influenced by the torch input power [353]. With the increase in power level, the plasma density increases leading to rise in enthalpy of the plasma jet and also thereby the temperature of the particles (coating material) residing within the jet. Hence at higher torch input power, better melting of the feed material during the

in-flight traverse through the plasma results in better inter-particle bonding which subsequently gives rise to a higher rate of coating deposition.

4.2.2 Deposition Efficiency

Deposition efficiency of coatings made within the scope of this investigation is evaluated because it is an important factor that determines the techno economics of the process. It depends on many factors that include the input power to the plasma torch, material properties such as melting point, particle size range, heat capacity of the powder being sprayed and the torch to base distance (TBD) etc. [29, 31]. For a given TBD and a specific coating material, torch input power appears to be an important factor for the deposition efficiency. The deposition efficiency is a measure of the fraction of the powder that is deposited on the substrate. Deposition efficiency values of 'LDS + Al_2O_3' and 'LDS + TiO_2' coatings made at different operating powers are presented in Figures 4.5 and 4.6 respectively.

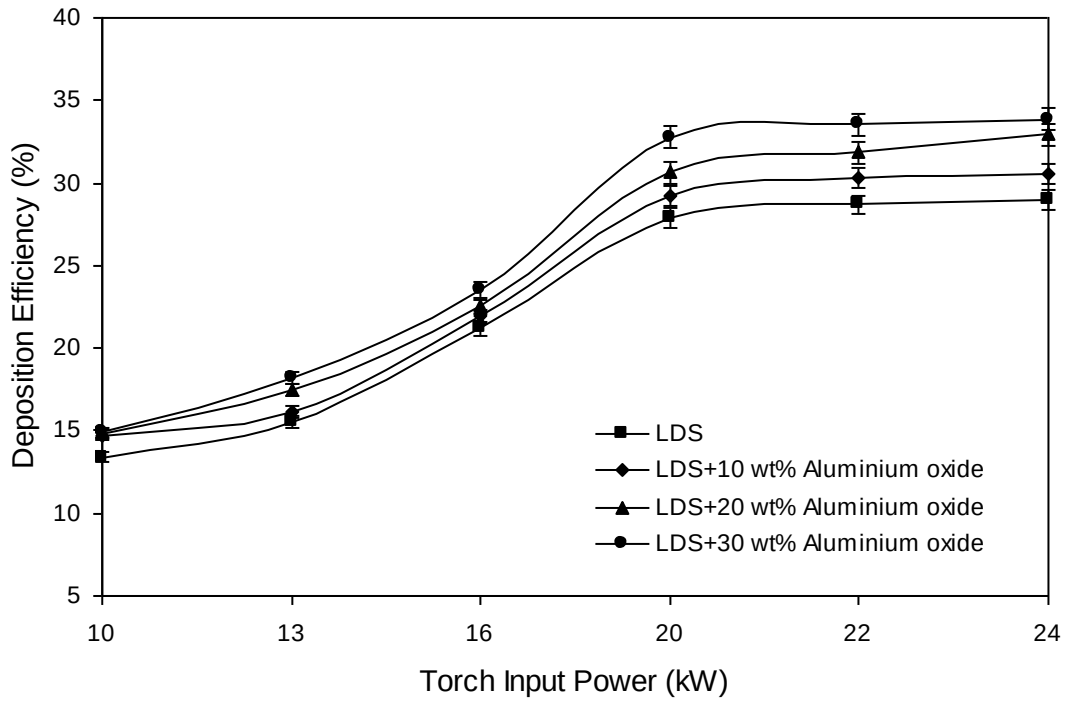

Figure 4.5 Coating deposition efficiency of LDS and 'LDS + Al_2O_3' mix at different torch input power on aluminium substrate

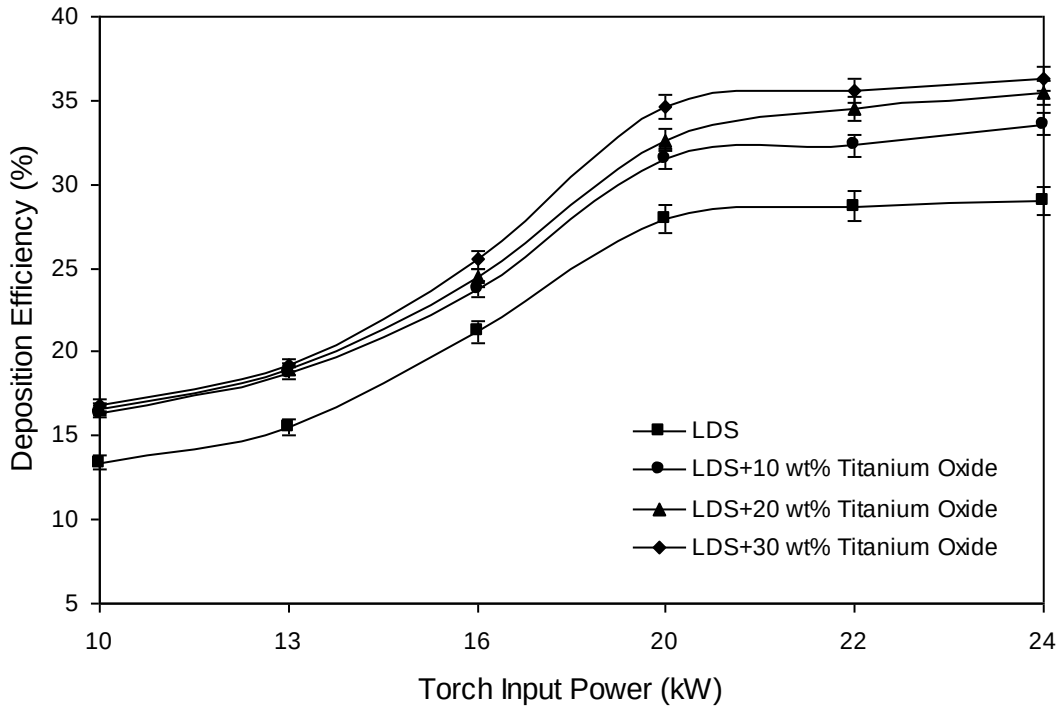

Figure 4.6 Coating deposition efficiency of LDS and 'LDS + TiO_2' mix at different torch input power on aluminium substrate

Figure 4.5 is representing the deposition efficiency for the feed materials: raw LDS and 'LDS + Al_2O_3' (with different weight proportions) on aluminium substrate. It is interesting to note that the deposition efficiency is increasing from lower to higher values as the weight percentage of aluminium oxide increases in the blend and also, as the torch input power increases. Al_2O_3 is a conventional coating material and exhibits excellent coatability on metallic substrates. Hence the increase in Al_2O_3 content in the mixture helps in enhancing the rate of deposition compared to that in case of raw LDS. Here, the deposition efficiency presents a sigmoid-type evolution with the increase in torch input power. As the power level increases, the net available energy in the plasma jet increases leading to a better in-flight particle melting and hence to higher probability for the molten particles to flatten. The deposition efficiency reaches a plateau for the highest power levels due to the plasma jet temperature increasing which in turn increases both the particle vaporization ratio and the plasma jet viscosity. Actually, deposition efficiency indicates the rate of deposition of the material on

the substrate and a constant deposition efficiency therefore does not mean that there is no deposition. On the other hand, coating thickness would increase with coating deposition even if the rate of deposition remains constant. This is evident from the experimental results shown in Figures 4.3 to 4.6.

Deposition efficiency of 33.84% is recorded as the highest for coating of 'LDS + 30 wt% Al_2O_3' at 24 kW torch input power level on aluminium substrate. Similarly, for 'LDS + TiO_2' mixture with different weight proportions, the coating deposition efficiency on aluminium substrate is also evaluated and plotted and a maximum deposition efficiency of 36.34% is obtained at 24 kW torch input power level and with 30 wt% of TiO_2 in the mixture. It is further evident from the graphs in Figures 4.5 and 4.6 that the coating deposition efficiency is higher for the 'LDS + TiO_2' deposition as compared to that in case of 'LDS + Al_2O_3' deposition under similar spraying conditions.

This study reveals that efficiency of coating deposition is significantly influenced by the input power to the torch. In fact, plasma spray deposition efficiency of a given material depends on its melting point, heat capacity, rate of heat dissipation at coating-substrate interface and on particle size of the sprayed powder etc. At lower power level, the plasma jet temperature is not high enough to melt the entire feed powder (particles) that enters the plasma jet. As the power level is increased, plasma temperature and enthalpy increases, thus melting a larger fraction of the feed powder. The spray efficiency therefore increases with increase in input power to the plasma torch. However, beyond a certain power level of the torch, temperature of the plasma becomes high enough leading to vaporization or dissociation of the particles. Thus there is not much increase in deposition efficiency. This tendency is generally observed in deposition of a wide range of plasma sprayed ceramic and cermet coatings [31]. However, the operating power above which no further increase of deposition efficiency is noticed depends on the chemical nature of the feed material i.e. powder and its particle size, thermal conductivity, in-situ phase transformations etc.

4.2.3 Coating Adhesion Strength

Adhesion tests have been carried out for several coatings by many investigators in the past [27, 99]. It has been stated that, the fracture mode is adhesive if it takes place at the coating-substrate interface and that the measured adhesion value is the value of practical adhesion, which is strictly an interface property, depending exclusively on the surface characteristics of the adhering phase and the substrate surface condition [91, 354]. From the microscopic point of view, adhesion is due to physico-chemical surface forces (Vander-walls, Covalent, Ionic etc.), which are established at the coating-substrate interface [355] and corresponds to the work of adhesion. From the mechanical point of view, strength of adherence can be estimated by the force corresponding to interfacial fracture and is essentially macroscopic in nature.

In the present investigation, to evaluate the coating adhesion strength, test is conducted by the pull out method following ASTM C-633 test standards. It is found that, in all the samples fracture occurred at the coating-substrate interface. The variations of adhesion strength of 'LDS + Al_2O_3' and 'LDS + TiO_2' coatings with torch input power are shown in Figures 4.7 and 4.8 respectively. Each data point is the average of three test runs. From the figures, it is seen that the adhesion strength varies with operating power of the plasma torch. The strength also differs from substrate to substrate and depends on the composition of the coating materials as well.

From the Figure 4.7, it is clear that the adhesion strength varies appreciably with torch input power (10-24 kW) of the plasma torch and the maximum adhesion strength is obtained at 20 kW invariably for all feed stock materials. Maximum adhesion strength of about 33.77 MPa is recorded with 'LDS + 30 wt% Al_2O_3' powder. The Figure 4.8 also shows almost similar trends as those obtained in case of 'LDS + Al_2O_3' coatings. Among all the coated samples, 'LDS + 30 wt% TiO_2' coating made at 20 kW exhibited a maximum adhesion strength of about 36 MPa. A drop in adhesion strength is noticed for all coatings deposited at a torch operating power beyond 20 kW.

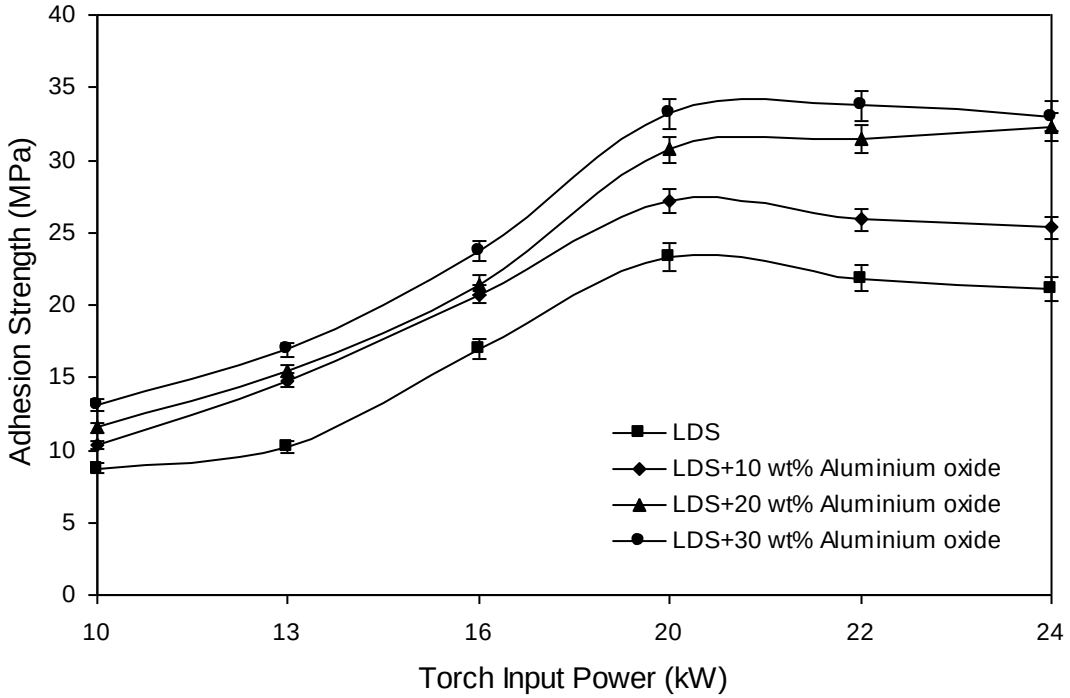

Figure 4.7 Variation in coating adhesion strength of LDS and 'LDS + Al_2O_3' coatings on aluminium substrate with torch input power

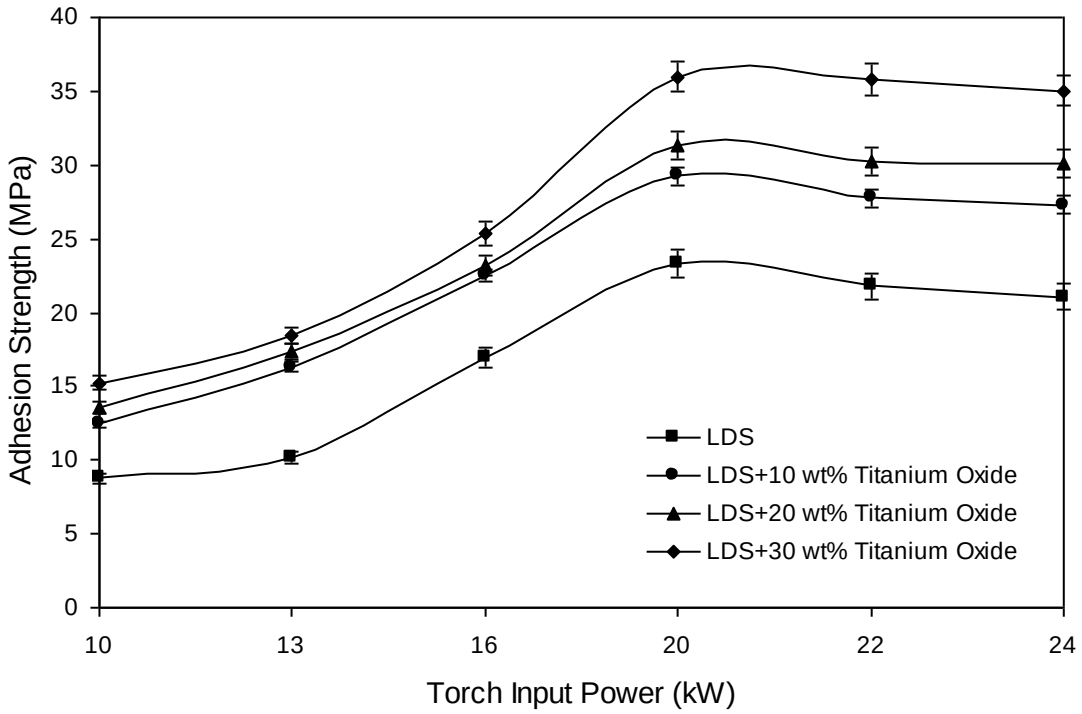

Figure 4.8 Variation in coating adhesion strength of LDS and 'LDS + TiO_2' coatings on aluminium substrate with torch input power

Initially, when the operating power level is increased from 10 to 20 kW, the melting fraction and velocity of the particles also increase. Therefore there is better splashing and mechanical inter-locking of molten particles on the substrate surface leading to increase in adhesion strength [356]. But, at higher power levels (beyond 20 kW), the amount of fragmentation and vaporization of the particles are likely to increase. There is also a greater chance of smaller particles (during in-flight traverse through the plasma) to fly off during spraying. This results in poor adhesion strength of the coatings. The presence of a suitable proportion of conventional ceramics like Al_2O_3 and TiO_2 is also found to have helped in interparticle as well as interfacial bonding. This could be one of the reasons for the greater adhesion strength with the presence of Al_2O_3 and TiO_2 powder in the raw material.

4.2.4 Coating Micro-hardness

Micro-hardness measurement is done on the optically distinguishable phases on the polished coating cross-section using a Leitz micro-hardness tester. Different phases bear different hardness values and the average of these values is recorded as the mean hardness of the coating. Each data point therefore is the mean of at least six or seven such readings. The values of coating micro-hardness for different coating materials at different torch input power are shown in Table 4.1.

Table 4.1 Coating micro-hardness for different feed materials deposited at different operating torch input power

Coating material	Coating micro-hardness (GPa) (at different plasma torch input power)					
	10 kW	13 kW	16 kW	20 kW	22 kW	24 kW
LDS	3.52	4.54	4.73	4.97	5.46	5.82
LDS+10wt% TiO_2	4.13	4.92	5.42	5.63	5.81	5.96
LDS+20wt% TiO_2	4.86	5.31	5.54	5.76	5.92	6.38
LDS+30wt% TiO_2	5.24	5.63	5.78	5.89	6.24	6.72
LDS+10wt% Al_2O_3	4.21	5.37	5.56	5.77	5.97	6.41
LDS+20wt% Al_2O_3	4.94	5.49	5.67	5.83	6.04	6.53
LDS+30wt% Al_2O_3	5.39	5.88	5.94	6.11	6.38	6.93

[*]LDS: Linz-Donawitz slag

For the raw LDS coatings, the coating micro-hardness is found to increase from 3.52 GPa to 5.82 GPa as the torch input power increases from 10 to 24 kW. It is also observed that the addition of either Al_2O_3 or TiO_2 to LDS in the feed stock results in substantial increase in the bulk hardness of the coatings. Influence of power level in terms of improvement of coating hardness is clearly seen from the results presented in the table.

4.2.5 Coating Porosity

Measurement of porosity is done using the image analysis technique. The results are tabulated in Table 4.2. It is observed that porosity in the LDS based coatings considered in this investigation lie in the range of 4-10%. The lowest porosity is recorded to be 5.64% for 'LDS + 30 wt% Al_2O_3' coatings and 5.62% for 'LDS + 30 wt% TiO_2' coatings, both at 24 kW power.

It is also noticed that with addition of both Al_2O_3 and TiO_2 to raw LDS in the feed stock, the percentage of pores can be reduced. In conventional plasma sprayed ceramic coatings, porosity of about 3-10 % is generally observed [27, 88, 357, 358]. Thus the values obtained for the coatings under this study are well within the acceptable range.

Table 4.2 Coating porosity for different feed materials deposited at different operating torch input power

Coating material	Porosity (%) (at different plasma torch input power)					
	10 kW	13 kW	16 kW	20 kW	22 kW	24 kW
LDS	8.42	8.31	9.27	8.73	9.31	8.58
LDS+10wt% Al_2O_3	7.24	7.21	8.45	7.94	8.68	7.54
LDS+20wt% Al_2O_3	6.46	6.68	7.53	6.74	7.87	6.96
LDS+30wt% Al_2O_3	6.08	5.78	6.71	5.69	6.67	5.64
LDS+10wt% TiO_2	7.43	7.25	8.43	7.82	8.64	7.57
LDS+20wt% TiO_2	6.57	6.72	7.58	6.78	7.86	5.94
LDS+30wt% TiO_2	6.14	5.84	6.76	5.67	6.73	4.62

**LDS: Linz-Donawitz slag*

The variation of coating porosity with torch input power can be explained as follows: during spraying the coating materials melt and travel at high speed and these molten species hit the substrate with a reasonably high impact velocity. On impact, they get flattened and adhere to the surface forming big splats. If the inter-lamellar bonding between these splats is strong and the area of contact between the lamellae is more, then it leads to less amount of porosity. Therefore, although there is decrease in coating thickness, a dense coating is formed. Similar trend of increase in porosity with coating thickness and vice versa has been observed by Sarikaya in case of alumina coatings [359].

X-Ray Diffraction Analysis

To ascertain the major phases after plasma spraying, the X-ray diffractograms are taken on some of chosen coating samples using a Phillips X-ray Diffractometer with Ni-filtered Cu Kα radiation.

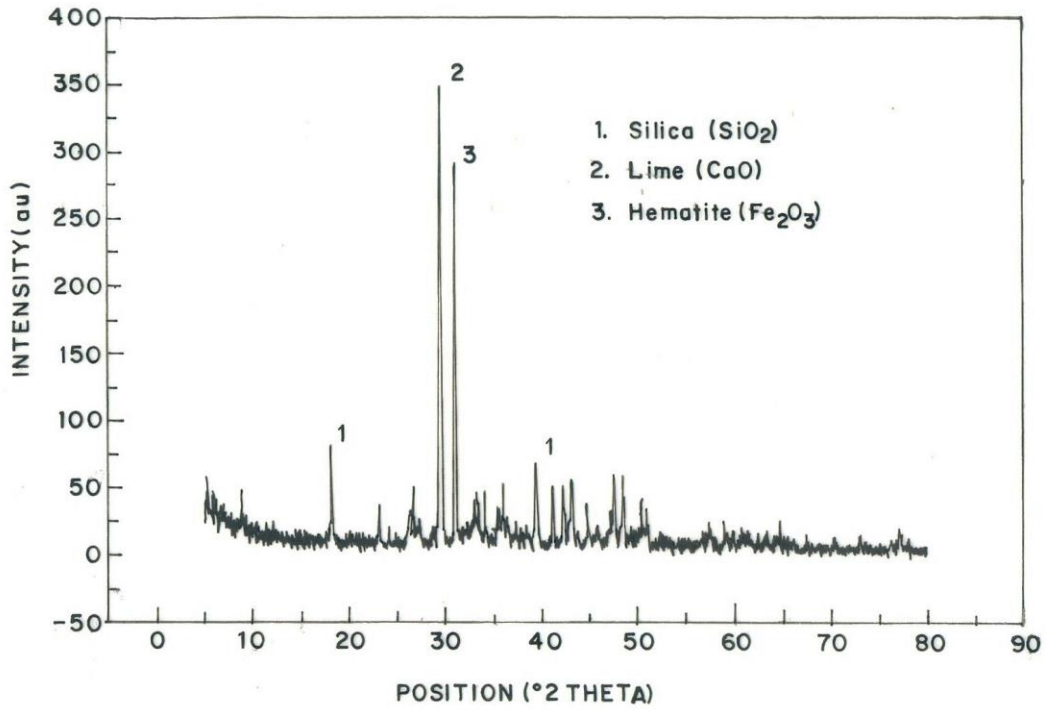

Figure 4.9 X-ray diffractogram of raw LDS

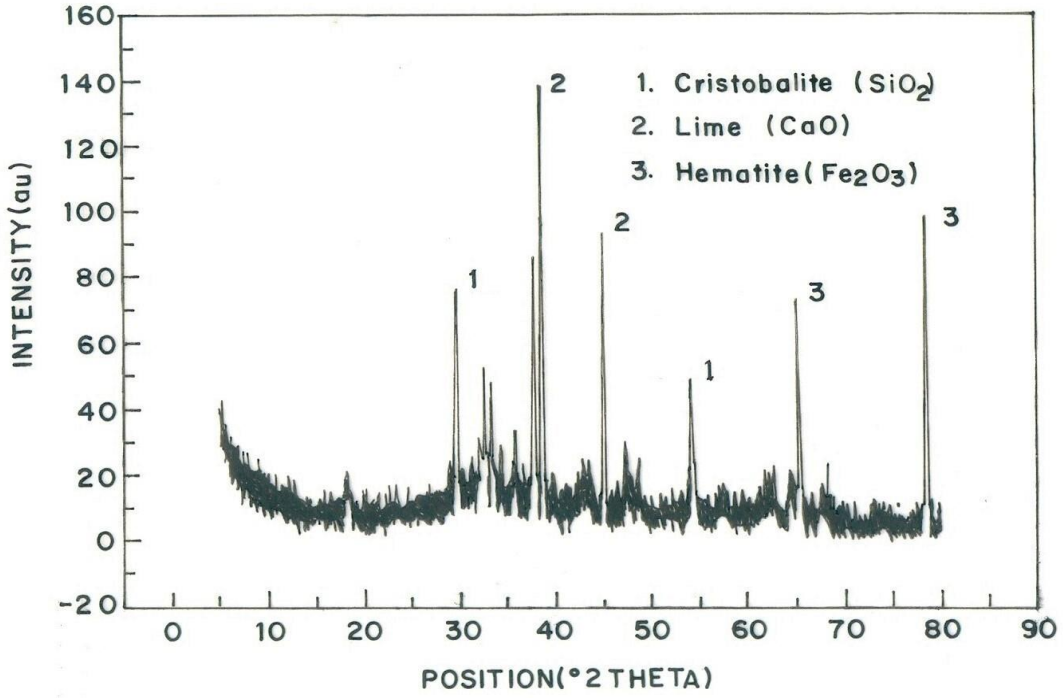

Figure 4.10 X-ray diffractogram of the LDS coating

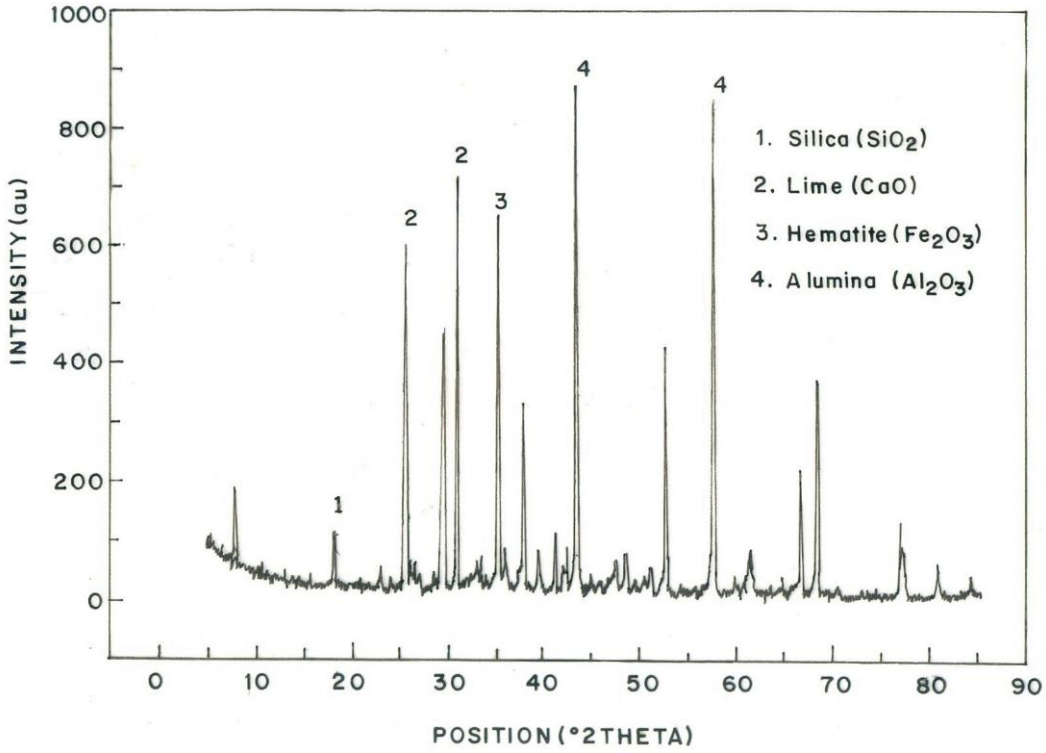

Figure 4.11 X-ray diffractogram of LDS-Al_2O_3 mix

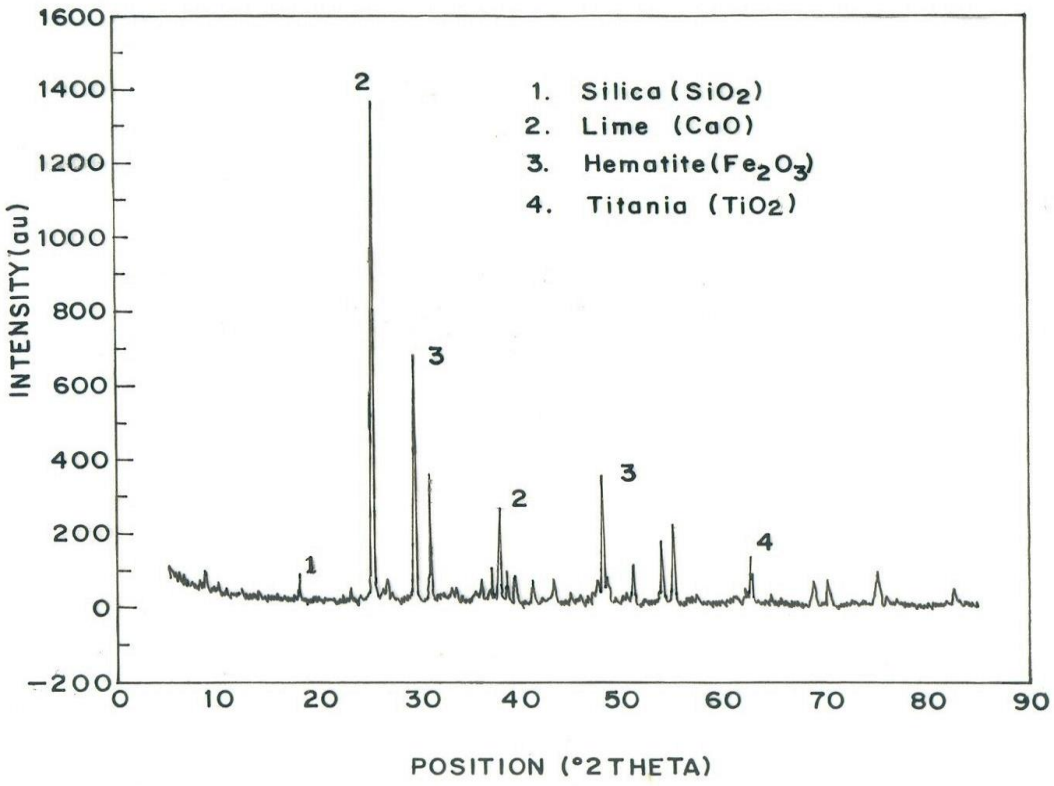

Figure 4.12 X-ray diffractogram of LDS-TiO_2 mix

Figure 4.9 presents the the X-ray diffractogram for raw LD slag particles. The XRDs for coatings of LDS, 'LDS + Al_2O_3' mix and 'LDS + TiO_2' mix are shown in Figures 4.10, 4.11 and 4.12 respectively. From the diffratogram for raw LDS, shown in Figure 4.9, it is seen that the major oxide phases present are silica (SiO_2), lime(CaO) and hematite (Fe_2O_3). The XRD of LDS coating reveals the presence of phases like cristobalite (SiO_2), lime (CaO) and hematite (Fe_2O_3). In the diffractogram for LDS-Al_2O_3 mix (Figure 4.11), crystalline phases like alumina (Al_2O_3) in addition to silica (SiO_2), lime (CaO) and hematite (Fe_2O_3) are identified. Similarly the diffractogram for LDS-TiO_2 coating indicates the presence of crystalline phases like rutile (TiO_2) apart from silica (SiO_2), lime(CaO) and hematite (Fe_2O_3).

Chapter Summary

This chapter has provided:

- The physical and mechanical characterization of the plasma sprayed coatings of LDS, 'LDS + Al_2O_3' and 'LDS + TiO_2' on aluminium substrate
- The relative effects of coating material composition and plasma torch input power on various coating characteristics
- The identification of various phases in the coatings made of materials of different compositions

The next chapter presents the solid particle erosion characteristics of plasma sprayed LDS based coatings.

*****

Chapter 5

Erosion Wear Response of Plasma Sprayed LD Slag (LDS) Coatings

Chapter 5

EROSION WEAR RESPONSE OF PLASMA SPRAYED LD SLAG (LDS) COATINGS

Erosion wear characteristics of plasma sprayed LDS, 'LDS + Al_2O_3' and 'LDS + TiO_2' coatings have been investigated in this study following a well planned experimental schedule based on the Taguchi technique which is used to acquire the erosion test data in a controlled way. This chapter reports the wear rates obtained from these erosion trials and presents a critical analysis of the test results. Further, erosion rate predictions following an ANN approach for different test conditions are presented. A correlation among various control factors influencing the erosion rate has also been proposed for predictive purpose. Possible wear mechanisms are identified from the scanning electron microscopy of the eroded surfaces.

5.1 Morphology of Coating Surfaces

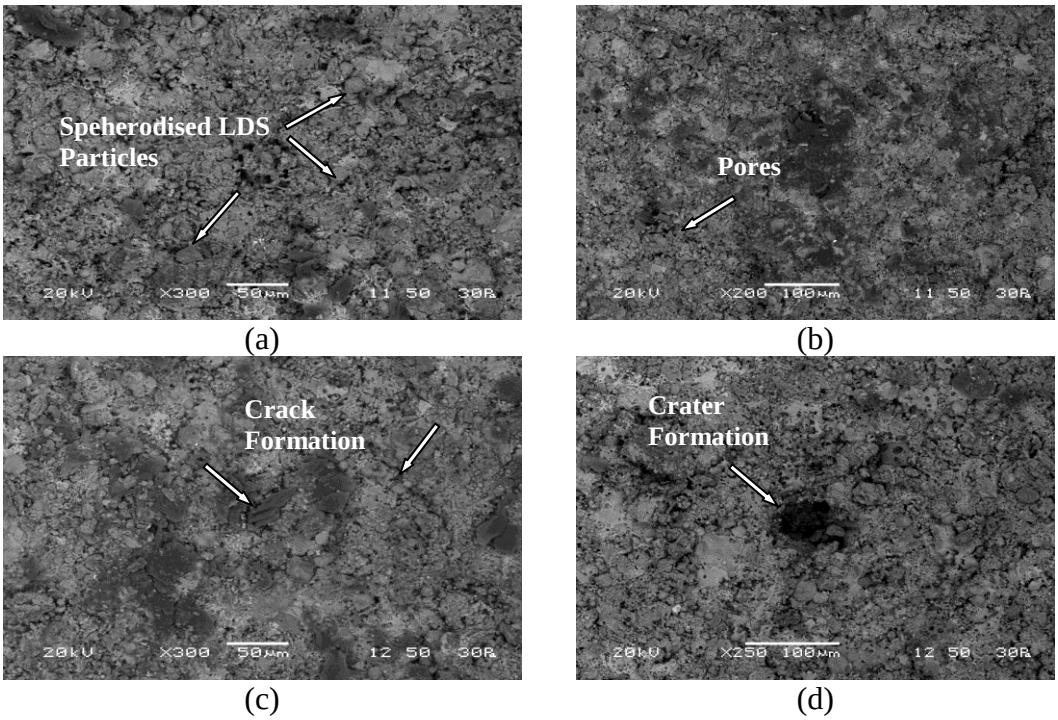

(a) (b) (c) (d)

Figure 5.1 SEM micrographs of uneroded and eroded surfaces of the LDS-TiO_2 coatings

Figure 5.1 shows some of typical the SEM micrographs of the surfaces coated with 'LDS + TiO_2' mix. As a result of plasma processing at very high temperature, the slag particles have been speherodised and on striking the substrate surface have formed splats as is seen in Figure 5.1 (a). Small pores are also visible on the coating surface (Figure 5.1 (b)). Figures 5.1 (c) and 5.1 (d) are the SEM microstructures for the coating surfaces after erosion and these images clearly indicate features like cracks, crater formation and chipping of the coating surface. These features are possibly the consequence of the repeated impacts of hard sand particles on the coating surface.

5.2 Erosion Test Results and Taguchi Analysis

The erosion wear rates of LDS coated substrate according to an L_{16} orthogonal design along with the corresponding signal-to-noise (S/N) ratios are shown in Table 5.1. The difference between the weights of the coating substrate before and after the erosion test is the wear loss or the mass loss of the specimen due to solid particle impact. The ratio of this mass loss to the mass of the eroding particles causing the loss is then computed as the dimensionless incremental erosion rate. All four control factors are represented in second to fifth columns of the table and the test results (i.e., erosion rate) are presented in sixth column. The S/N ratio for each test run is calculated and is shown in last column of Table 5.1. The overall mean for the S/N ratio of erosion rate is found to be -26.3218 db. The analysis is made using the popular software specifically used for design of experiment applications known as MINITAB 14. The response table for S/N ratio with smaller-is-better characteristic is given in Table 5.2. This table shows the delta value of the factors and according to that the factors are ranked. In this study, the impact velocity, with a higher delta value, is found to be the most significant factor, followed by the impingement angle and erodent size, influencing the erosion wear rate of the LDS coatings. Figure 5.2 shows the main effect plot for S/N ratios of individual control factors. The effects of individual control factors are assessed by calculating the response and the results

of response analysis lead to the conclusion that factor combination of A_1, B_1, C_1 and D_1 gives the minimum wear rate

Table 5.1 Experimental design using L_{16} orthogonal array and the wear test results for LDS coatings

Test Run	Impact Velocity (A) m/sec	Impingement Angle (B) degree	Erodent Size (C) µm	Erodent Temperature (D) ^oC	Erosion Rate (ER) mg/kg	S/N Ratio db
1	32	30	100	30	14.004	-22.9250
2	32	45	200	40	16.113	-24.1435
3	32	60	300	50	19.234	-25.6814
4	32	90	400	60	20.342	-26.1679
5	40	30	200	50	17.204	-24.7126
6	40	45	100	60	18.943	-25.5490
7	40	60	400	30	22.042	-26.8650
8	40	90	300	40	23.114	-27.2775
9	48	30	300	60	19.114	-25.6270
10	48	45	400	50	20.914	-26.4087
11	48	60	100	40	23.452	-27.4036
12	48	90	200	30	25.674	-28.1899
13	56	30	400	40	21.078	-26.4766
14	56	45	300	30	22.744	-27.1373
15	56	60	200	60	24.952	-27.9421
16	56	90	100	50	27.047	-28.6424

Table 5.2 S/N ratio response table for erosion rate of LDS coatings

Level	A	B	C	D
1	-24.73	-24.94	-26.13	-26.28
2	-26.10	-25.81	-26.25	-26.33
3	-26.91	-26.97	-26.43	-26.36
4	-27.55	-27.57	-26.48	-26.32
Delta	2.82	2.63	0.35	0.08
Rank	**1**	**2**	**3**	**4**

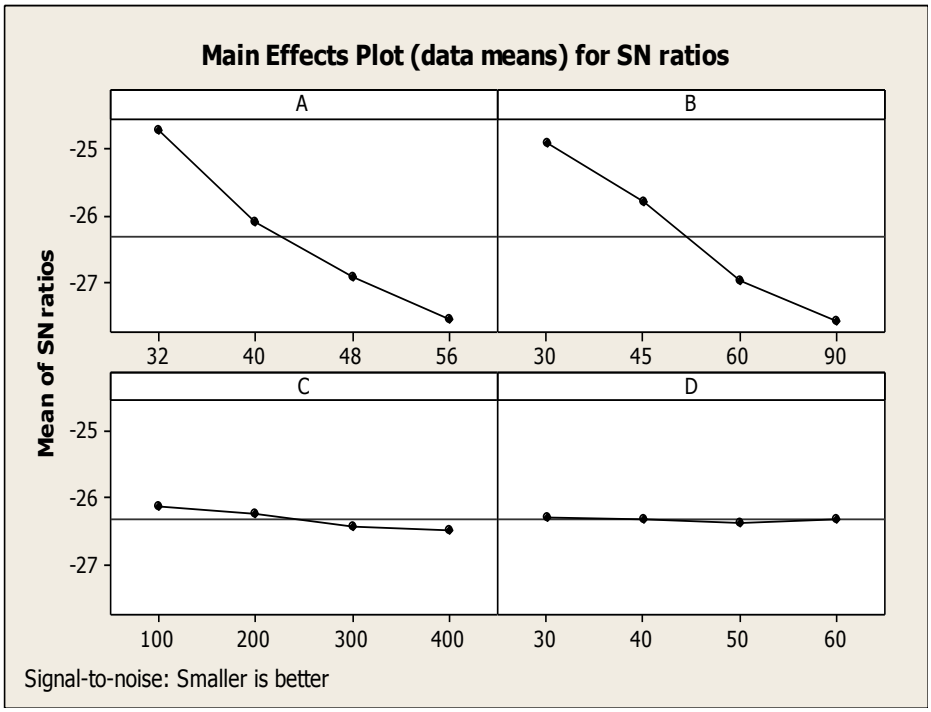

Figure 5.2 Effect of control factors on erosion rate for LDS coatings

The results of erosion experiments carried out according to the predetermined design on LDS coatings premixed with Al_2O_3 and TiO_2 particles are presented in Table 5.3. This table provides the experimental erosion rate along with the S/N ratio for each individual test run. The overall mean of the S/N ratios for 'LDS + Al_2O_3' coating is found to be -25.2434 db and for 'LDS + TiO_2' coating is found to be -25.8055 db.

The S/N ratio response analyses are presented in Tables 5.4 and 5.5 for 'LDS + Al_2O_3' and 'LDS + TiO_2' coatings respectively. These tables show the hierarchical order of the control factors as impact velocity (A), impingement angle (B), feed stock composition (E), erodent size (C) and erodent temperature (D) in decreasing order according to their significance on the erosion rate for both the coatings. It can thus be concluded that the erodent temperature (D) has negligible effect on the wear rate.

Table 5.3 Experimental design using L_{16} orthogonal array and the wear test results for 'LDS + Al_2O_3' and 'LDS + TiO_2' coatings

Test Run	A	B	C	D	E	LDS + Al_2O_3		LDS + TiO_2	
						ER	S/N Ratio	ER	S/N ratio
1	32	30	100	30	0	14.004	-22.9250	14.004	-22.9250
2	32	45	200	40	10	13.675	-22.7185	14.894	-23.4602
3	32	60	300	50	20	16.008	-24.0867	17.621	-24.9206
4	32	90	400	60	30	17.023	-24.6207	18.682	-25.4285
5	40	30	200	50	30	13.998	-22.9213	15.601	-23.8630
6	40	45	100	60	20	15.654	-23.8925	17.298	-24.7599
7	40	60	400	30	10	19.003	-25.5764	20.522	-26.2444
8	40	90	300	40	0	23.114	-27.2775	23.114	-27.2775
9	48	30	300	60	10	16.112	-24.1430	17.613	-24.9167
10	48	45	400	50	0	20.914	-26.4087	20.914	-26.4087
11	48	60	100	40	30	19.323	-25.7215	21.387	-26.6030
12	48	90	200	30	20	22.987	-27.2296	24.331	-27.7232
13	56	30	400	40	20	18.073	-25.1406	19.575	-25.8340
14	56	45	300	30	30	18.988	-25.5696	20.866	-26.3888
15	56	60	200	60	0	24.952	-27.9421	24.952	-27.9421
16	56	90	100	50	10	24.324	-27.7207	25.685	-28.1936

Note : *Factor A: Impact Velocity (m/sec), Factor B: Impingement Angle (degree)*
Factor C: Erodent Size (µm), Factor D: Erodent Temperature (^oC)
Factor E: Al_2O_3/ TiO_2 Content in the feedstock (wt%)
ER: Erosion Rate (mg/kg), S/N Ratio: Signal to Noise Ratio (db)
LDS: Linz-Donawitz slag

Table 5.4 S/N ratio response table for erosion rate of 'LDS + Al_2O_3' coatings

Level	A	B	C	D	E
1	-23.59	-23.78	-25.06	-25.33	-26.14
2	-24.92	-24.65	-25.20	-25.21	-25.04
3	-25.88	-25.83	-25.27	-25.28	-25.09
4	-26.59	-26.71	-25.44	-25.15	-24.71
Delta	3.01	2.93	0.37	0.18	1.43
Rank	**1**	**2**	**4**	**5**	**3**

Table 5.5 S/N ratio response table for erosion rate of 'LDS + TiO_2' coatings

Level	A	B	C	D	E
1	-24.18	-24.38	-25.62	-25.82	-26.14
2	-25.54	-25.25	-25.75	-25.79	-25.70
3	-26.41	-26.43	-25.88	-25.85	-25.81
4	-27.09	-27.16	-25.98	-25.76	-25.57
Delta	2.91	2.77	0.36	0.08	0.57
Rank	**1**	**2**	**4**	**5**	**3**

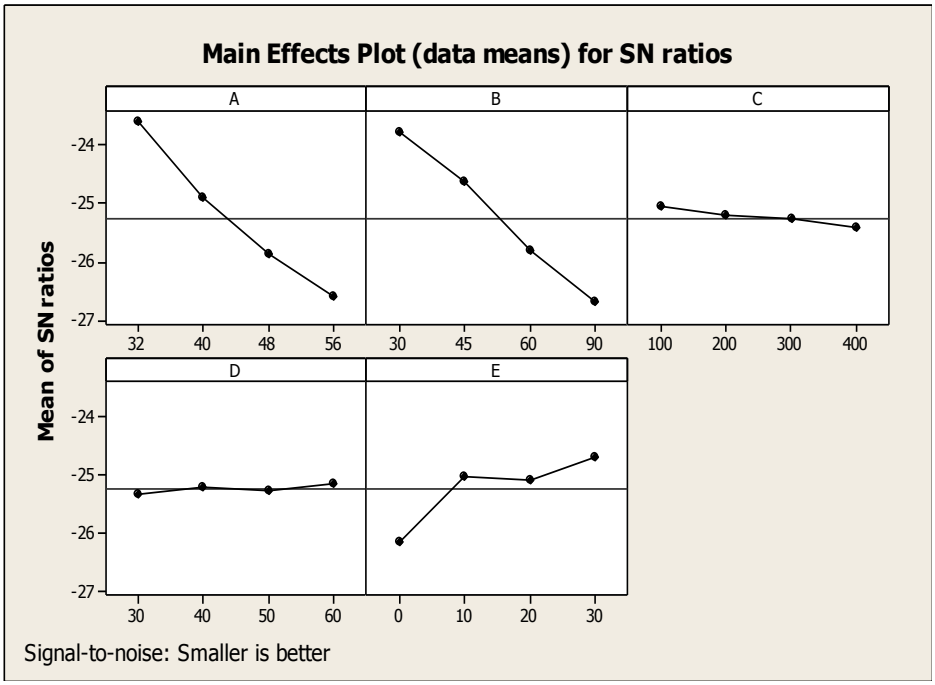

Figure 5.3 Effect of control factors on erosion rate for 'LDS + Al_2O_3'coatings

Figures 5.3 and 5.4 illustrate the effect of control factors on erosion rate for 'LDS + Al_2O_3' and 'LDS + TiO_2' coatings respectively. Analysis of the results leads to the conclusion that factor combination of A_1, B_1, C_1, D_4 and E_4 gives minimum erosion rate (Figure 5.3) for 'LDS + Al_2O_3' coatings and factor combination A_1, B_1, C_1, D_4 and E_4 gives minimum erosion rate (Figure 5.4) for 'LDS + TiO_2' coatings.

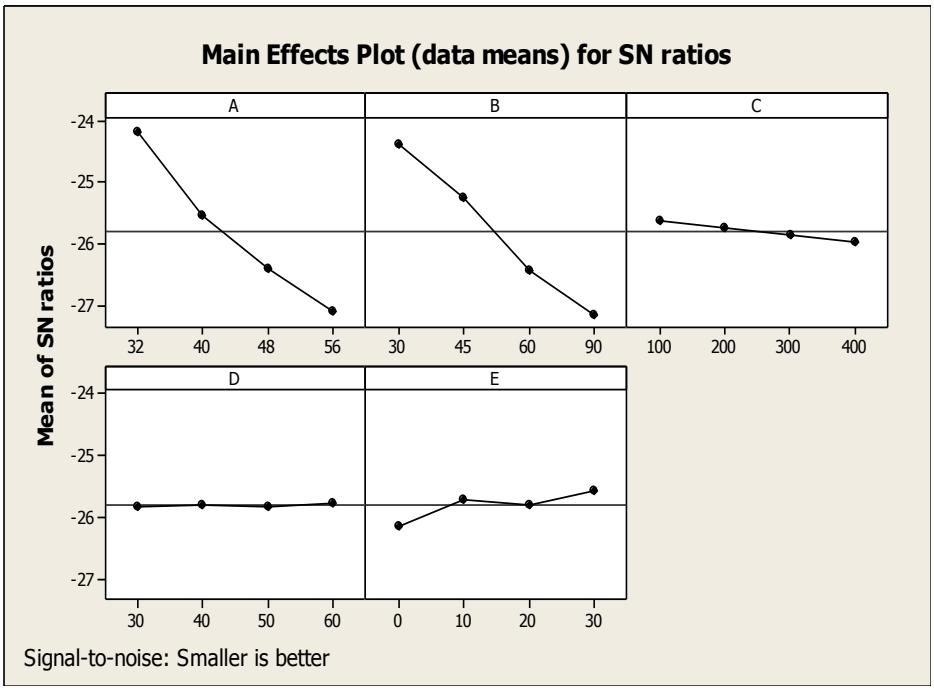

Figure 5.4 Effect of control factors on erosion rate for 'LDS + TiO_2'coatings

5.3 Confirmation Experiment

The confirmation experiment is the final test in the design-of-experiment process. The purpose of the confirmation experiment is to validate the conclusions drawn during the analysis phase. It is performed by considering a new arbitrary set of factors other than the optimal factor setting to evaluate the erosion rate. For this investigation $A_2B_3C_4D_1$, $A_2B_3C_1D_4E_2$ and $A_3B_2C_3D_1E_3$ for LDS, 'LDS + Al_2O_3' and 'LDS + TiO_2' coatings respectively are chosen as the arbitrary sets considering which prediction equations can be formulated using Taguchi's approach to estimate S/N ratios for erosion rate as [360]:

$$\overline{\eta_1} = \overline{T} + \left(\overline{A_2} - \overline{T}\right) + \left(\overline{B_3} - \overline{T}\right) + \left(\overline{C_4} - \overline{T}\right) + \left(\overline{D_1} - \overline{T}\right) \quad \textbf{(5.1)}$$

$$\overline{\eta_2} = \overline{T} + \left(\overline{A_2} - \overline{T}\right) + \left(\overline{B_3} - \overline{T}\right) + \left(\overline{C_1} - \overline{T}\right) + \left(\overline{D_4} - \overline{T}\right) + \left(\overline{E_2} - \overline{T}\right) \quad \textbf{(5.2)}$$

$$\overline{\eta_3} = \overline{T} + \left(\overline{A_3} - \overline{T}\right) + \left(\overline{B_2} - \overline{T}\right) + \left(\overline{C_3} - \overline{T}\right) + \left(\overline{D_1} - \overline{T}\right) + \left(\overline{E_3} - \overline{T}\right) \quad \textbf{(5.3)}$$

$\overline{\eta_1}$, $\overline{\eta_2}$, $\overline{\eta_3}$	Predicted average for LDS, 'LDS + Al_2O_3' and 'LDS + TiO_2' coatings respectively
$\overline{T}$	Overall experimental average
$\overline{A}, \overline{B}, \overline{C}, \overline{D}, \overline{E}$	Mean response for factors

By combining like terms, the equations reduce to

$$\overline{\eta_1} = \overline{A_2} + \overline{B_3} + \overline{C_4} + \overline{D_1} - 3\overline{T} \quad \textbf{(5.4)}$$

$$\overline{\eta_2} = \overline{A_2} + \overline{B_3} + \overline{C_1} + \overline{D_4} + \overline{E_2} - 4\overline{T} \quad \textbf{(5.5)}$$

$$\overline{\eta_3} = \overline{A_3} + \overline{B_2} + \overline{C_3} + \overline{D_1} + \overline{E_3} - 4\overline{T} \quad \textbf{(5.6)}$$

Table 5.6 Results of the confirmation experiments for erosion rate

	Optimal Control Parameters					
	LDS Coatings		**LDS+Al_2O_3 Coatings**		**LDS+TiO_2 Coatings**	
	Pred.	**Exp.**	**Pred.**	**Exp.**	**Pred.**	**Exp.**
Level	$A_1B_1C_1D_1$	$A_1B_1C_1D_1$	$A_1B_1C_1D_4E_4$	$A_1B_1C_1D_4E_4$	$A_1B_1C_1D_4E_4$	$A_1B_1C_1D_4E_4$
S/N ratio for erosion rate (db)	-22.1086	-22.6271	-21.3191	-21.5454	-22.2990	-22.6814
Percentage Error	2.29%		1.05%		1.68%	

	Arbitrary set of Control Parameters					
	LDS Coatings		**LDS+Al_2O_3 Coatings**		**LDS+TiO_2 Coatings**	
	Pred.	**Exp.**	**Pred.**	**Exp.**	**Pred.**	**Exp.**
Level	$A_2B_3C_4D_1$	$A_2B_3C_4D_1$	$A_2B_3C_1D_4E_2$	$A_2B_3C_1D_4E_2$	$A_3B_2C_3D_1E_3$	$A_3B_2C_3D_1E_3$
S/N ratio for erosion rate (db)	-26.8674	-27.7702	-25.0292	-25.3174	-25.9507	-26.4352
Percentage Error	3.25%		1.13%		1.83%	

For these arbitrarily chosen combinations of factors, the S/N ratios for LDS, 'LDS + Al_2O_3' and 'LDS + TiO_2' coatings are found to be -26.8674, -25.0292 and -25.9507 db respectively while those for the optimal combinations of factors happen to be -22.1086, -21.3191 and -22.2990 db respectively. Each of these

values is smaller than the S/N ratio value for the corresponding optimal factor combination. This confirms the optimized combinations of control factors for the respective coatings. Further, an experiment is also conducted taking the same factor combination and the test results are compared with values obtained from the predictive Equations 5.4, 5.5 and 5.6. The comparison of the experimental and the predicted results along with the associated error percentage are given in Table 5.6. The proposed correlations are thus capable of predicting erosion rate to a reasonable accuracy.

5.4 Predictive Equation for Determination of Erosion Rate

The solid particle erosion wear rate of the coated sample can also be predicted using a nonlinear regressive predictive equation showing the relationship between the erosion rate and the individual control factors. This correlation is developed statistically using the standard software SYSTAT 7. In order to express the erosion rate in terms of a nonlinear regressive mathematical equation, the following form is suggested:

$$ER = k_0 + k_1 \times A + k_2 \times B + k_3 \times C + k_4 \times D + k_5 \times E \quad \textbf{(5.7)}$$

Here, ER is the performance output term i.e. the erosion rate in mg/kg and k_i (i = 0, 1, 2, 3, 4, 5) are the model constants. A is the impact velocity (m/sec), B is the impingement angle (degree), C is the erodent size (µm) and D is the erodent temperature (^{0}C) and E is the Al_2O_3/ TiO_2 content in the feedstock (wt%).

By using the software, the values of all of the constants are calculated and the final nonlinear regression expressions for the LDS, 'LDS + Al_2O_3' and 'LDS + TiO_2' coatings are obtained by the Equations 5.8, 5.9 and 5.10 respectively.

$$ER = 3.379 + 0.269 \times A + 0.104 \times B + 0.001 \times C - 0.007 \times D \quad \textbf{(5.8)}$$

$$ER = 2.658 + 0.264 \times A + 0.106 \times B + 0.001 \times C - 0.007 \times D - 0.103 \times E \quad \textbf{(5.9)}$$

$$ER = 2.965 + 0.267 \times A + 0.105 \times B + 0.001 \times C - 0.007 \times D - 0.048 \times E \quad \textbf{(5.10)}$$

The correctness of the calculated constants is confirmed because very high correlation coefficients (r^2) of 0.999, 0.998 and 0.999 for the LDS, 'LDS + Al_2O_3' and 'LDS + TiO_2' coatings respectively are obtained for Equation (5.7); therefore, the models are quite suitable for further analysis. Comparisons between the wear rates obtained from experimental results and the predictive equations for all the three coating types are shown in Table 5.7, which indicates that the percentage error associated with the predicted values with respect to the experimental one varies in the range of 0 to 9 %.

Table 5.7 Comparison of experimental and predicted values for erosion rate

LDS			LDS + Al_2O_3			LDS + TiO_2		
ER Exp.	**ER Pred.**	**% Error**	**ER Exp.**	**ER Pred.**	**% Error**	**ER Exp.**	**ER Pred.**	**% Error**
14.004	14.997	7.090	14.004	14.176	1.228	14.004	14.549	3.891
16.113	16.587	2.941	13.675	14.866	8.709	14.894	15.674	5.237
19.234	18.177	5.495	16.008	15.356	4.072	17.621	16.799	4.664
20.342	21.327	4.842	17.023	17.536	3.013	18.682	19.499	4.373
17.204	17.109	0.552	13.998	13.158	6.000	15.601	15.205	2.538
18.943	18.499	2.343	15.654	15.608	0.293	17.298	17.090	1.202
22.042	20.569	6.682	19.003	18.738	1.394	20.522	19.655	4.224
23.114	23.519	1.752	23.114	22.778	1.453	23.114	23.115	0.004
19.114	19.291	0.926	16.112	17.360	7.745	17.613	18.331	4.076
20.914	21.021	0.511	20.914	20.150	3.653	20.914	20.556	1.711
23.452	22.351	4.694	19.323	18.420	4.673	21.387	20.461	4.329
25.674	25.641	0.128	22.987	22.800	0.813	24.331	24.261	0.287
21.078	21.683	2.870	18.073	18.682	3.369	19.575	20.227	3.330
22.744	23.213	2.062	18.988	19.212	1.179	20.866	21.292	2.041
24.952	24.463	1.959	24.952	23.582	5.490	24.952	23.997	3.827
27.047	27.553	1.870	24.324	25.702	5.665	25.685	26.637	3.706

Note: *ER: Erosion Rate (mg/kg)*

LDS: Linz-Donawitz slag

5.5 Analysis and Prediction of Erosion Response using ANN

As mentioned earlier, artificial neural network (ANN) is a technique that involves database training to predict input-output evolutions. In this attempt to simulate the erosion wear process and to predict the erosion rate for LDS, 'LDS + Al_2O_3' and 'LDS + TiO_2' coatings under different operating conditions, certain input parameters are taken each of which is characterized by one neuron in the input layer of the ANN structure. Different ANN structures with varying number of neurons in the hidden layer are tested at constant cycles, learning rate, error tolerance, momentum parameter, noise factor and slope parameter. Based on least error criterion, three ANN structures (one structure for each coating type) shown in Tables 5.8, 5.9 and 5.10 are selected for training of the input-output data for different types of coatings.

Table 5.8 Input parameters for training (LDS coatings)

Input Parameters for Training	Values
Error tolerance	0.003
Learning rate (β)	0.002
Momentum parameter (α)	0.002
Noise factor (NF)	0.001
Number of epochs	1,00,00,000
Slope parameter (£)	0.6
Number of hidden layer neurons (H)	7
Number of input layer neurons (I)	4
Number of output layer neurons (O)	1

Table 5.9 Input parameters for training ('LDS + Al_2O_3' coatings)

Input Parameters for Training	Values
Error tolerance	0.003
Learning rate (β)	0.002
Momentum parameter (α)	0.002
Noise factor (NF)	0.001
Number of epochs	1,00,00,000
Slope parameter (£)	0.6
Number of hidden layer neurons (H)	9
Number of input layer neurons (I)	5
Number of output layer neurons (O)	1

Table 5.10 Input parameters for training ('LDS + TiO_2' coatings)

Input Parameters for Training	Values
Error tolerance	0.003
Learning rate (β)	0.002
Momentum parameter (α)	0.002
Noise factor (NF)	0.001
Number of epochs	1,00,00,000
Slope parameter (£)	0.6
Number of hidden layer neurons (H)	7
Number of input layer neurons (I)	5
Number of output layer neurons (O)	1

The optimized three-layer neural networks used in these simulations are shown in Figures 5.5, 5.6 and 5.7 which are for the three different types of coatings taken in this study. A software package NEURALNET for neural computing based on back propagation algorithm is used as the prediction tool for erosion wear rate of the coatings under various test conditions.

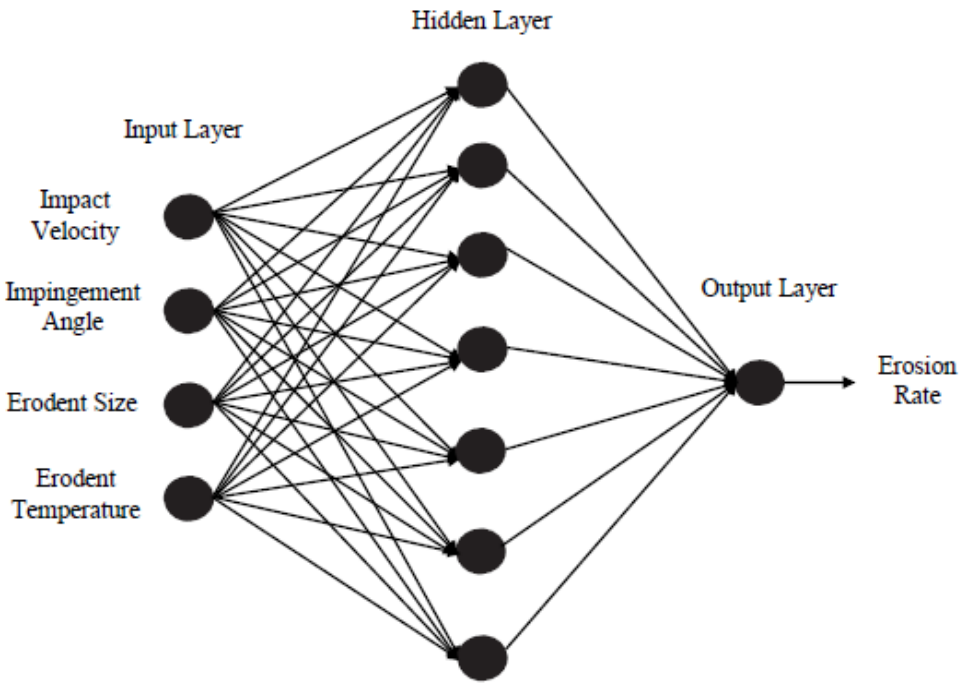

Figure 5.5 Three layer neural network (LDS coatings)

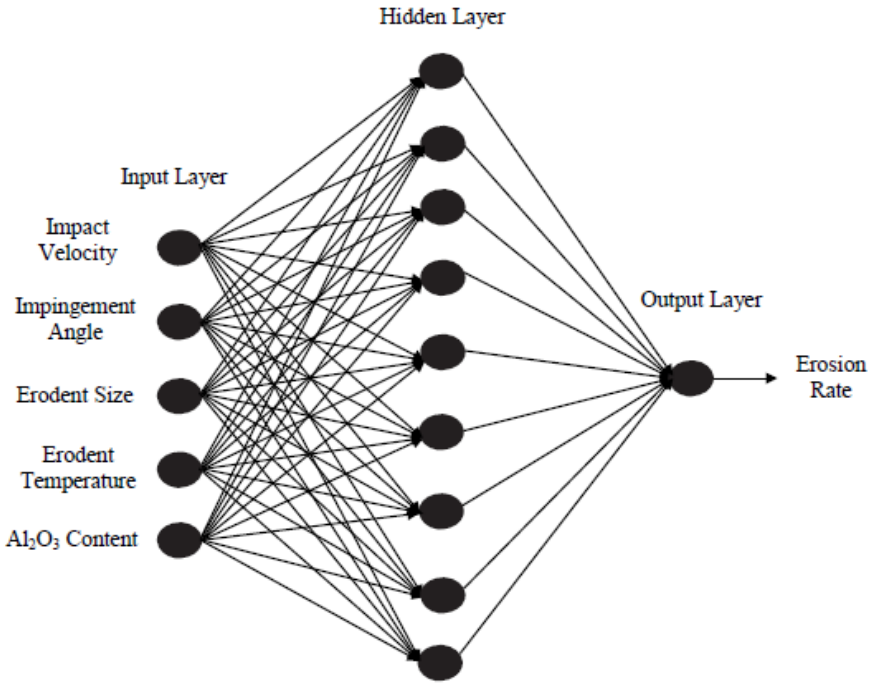

Figure 5.6 Three layer neural network ('LDS + Al_2O_3' coatings)

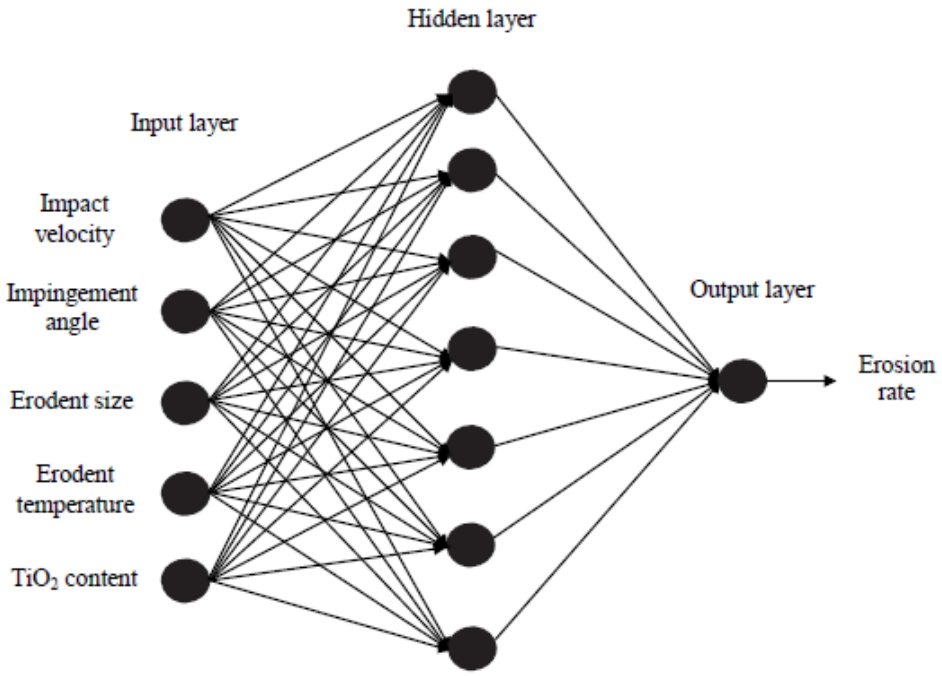

Figure 5.7 Three layer neural network ('LDS + TiO_2' coatings)

The ANN predictive results of erosion wear rates for all the 16 test conditions and for all the coating material combinations are shown and compared with the corresponding experimental values along with the associated percentage errors in Table 5.11. It is observed that the errors lie in the range of 0-7%, which establishes the validity of the neural computation. The errors, however, can still be reduced and the quality of predictions can be further improved by enlarging the data sets and optimizing the construction of the neural network.

Table 5.11 Percentage error between experimental results and ANN predictions

LDS			LDS + Al_2O_3			LDS + TiO_2		
ER Exp.	**ER ANN**	**% Error**	**ER Exp.**	**ER ANN**	**% Error**	**ER Exp.**	**ER ANN**	**% Error**
14.004	14.8253	5.864	14.004	14.3254	2.295	14.004	14.5482	3.886
16.113	16.8550	4.604	13.675	14.3563	4.982	14.894	15.7984	6.072
19.234	18.5693	3.455	16.008	15.7347	1.707	17.621	16.9258	3.945
20.342	20.7600	2.054	17.023	17.3154	1.717	18.682	19.1835	2.684
17.204	16.8853	1.852	13.998	13.1830	5.822	15.601	14.9652	4.075
18.943	18.3712	3.018	15.654	15.7411	0.556	17.298	16.9536	1.990
22.042	21.2310	3.679	19.003	18.8177	0.975	20.522	19.8736	3.159
23.114	23.2823	0.728	23.114	23.2437	0.561	23.114	23.2425	0.555
19.114	19.0403	0.385	16.112	16.7724	4.098	17.613	17.9750	2.055
20.914	21.3766	2.211	20.914	20.1831	3.494	20.914	20.7965	0.561
23.452	22.3304	4.782	19.323	18.5651	3.922	21.387	20.3430	4.881
25.674	25.5869	0.339	22.987	22.7418	1.066	24.331	24.2487	0.338
21.078	21.1119	0.160	18.073	18.2506	0.982	19.575	19.8185	1.243
22.744	23.1881	1.952	18.988	19.3581	1.949	20.866	21.1811	1.510
24.952	24.6461	1.225	24.952	24.8850	0.268	24.952	24.6702	1.129
27.047	27.0762	0.107	24.324	25.8285	6.185	25.685	27.2898	6.248

Note: *ER: Erosion Rate (mg/kg)*

LDS: Linz-Donawitz slag

A well-trained ANN is expected to be very helpful for the analysis of erosion wear characteristics of any given coating and permits to study quantitatively the effect of each of the considered input parameters on the wear rate. The range of any chosen parameter can be beyond the actual experimental limits, thus offering the possibility to use the generalization property of ANN in a large parameter space. In the present investigation, this possibility has been explored by selecting the most significant factor i.e. the impact velocity in a range from 25 to 75 m/sec. Sets of predictions for erosion wear rate of LDS, 'LDS + Al_2O_3' and 'LDS + TiO_2' coatings at different impact velocities and impingement angles are evolved and the predicted evolutions are presented in Figures 5.8, 5.9 and 5.10 respectively.

It is interesting to see that the erosion rate presents either a linear or an exponential type evolution with the impact velocity (Figures 5.8 (a), 5.9 (a) and 5.10 (a)). As the velocity of impact of the erodent increases, the kinetic energy carried by it also increases. This causes transfer of greater amount of energy to the target coating surface upon impact and leads to higher material loss due to erosion. The results are presented in Figures 5.8 (b), 5.9 (b) and 5.10 (b) which shows at an impingement angle of 90^0 the peak erosion takes place for all the coatings made of LDS pre-mixed with Al_2O_3/TiO_2. Thus, it suggests that these coatings respond to solid particle erosion in a purely brittle manner. In fact, the angle of impact determines the relative magnitude of the two components of the impact velocity namely, the components normal to the surface and parallel to the surface. The normal component will determine how long the impact will last (i.e. contact time) and the load. The product of this contact time and the tangential (parallel) velocity component determines the amount of sliding that takes place. The tangential velocity component also provides a shear loading to the surface, which is in addition to the normal load that the normal velocity component causes. Hence, as this angle changes the amount of sliding that takes place also changes the nature and magnitude of the stress system. Both of these aspects influence the way a coating wears out.

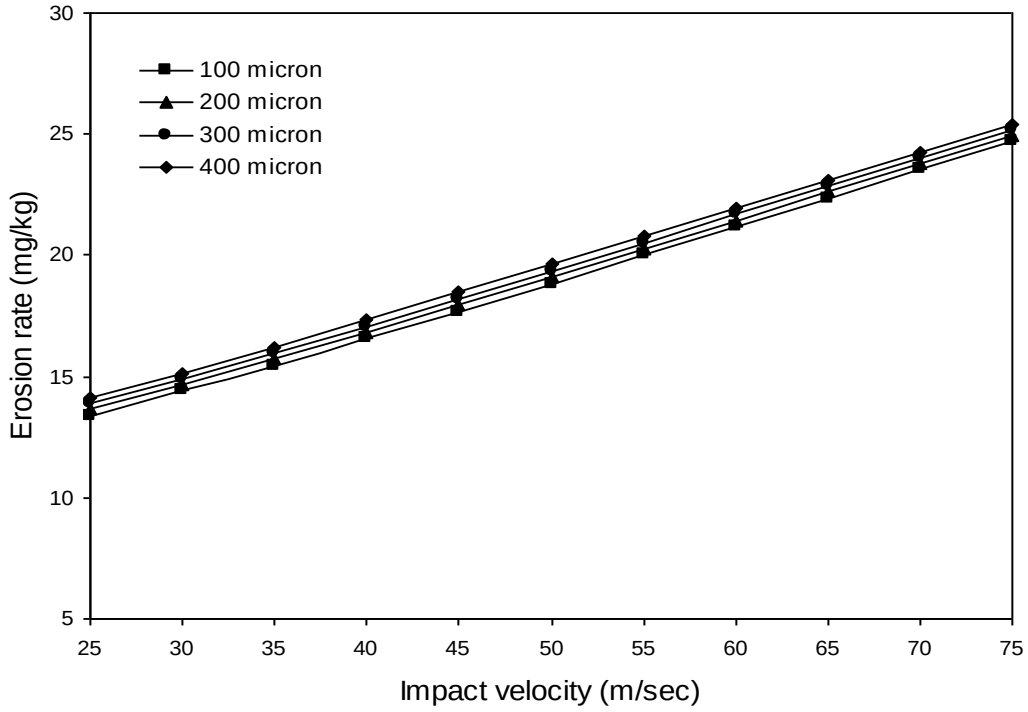

(a)

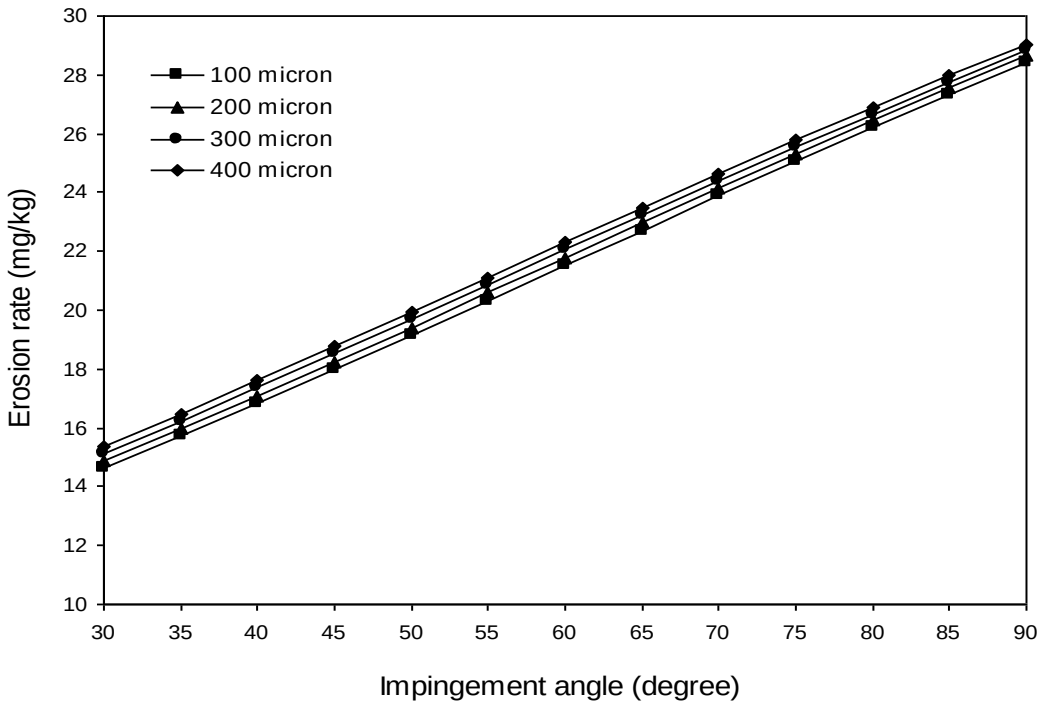

(b)

Figure 5.8 Effect of (a) impact velocity and (b) impingement angle on erosion rate for different erodent size for LDS coatings

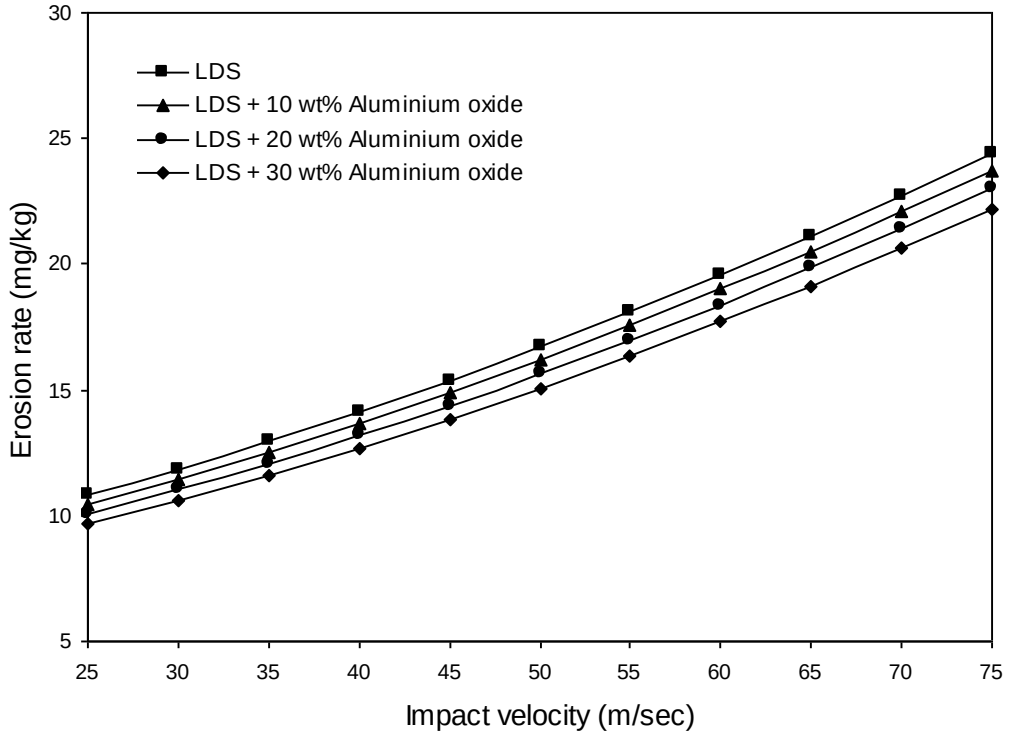

(a)

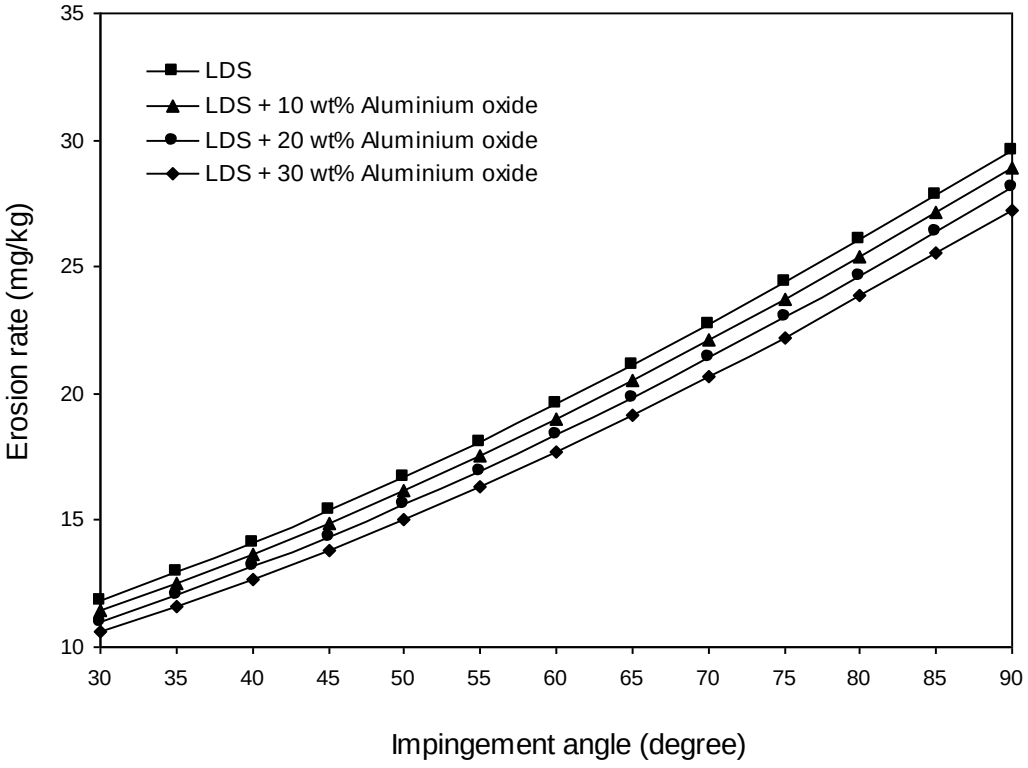

(b)

Figure 5.9 Effect of (a) impact velocity and (b) impingement on erosion rate for different LDS content for 'LDS + Al_2O_3' coatings

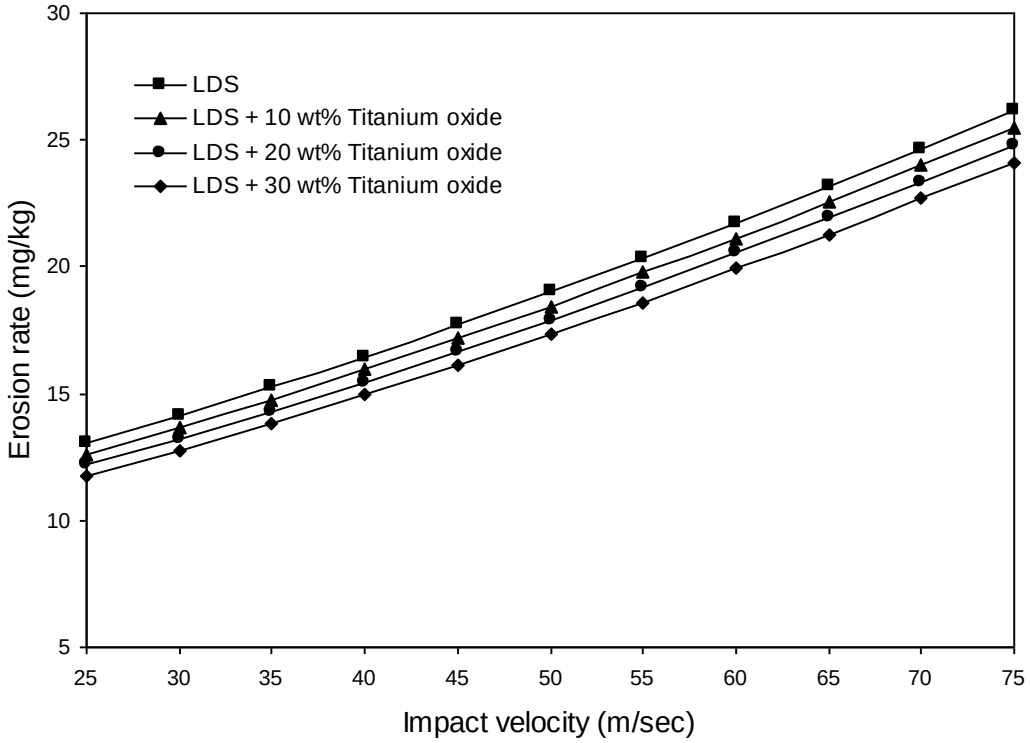

(a)

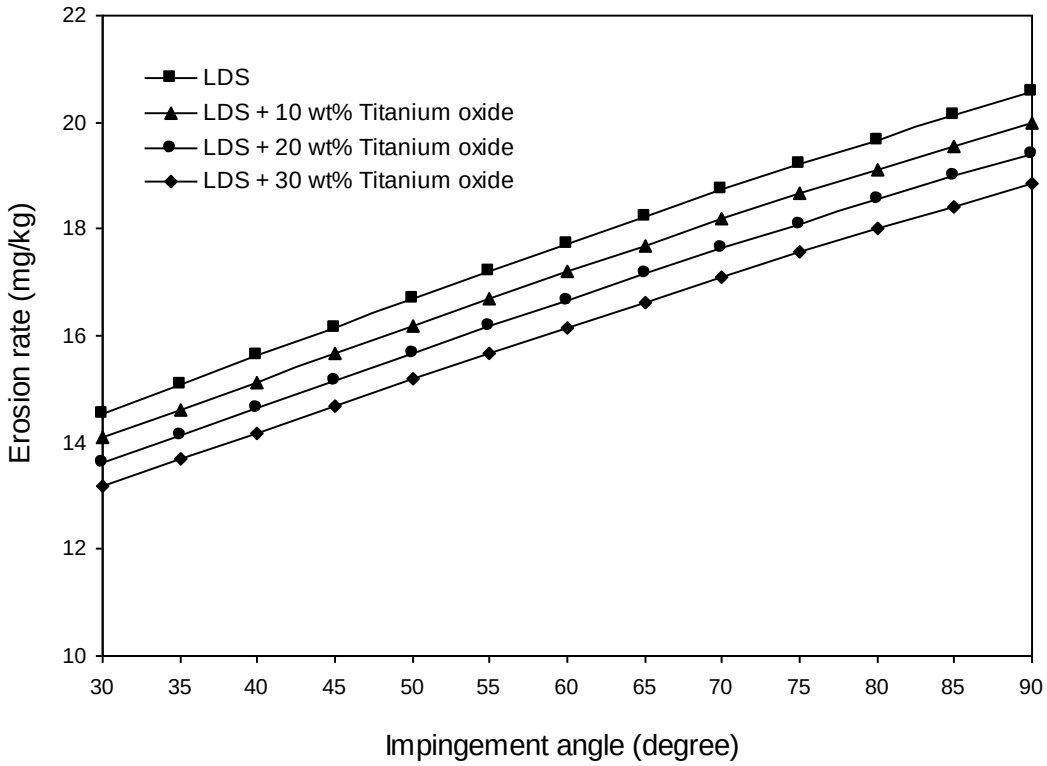

(b)

Figure 5.10 Effect of (a) impact velocity and (b) impingement on erosion rate for different LDS content for 'LDS + TiO_2' coatings

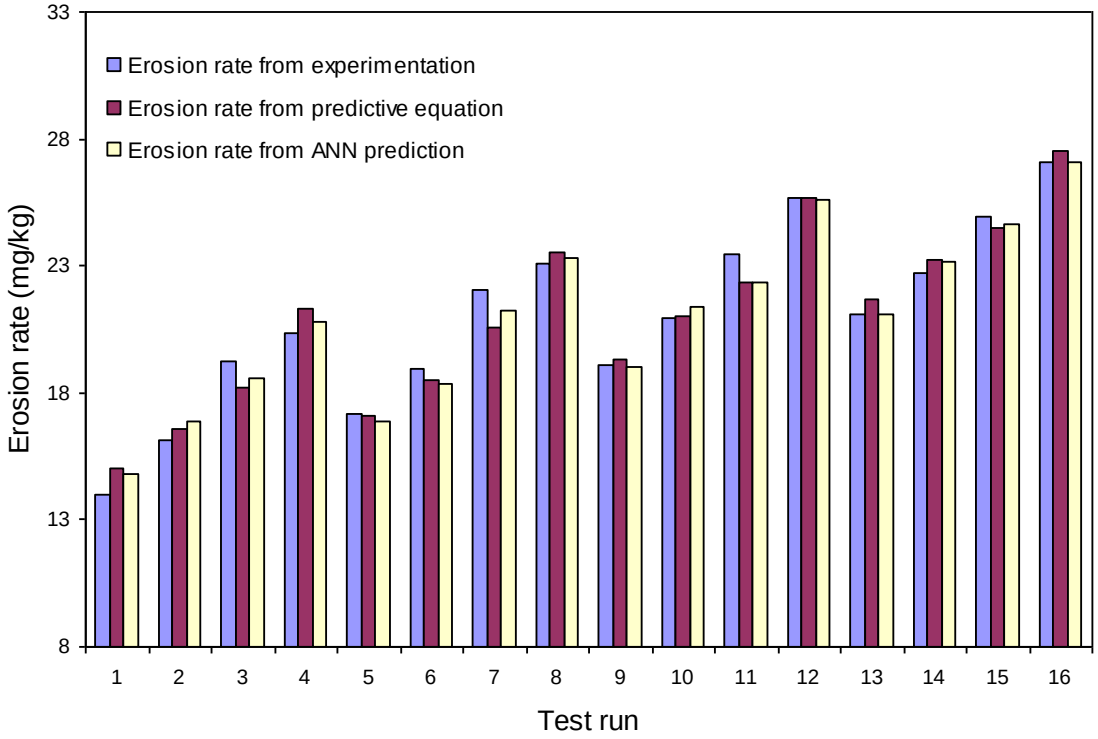

Figure 5.11 Comparison of erosion rates of LDS coatings obtained from different methods

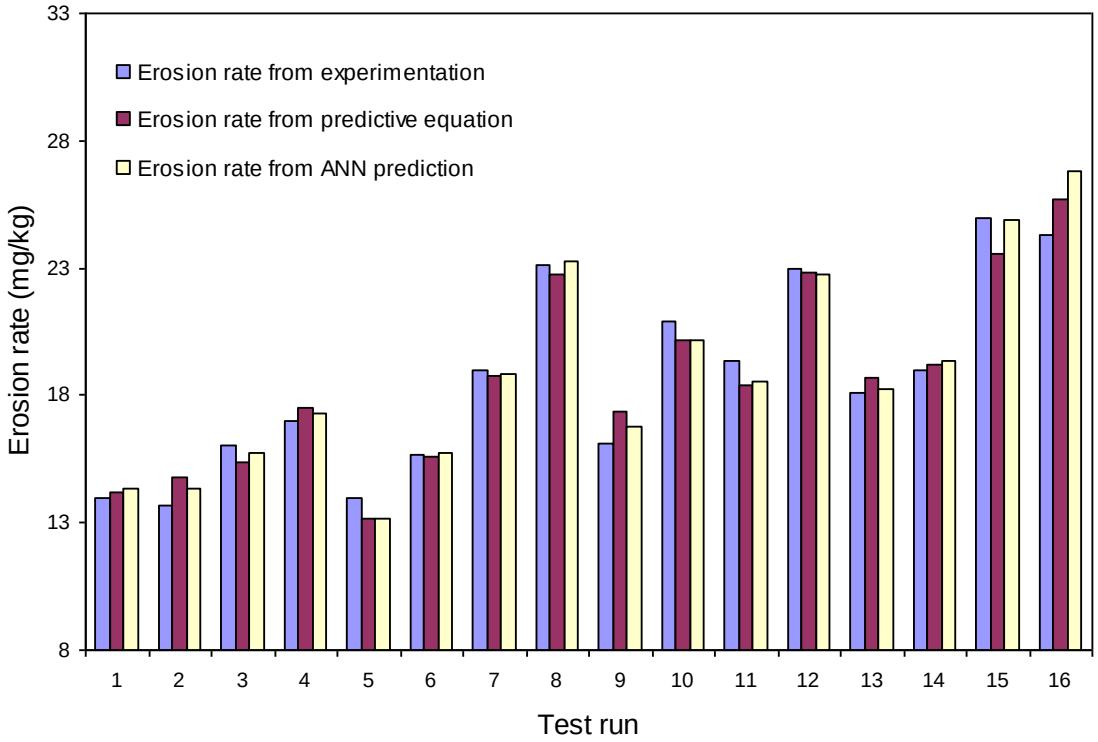

Figure 5.12 Comparison of erosion rates of 'LDS + Al_2O_3' coatings obtained from different methods

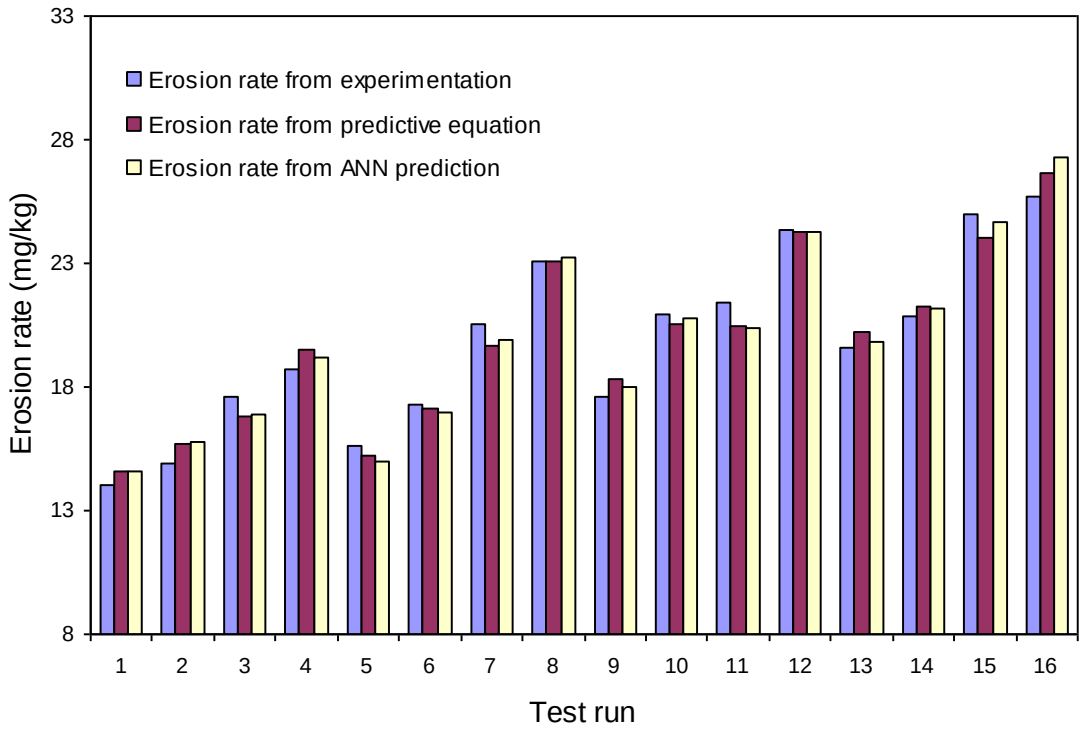

Figure 5.13 Comparison of erosion rates of 'LDS + TiO_2' coatings obtained from different methods

Similar observations have also been reported by previous investigators for other plasma sprayed ceramic coatings [90, 215, 361, 362]. It has also been reported in the past that impact velocity happens to be an important test variable in any erosion test and can easily overshadow changes in other variables such as erodent size, impingement angle etc. [362]. Erosion rate (ER) depends on velocity (V) by a power law, given as $ER = k.V^n$, where k is a material constant. However, the exponent n is reported to be material independent and is governed by test conditions including particle characteristics and the erosion test apparatus [298, 363, 364].

Comparison of the measured erosion rates of LDS, 'LDS + Al_2O_3' and 'LDS + TiO_2' coatings with those obtained using the two prediction models proposed in this work are presented in Figures 5.11, 5.12 and 5.13 respectively. While the errors associated with the ANN predictions lie in the range of 0-7 %, the same

for results obtained from the proposed correlation lie in the range of 0-9%. Thus it can be concluded that the results obtained from the predictive model based on ANN are relatively closer to the measured values of erosion rates. However, both the ANN and the predictive equations are equally useful for wear rate prediction in similar situations.

Chapter Summary

This chapter has provided a critical analysis of the test results related to the solid particle erosion characteristics of LDS, 'LDS + Al_2O_3' and 'LDS + TiO_2' coatings using Taguchi experimental design. Significant control factors affecting the erosion rate have been identified through successful implementation of this technique. Impact velocity and impingement angle in declining sequence are found to be highly significant for minimizing the erosion rate.

The experimental results suggest the potential of LD slag to be used as a wear resistant coating material for deposition on aluminium substrates. The research presented in this chapter further illustrates that the use of a neural network model to simulate experiments with parametric design strategy is effective, efficient and helps to predict the solid particle erosion response of LDS based coatings under different test conditions within and beyond the experimental domain. The predicted and the experimental values of erosion wear rate exhibit good agreement and validate the remarkable prediction capability of a well-trained neural network for this kind of processes.

The next chapter presents the physical and mechanical properties of the LDS filled polymer composites.

*****

Chapter 6

Composite Characterization

Chapter 6

COMPOSITE CHARACTERIZATION

This chapter provides the physical and mechanical characterization of the composites under the present investigation. The measured values of different properties of the epoxy and polypropylene composites filled with different weight fractions of Linz-Donawitz slag (LDS) with and without fiber reinforcement are reported. The results of various characterization tests are presented and the effects of LDS on the modified composite properties are discussed.

6.1 Physical Characterization

Density and Void Fraction

Density is a material property which is of prime importance in several weight sensitive applications. Thus, in many such applications, polymer composites are found to replace conventional metals and materials primarily for their low densities. Density of a composite depends on the relative proportion of matrix and the reinforcing materials and this is one of the most important factors determining the properties of the composites. There is always a difference between the measured and the theoretical density values of a composite due to the presence of voids and pores. These voids significantly affect some of the mechanical properties and even the performance of composites. Higher void contents usually mean lower fatigue resistance, greater susceptibility to water penetration and weathering [348]. The information about the amount of void content is desirable for estimation of the quality of the composites. In the present research work, the measured and theoretical densities of LDS filled epoxy and polypropylene composites (with and without fiber reinforcement) are reported along with the corresponding volume fraction of voids in Table 6.1 and Table 6.2 respectively.

Table 6.1 Measured and theoretical densities along with the void fractions of the Epoxy-LDS composites with and without glass fiber

Composition	Measured density (g/cm^3)	Theoretical density (g/cm^3)	Volume fraction of voids (%)
Epoxy + 0 wt% LDS	1.098	1.100	0.18
Epoxy + 7.5 wt% LDS	1.159	1.163	0.34
Epoxy + 15 wt% LDS	1.217	1.223	0.49
Epoxy + 22.5 wt% LDS	1.261	1.269	0.63
Epoxy + 30 wt% LDS	1.312	1.322	0.75
Epoxy + 20 wt% SGF + 0 wt% LDS	1.223	1.238	1.211
Epoxy + 20 wt% SGF + 7.5 wt% LDS	1.285	1.307	1.683
Epoxy + 20 wt% SGF + 15 wt% LDS	1.364	1.401	2.640
Epoxy + 20 wt% SGF + 22.5 wt% LDS	1.468	1.521	3.484

** LDS: Linz-Donawitz slag; SGF: Short Glass Fiber*

Table 6.2 Measured and theoretical densities along with the void fractions of the Polypropylene-LDS composites with and without glass fiber

Composition	Measured density (gm/cc)	Theoretical density (gm/cc)	Volume fraction of voids (%)
PP + 0 wt% LDS	0.899	0.900	0.01
PP + 7.5 wt% LDS	0.953	0.956	0.31
PP + 15 wt% LDS	0.981	0.985	0.40
PP + 22.5 wt% LDS	1.018	1.024	0.58
PP + 30 wt% LDS	1.106	1.113	0.62
PP + 20 wt% SGF + 0 wt% LDS	1.027	1.035	0.772
PP + 20 wt% SGF + 7.5 wt % LDS	1.092	1.107	1.355
PP + 20 wt% SGF + 15 wt% LDS	1.178	1.204	2.159
PP + 20 wt% SGF + 22.5 wt% LDS	1.286	1.318	2.427

**PP: Polypropylene; LDS: Linz-Donawitz Slag; SGF: Short Glass Fiber*

The difference between the measured and theoretical density is a measure of voids and pores present in the composites. It is observed that, by the addition of LDS, the density of the composites gradually increases. It is obvious as the density of LDS (1.75 g/cm^3) is higher than those of the polymers taken in this work. As the filler content in the composite increases from 0 to 30 wt%, the volume fraction of voids is also found to be increasing. Similar observations have been reported earlier by previous researchers [176, 285]. Similar trends are noticed for these composites even when they are reinforced with glass fibers. It is also observed that the void fraction in PP based composites is much less compared to the epoxy based composites with similar reinforcement. This difference is attributed to the fact that the processing routes for these two types of composites are different. The PP composites are fabricated by injection molding route while the epoxy composites are made by hand lay-up technique.

It is understandable that a good composite should have fewer voids [365]. However, presence of void is unavoidable in composite making particularly through hand lay-up route. The composites under the present investigation possess very less voids (maximum ≈ 4%) and can thus be termed as good composites.

6.2 Mechanical Characterization

Evaluation of strength and other mechanical properties of any new composite is essential from research as well as functionality point of view. Various authors have earlier characterized mechanical properties of different polymeric materials on different occasions [366-370]. In the present work, a wealth of property data has been generated by conducting different characterization tests under controlled laboratory conditions to evaluate various mechanical characteristics of the composites fabricated for this work. The property values are presented in Table 6.3.

6.2.1 Micro-hardness

Hardness is considered as one of the most important material properties that govern the wear resistance of any material. In the present work, micro-hardness

values of the epoxy and PP based composites filled with LDS particles (with and without fiber reinforcement) are measured. The test results are presented in Table 6.3 and are shown graphically in Figure 6.1. It is evident that with addition of LDS particles, micro-hardness values of the composites are improved irrespective of the matrix type and this improvement is a function of the filler content. As far as the comparison between the epoxy and PP composites is concerned, the PP based composites exhibit superior micro-hardness values than the epoxy composites. Among all the composites under this investigation, the maximum hardness value is recorded for PP reinforced with 30 wt% LDS (79.03 Hv) and this value is about 13 times the hardness of neat PP.

Table 6.3 Mechanical properties of the composites

Sample Composition	Tensile strength (MPa)	Tensile modulus (GPa)	Flexural strength (MPa)	Impact strength (kJ/m^2)	Micro-hardness (Hv)
EP + 0 wt% LDS	48.00	3.20	22.50	17.2	8.667
EP + 7.5 wt% LDS	41.85	2.82	18.43	19.6	10.60
EP + 15 wt% LDS	39.17	2.64	14.72	21.3	16.52
EP + 22.5 wt% LDS	37.28	2.43	12.67	23.7	21.72
EP + 30 wt% LDS	36.43	2.21	10.51	25.8	27.94
EP + 20 wt% SGF + 0 wt% LDS	221.37	5.41	204.23	28.7	22.53
EP + 20 wt% SGF + 7.5 wt% LDS	208.82	4.96	172.94	31.4	24.61
EP + 20 wt% SGF + 15 wt% LDS	179.63	4.51	158.57	33.7	28.48
EP + 20 wt% SGF + 22.5 wt% LDS	154.37	4.36	146.26	34.6	31.74
PP + 0 wt% LDS	39.00	1.83	29.23	17.9	5.91
PP + 7.5 wt% LDS	35.25	1.58	23.71	20.4	20.19
PP + 15 wt% LDS	30.74	1.46	19.82	25.6	41.6
PP + 22.5 wt% LDS	28.46	1.41	15.17	27.2	68.11
PP + 30 wt% LDS	26.63	1.32	13.42	29.7	79.03
PP + 20 wt% SGF + 0 wt% LDS	180.32	6.32	243.25	32.8	11.73
PP + 20 wt% SGF + 7.5 wt % LDS	144.58	5.86	215.42	34.8	35.89
PP + 20 wt% SGF + 15 wt% LDS	126.35	5.54	192.35	37.3	66.38
PP + 20 wt% SGF + 22.5 wt% LDS	115.63	5.37	174.51	40.2	76.68

**EP: Epoxy; PP: Polypropylene; SGF: Short Glass Fiber; LDS: Linz-Donawitz Slag*

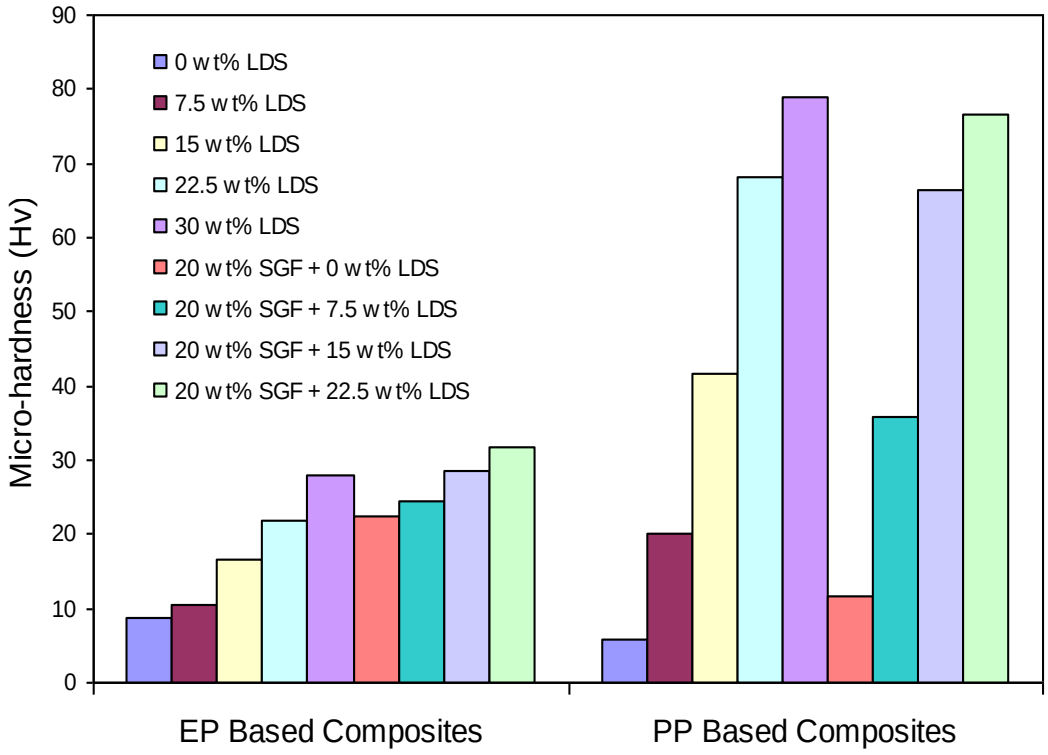

Figure 6.1 Micro-hardness of LDS filled composites

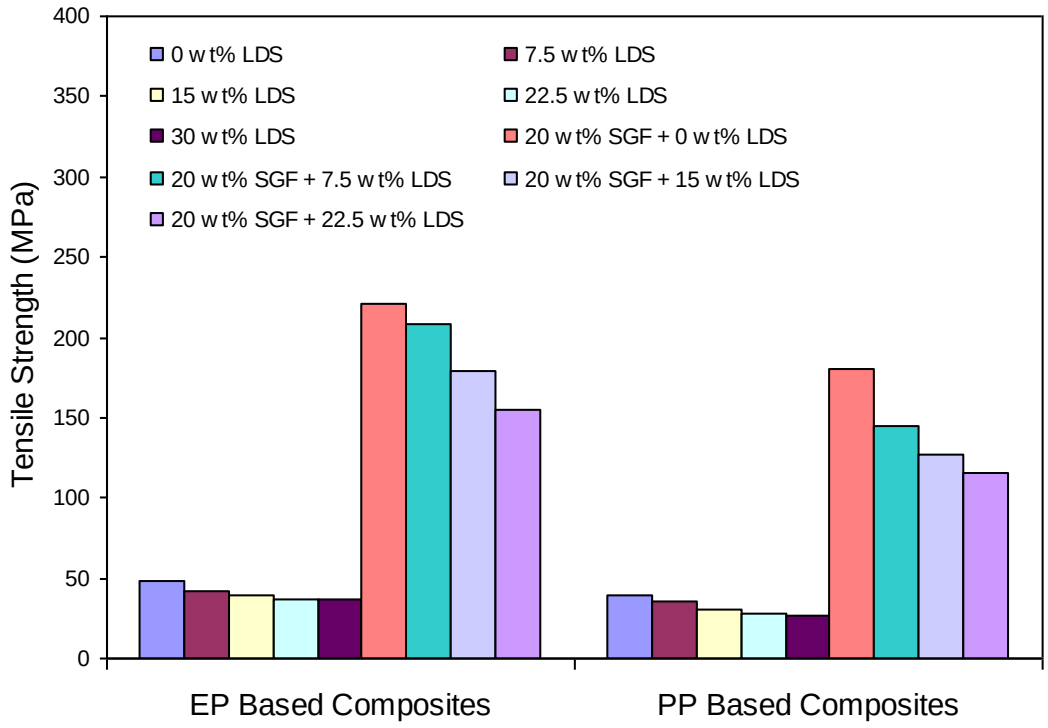

Figure 6.2 Tensile strength of LDS filled composites

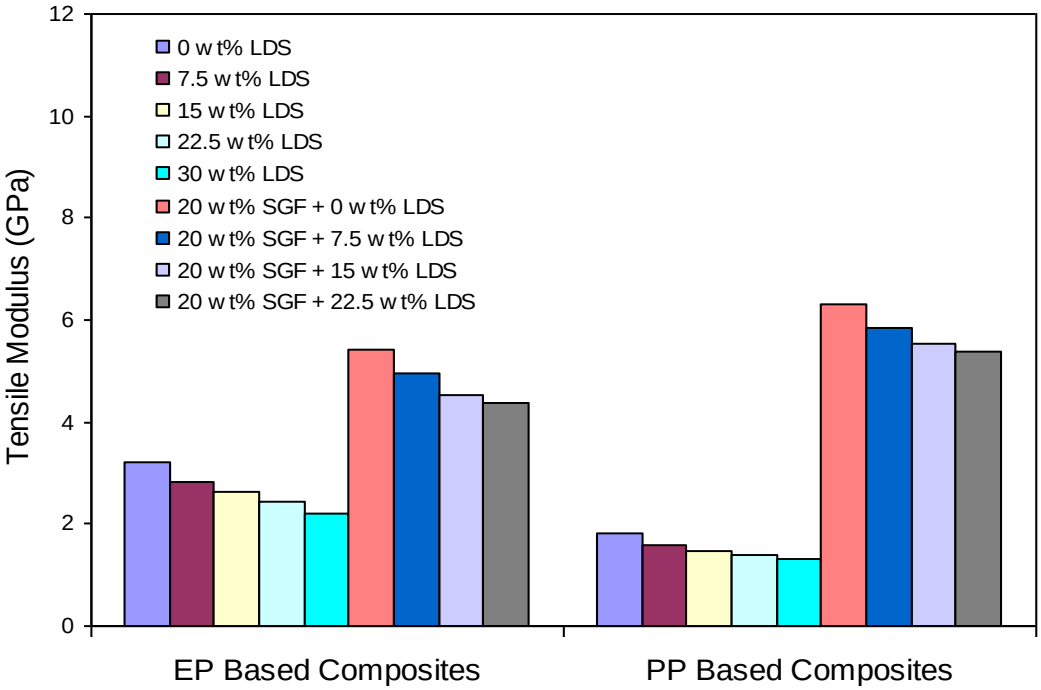

Figure 6.3 Tensile modulus of LDS filled composites

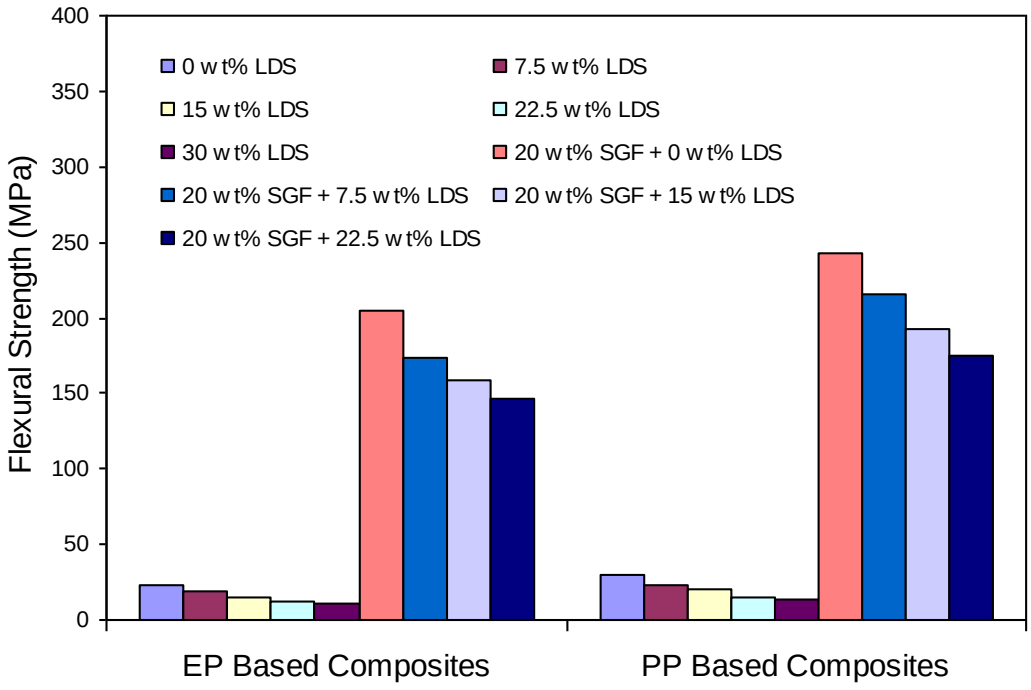

Figure 6.4 Flexural strength of LDS filled composites

6.2.2 Tensile Strength

The variation of tensile strength with LDS content for both the epoxy and PP based composites (with and without fiber reinforcement) is shown in Figure 6.2. It is found that with increase in LDS content from 0 to 30 wt%, the tensile strengths of both the epoxy as well as PP based composites decrease. However, this decrement is very marginal in case of both the epoxy and PP based the composites without SGF reinforcement. But in case of SGF reinforced composites, it is seen that this drop in tensile strength is significant (about 30 % in epoxy based composites and about 35% in PP composites) as the LDS content is varied from 0 to 22.5 wt%. This reduction might be due to the voids present in the composite body and due to stress concentration arising out of the sharp corners of the irregular shaped LDS particles.

Figure 6.3 presents the variation of tensile modulus with LDS content for both the epoxy and PP based composites (with and without glass fiber reinforcement). It shows a trend very similar to that of variation of tensile strength with filler content as mentioned earlier. The tensile moduli of the composite samples are also found to be decreasing as the LDS content in composites increases from 0 to 30 wt%. Thus, it can be seen that both the strength and modulus are distinctly reduced for all the composites as the LDS content in them increases. This can be attributed to the fact that the reinforcing fibers and filler particles strongly restrain the deformation of the matrix polymer as demonstrated in several previous studies [371]. This reduces the strain rate; but with both the tensile strength and strain decreasing, it seems that a synergistic effect takes place which ultimately leads to a small reduction in modulus.

6.2.3 Flexural Strength

Composite materials used in structures are prone to fail in bending and therefore development of new composites with improved flexural characteristics is essential. In the present work, the variation of flexural strength of epoxy and PP based composites with LDS content is shown in Figure 6.4. A gradual decrement

in flexural strength is recorded for all the composite samples with the incorporation of LDS particles. The reduction in flexural strength of the composites with filler content may be attributed to poor interfacial bonding, fiber to fiber interaction, voids and dispersion problems etc. Influence of particulate fillers on flexural strength is clearly observed in case of SGF reinforced composites also. It is evident from this study that as far as flexural strength is concerned, the SGF reinforced composites exhibit superior properties as compared to the composites without fiber reinforcement.

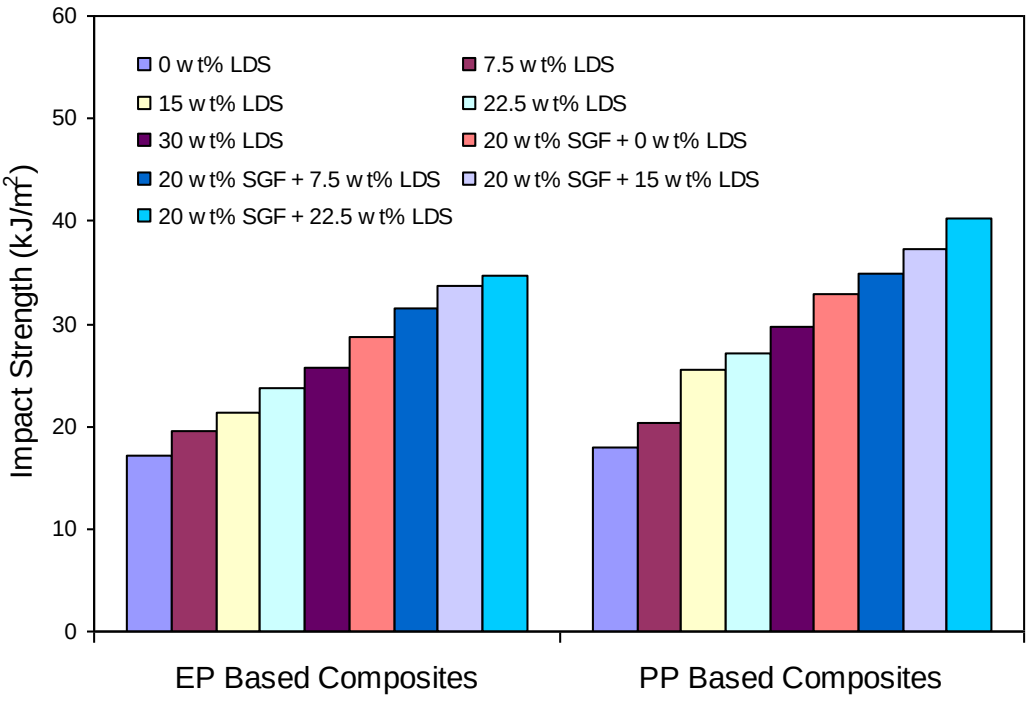

Figure 6.5 Impact strength of LDS filled composites

6.2.4 Impact Strength

The impact strength of a material is its capacity to absorb and dissipate energies under impact or shock loading. The suitability of a composite for certain applications is determined not only by usual design parameters, but also by its impact or energy absorbing properties. Figure 6.5 shows measured impact energy values of LDS filled composites under this investigation. It is seen from the figure that the impact energies of the composites improves gradually with

filler content increasing from 0 to 30 wt% in case of both epoxy and PP composites. Reinforcement of SGF also contributes to the enhancement of impact strength as is seen in the Figure 6.5. An increase of about 50% in impact strength is recorded for epoxy based composites when filled with 30 wt% LDS. Similar trend of improvement in impact strength is also observed in case of PP based composites.

Chapter Summary

This chapter has provided:

- The physical and mechanical characterization of epoxy and polypropylene composites filled with different weight fractions of LD slag with and without short glass fiber reinforcement
- The effects of filler addition and fiber reinforcement on the composite properties

The next chapter presents the results and discussion for erosion wear performance of the epoxy and polypropylene based composites under different test conditions.

*****

Chapter 7

Erosion Wear Response of LD Slag (LDS) Filled Polymer Composites

Chapter 7

EROSION WEAR RESPONSE OF LD SLAG (LDS) FILLED POLYMER COMPOSITES

Erosion wear characteristics of LD slag (LDS) filled epoxy (EP) and polypropylene (PP) composites with and without short glass fiber (SGF) reinforcement have been investigated following a well planned experimental schedule based on Taguchi design-of-experiment which is used to acquire the erosion test data in a controlled way. This chapter reports the wear rates obtained from these erosion trials and presents a critical analysis of the test results. Further, erosion rate predictions following an ANN approach for different test conditions are presented. A correlation among various control factors influencing the erosion rate has also been proposed for predictive purpose. Possible wear mechanisms are identified from the scanning electron microscopy of the eroded surfaces.

7.1 Morphology of Composite Surfaces

Some typical SEM micrographs of the uneroded and eroded surfaces of LDS filled epoxy composites are shown in Figure 7.1. The surface of the composite before being subjected to solid particle erosion, shown in Figure 7.1 (a), appears to be smooth with no wear grooves. Figure 7.1 (b) shows the formation of small craters due to penetration of hard sand particles onto the surface and cause material removal mostly from the relatively softer matrix regime. Figures 7.1 (c) and 7.1 (d) show the material getting dislodged from the matrix body leading to a greater degree of surface damage. This is a case of the erodent particles striking aggressively the composite surface at high impact velocity. Due to repeated impact of the erodent particles carrying higher kinetic energy, the LD slag particles in the matrix body break and subsequently get fragmented resulting in loose wear debris. But in the process, the hard slag particles absorb a

good fraction of the erodent kinetic energy and the energy available for the plastic deformation of epoxy becomes less. This way material removal and surface degradation of particulate filled composites are mitigated to a large extent. Figures 7.1 (e) and 7.1 (f) present SEM micrographs of eroded epoxy composites with maximum filler content (30 wt%) clearly indicating the role of hard LD slag particles in resisting the solid particle erosion.

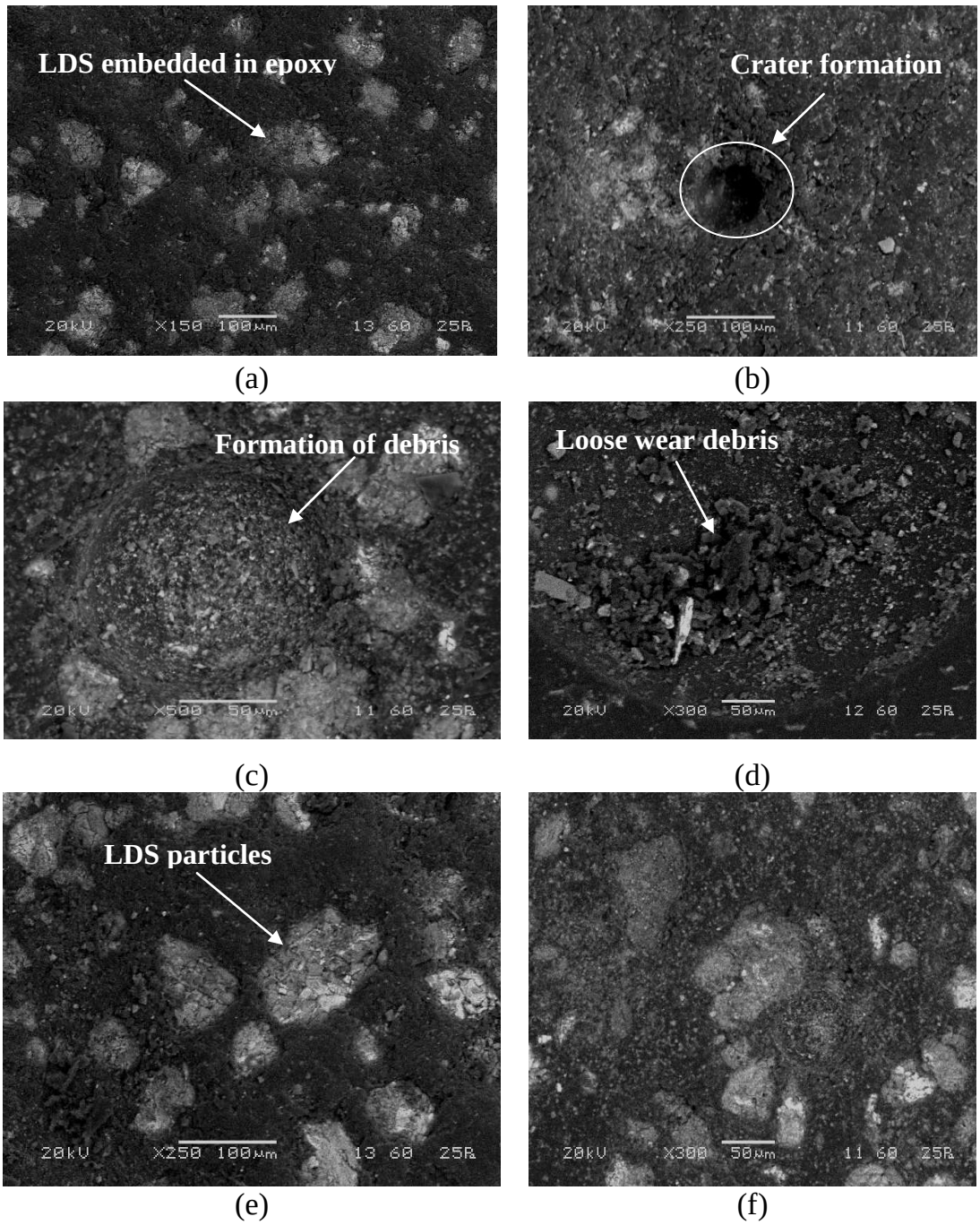

Figure 7.1 SEM micrographs of uneroded and eroded surfaces of the epoxy composites

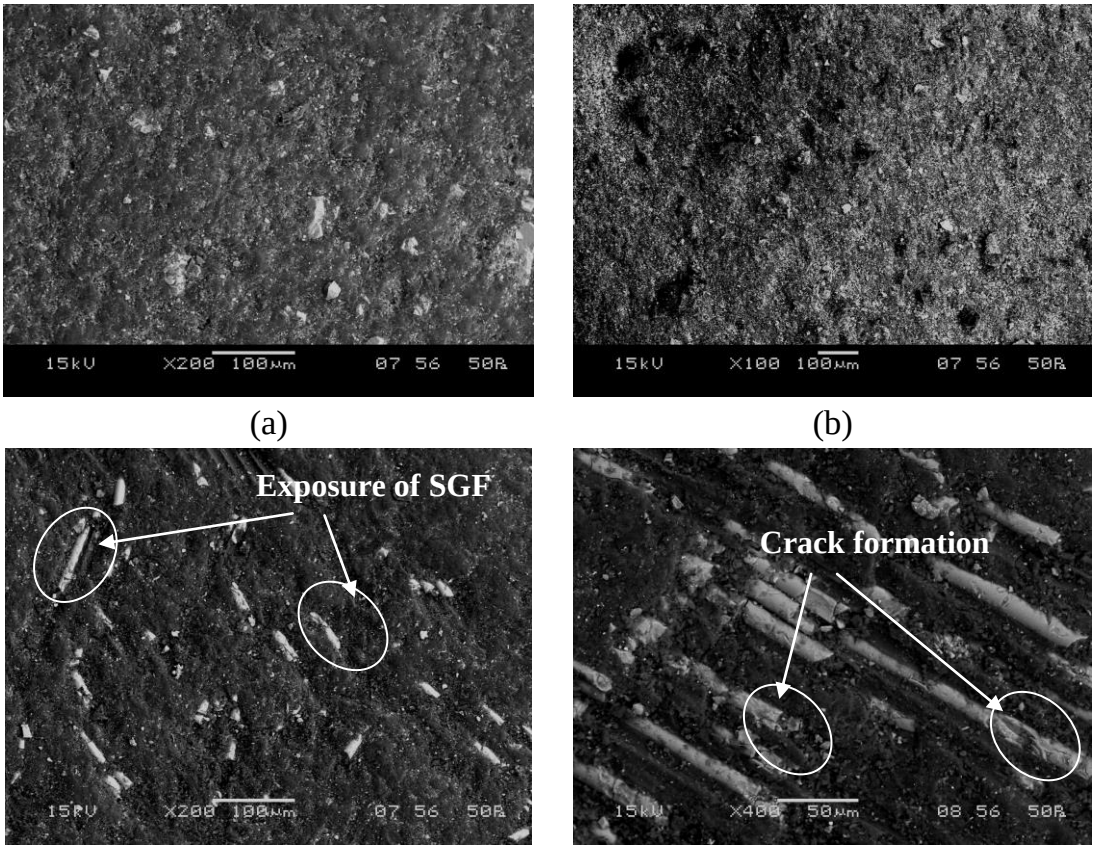

Figure 7.2 SEM micrographs of uneroded and eroded surfaces of the EP-LDS-SGF composites

Figure 7.2 shows the surface morphologies of some typical LDS filled epoxy-SGF composites. The distribution of slag particles in the matrix body can be clearly seen on the uneroded surfaces shown by the SEM images in Figures 7.2 (a) and 7.2 (b). The short fibers are however not visible on the outer surface. When the composites are subjected to repeated impact of hard erodent particles, the short fibers start appearing on the surface after the local removal of the soft matrix layer as seen in Figure 7.2 (c). Further impact of the hard silica sand particles even cause fracture of these short fiber bodies which is evident from the features like crack formation and propagation as clearly seen in Figure 7.2 (d). The fracture of the matrix layer and the fibers ultimately result in dislodgement of material which is characterized as erosion loss.

Table 7.1 Experimental design using L_{25} orthogonal array and the wear test results for epoxy and polypropylene composites without glass fiber

Test Run	A	B	C	D	E	EP-LDS		PP-LDS	
						ER	S/N Ratio	ER	S/N Ratio
1	32	30	0	50	30	40.6209	-32.1750	37.4214	-31.4624
2	32	45	7.5	100	40	39.3187	-31.8920	30.1724	-29.5922
3	32	60	15	150	50	36.1134	-31.1534	26.5724	-28.4886
4	32	75	22.5	200	60	34.7634	-30.8224	20.8624	-26.3873
5	32	90	30	250	70	30.6209	-29.7204	12.3571	-21.8383
6	40	30	7.5	150	60	41.4581	-32.3522	37.7542	-31.5393
7	40	45	15	200	70	38.9123	-31.8017	32.3524	-30.1981
8	40	60	22.5	250	30	36.8796	-31.3357	28.9425	-29.2307
9	40	75	30	50	40	34.4532	-30.7446	14.6471	-23.3150
10	40	90	0	100	50	45.2709	-33.1164	45.8257	-33.2222
11	48	30	15	250	40	48.4581	-33.7073	42.9358	-32.6564
12	48	45	22.5	50	50	45.9123	-33.2386	38.6759	-31.7488
13	48	60	30	100	60	42.8796	-32.6450	21.8735	-26.7984
14	48	75	0	150	70	57.4538	-35.1864	54.5785	-34.7404
15	48	90	7.5	200	30	54.6432	-34.7507	45.8546	-33.2277
16	56	30	22.5	100	70	49.8712	-33.9570	41.2687	-32.3124
17	56	45	30	150	30	44.9623	-33.0570	26.6238	-28.5054
18	56	60	0	200	40	65.4539	-36.3187	63.4257	-36.0453
19	56	75	7.5	250	50	62.9834	-35.9845	52.5823	-34.4168
20	56	90	15	50	60	58.5463	-35.3500	47.4684	-33.5281
21	64	30	30	200	50	49.6721	-33.9223	24.8457	-27.9050
22	64	45	0	250	60	73.9231	-37.3756	62.6984	-35.9451
23	64	60	7.5	50	70	70.0989	-36.9142	58.5847	-35.3557
24	64	75	15	100	30	65.9348	-36.3823	52.8457	-34.4602
25	64	90	22.5	150	40	60.7837	-35.6757	46.3574	-33.3224

Note : *Factor A denotes Impact Velocity (m/sec)*
Factor B denotes Impingement Angle (^{0})
Factor C denotes LDS content (wt%)
Factor D denotes Erodent Size (µm)
Factor E denotes Erodent Temperature (^{0}C)
ER denotes Erosion Rate (mg/kg)
S/N Ratio denotes Signal to Noise Ratio (db)
EP: Epoxy, PP: Polypropylene, LDS: Linz-Donawitz slag

7.2 Erosion Test Results and Taguchi Analysis

The erosion wear rates of LDS filled epoxy and PP composites without glass fiber obtained for all the 25 test runs along with the corresponding signal-to-noise (S/N) ratios are presented in Table 7.1. Each data point (value of erosion rate) is in fact the average of three replications. From this table, the overall mean for the S/N ratio of the wear rate for epoxy and PP composites are found to be -33.5831 db and -31.0496 db respectively. This is done using the software MINITAB 14 specifically used for design-of-experiment applications.

Table 7.2 S/N ratio response table for erosion rate of EP-LDS composites

Level	A	B	C	D	E
1	-31.15	-33.22	-34.83	-33.68	-33.54
2	-31.87	-33.47	-34.38	-33.60	-33.67
3	-33.91	-33.67	-33.68	-33.48	-33.48
4	-34.93	-33.82	-33.01	-33.52	-33.71
5	-36.05	-33.72	-32.02	-33.62	-33.52
Delta	4.90	0.60	2.82	0.20	0.23
Rank	**1**	**3**	**2**	**5**	**4**

The S/N ratio response analyses are presented in Tables 7.2 and 7.3 for EP-LDS and PP-LDS composites respectively. These tables show the hierarchical order of the control factors as per their significance on the composite erosion rate.

Figures 7.3 and 7.4 illustrate the effect of control factors on erosion rate for EP-LDS and PP-LDS composites respectively. Analysis of the results leads to the conclusion that factor combination of A_1 (Impact velocity), B_1 (Impingement

angle), C_5 (LDS content), D_3 (Erodent size) and E_3 (Erodent temperature) gives minimum erosion rate (Figure 7.3) for EP-LDS composites and factor combination A_1 (Impact velocity), B_4 (Impingement angle), C_5 (LDS content), D_4 (Erodent size) and E_4 (Erodent temperature) gives minimum erosion rate (Figure 7.4) for PP-LDS composites.

Table 7.3 S/N ratio response table for erosion rate of PP-LDS composites

Level	A	B	C	D	E
1	-27.55	-31.18	-34.28	-31.08	-31.38
2	-29.50	-31.20	-32.83	-31.28	-30.99
3	-31.83	-31.18	-31.87	-31.32	-31.16
4	-32.96	-30.66	-30.60	-30.75	-30.84
5	-33.40	-31.03	-25.67	-30.82	-30.89
Delta	5.84	0.53	8.61	0.57	0.54
Rank	**2**	**5**	**1**	**3**	**4**

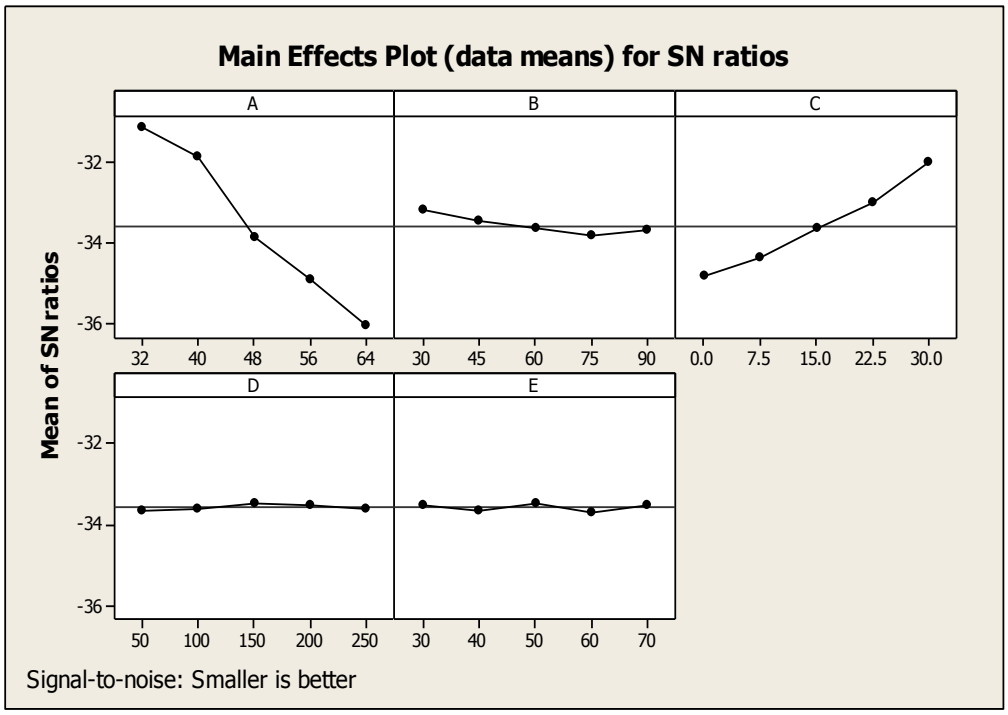

Figure 7.3 Effect of control factors on erosion rate for EP-LDS composites

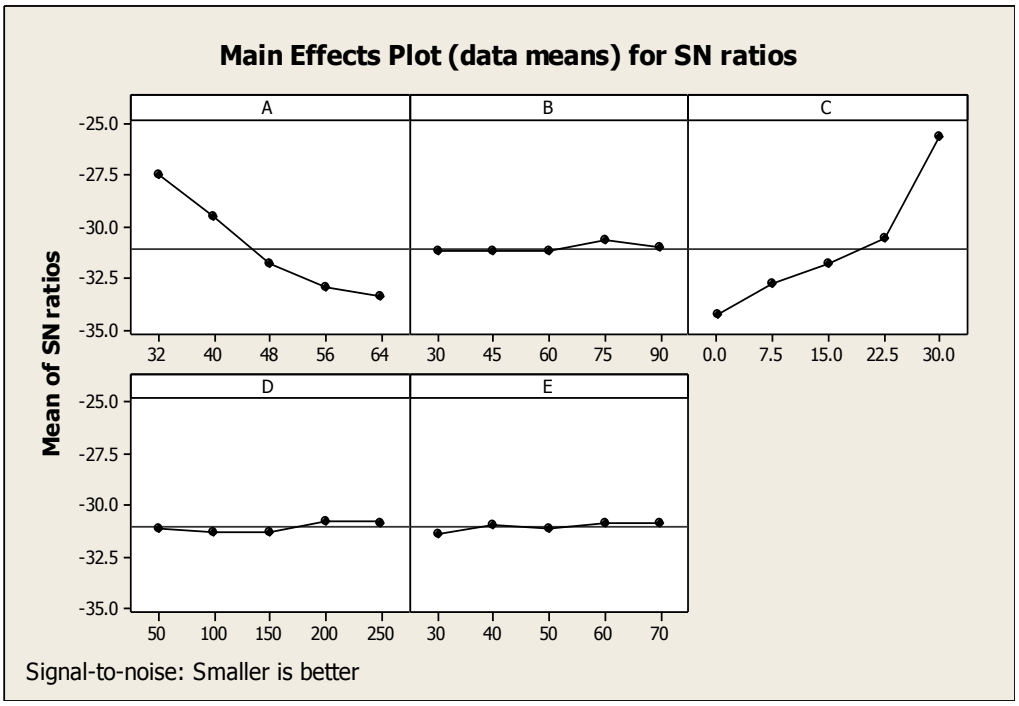

Figure 7.4 Effect of control factors on erosion rate for PP-LDS composites

The erosion wear rates of LDS filled epoxy and PP composites with 20 wt% short glass fiber obtained for all the 16 test runs along with the corresponding S/N ratios are presented in Table 7.4. Each data point (value of erosion rate) is in fact the average of three replications. From this table, the overall mean for the S/N ratio of the wear rate for EP-LDS-SGF and PP-LDS-SGF composites are found to be -46.5664 db and -44.9641 db respectively.

The S/N ratio response analyses are presented in Tables 7.5 and 7.6 for EP-LDS-SGF and PP-LDS-SGF composites respectively. These tables show the hierarchical order of the control factors as per their significance on the composite erosion rate.

Figures 7.5 and 7.6 illustrate the effects of control factors on erosion rate for EP-LDS-SGF and PP-LDS-SGF composites respectively. Analysis of the results leads to the conclusion that factor combination of A_1, B_2, C_4, D_1 and E_1 gives minimum erosion rate (Figure 7.5) for EP-LDS-SGF composites and factor combination A_1, B_2, C_3, D_1 and E_2 gives minimum erosion rate (Figure 7.6) for PP-LDS-SGF composites.

Table 7.4 Experimental design using L_{16} orthogonal array and the wear test results for epoxy and polypropylene composites with glass fiber

Test Run	A	B	C	D	E	EP-LDS-SGF		PP-LDS-SGF	
						ER	S/N Ratio	ER	S/N Ratio
1	32	30	0	50	30	197.186	-45.8975	263.63	-48.4199
2	32	45	7.5	100	40	158.432	-43.9969	108.25	-40.6886
3	32	60	15	150	50	128.521	-42.1795	101.98	-40.1703
4	32	90	22.5	200	60	110.236	-40.8465	90.86	-39.1675
5	40	30	7.5	150	60	262.721	-48.3899	205.72	-46.2655
6	40	45	0	200	50	320.525	-50.1172	308.57	-49.7871
7	40	60	15	50	40	165.853	-44.3945	100.14	-40.0122
8	40	90	22.5	100	30	209.857	-46.4385	190.36	-45.5915
9	48	30	15	200	40	202.384	-46.1235	122.42	-41.7570
10	48	45	22.5	150	30	150.652	-43.5595	140.84	-42.9745
11	48	60	0	100	60	411.095	-52.2788	323.39	-50.1945
12	48	90	7.5	50	50	290.892	-49.2746	238.93	-47.5654
13	56	30	22.5	100	50	162.875	-44.2371	159.74	-44.0683
14	56	45	15	50	60	182.657	-45.2327	135.53	-42.6407
15	56	60	7.5	200	30	302.895	-49.6258	304.95	-49.6846
16	56	90	0	150	40	420.235	-52.4698	332.64	-50.4395

Note : *Factor A denotes Impact Velocity (m/sec)*
Factor B denotes Impingement Angle (^{0})
Factor C denotes LDS content (wt%)
Factor D denotes Erodent Size (µm)
Factor E denotes Erodent Temperature (^{0}C)
ER denotes Erosion Rate (mg/kg)
S/N Ratio denotes Signal to Noise Ratio (db)
EP: Epoxy, PP: Polypropylene, LDS: Linz-Donawitz slag
SGF: Short glass fiber

Table 7.5 S/N ratio response table for erosion rate of EP-LDS-SGF composites

Level	A	B	C	D	E
1	-43.23	-46.16	-50.19	-46.20	-46.38
2	-47.34	-45.73	-47.82	-46.74	-46.75
3	-47.81	-47.12	-44.48	-46.65	-46.45
4	-47.89	-47.26	-43.77	-46.68	-46.69
Delta	4.66	1.53	6.42	0.54	0.37
Rank	**2**	**3**	**1**	**4**	**5**

Table 7.6 S/N ratio response table for erosion rate of PP-LDS-SGF composites

Level	A	B	C	D	E
1	-42.11	-45.13	-49.71	-44.66	-46.67
2	-45.41	-44.02	-46.05	-45.14	-43.22
3	-45.62	-45.02	-41.15	-44.96	-45.40
4	-46.71	-45.69	-42.95	-45.10	-44.57
Delta	4.60	1.67	8.57	0.48	3.44
Rank	**2**	**4**	**1**	**5**	**3**

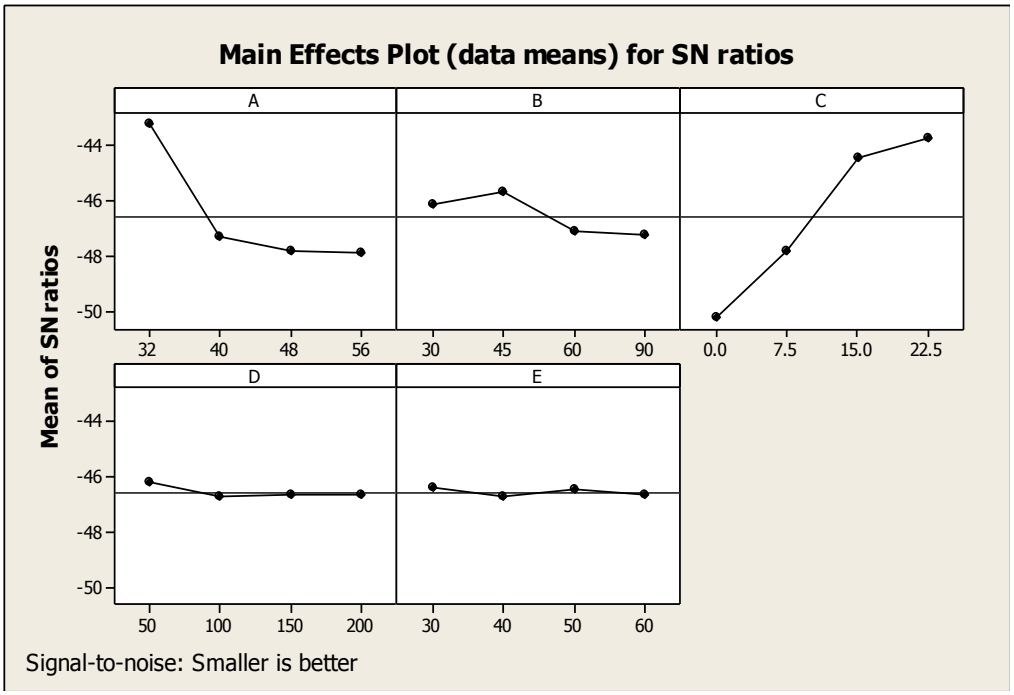

Figure 7.5 Effect of control factors on erosion rate for EP-LDS-SGF composites

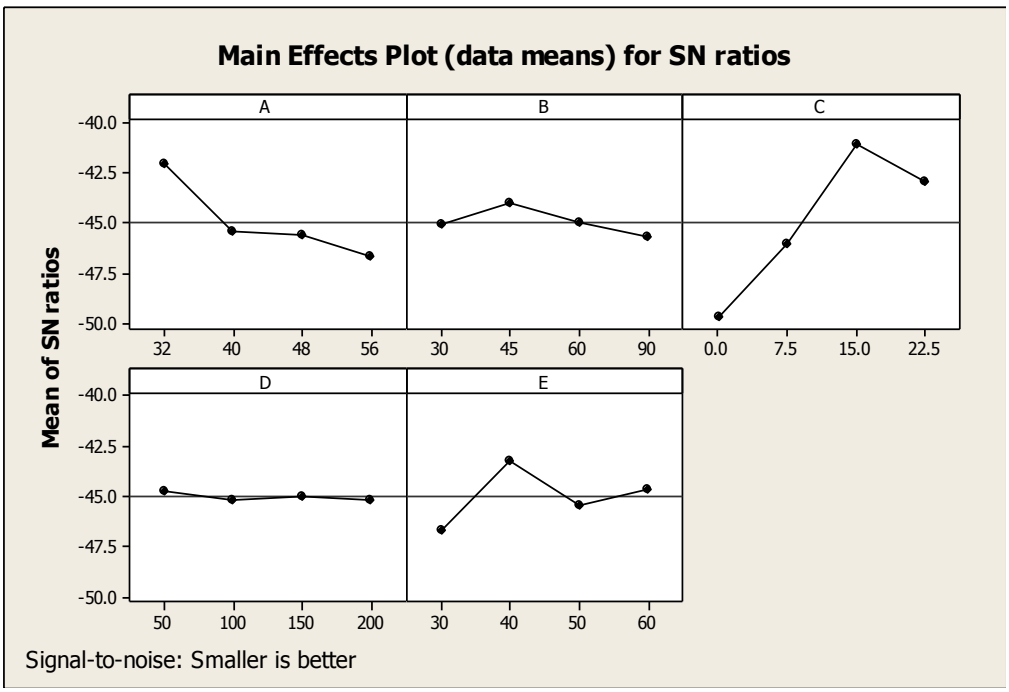

Figure 7.6 Effect of control factors on erosion rate for PP-LDS-SGF composites

7.3 Confirmation Experiment

To validate the conclusions drawn during the analysis, confirmation experiments are performed by considering a new arbitrary set of factors other than the optimal factor setting to evaluate the erosion rate. For this investigation $A_1B_3C_4D_2E_2$, $A_2B_4C_3D_4E_5$, $A_4B_3C_2D_4E_1$ and $A_3B_2C_3D_2E_4$ for EP-LDS, PP-LDS, EP-LDS-SGF and PP-LDS-SGF composites respectively are chosen as the arbitrary sets considering which prediction equations can be formulated using Taguchi's approach to estimate S/N ratios for erosion rate as [294]:

$$\overline{\eta_1} = \overline{T} + \left(\overline{A_1} - \overline{T}\right) + \left(\overline{B_3} - \overline{T}\right) + \left(\overline{C_4} - \overline{T}\right) + \left(\overline{D_2} - \overline{T}\right) + \left(\overline{E_2} - \overline{T}\right) \quad \textbf{(7.1)}$$

$$\overline{\eta_2} = \overline{T} + \left(\overline{A_2} - \overline{T}\right) + \left(\overline{B_4} - \overline{T}\right) + \left(\overline{C_3} - \overline{T}\right) + \left(\overline{D_4} - \overline{T}\right) + \left(\overline{E_5} - \overline{T}\right) \quad \textbf{(7.2)}$$

$$\overline{\eta_3} = \overline{T} + \left(\overline{A_4} - \overline{T}\right) + \left(\overline{B_3} - \overline{T}\right) + \left(\overline{C_2} - \overline{T}\right) + \left(\overline{D_4} - \overline{T}\right) + \left(\overline{E_1} - \overline{T}\right) \quad \textbf{(7.3)}$$

$$\overline{\eta_4} = \overline{T} + \left(\overline{A_3} - \overline{T}\right) + \left(\overline{B_2} - \overline{T}\right) + \left(\overline{C_3} - \overline{T}\right) + \left(\overline{D_2} - \overline{T}\right) + \left(\overline{E_4} - \overline{T}\right) \quad \textbf{(7.4)}$$

$\overline{\eta_1}$, $\overline{\eta_2}$, $\overline{\eta_3}$, $\overline{\eta_4}$ Predicted average for EP-LDS, PP-LDS, EP-LDS-SGF and PP-LDS-SGF composites respectively

$\overline{T}$ Overall experimental average

$\overline{A}, \overline{B}, \overline{C}, \overline{D}, \overline{E}$ Mean response for factors

By combining like terms, the equation reduces to

$$\overline{\eta_1} = \overline{A_1} + \overline{B_3} + \overline{C_4} + \overline{D_2} + \overline{E_2} - 4\overline{T} \quad \textbf{(7.5)}$$

$$\overline{\eta_2} = \overline{A_2} + \overline{B_4} + \overline{C_3} + \overline{D_4} + \overline{E_5} - 4\overline{T} \quad \textbf{(7.6)}$$

$$\overline{\eta_3} = \overline{A_4} + \overline{B_3} + \overline{C_2} + \overline{D_4} + \overline{E_1} - 4\overline{T} \quad \textbf{(7.7)}$$

$$\overline{\eta_4} = \overline{A_3} + \overline{B_2} + \overline{C_3} + \overline{D_2} + \overline{E_4} - 4\overline{T} \quad \textbf{(7.8)}$$

Table 7.7 Results of the confirmation experiments for erosion rate without glass fiber

	Optimal Control Parameters			
	EP-LDS Composites		**PP-LDS Composites**	
	Pred.	**Exp.**	**Pred.**	**Exp.**
Level	$A_1B_1C_5D_3E_3$	$A_1B_1C_5D_3E_3$	$A_1B_4C_5D_4E_4$	$A_1B_4C_5D_4E_4$
S/N ratio for erosion rate (db)	-29.0286	-29.4721	-21.2838	-21.5361
Percentage Error	1.50%		1.17%	

	Arbitrary set of Control Parameters			
	EP-LDS Composites		**PP-LDS Composites**	
	Pred.	**Exp.**	**Pred.**	**Exp.**
Level	$A_1B_3C_4D_2E_2$	$A_1B_3C_4D_2E_2$	$A_2B_4C_3D_4E_5$	$A_2B_4C_3D_4E_5$
S/N ratio for erosion rate (db)	-30.7655	-31.4215	-29.4742	-29.9651
Percentage Error	2.08%		1.63%	

Table 7.8 Results of the confirmation experiments for erosion rate with glass fiber

	Optimal Control Parameters			
	EP-LDS-SGF Composites		**PP-LDS-SGF Composites**	
	Pred.	**Exp.**	**Pred.**	**Exp.**
Level	$A_1B_2C_4D_1E_1$	$A_1B_2C_4D_1E_1$	$A_1B_2C_3D_1E_2$	$A_1B_2C_3D_1E_2$
S/N ratio for erosion rate (db)	-39.0415	-39.8652	-35.3066	-35.8537
Percentage Error	2.06%		1.52%	

	Arbitrary set of Control Parameters			
	EP-LDS-SGF Composites		PP-LDS-SGF Composites	
	Pred.	**Exp.**	**Pred.**	**Exp.**
Level	$A_4B_3C_2D_4E_1$	$A_4B_3C_2D_4E_1$	$A_3B_2C_3D_2E_4$	$A_3B_2C_3D_2E_4$
S/N ratio for erosion rate (db)	-49.6258	-51.5752	-42.0315	-43.2713
Percentage Error	3.77%		2.86%	

For this chosen combination of factors, the S/N ratios for EP-LDS, PP-LDS, EP-LDS-SGF and PP-LDS-SGF composites are found to be -30.7655, -29.4742, -49.6258 and -42.0315 db respectively while those for the optimal combinations of factors happen to be -29.0286, -21.2838, -39.0415 and -35.3066 db respectively. Each of these values is smaller than the S/N ratio value for the corresponding optimal factor combination. This confirms the optimized combinations of control factors leading to minimum erosion rate for the respective composites. Further, an experiment is also conducted taking the same factor combination and the test results are compared with value obtained from the predictive Equations 7.5, 7.6, 7.7 and 7.8. The comparison of the experimental and the predicted results along with the associated percentage errors are given in Tables 7.7 and 7.8. Thus, the proposed correlations seem to be capable of predicting erosion rate to a reasonable accuracy.

7.4 Predictive Equation for Determination of Erosion Rate

The solid particle erosion wear rate of the composite samples can also be predicted using a nonlinear regressive predictive equation showing the relationship between the erosion rate and combination of control factors. This correlation is developed statistically using standard software SYSTAT 7.

In order to express the erosion rate in terms of a nonlinear regressive mathematical equation, the following form is suggested:

$$ER = k_0 + k_1 \times A + k_2 \times B + k_3 \times C + k_4 \times D + k_5 \times E \quad \textbf{(7.9)}$$

Here, ER is the performance output term i.e. the erosion rate in mg/kg and k_i (i = 0, 1, 2, 3, 4, 5) are the model constants. A is the impact velocity (m/sec), B is the impingement angle (degree), C is the LDS content in the composite (wt%), D is the erodent size (micron) and E is the erodent temperature (^{0}C).

By using the software, the values of all of the constants are calculated and the final nonlinear regression expressions for the EP-LDS, PP-LDS, EP-LDS-SGF and PP-LDS-SGF composites are obtained by the Equations 7.10, 7.11, 7.12 and 7.13 respectively.

$$ER = 8.025 + 0.907 \times A + 0.070 \times B - 0.535 \times C + 0.003 \times D + 0.022 \times E \quad \textbf{(7.10)}$$

$$ER = 13.383 + 0.769 \times A + 0.043 \times B - 1.003 \times C + 0.000 \times D + 0.016 \times E \quad \textbf{(7.11)}$$

$$ER = 3.661 + 4.747 \times A + 1.234 \times B - 8.570 \times C + 0.223 \times D + 0.364 \times E \quad \textbf{(7.12)}$$

$$ER = 109.26 + 3.516 \times A + 0.786 \times B - 8.080 \times C + 0.193 \times D - 1.021 \times E \quad \textbf{(7.13)}$$

The correctness of the calculated constants is confirmed because very high correlation coefficients (r^2) of 0.998, 0.993, 0.984 and 0.968 for the EP-LDS, PP-LDS, EP-LDS-SGF and PP-LDS-SGF composites respectively are obtained for Equation (7.5); therefore, the models are quite suitable for further analysis. A comparison between the wear rate obtained from experimental results and the predictive equation for composite with and without fiber reinforcement combination are shown in Tables 7.9 and 7.10, which indicates that the percentage errors associated with the predicted values with respect to the experimental ones vary in the range of 0 to 13%.

Table 7.9 Comparison between experimental and predicted values for erosion rate without glass fiber

EP-LDS			PP-LDS		
ER Experimental	**ER Predicted**	**% Error**	**ER Experimental**	**ER Predicted**	**% Error**
40.6209	39.9590	1.629	37.4214	39.7610	6.252
39.3187	37.3665	4.965	30.1724	33.0435	9.515
36.1134	34.7740	3.708	26.5724	26.3260	0.927
34.7634	32.1815	7.427	20.8624	19.6085	6.010
30.6209	29.5890	3.369	12.3571	12.8910	4.320
41.4581	44.1625	6.523	37.7542	38.8705	2.956
38.9123	41.5700	6.829	32.3524	32.1530	0.616
36.8796	37.8775	2.705	28.9425	26.6355	7.970
34.4532	34.5350	0.237	14.6471	15.9180	8.676
45.2709	50.0050	10.457	45.8257	48.8130	6.518
48.4581	47.2660	2.460	42.9358	38.1800	11.076
45.9123	43.9235	4.331	38.6759	34.4625	10.894
42.8796	41.3310	3.611	21.8735	23.7450	8.556
57.4538	58.8010	2.344	54.5785	54.6400	0.112
54.6432	55.1085	0.851	45.8546	47.1225	2.765
49.8712	50.7195	1.700	41.2687	37.2895	9.642
44.9623	47.0270	4.592	26.6238	28.7720	8.068
65.4539	64.4970	1.461	63.4257	59.6670	5.926
62.9834	61.9045	1.712	52.5823	52.9495	0.698
58.5463	58.5620	0.026	47.4684	46.2320	2.604
49.6721	53.8230	8.356	24.8457	27.5990	11.081
73.9231	71.2930	3.557	62.6984	65.4940	4.458
70.0989	67.9505	3.064	58.5847	58.7765	0.327
65.9348	64.2580	2.543	52.8457	51.2590	3.002
60.7837	61.6655	1.450	46.3574	44.5415	3.917

Note: *ER: Erosion Rate (mg/kg), EP: Epoxy, PP: Polypropylene, LDS: Linz-Donawitz slag*

Table 7.10 Comparison between experimental and predicted values for erosion rate with glass fiber

EP-LDS-SGF			PP-LDS-SGF		
ER Experimental	**ER Predicted**	**% Error**	**ER Experimental**	**ER Predicted**	**% Error**
197.186	214.655	8.859	263.63	250.372	5.029
158.432	175.680	10.886	108.25	121.002	11.780
128.521	140.705	9.480	101.98	112.632	10.445
110.236	123.240	11.796	90.86	88.052	3.090
262.721	248.576	5.384	205.72	180.570	12.225
320.525	311.871	2.699	308.57	272.820	11.585
165.853	164.741	0.670	100.14	110.670	10.515
209.857	195.996	6.604	190.36	173.510	8.851
202.384	199.147	1.599	122.42	137.168	12.047
150.652	138.592	8.005	140.84	129.918	7.754
411.095	378.697	7.880	323.39	283.228	12.419
290.892	307.652	5.761	238.93	246.768	3.280
162.875	154.188	5.333	159.74	142.186	10.989
182.657	190.463	4.273	135.53	121.716	10.192
302.895	334.778	10.526	304.95	300.686	1.398
420.235	428.563	1.981	332.64	365.006	9.730

Note: *ER: Erosion Rate (mg/kg), EP: Epoxy, PP: Polypropylene, LDS: Linz-Donawitz slag, SGF: Short glass fiber*

7.5 Analysis and Prediction of Erosion Response using ANN

As mentioned earlier, artificial neural network (ANN) is a technique that involves database training to predict input-output evolutions. In this attempt to simulate the erosion wear process and to predict the erosion rates of EP-LDS and PP-LDS composites with and without fiber reinforcement under different operating conditions, five input parameters (impact velocity, impingement angle, LDS content, erodent size and erodent temperature) are taken, each of which is characterized by one neuron in the input layer of the ANN structure. Different ANN structures with varying number of neurons in the hidden layer are tested at constant cycles, learning rate, error tolerance, momentum parameter, noise factor

and slope parameter. Based on least error criterion, one structure for each composite type, shown in Tables 7.11, 7.12, 7.13 and 7.14 are selected for training of the input-output data for EP-LDS, PP-LDS, EP-LDS-SGF and PP-LDS-SGF composites respectively.

The optimized three-layer neural networks used in these simulations are shown in Figures 7.7, 7.8, 7.9 and 7.10. A software package NEURALNET for neural computing based on back propagation algorithm is used as the prediction tool for estimating the erosion wear rates of the composites under various test conditions.

Table 7.11 Input parameters for training (EP-LDS)

Input Parameters for Training	Values
Error tolerance	0.001
Learning rate (β)	0.002
Momentum parameter (α)	0.002
Noise factor (NF)	0.001
Number of epochs	1,00,00,000
Slope parameter (£)	0.6
Number of hidden layer neurons (H)	8
Number of input layer neurons (I)	5
Number of output layer neurons (O)	1

Table 7.12 Input parameters for training (PP-LDS)

Input Parameters for Training	Values
Error tolerance	0.001
Learning rate (β)	0.002
Momentum parameter (α)	0.002
Noise factor (NF)	0.001
Number of epochs	1,00,00,000
Slope parameter (£)	0.6
Number of hidden layer neurons (H)	9
Number of input layer neurons (I)	5
Number of output layer neurons (O)	1

Table 7.13 Input parameters for training (EP-LDS-SGF)

Input Parameters for Training	Values
Error tolerance	0.001
Learning rate (β)	0.002
Momentum parameter (α)	0.002
Noise factor (NF)	0.001
Number of epochs	1,00,00,000
Slope parameter (£)	0.6
Number of hidden layer neurons (H)	7
Number of input layer neurons (I)	5
Number of output layer neurons (O)	1

Table 7.14 Input parameters for training (PP-LDS-SGF)

Input Parameters for Training	Values
Error tolerance	0.001
Learning rate (β)	0.002
Momentum parameter (α)	0.002
Noise factor (NF)	0.001
Number of epochs	1,00,00,000
Slope parameter (£)	0.6
Number of hidden layer neurons (H)	9
Number of input layer neurons (I)	5
Number of output layer neurons (O)	1

The ANN predictive results of erosion wear rate of LDS filled epoxy and PP composites without fiber reinforcement obtained for all the 25 test conditions and with fiber reinforcement obtained for all the 16 test conditions for all the composite combinations are shown and compared with the experimental values along with the associated percentage errors in Tables 7.15 and 7.16 respectively. It is observed that the errors lie in the range of 0-10%, which establishes the validity of the neural computation. The errors, however, can still be reduced and the quality of predictions can be further improved by enlarging the data sets and optimizing the construction of the neural network.

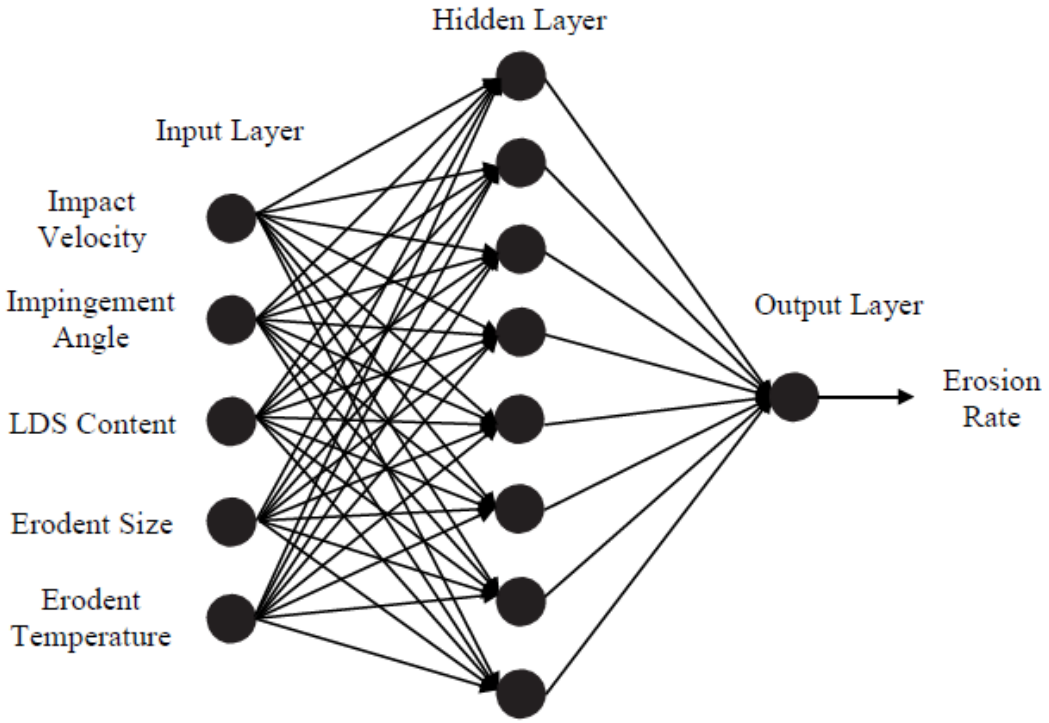

Figure 7.7 Three layer neural network (EP-LDS)

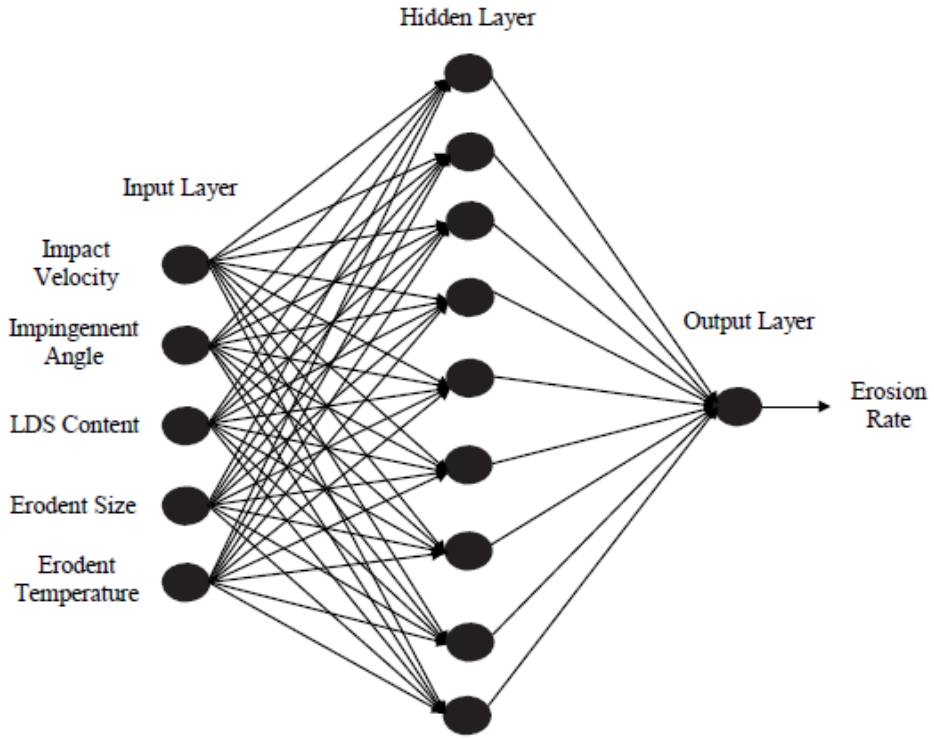

Figure 7.8 Three layer neural network (PP-LDS)

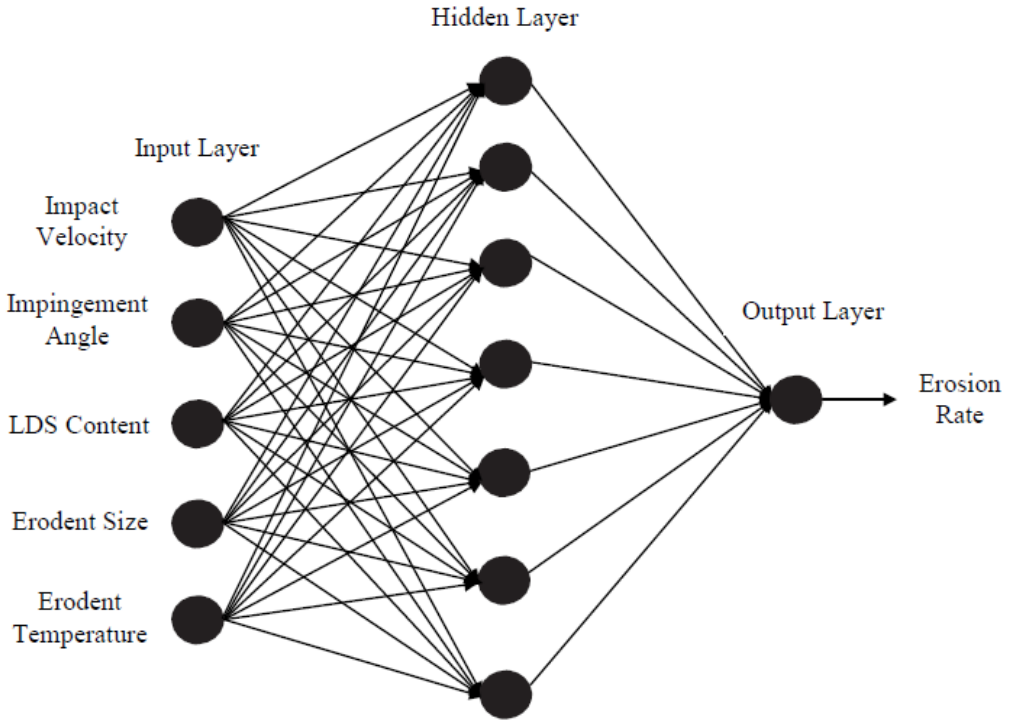

Figure 7.9 Three layer neural network (EP-LDS-SGF)

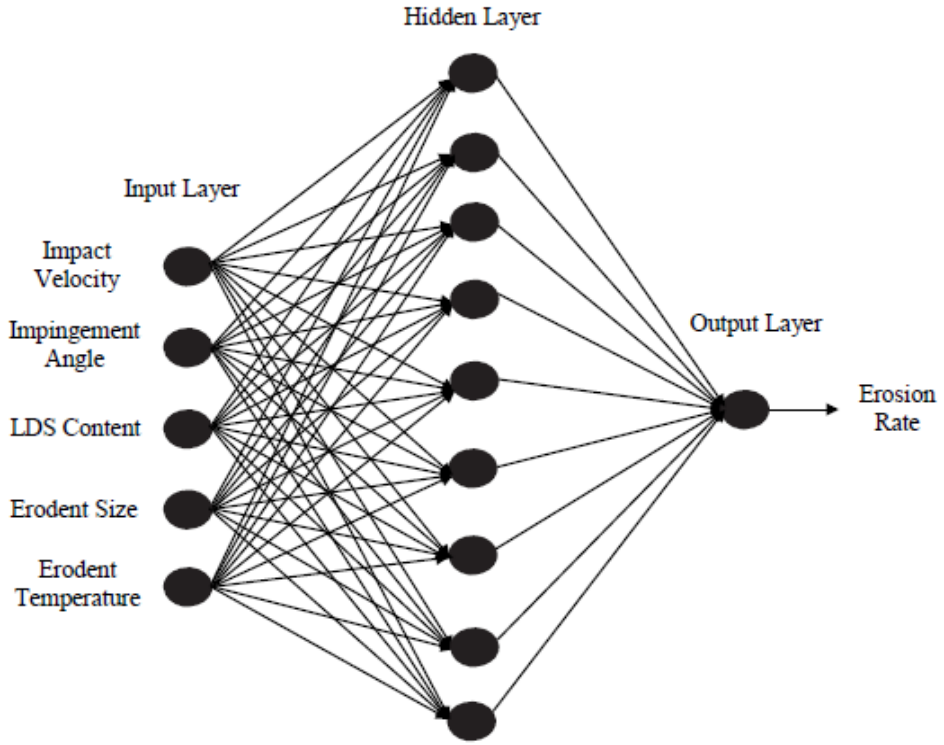

Figure 7.10 Three layer neural network (PP-LDS-SGF)

Table 7.15 Percentage error between experimental result and ANN prediction for erosion rate without glass fiber

EP-LDS			PP-LDS		
ER Experimental	**ER ANN**	**% Error**	**ER Experimental**	**ER ANN**	**% Error**
40.6209	38.7126	4.697	37.4214	34.0102	9.115
39.3187	38.2689	2.669	30.1724	31.7275	5.154
36.1134	36.6686	1.537	26.5724	26.9113	1.275
34.7634	34.0706	1.992	20.8624	19.8393	4.904
30.6209	30.7804	0.520	12.3571	12.7979	3.567
41.4581	42.4863	2.480	37.7542	37.4047	0.925
38.9123	41.9489	7.803	32.3524	35.2267	8.884
36.8796	37.5475	1.811	28.9425	29.0930	0.519
34.4532	34.5982	0.420	14.6471	14.5770	0.478
45.2709	45.6969	0.941	45.8257	44.8981	2.024
48.4581	47.6735	1.619	42.9358	42.4486	1.134
45.9123	46.3812	1.021	38.6759	38.1074	1.469
42.8796	43.3818	1.171	21.8735	23.5368	7.604
57.4538	57.0711	0.666	54.5785	54.6957	0.214
54.6432	54.3264	0.579	45.8546	46.0310	0.384
49.8712	49.1190	1.508	41.2687	41.1316	0.332
44.9623	44.2322	1.623	26.6238	26.4112	0.798
65.4539	66.2073	1.151	63.4257	62.3669	1.669
62.9834	64.1678	1.880	52.5823	57.6706	9.676
58.5463	58.3506	0.334	47.4684	48.4391	2.044
49.6721	50.5943	1.856	24.8457	25.2068	1.453
73.9231	73.5361	0.523	62.6984	63.6709	1.551
70.0989	70.3196	0.314	58.5847	58.1864	0.679
65.9348	65.8883	0.070	52.8457	53.0079	0.306
60.7837	62.3329	2.548	46.3574	47.5160	2.499

Note: *ER: Erosion Rate (mg/kg), EP: Epoxy, PP: Polypropylene, LDS: Linz-Donawitz slag*

Table 7.16 Percentage error between experimental result and ANN prediction for erosion rate with glass fiber

EP-LDS-SGF			PP-LDS-SGF		
ER Experimental	**ER ANN**	**% Error**	**ER Experimental**	**ER ANN**	**% Error**
197.186	205.524	4.228	263.63	258.766	1.845
158.432	166.685	5.209	108.25	118.174	9.167
128.521	134.347	4.533	101.98	101.016	0.945
110.236	107.769	2.237	90.86	92.100	1.364
262.721	256.185	2.487	205.72	200.340	2.615
320.525	328.875	2.605	308.57	302.903	1.836
165.853	153.489	7.454	100.14	91.024	9.103
209.857	213.517	1.744	190.36	178.612	6.171
202.384	203.771	0.685	122.42	130.502	6.601
150.652	155.938	3.508	140.84	128.453	8.795
411.095	390.080	5.111	323.39	326.212	0.872
290.892	295.702	1.653	238.93	239.034	0.043
162.875	148.498	8.827	159.74	151.419	5.209
182.657	192.323	5.291	135.53	144.533	6.642
302.895	309.889	2.309	304.95	309.323	1.434
420.235	420.457	0.052	332.64	332.986	0.104

Note: *ER: Erosion Rate (mg/kg), EP: Epoxy, PP: Polypropylene LDS: Linz-Donawitz slag, SGF: Short glass fiber*

A well-trained ANN is expected to be very helpful for the analysis of erosion wear characteristics of any given composites and permits to study quantitatively the effect of each of the considered input parameters on the wear rate. The range of any chosen parameter can be beyond the actual experimental limits, thus offering the possibility to use the generalization property of ANN in a large parameter space. In the present investigation, this possibility has been explored by selecting the most significant factor i.e. the impact velocity for EP-LDS composites in a range from 25 to 75 m/sec and the LDS content for PP-LDS, EP-LDS-SGF and PP-LDS-SGF composites in a range of 0 to 50 wt%. Sets of predictions for erosion wear rate of these composites of varied compositions at different impact velocities and LDS contents are evolved and these predicted evolutions are presented in Figures 7.11, 7.12, 7.13 and 7.14. It is interesting to see that the erosion rate presents a linear or an exponential type evolution with the impact velocity.

These figures indicate the effects of impact velocity and LDS content on the erosion rate of these composites. It is noted that while the rate of erosion increases almost linearly or exponentially with increase in impact velocity, there is a gradual drop in it as the LDS content is increased in the composites. The increase in erosion rate with increased impact velocity is obvious. As the velocity of impact of the erodent increases, the kinetic energy carried by it also increases. This causes transfer of greater amount of energy to the target surface upon impact and leads to higher material loss due to erosion. This leads to more surface damage, enhanced sub-critical crack growth etc. and consequently to the reduction in erosion resistance. Similarly the drop in erosion rate with increase in LDS content can be explained as follows: One is the improvement in the bulk hardness of the composite with addition of these hard filler particles. Secondly, during the erosion process, the filler particles absorb a good part of the kinetic energy associated with the erodent. This results in less amount of energy being available to be absorbed by the matrix body and the reinforcing fiber phase.

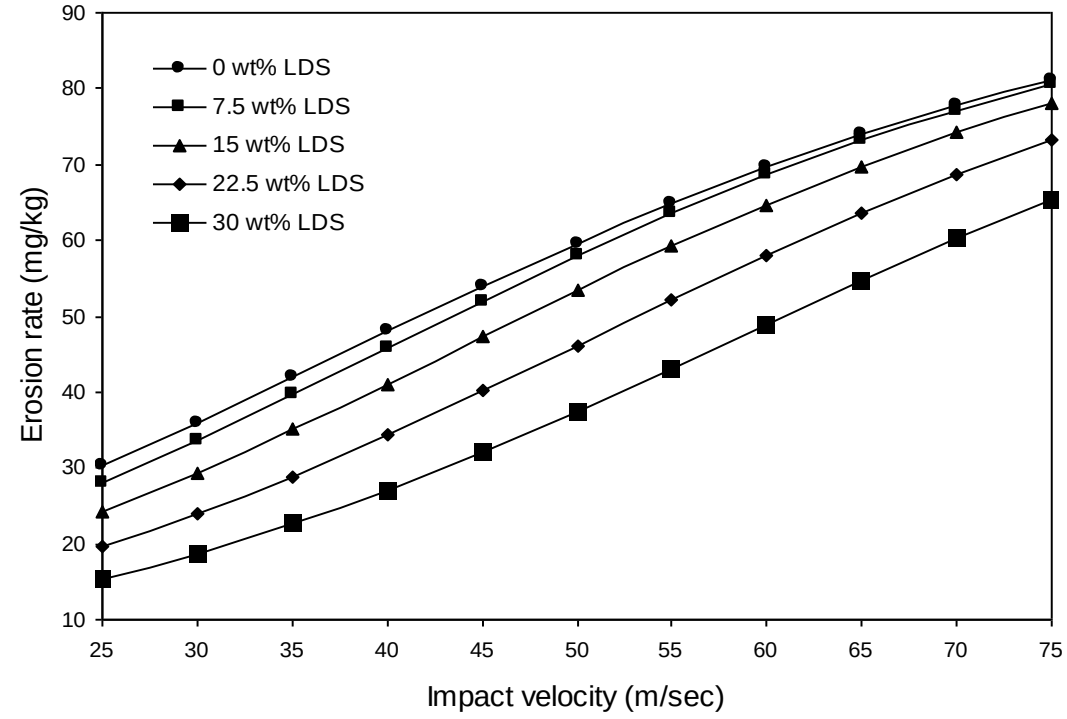

(a)

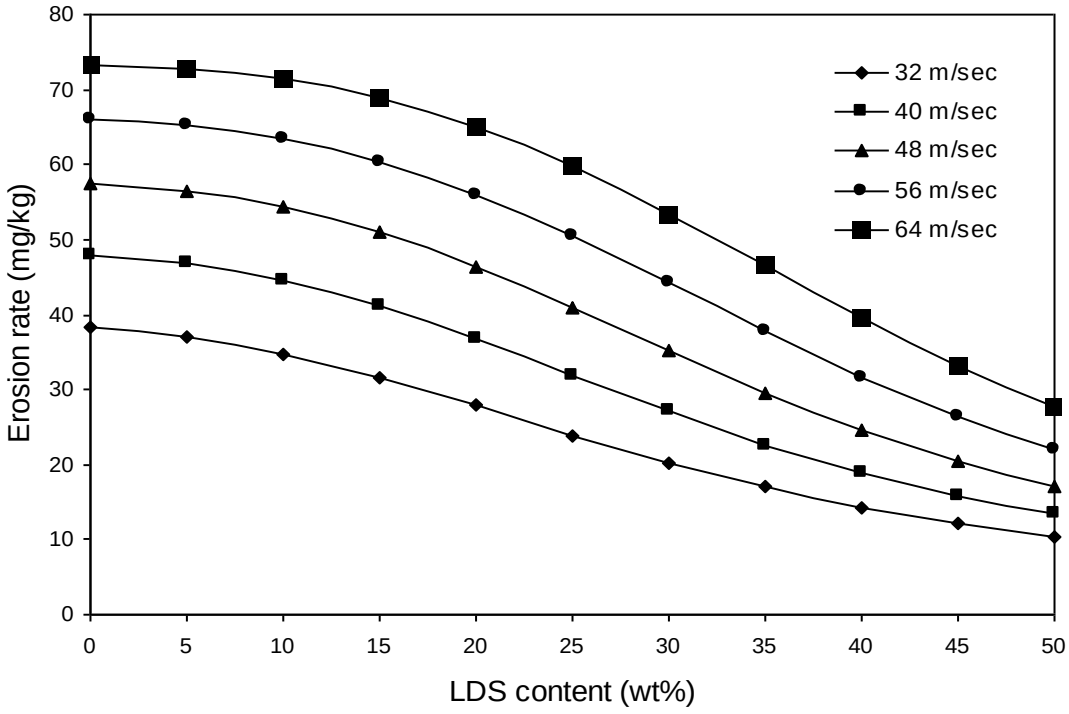

(b)

Figure 7.11 Variation of erosion rate with (a) impact velocity and (b) LDS content for EP-LDS composites

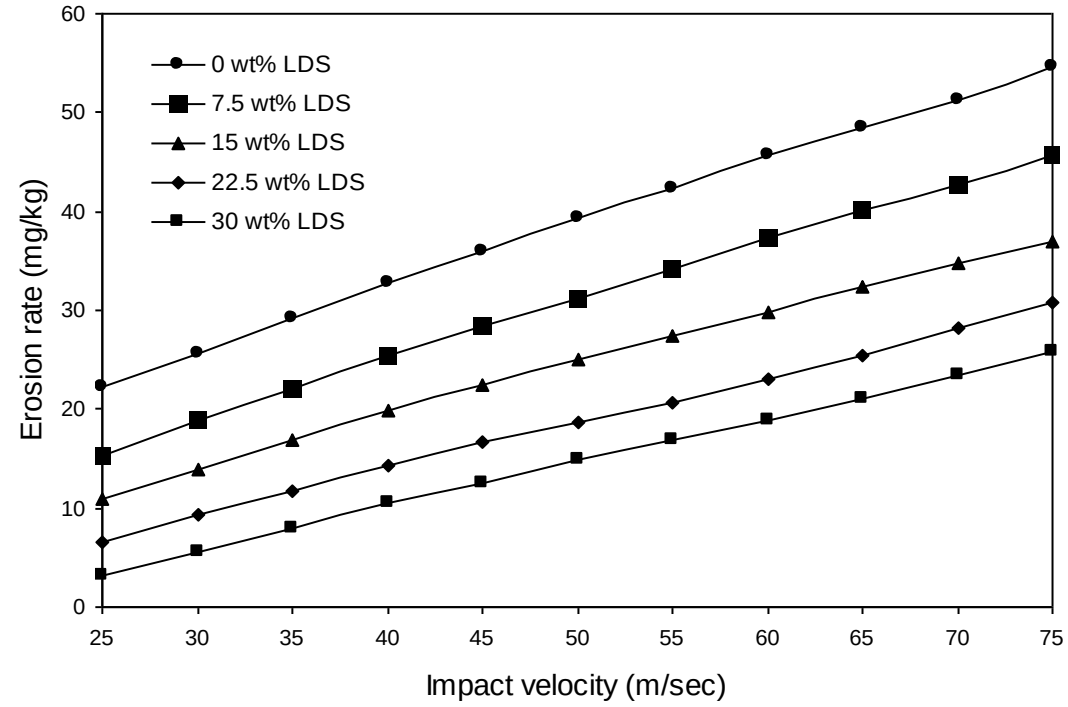

(a)

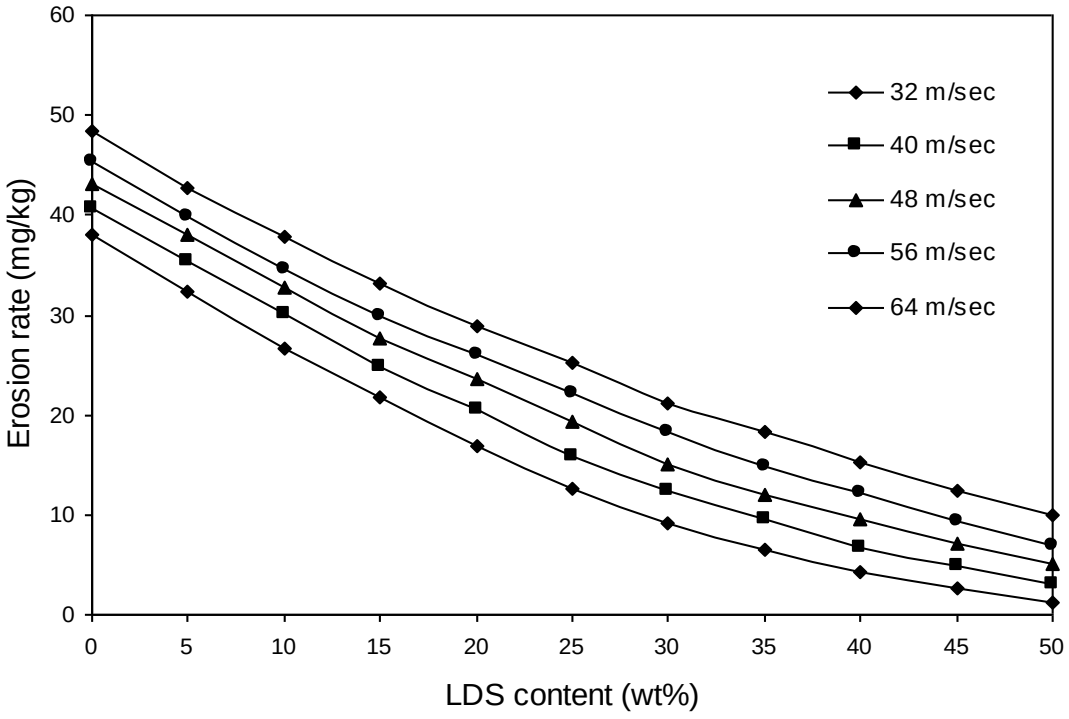

(b)

Figure 7.12 Variation of erosion rate with (a) impact velocity and (b) LDS content for PP-LDS composite

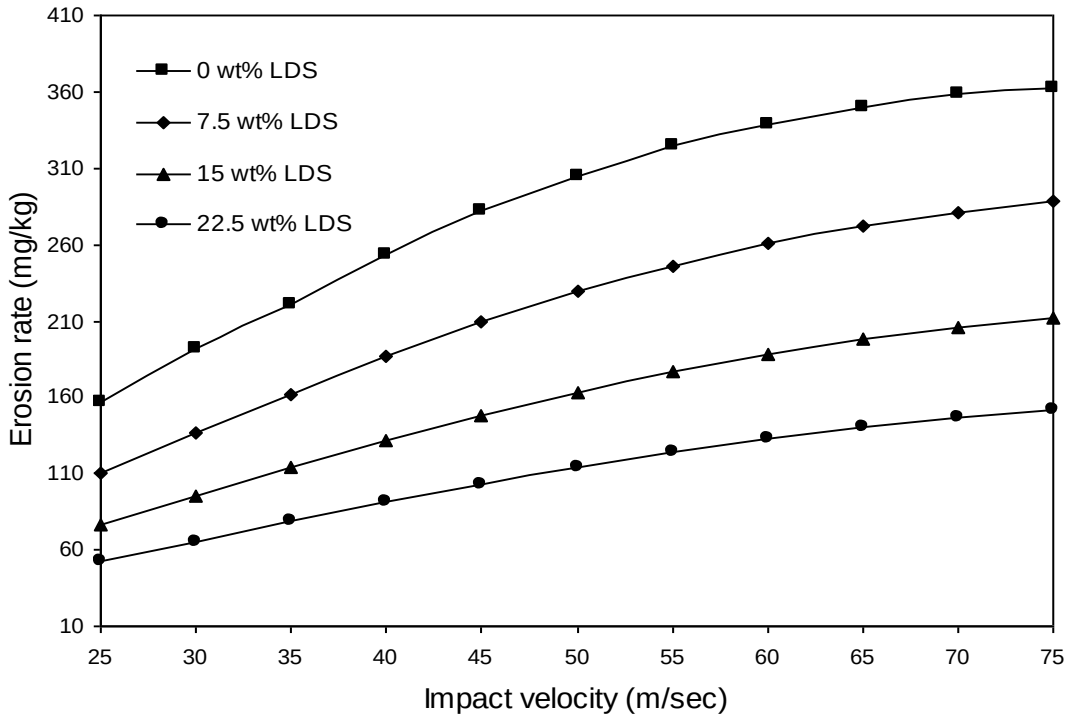

(a)

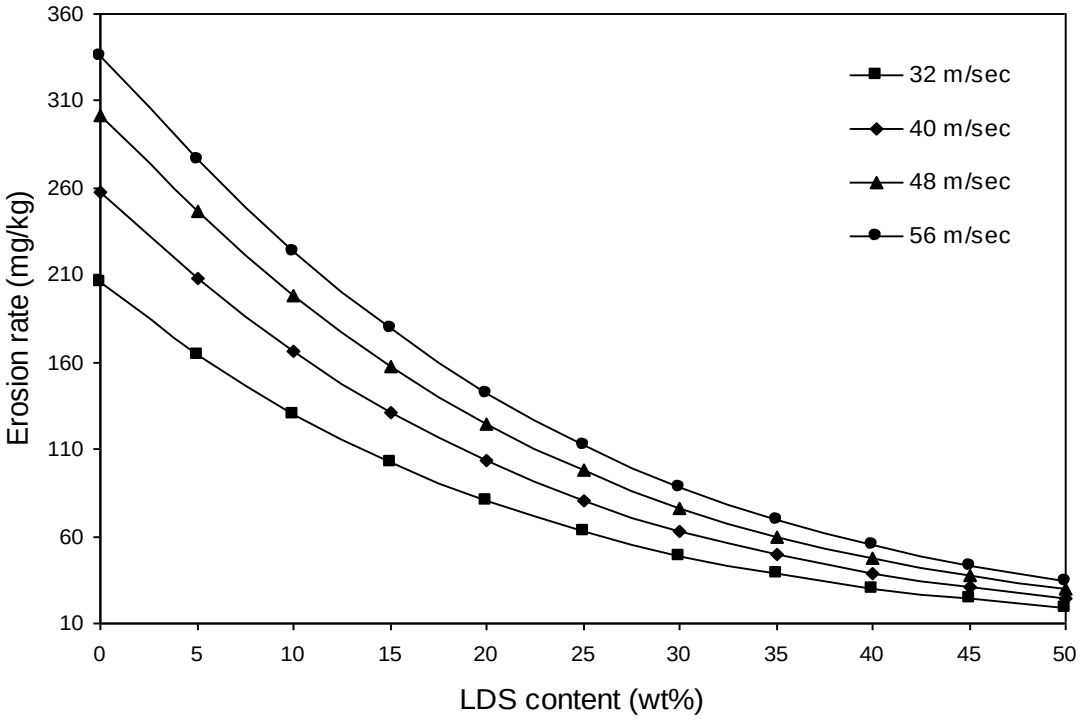

(b)

Figure 7.13 Variation of erosion rate with (a) impact velocity and (b) LDS content for EP-LDS-SGF composite

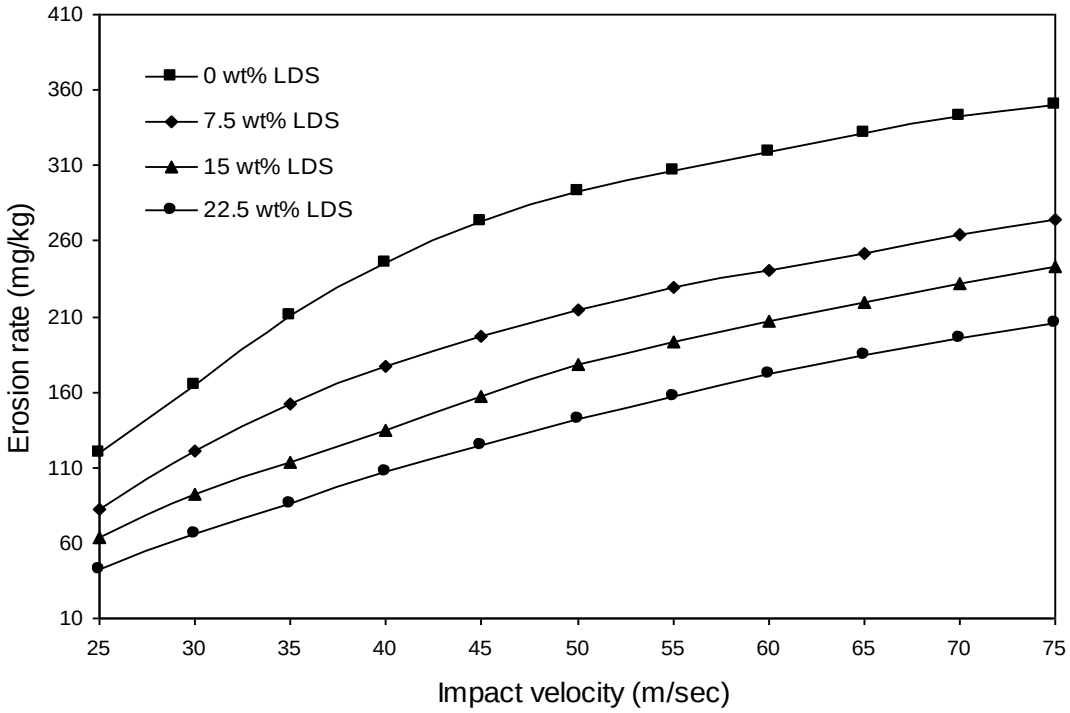

(a)

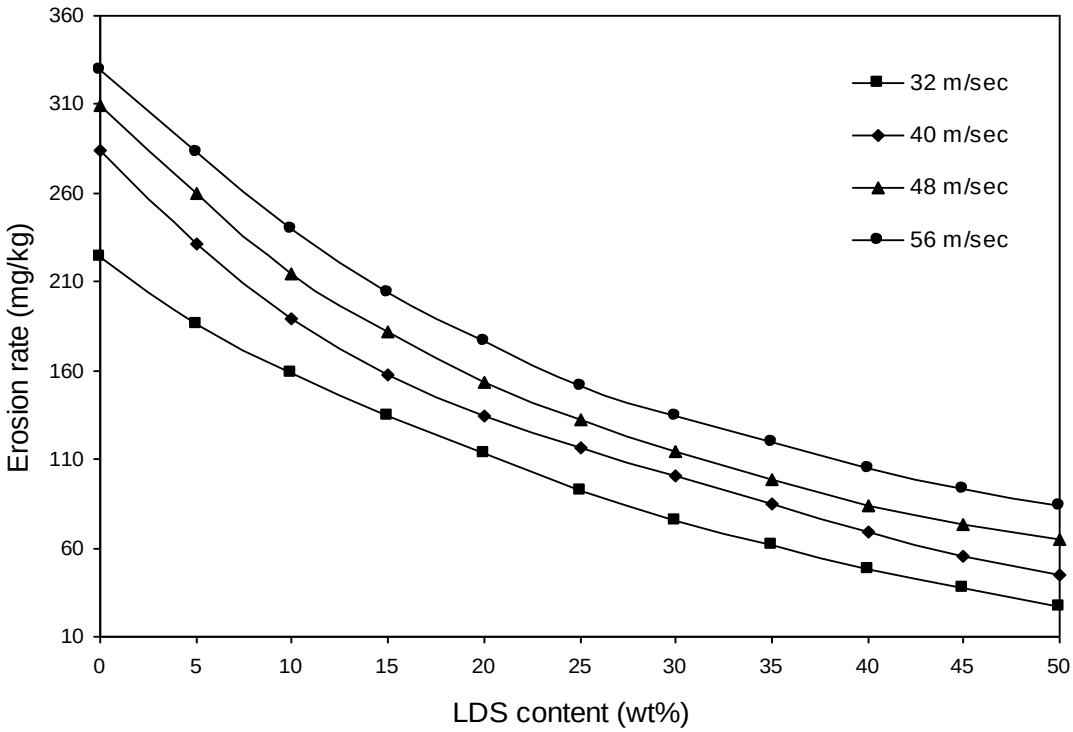

(b)

Figure 7.14 Variation of erosion rate with (a) impact velocity and (b) LDS content for PP-LDS-SGF composite

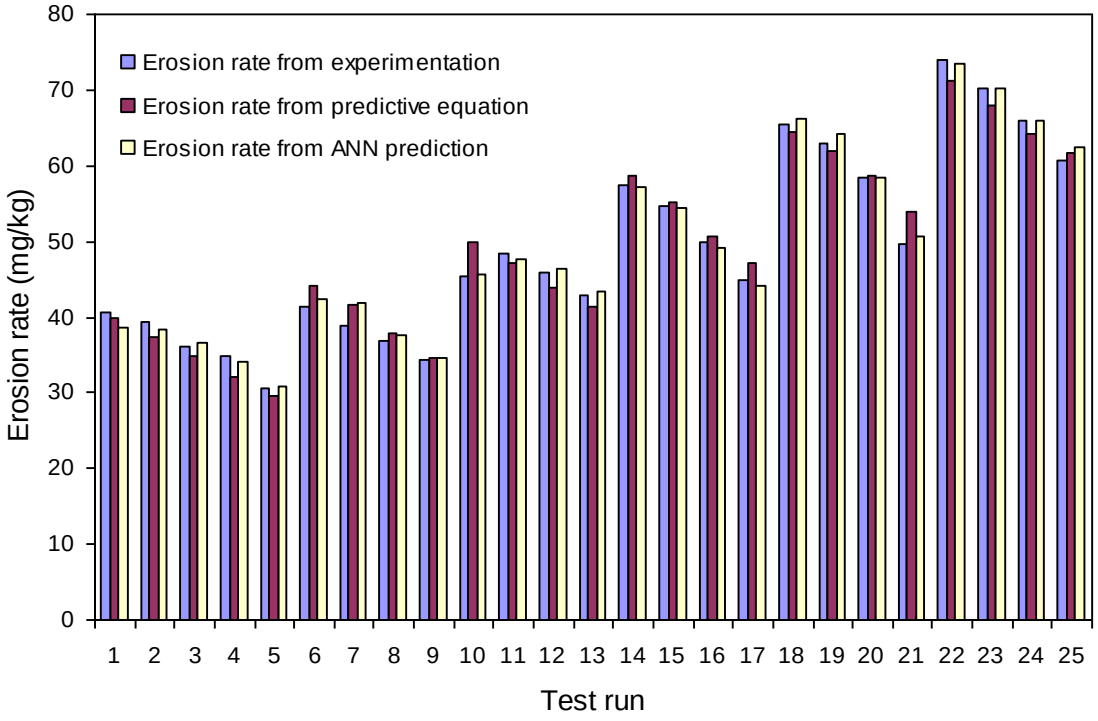

Figure 7.15 Comparison of erosion rates of EP-LDS composites obtained from different methods

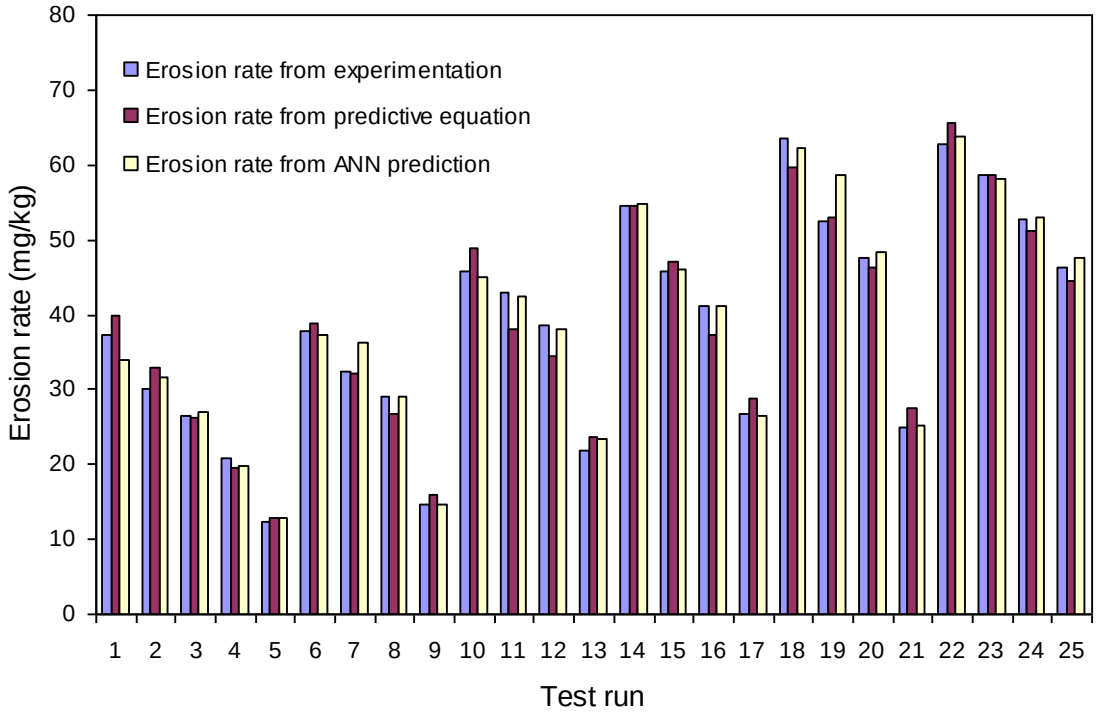

Figure 7.16 Comparison of erosion rates of PP-LDS composites obtained from different methods

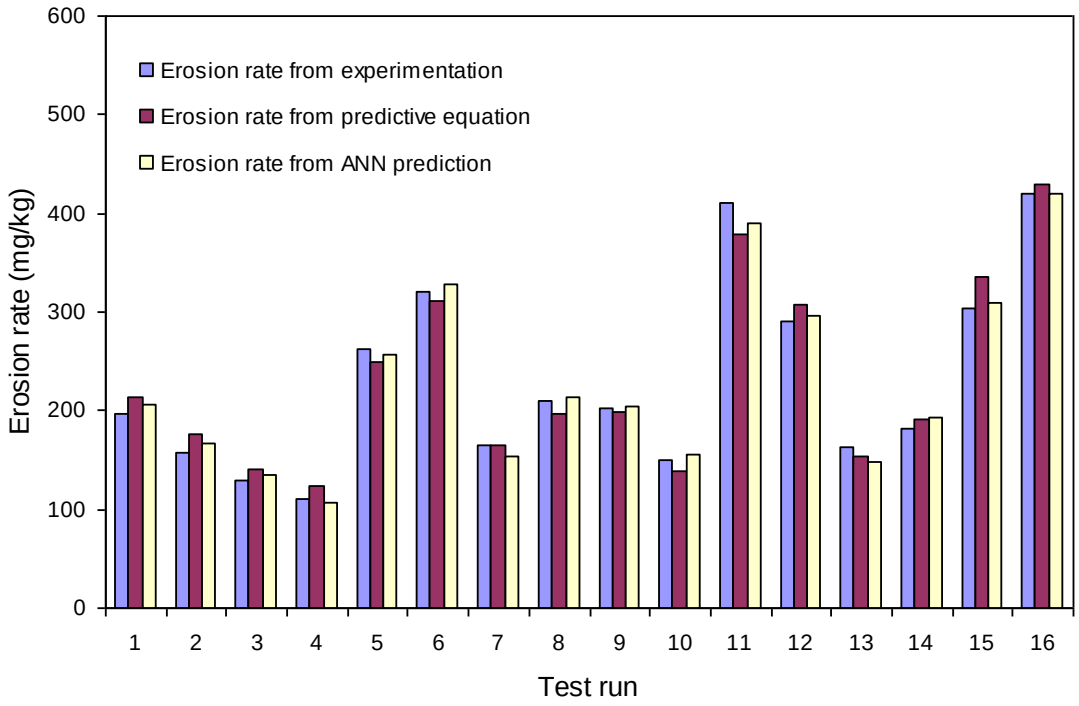

Figure 7.17 Comparison of erosion rates of EP-LDS-SGF composites obtained from different methods

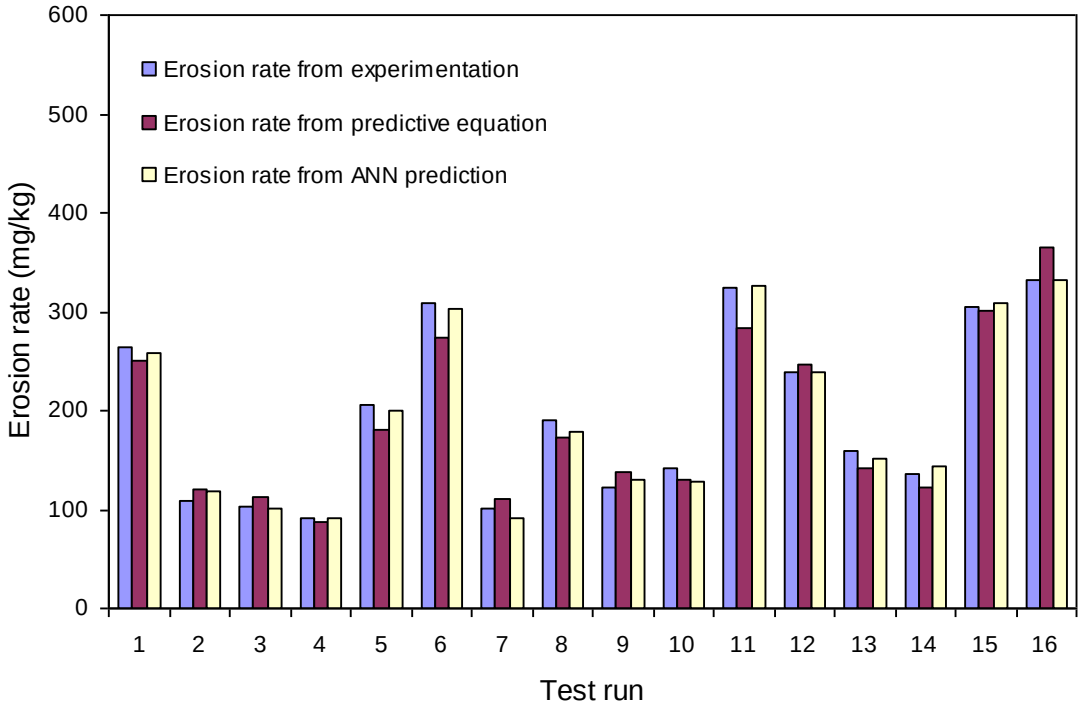

Figure 7.18 Comparison of erosion rates of PP-LDS-SGF composites obtained from different methods

Figures 7.15, 7.16, 7.17 and 7.18 present the comparison of the measured erosion rates with those obtained from the ANN prediction and from the proposed predictive equation for EP-LDS, PP-LDS, EP-LDS-SGF and PP-LDS-SGF composites respectively. While the errors associated with the ANN predictions lie in the range of 0-10%, the same for results obtained from the proposed correlations lie in the range of 0-13%. Thus it can be concluded that both ANN and the proposed correlations can be used for predictive purpose as far as the estimation of erosion wear rate of the composites under this investigation is concerned.

7.6 Effect of Impingement Angle on Erosion Rate

The erosion wear response of polymer composites can be grouped into ductile and brittle categories although this grouping is not definitive because the erosion characteristics depend on the experimental conditions as much as on the composition of the target material. It is well known that impingement angle is one of the important parameters in the erosion process and for ductile materials the peak erosion normally occurs at 15-30^0 angle while for brittle materials, the erosion damage is maximum usually at normal impact i.e. at 90^0 impingement angle.

In the present study, the variation of erosion wear rate of the composites with impingement angle is studied by conducting experiments under specified operating conditions. The results are presented in Figures 7.19 and 7.20 which shows that the peak erosion for hardened neat epoxy occurs at 45^0 impingement angle and for neat PP, peak erosion occurs at 30^0 impingement angle. It is obvious as thermoplastic polymers normally exhibit ductile erosion response. But for the LDS filled epoxy and PP composites, as shown in Figures 7.19 and 7.20, the peak erosion takes place at an impingement angle of 75^0 for EP-LDS composites and at 60^0 for PP-LDS composites irrespective of the filler content, indicating a semi-brittle response. This behaviour may be attributed to the incorporation of hard crystalline LDS particles within the matrix body.

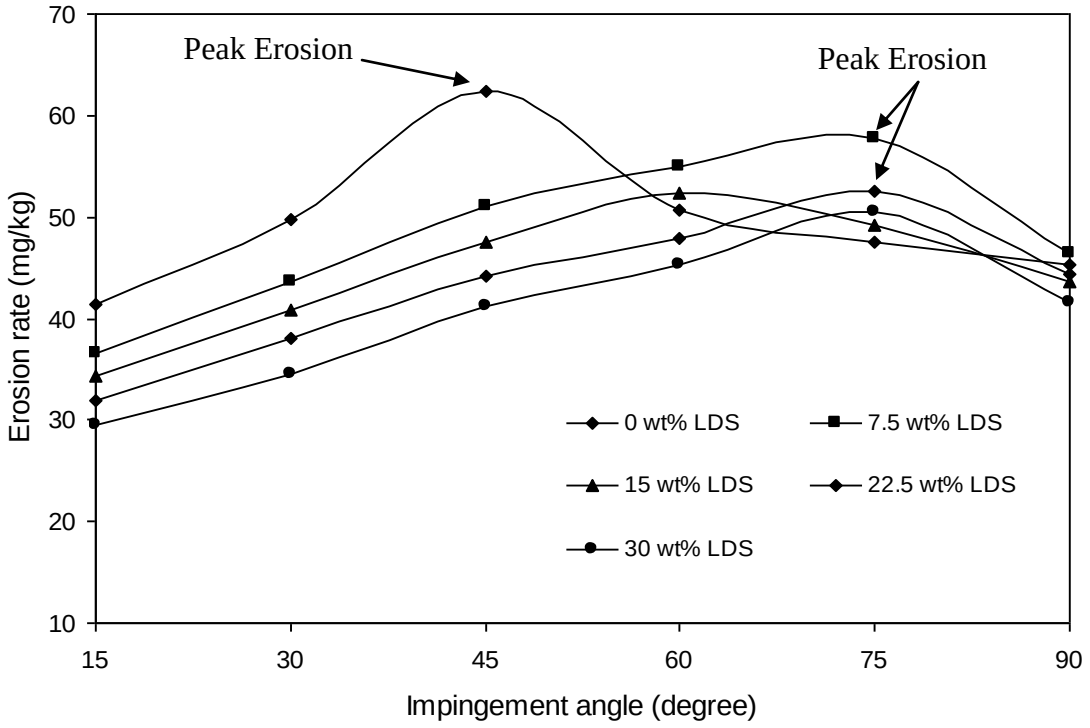

Figure 7.19 Effect of impingement angle on erosion rate of EP-LDS composites (Impact vel. 40 m/sec, erodent size 100 micron, erodent temp. 50^0C)

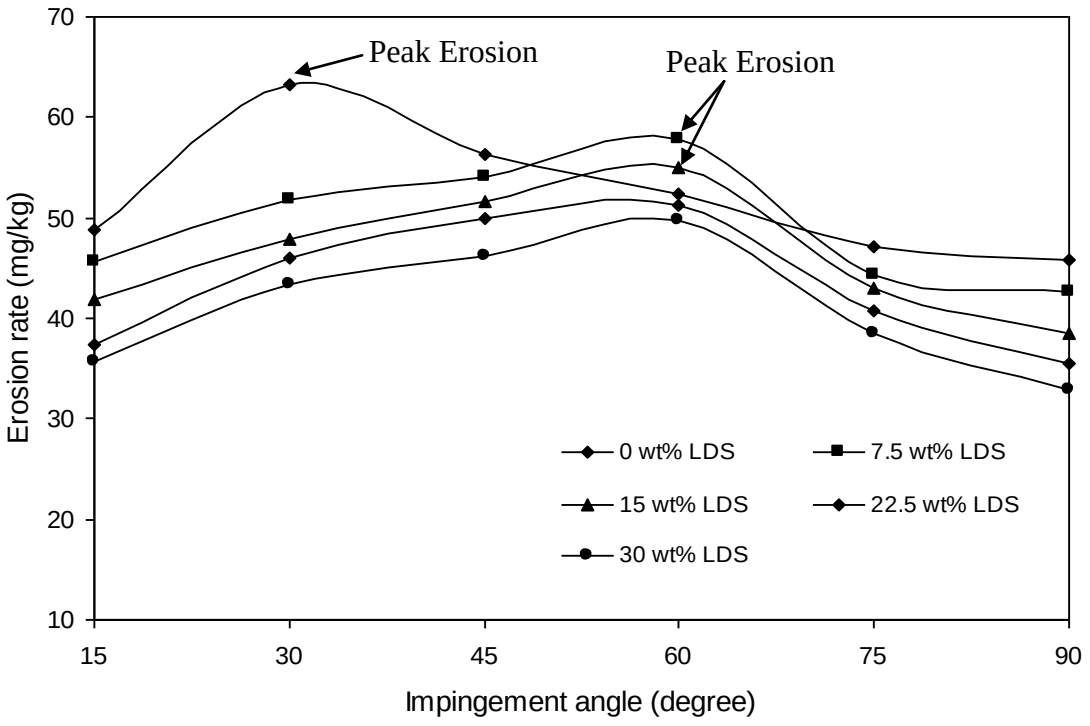

Figure 7.20 Effect of impingement angle on erosion rate of PP-LDS composites (Impact vel. 40 m/sec, erodent size 100 micron, erodent temp. 50^0C)

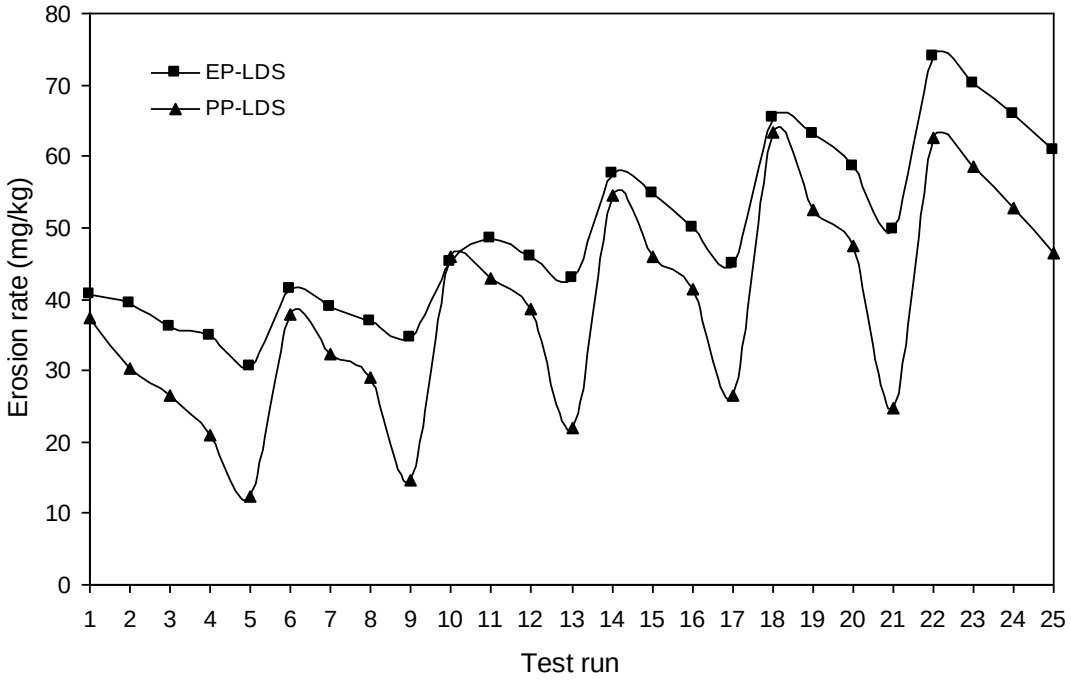

Figure 7.21 Comparison of wear rates of composites without fiber reinforcement under different test conditions

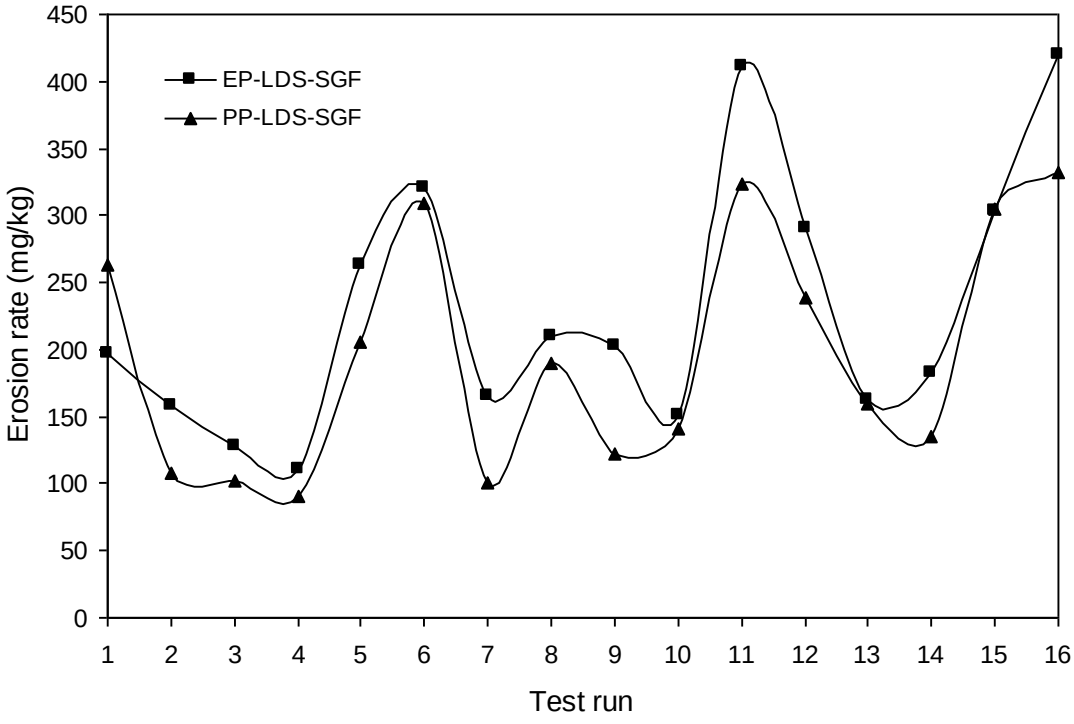

Figure 7.22 Comparison of wear rates of composites with fiber reinforcement under different test conditions

Comparisons of the erosion responses of LDS filled epoxy and PP composites with and without fiber reinforcement are presented in Figures 7.21 and 7.22. The factors which govern the erosion rate of fiber reinforced polymers are: the brittleness of the fibers and the interfacial bond strength between the fibers and the matrix. The sequence of damage due to erosion is in this order (a) local removal of material in the polymer-rich zones, (b) erosion in the fiber zones associated with breakage of fibers and (c) erosion of the matrix-fiber interface zones. Another factor which governs the erosion rate of glass fiber reinforced polymers is the nature of the matrix being either thermosetting or thermoplastic. Thermoplastic polymers become soft and formable when heated and the polymer melt can be formed or shaped when it is in this softened state. On the other hand, thermosetting polymers cannot be shaped or formed to any great extent and will definitely not flow. Hence in the present work, while plastic deformation is predominant in polypropylene (thermoplastic) based composites, features like micro-cutting and matrix-fracture characterize the epoxy (thermosetting) based composites.

Chapter Summary

This chapter has provided:

- The results of erosion tests for LDS filled epoxy and polypropylene composites with and without short glass fiber reinforcement
- The analysis of the experimental results using Taguchi method
- The surface morphologies of uneroded and eroded composites using SEM
- Simulated wear predictions under different test conditions within and beyond the experimental domain using ANN model
- The effect of impingement angle on erosion response of the composites

*****

Chapter 8

Summary and Conclusions

Chapter 8

SUMMARY AND CONCLUSIONS

The research reported in this thesis broadly consists of two parts:

- The first part has provided the description of the materials used, the experimental details and the methods adopted for analysis of experimental results. This part has also presented various physical and mechanical characteristics of the plasma sprayed coatings of LD slag (LDS, 'LDS + Al_2O_3' and 'LDS + TiO_2' coatings) and LD slag filled epoxy and polypropylene composites with and without glass fiber reinforcement. An assessment of LDS as a potential coating material and a particulate filler in polymers has been made by evaluating the physical and mechanical properties of these coatings and composites under controlled laboratory conditions. Effects of premixing of Al_2O_3 and TiO_2 powders on the physical and mechanical properties of LD slag coatings have also been reported in this part.

- The second part reports on the erosion wear characteristics of these coatings and composites. The wear response of LDS, 'LDS + Al_2O_3' and 'LDS + TiO_2' coatings have been discussed separately. Comparisons between the erosion characteristics of LD slag filled epoxy and polypropylene composites with and without fiber reinforcement have also been presented. Parametric analysis and wear response prediction has been made for all the coatings and composites under this study using statistical techniques namely Taguchi experimental design and artificial neural networks (ANN). Correlations have been developed to predict the wear rate for these coatings and composites under different test conditions.

8.1 Summary of Research Findings

This research includes the characterization and wear performance of a new class of plasma sprayed coatings and polymer composites developed using LD slag. For this purpose, a wealth of property data has been generated by conducting various characterization tests on these coatings and composites under controlled laboratory conditions. Some of the worth noting findings of these tests are summarized below.

Plasma spray is the most versatile of the thermal spray processes. Plasma is capable of spraying all materials that are considered sprayable. The quality of coating in terms of mechanical, micro-structural and functional characteristics depends on a large number of variables that include both material as well as operational parameters. While the composition of coating material and the substrate play an important role in determining the coating quality, the influence of plasma torch operating power is also equally important; this is reflected in the research findings of the present investigation. The dependence of different coating characteristics such as coating deposition efficiency, thickness, adhesion strength and micro-hardness on the plasma torch input power is evident in the illustrations presented in this thesis. The erosion rates of 'LDS + Al_2O_3' and 'LDS + TiO_2' coatings are found to be lower than those of LDS coatings under similar test conditions. It is further found that the premixing of Al_2O_3/TiO_2 with LDS improves its coatabilty and the other primary coating characteristics like adhesion strength, thickness etc.

This work also shows that LD slag is successfully used as a functional filler material in both thermoset and thermoplastic polymers. By incorporating micro-sized LDS particles in epoxy and polypropylene, synergistic effects, as expected are achieved in the form of modified mechanical properties and wear resistance. Inclusion of LDS in these polymeric resins has not resulted in any improvement in the load bearing capacity (tensile strength) or in the ability to withstand bending (flexural strength) of the composites. Hardness values have been found to have improved invariably for all the composites on addition of LDS. The

reduction in tensile strength and the improvement in hardness with the incorporation of LDS particles can be further explained as follows: under the action of a tensile force, the filler-matrix interface is vulnerable to debonding depending on interfacial bond strength and this may lead to a break in the composite. But in case of hardness test, a compression or pressing stress is in action. So the polymeric matrix phase and the solid filler phase would be pressed together and touch each other more tightly. Thus, the interface can transfer pressure more effectively although the interfacial bond may be poor. This might have resulted in an enhancement of hardness.

In the present work, it is noticed that the composites filled with LDS have higher void fraction compared to the unfilled composites. The presence of pores and voids in the composite structure significantly affects some of the mechanical properties and even the performance of the composites. Higher void contents usually mean lower fatigue resistance, greater susceptibility to water penetration and weathering. However, presence of void is unavoidable in composite making particularly through hand-lay-up route and that is the reason for the presence of more voids and pores in the LDS filled epoxy composites as compared to the polypropylene composites.

The erosion wear rates of the coatings and composites are found to be dependent on the impingement angle. In fact, the impingement angle determines the relative magnitude of the two components of the impact velocity, namely the components normal and parallel to the surface respectively. The normal component will determine how long the impact will last (that is the contact time and the load). The product of this contact time and the tangential (parallel) velocity component determines the amount of sliding that takes place. The tangential velocity component also provides a shear loading to the surface which is in addition to the normal load that the normal velocity component causes. Hence, as this angle changes, the amount of sliding that takes place also changes the nature and magnitude of the stress system. Both of these aspects influence the way a coating wears out.

It is further observed that invariably in the erosion wear situations, the composites with glass fiber reinforcement suffer from greater material loss (i.e. high wear rate) as compared to the ones without glass fiber reinforcement under similar test conditions. The factors which govern the wear rate of fiber-reinforced polymers are: the brittleness of the fibers and the interfacial bond strength between the fibers and the matrix. Another factor which governs the wear rate of glass fiber-reinforced polymers is the nature of the matrix being either thermosetting or thermoplastic. Thermoplastic polymers become soft and formable when heated and the polymer melt can be formed or shaped when it is in this softened state. On the other hand, thermosetting polymers cannot be shaped or formed to any great extent.

Erosion wear characteristics of these coatings and composites have been analyzed in this work using Taguchi experimental design. Significant control factors affecting the erosion rate have been identified through successful implementation of this technique. Functional coatings and composites have to fulfill various requirements when employed in tribological applications. The wear rate is one such requirement as it is directly related to the service life period of the coatings and composites. In order to achieve certain degree of erosion wear resistance accurately and repeatedly, the influencing parameters of the process have to be controlled accordingly. The present research has shown that neural computation can be successfully applied in this investigation to predict and simulate the wear response of the coatings and composites under various test conditions within and beyond the experimental domain.

8.2 Conclusions

This analytical and experimental investigation on using LD slag in erosion resistant coatings and polymer composites has led to the following specific conclusions:

1. LD slag, in spite of being a waste, is found to be eminently coatable on aluminium substrates. Maximum coating deposition efficiency of about

33% is recorded for this slag by plasma spraying route and it can therefore be gainfully used as a potential cost-effective coating material. Such coatings also possess desirable coating characteristics such as good adhesion strength, hardness etc.

2. Pre-mixing of conventional coating materials like Al_2O_3 or TiO_2 in small proportions with LDS is found to help in further improving the coatability of LDS. The mixture of LDS and Al_2O_3 particles exhibited a deposition efficiency of 33.84% on aluminium substrate and for the mixture of LDS and TiO_2 particles, a coating deposition efficiency of 36.34% is obtained. It is also noted that the coating deposition efficiency presents a sigmoid type evolution with the plasma torch input power.

3. Pre-mixing of Al_2O_3/TiO_2 with LDS leads to production of coatings of improved interfacial adhesion as compared to raw LD slag coatings. Maximum adhesion strength of about 33.77 MPa is recorded in coatings with 30 wt% of Al_2O_3 in the LDS-Al_2O_3 mix and of about 36 MPa in coatings with 30 wt% of TiO_2 in the LDS-TiO_2 mix on aluminium substrate deposited at 20 kW.

4. The coating adhesion strength is noticed to be greatly affected by the plasma torch input power. Adhesion strength of the coatings varied with the plasma power input. The interface bond strength increases with the torch input power up to a certain level and with further increase in input power, there is a drop in coating adhesion strength.

5. The input power to the plasma torch also affects other important coating characteristics such as thickness, porosity and hardness appreciably.

6. LD slag, in spite of being an industrial waste, possesses good reinforcing potential to be used as a filler material in both thermoset and thermoplastic polymer matrices. Successful fabrication of epoxy and polypropylene matrix composites reinforced with micro-sized LDS

particles is possible by simple hand-lay-up technique and by injection molding route respectively. With additional reinforcement of short E-glass fibers, hybrid composites can also be successfully fabricated.

7. Incorporation of this filler modifies the tensile, flexural and impact strengths of the composites. The micro-hardness and density of the composites are also greatly influenced by the type and content of fillers. However, while fabricating a composite of specific requirements, there is a need for the choice of appropriate fiber and filler material for optimizing the composite system.

8. Erosion wear characteristics of LD slag coatings and LD slag filled polymer composites have been analyzed using Taguchi technique. Significant factors affecting the erosion rate of these coatings and composites are identified through successful implementation of this technique. It can be concluded that for all types of coatings and LDS filled epoxy composites without fiber reinforcement, among all the factors, impact velocity is the most significant factor as far as the erosion wear rate is concerned. On the other hand, for LD slag filled polypropylene composites with and without fiber reinforcement and epoxy based composites with fiber reinforcement, among all the factors, LDS content is the most significant factor followed by impact velocity. Erodent size is identified as the factor having very less significance on the erosion rate of the composites irrespective of the matrix type.

9. Impingement angle is found to be another major operating parameter affecting the erosion rate of LD slag filled composites. A study on the variation of erosion rate with impingement angle reveals the semi-brittle erosion response of the composites under this investigation. The peak erosion rate is found to occur at 75^0 impingement angle for all the epoxy based composites and at 60^0 impingement angle for all the polypropylene based composites under similar experimental conditions.

10. Two predictive models; one based on artificial neural networks (ANN) approach and the other on Taguchi approach are proposed in this work. It is demonstrated that these models well reflect the effects of various factors on the wear loss and their predictive results are consistent with the experimental observations. Neural computation is successfully applied in this investigation to predict and simulate the wear response of these coatings and composites under various test conditions within and beyond the experimental domain. The predicted and the experimental values of erosion wear rate exhibit good agreement and validate the remarkable capability of a well-trained neural network for these kinds of processes.

8.3 Recommendation for Potential Applications

The plasma sprayed LDS based coatings developed for this investigation are expected to have adequate potential for a wide variety of applications particularly in erosive environment. In places where cost is a major consideration, the components can be coated with raw LDS particles of suitable size. However, when the possibility of surface degradation due to solid particle erosion is higher and durability of the component is important, coatings of 'LDS + Al_2O_3' and 'LDS + TiO_2' can be employed instead of raw LDS. The use of such coatings is suggested in structural applications such as electric towers and engineering trusses in deserts and mining sites. These coatings can also be recommended for engineering applications such as pipelines and valves carrying particulate matters, transport tubes carrying abrasive materials in an air stream, coal bends carrying pulverized coal, rocket motors trail nozzle, gun barrel, compressor, turbine and exhaust fan blades, burner nozzle, reheater, super heater and economizer tube banks etc.

Composite materials show excellent performance, these days, starting from manufacturing point of view to sports goods. It is due to their light weight, high stiffness-to-weight and strength-to-weight ratios and potentially high resistance to environmental degradation resulting in lower life-cycle costs. The LDS filled epoxy and polypropylene composites with and without fiber reinforcement

fabricated and experimented upon in this investigation are found to have adequate potential for a wide variety of applications particularly in wear prone environment. However, the weight fraction of fiber in the composite is to be decided from the view point of required strength. If the place of use is hostile and highly erosive, then LDS filled glass-epoxy composites are to be preferred due to their fairly good wear resistance. These composites, in general, may also be recommended for applications like partition boards, false ceilings, pipe lines carrying coal dust, chute liners, pulley laggings, exhaust fan blades, nozzles and diffusers, light weight vehicles etc. Use of these composites may also be suggested in applications like engineering structures in dusty environment and low cost building materials in deserts.

8.4 Scope for Future Work

This study opens up a new avenue for the value added utilization of an industrial waste like LD slag and leaves wide scope for future investigators to explore many other aspects of such coatings and composites. Some recommendations for future research include:

- Possible use of ceramic/metallic powders as additive in the development of LD slag based composite coatings.
- Possible use of other industrial wastes, polymeric resins and natural fibers in the development of new wear resistant hybrid composites.
- Study on the response of these coatings and composites to other wear modes such as sliding, abrasion and slurry erosion.
- Cost analysis of these coatings and composites to assess their economic viability in industrial applications.

*****

References

REFERENCES

1. Maslehuddin M., Alfarabi A.M., Sharif M., Shameen M., Ibrahim M. and Barry M.S. (2003), Comparison of properties of steel slag and crushed limestone aggregate concretes, Construct Build Mater, 17(2), pp. 105-12.

2. Patnaik A. (2009), Development, Characterization and Solid Particle Erosion Response of Polyester based Hybrid Composites, Ph.D. Thesis, NIT, Rourkela, India.

3. Pool K.V., Dharan C.K.H. and Finnie I. (1986), Erosive wear of composite materials, Wear, 107, pp. 1-12.

4. Wahl H. and Hartenstein F. (1946), Strahlverschleiss, Frankh'sche Verlagshandlung, Stuttgart.

5. Bitter J.G.A. (1963), A study of erosion phenomena, Part II, Wear, 6, pp. 169-190.

6. Raask E. (1969), Tube erosion by ash impaction, Wear, 13, pp. 301-315.

7. Hibbert W.A. and Roy J. (1965), Aero. Soc, 69, pp. 769-776.

8. Cai K., Xia J., Li L. and Gui Z. (2005), Analysis of the Electrical Properties of PZT by a BP Artificial Neural Network, Comp. Mat. Sc., 34, pp. 166-172.

9. Guo D., Li L., Nan C., Xia J. and Gui Z. (2003), Modeling and Analysis of the Electrical Properties of PZT Through Neural Networks, J. Eur. Cer. Soc., 23, pp. 2177-2181.

10. Bhadeshia M.K.D.H. (1999), Estimation of the Hot-Torsion Stress-Strain Curves in Iron Alloys Using Neural Network Analysis, ISIJ Int., 39 (10), pp. 966-979.

11. Robert B.H. (1996), Plasma Sprayed Coatings; Principles and Applications, VCH Publishing, New York.

12. Maejka D. and Benko B. (1989), Plasma Spraying of and Ceramic Materials, John Wiley, New York.

13. Liu C.T., White C.L., Koch C.C., Liu C.T. and Stollof N.S. (1985), High Temp Ordered Intermetallic Alloys, Mat Res Soc, pp. 365-71.

14. Briscoe B.J. (1985), Wear of Poly (Tetrafluoroethylene) Polymer and Its Control, Polymer Wear and Control, American Chemical Society, pp. 151-170.

15. Briscoe B.J., Lao L.H. and Stolarski T.A. (1985), Wear of Materials, American Society of Mechanical Engineers, pp. 725-731.

16. Lu X.C., Wen S.Z., Tong J., Chen Y.T. and Ren L.Q. (1996), Wettability, Soil Adhesion Abrasion and Friction Wear of PTFE (+PPS) +Al_2O_3 Composites, Wear, 193, pp. 48-55.

17. Ivosevic M., Knight R., Kalidindi S.R., Palmese G.R. and Sutter J.K. (2005), Adhesive/Cohesive Properties of Thermally Sprayed Functionally Graded Coatings for Polymer Matrix Composites, Journal of Thermal Spray Technology, 14(1), pp. 45-51.

18. Niebuhr D. and Scholl M. (2005), Synthesis and Performance of Plasma Sprayed Polymer/Steel Coating System, Journal of Thermal Spray Technology, 14(4), pp. 487-494.

19. Wang B.Q., Geng G.Q. and Levy A.V. (1992), Erosion and erosion- corrosion behavior of chromized-siliconized steel, Surface and Coatings Technology, 54-55 (2), pp. 529-535.

20. Modi M.D., Modi S.C. and Mayuram M.M. (1986), A case study on the use of plasma sprayed oxide ceramic coatings in hot extrusion dies for nonferrous metals, In: Proceedings of the 11th international thermal spraying conference, 8-12 September, Montreal, Canada, pp. 359-366.

21. Fu Y.Q., Batchelor A.W., Wang Y. and Khor K.A. (1998), Fretting wear behaviors of thermal sprayed hydroxyapatite (HA) coating under unlubricated conditions, Wear, 217, pp. 132-139.

22. Liao H., Normand B. and Coddet C. (2000), Influence of coating microstructure on the abrasive wear resistance of WC/Co cermet coatings, Sur. and Coat. Tech., 124, pp. 235-242.

23. Auciello O. and Flamm D.L. (1989), Plasma diagnostics, Plasma-materials Interactions, Vol. 1, Academic Press, Boston, Mass.

24. Tucker (Jr.) R.C. (2002), Thermal spray coatings: broad and growing applications, International Journal of Powder Metallurgy, 38 (7), pp. 45-53.

25. Westergard R., Erickson L.C., Axen N., Hawthorne H.M. and Hogmark S. (1998), The erosion and abrasion characteristics of alumina coatings plasma sprayed under different spraying conditions, Tribology International, 1 (5), pp. 271-279.

26. Toma D., Brandl W. and Marginean G. (2001), Wear and corrosion behaviour of thermally sprayed cermet coatings, Surface and Coatings Technology, 138 (2-3), pp. 149-158.

27. Satapathy A., Sahu S.P. and Mishra D. (2010), Development of protective coatings using fly ash premixed with metal powder on aluminium substrates, Waste Management & Research, 28 (7), pp. 660-666.

28. Budinski K.G. (1998), Surface engineering for wear resistance, Prentice Hall, Englewood Cliffs, New Jersey, USA, pp. 209.

29. Heimann R.B. (1996), Plasma spray coating, principle and application, VCH, Weinheim, Germany.

30. Little R.L. (1979), Welding and welding technology, TMH Publications, New Delhi, India.

31. Pawlowski L. (1995), The science and engineering of thermal spraying, Willey, USA.

32. Metco Plasma Spraying Manual (1993), Metco, USA.

33. Novak R.C. (1988), Processing aspects of plasma sprayed ceramic coatings, Journal of Engineering for Gas Turbines and Power, 110 (4), pp. 617-620.

34. Nash D.R., Weare N.E. and Walker D.L. (1961), Process variables in plasma-jet spraying, Journal of Metals, 13 (7), pp. 483-486.

35. Gruner H. (1984), Vacuum plasma spray quality control, Thin Solid Films, 118 (4), pp. 409-420.

36. Eaton H. and Novak R.C. (1986), A study of the effects of variations in parameters on the strength and modulus of plasma sprayed zirconia, Surface and Coatings Technology, 27 (3), pp. 257-267.

37. Wielage B., Hofmann V., Steinhauser A. and Zimmerman G. (1998), Improving wear and corrosion resistance of thermal sprayed coatings, Surface Engineering, 14 (2), pp. 136-138.

38. Lee W.Y., Stinton D.P., Brandt C.C., Erdogan F., Lee Y.D. and Mutasim Z.Z. (1996), Thermal barrier coatings, Journal of Americal Ceramic Society, 79 (12), pp. 3003-3012.

39. Guessasma S., Bounazef M., Nardin P. and Sahraoui T. (2006), Wear behavior of alumina Titania coatings: analysis of process and parameters, Cer. Int., 32, pp. 13-19.

40. Ouyang J.H. and Sasaki S. (2005), Tribological characteristics of low pressure plasma-sprayed Al_2O_3 coating from room temperature to 800^0C, Trib. Int., 38 (1), pp. 49-57.

41. Kov´aˇr´ık O., Siegl J., Nohava J. and Chr´aska P. (2005), Young's modulus and fatigue behavior of plasma-sprayed alumina coatings, J. of Ther. Sp. Tech., 14, pp. 231-238.

42. Ramachandran K., Selvarajan V., Ananthapadmanabhan P. V. and Sreekumar K. P. (1998), Microstructure, adhesion, micro-hardness, abrasive wear resistance and electrical resistivity of the plasma sprayed alumina and alumina-titania coatings, Thin Sol. Films, 315 (1-2), pp. 144-152.

43. Xie Y. and Hawthorne H.M. (1999), The damage mechanisms of several plasma sprayed ceramic coatings in controlled scratching, Wear, 233-235, pp. 293-305.

44. Erickson L.C., Hawthorne H.M. and Troczynski T. (2001), Correlations between microstructural parameters, micromechanical properties and wear resistance of plasma-sprayed cermaic coatings, Wear, 250 (1), pp. 569-575.

45. Fernandez J.E., Rodriguez R., Wang Y., Vijande R. and Rincon A. (1995), Sliding wear of a plasma-sprayed Al_2O_3 coating, Wear, 181-183 (1), pp. 417-425.

46. Budinsky K.G. (1995), Abrasion resistance of transport roll surfaces, Wear, 181-183 (2), pp. 938-943.

47. Bolelli G., Cannillo V., Lusvarghi L. and Ricc`o S. (2006), Mechanical and tribological properties of electrolytic hard chrome and HVOF-sprayed coatings, Surf. and Coat. Tech., 200, pp. 2995-3009.

48. Hsu S.M. and Shen M. (2004), Wear prediction of ceramics, Wear, 256, pp. 867-878.

49. Kato K. and Adachi K. (2002), Wear of advanced ceramics, Wear, 253, pp. 1097-1104.

50. Adachi K., Kato K. and Chen N. (1997), Wear map of ceramics, Wear, 203-204, pp. 291-301.

51. Cadenas M., Vijande R., Montes H.J. and Sierra J.M. (1997), Wear behaviour of laser cladded and plasma sprayed WC-Co coatings, Wear, 212 (2), pp. 244-253.

52. Roy M., Rao C.V.S., Rao D.S. and Sundarrajan G. (1999), Abrasive wear behaviour of detonation sprayed WC-Co coatings on mild steel, Surf. Eng., 15 (2), pp. 129-136.

53. Chuanxian D., Bingtang H., Huiling L. (1984), Plasma-sprayed wear- resistant ceramic and cermet coating materials, Thin Sol. Films, 118 (4), pp. 485-493.

54. Guilemay J.M., Nutting J., and de Paco J.M. (1995), In: Proc. 4th Eur. Conf. Advanced Materials Processing, Venice, Sept. 25-28, Association Italiana di Metallurgica, Milan, 1996, pp. 395-398.

55. Wang Y. (1993), Friction and wear performances of detonation gun and plasma-sprayed ceramic and cermet hard coatings under dry friction, Wear, 161 (1-2), pp. 69-78.

56. Wang Y., Yansheng J. and Shizhu W. (1988), The Analysis of the Friction and Wear Mechanisms of Plasma Sprayed Ceramic Coatings at 450^0, Wear, 128, pp. 265-276.

57. Tronche A. and Fauchais P. (1988), Frictional behaviour against steel of aluminium substrates plasma-sprayed with hard coatings, Mat. Sc. and Eng.: A, 102 (1), pp. 1-12.

58. Stuart D.A., Shipway P.H. and McCartney D.G. (1999), Abrasive wear behaviour of conventional and nanocomposite HVOF-sprayed WC-Co coatings, Wear, 225-229 (2), pp. 789-798.

59. Mohanty M., Smith R.W., De Bonte M., Celis J.P. and Lugscheider E. (1996), Sliding wear behavior of thermally sprayed 75/25 Cr_3C_2/NiCr wear resistant coatings, Wear, 198 (1-2), pp. 251-266.

60. Li J.F., Ding C.X., Huang J.Q. and Zhang P.Y. (1997), Wear Mechanism of Plasma Sprayed Cr_3C_2-NiCr Against TiO_2 Coatings, Wear, 211 (2), pp. 177-184.

61. Gee M.G. (1992), The formation of aluminium hydroxide in the sliding wear of alumina, Wear, 153 (1), pp. 201-227.

62. McPherson R. (1973), The enthalpy of formation of aluminium titanate, J. of Mat. Sc., 8, pp. 851-858.

63. McPherson R. (1980), On the formulation of thermally sprayed alumina coating, J. of Mat. Sc., 15, pp. 3141-3149.

64. López A.R.D.A. and Faber K.T. (1999), Microstructural Characterization of Small-Particle Plasma Spray Coatings, J. of the Am. Cer. Soc., 82 (8), pp. 2204-2208.

65. Mendelson M.I. (1978), Theoretical evaluation of wear in plasma-sprayed TiO_2 against grey cast iron, Wear, 50 (1), pp. 71-83.

66. Metco Technical Bulletin on TiO_2. (1971), Metco Inc., NY, USA.

67. Dai W.W., Ding C.X., Li J. F., Zhang Y.F. and Zhang P.Y. (1996), Wear mechanism of plasma-sprayed TiO_2 coating against stainless steel, Wear, 196 (1-2), pp. 238-242.

68. Suh N.P. (1979), Comments on "The metallography of worn surfaces and some theories of wear, Wear, 56 (2), pp. 423-424

69. So H. (1995), The mechanism of oxidational wear, Wear, 184, pp. 161-167.

70. Eyre T.S. (1975), Effect of Boronising on Friction and Wear of Ferrous Metals, Wear, 34, pp. 383-397.

71. Halling J. (1975), Principles of Tribology, The Mcmillan Press Ltd, NY, USA.

72. Guilmad Y., Denape J. and Patil J. A. (1993), Friction and Wear Thresholds of Alumina-Chromium Steel Pairs Sliding at High Speeds Under Dry and Wet Conditions, Trib. Int., 26, pp. 29-39.

73. Bayrak G. and Yılmaz S. (2006), Crystallization kinetics of plasma sprayed basalt coatings, Cer. Int., 32 (4), pp. 441-446.

74. Hebsur M.G. and Miner R.V. (1986), High temperature tensile and creep behaviour of low pressure plasma-sprayed Ni-Co-Cr-Al-Y coating alloy, Mat. Sc. Eng., 83 (2), pp. 239-245.

75. Metals Handbook, ASM, Metals Park, Ohio, USA.

76. Moore M.A. (1974), The relationship between the abrasive wear resistance, hardness and microstructure of ferritic materials, Wear, 28 (1), pp. 59-68.

77. Hurricks P.L. (1972), Some aspects of the metallurgy and wear resistance of surface coatings, Wear, 22 (3), pp. 291-320.

78. Spear A.E. (1989), Diamond-Ceramic Coating of the Future, J. of the Am. Cer. Soc., 73, pp. 171.

79. Marakawa A. (1997), Surface Coatings of Super Hard Materials for Tool Applications, Mat. Sc. Forum, 246, pp. 1-28.

80. Zhu W., Tan B.H. and Tan H.S. (1993), Diamond thin films synthesized by a multinozzle oxy-acetylene chemical vapour deposition method, Thin Sol. Films, 236 (1-2), pp. 106-110.

81. Hollman P., Alhelisteten A., Bjorke T. and Hogmark S. (1994), CVD- diamond coatings in sliding contact with Al, Al-17Si and steel, Wear, 179 (1-2), pp. 11-16.

82. Alahelisten A. (1995), Abrasion of Hot Flame-Deposited Diamond Coatings, Wear, 185 (1-2), pp. 213-224.

83. Wu C., Ramaswamy Y., Liu X., Wang G. and Zreiqat H. (2009), Plasma-sprayed $CaTiSiO_5$ ceramic coating on Ti-6Al-4V with excellent bonding strength, stability and cellular bioactivity, J.R.Soc. InterfaceR. Soc., 31 (6), pp. 159-168.

84. Amiruddin A.M.H., Shamsudin R., Jalar A. and Hamid M.A.A. (2012), Single layer of brushite coating onto stainless steel substrate using dip-coating technique, Adv. Mater. Res., 399-401, pp. 2004-2007.

85. Cao X.Q., Vassen R., Schwartz S., Jungen W., Tietz F. and Stöever D. (2000), Spray-drying of ceramics for plasma-spray coating, J. Eur. Ceram. Soc., 20 (14-15), pp. 2433–2439.

86. Brogan J.A., Gross K.A., Chen Z., Berndt C.C., Herman H. and Sampath S. (1994), Thermal spray industrial applications, ASM Int. (pub.).

87. Mishra S.C., Satapathy A., Behera R.K., Dhar R.K., Sreekumar K.P. and Ananthapadmanabhan P.V. (2002), Plasma Spray Coating of Red Mud on Metals, PBAMP, BARC, Mumbai, pp. 9-12.

88. Satapathy A. (2005), Thermal Spray Coating of Red Mud on Metals, Ph.D. Thesis, NIT, Rourkela, India.

89. Mishra S.C., Das S., Satapathy A., Sarkar S., Ananthapadmanabhan P.V. and Sreekumar K.P. (2009), Investigation on Composite Coating of Low Grade Minerals, J. of Rein. Plas. and Comp., 28(24), pp. 3061-3067.

90. Sahu S.P., Satapathy A., Patnaik A., Sreekumar K.P. and Ananthapadmanabhan P.V. (2010), Development, characterization and erosion wear response of plasma sprayed fly ash-aluminum coatings, Materials and Design, 31, pp. 1165-1173.

91. Yilmaz S., Okumus S.C., Demirkiran A.S. and Bindal C. (2004), Fly ash based plasma spray coating, Key Eng. Mat., 264-268, pp. 533-536.

92. Krishna L.R., Sen D., Rao D.S. and Sundararajan G., (2003), Cotability and Characterization of Fly Ash Deposited on Mild Steel by Detonation Spraying, J. of Ther. Sp. Tech., 12 (1), pp. 77-79.

93. Ramesh C.S., Seshadri S.K. and Iyer K.J.L. (1991), Wear resistance of Nickel-fly ash composite coatings, Wear, 145, pp. 189-195.

94. Ramesh C.S. and Seshadri S.K. (2003), Tribological characteristics of nickel based composite coatings, Wear, 255, pp. 893-902.

95. Mishra S.C., Rout K.C., Ananthapadmanabhan P.V. and Mills B. (2000), Plasma Spray Coating of Fly Ash Pre-Mixed with Aluminium Powder Deposited on Metal Substrates, J. Mat. Proc. Tech., 102 (1-3), pp. 9-13.

96. Sidhu B.S., Singh H., Puri D. and Prakash S. (2007), Wear and oxidation behaviour of shrouded plasma sprayed fly ash coatings, Trib. Int., 40, pp. 800-808.

97. Muhammad M.M., Isa M.C., Shamsudin R. and Jalar A. (2014), Plasma spray deposition of fly ash onto mild steel substrates using a fractional factorial design approach, Ceramics International, 40, pp. 13635-13642.

98. Mantry S., Behera D., Mishra S.K., Debasish D., Jha B.B. and Mishra B.K. (2013), Erosive Wear Analysis of Plasma-Sprayed Cu Slag-Al Composite Coatings, Tribology Transactions, 56, pp. 196-202.

99. Mantry S., Jha B.B. and Satapathy A. (2013), Evaluation and Characterization of Plasma sprayed Cu slag-Al composite coatings on metal substrates, Journal of Coatings, DOI: 10.1155/2013/842865.

100. Takei T., Hatta H. and Taya M. (1991), Thermal expansion behavior of particulate-filled composites with single reinforcing phase, Materials Science and Engineering: A, 131, pp. 133-143.

101. Ranganath S. (1997), A review on particulate-reinforced titanium matrix composites, Journal of Materials Science, 32 (1), pp. 1-16.

102. Sawyer W.G., Freudenberg K.D., Bhimaraj P. and Schadler L.S. (2003), A study on the friction and wear behavior of PTFE filled with alumina nanoparticles, Wear, 254 (5-6), pp. 573-580.

103. Kim J, Kang P.H. and Nho Y.C. (2004), Positive temperature coefficient behavior of polymer composites having a high melting temperature, Journal of Applied Polymer Science, 92 (1), pp. 394-401.

104. Nikkeshi S., Kudo M. and Masuko T. (1998), Dynamic visco-elastic properties and thermal properties of powder-epoxy resin composites, Journal of Applied Polymer Science, 69 (13), pp. 2593-2598.

105. Nielsen L.E and Landel R.F. (1994), Mechanical properties of polymers and composites, 2nd ed. New York: Marcel Dekker, pp. 557.

106. Peters S.T. (1998), Handbook of composites, 2nd ed. London: Chapman and Hall, pp. 242-243.

107. Sumita M., Shizuma T., Miyasaka K. and Ishikawa K. (1983), Effect of reducible properties of temperature, rate of strain, and filler content on the tensile yield stress of nylon 6 composites filled with ultrafine particles, Journal of Macromolecular Science: Part B, 22 (4), pp. 601-618.

108. Bartczak Z., Argon A.S., Cohen R.E. and Weinberg M. (1999), Toughness mechanism in semi-crystalline polymer blends: II. High-density polyethylene toughened with calcium carbonate filler particles, Polymer, 40 (9), pp. 2347-2365.

109. Radford K.C. (1971), The mechanical properties of an epoxy resin with a second phase dispersion, Journal of Materials Science, 6 (10), pp. 1286-1291.

110. Imanaka M., Takeuchi Y., Nakamura Y., Nishimura A. and Lida T. (2001), Fracture toughness of spherical silica-filled epoxy adhesives, International Journal of Adhesion Adhesives, 21 (5), pp. 389-396.

111. Wang H., Bai Y., Liu S., Wu J. and Wong C.P. (2002), Combined effects of silica filler and its interface in epoxy resin, Acta Materialia, 50 (17), pp. 4369-4377.

112. Yamamoto I., Higashihara T. and Kobayashi T. (2003), Effect of silica particle characteristics on impact/usual fatigue properties and evaluation of mechanical characteristics of silica-particle epoxy resins, JSME International Journal-Series A: Solid Mechanics and Material Engineering, 46 (2), pp. 145-153.

113. Nakamura Y., Yamaguchi M., Kitayama A., Okubo M. and Matsumoto T. (1991), Effect of particle size on fracture toughness of epoxy resin filled with angular-shaped silica, Polymer, 32 (12), pp. 2221-2229.

114. Nakamura Y., Yamaguchi M., Okubo M. and Matsumoto T. (1992), Effects of particle size on mechanical and impact properties of epoxy resin filled with spherical silica, Journal of Applied Polymer Science, 45 (7), pp. 1281-1289.

115. Pukanszky B. and Voros G. (1993), Mechanism of interfacial interactions in particulate filled composite, Composite Interfaces, 1 (5), pp. 411-427.

116. Nicolais L. and Nicodemo L. (1974), The Effect of particles shape on tensile properties of glassy thermoplastic composites, International Journal of Polymeric Materials, 3 (3), pp. 229-243.

117. Patnaik A., Satapathy A., Mahapatra S.S. and Dash R.R. (2009), A comparative study on different ceramic fillers affecting mechanical properties of glass-polyester composites, Journal of Reinforced Plastics and Composites, 28 (11), pp. 1305-1318.

118. Padhi P.K., Satapathy A. and Nakka A.M. (2013), Processing, characterization, and wear analysis of short glass fiber-reinforced polypropylene composites filled with blast furnace slag, Journal of Thermoplastic Composite Materials, DOI: 10.1177/0892705713486142.

119. Tagliavia G., Porfiri M. and Gupta N. (2010), Analysis of flexural properties of hollow-particle filled composites, composites Part B: Engineering, 41(1), pp. 86-93.

120. Weidenfeller B., Höfer M. and Schilling F.R. (2005), Cooling behavior of particle filled polypropylene during injection molding process, Composites Part A: Applied Science and Manufacturing, 36 (3), pp. 345-351.

121. Hassan S.B., Oghenevweta J.E. and Aigbodion V.S. (2012), Morphological and mechanical properties of carbonized waste maize stalk as reinforcement for eco-composites, Composites Part B: Engineering, 43 (5), pp. 2230-2236.

122. Omar M.F., Akil H.M. and Ahmad Z.A. (2013), Particle size- Dependent on the static and dynamic compression properties of polypropylene/silica composites, Materials and Design , 45, pp. 539-547.

123. Gupta G. and Satapathy A. (2014), Processing, Characterization and Erosion Wear Characteristics of Borosilicate Glass Microspheres Filled Epoxy Composites, Polymer Composites, DOI: 10.1002/pc.23079.

124. Lauke B. and Fu S.Y. (2013), Aspects of fracture toughness modeling of particulate filled polymer composites, Composites Part B: Engineering, 45 (1), pp. 1569-1574.

125. Jerabek M., Major Z., Renner K., Moczo J., Pukanszky B. and Lang R.W. (2010), Filler/matrix-debonding and micro-mechanisms of deformation in particulate filled polypropylene composites under tension, Polymer, 51 (9), pp. 2040-2048.

126. Bishay I.K., Abd-El-Messieh S.L., Mansour S.H. (2011), Electrical, mechanical and thermal properties of polyvinyl chloride composites filled with aluminum powder, Materials and Design, 32 (1), pp. 62-68.

127. Agrawal A. and Satapathy A. (2013), Development of a heat conduction model and investigation on thermal conductivity enhancement of AlN/epoxy composites, Procedia Engineering, 51, pp. 573-578.

128. Agrawal A. and Satapathy A. (2014), Effects of aluminium nitride inclusions on thermal and electrical properties of epoxy and polypropylene: An experimental investigation, Composites Part A: Applied Science and Manufacturing, 63, pp. 51-58.

129. Khalil Abdul H.P.S., Tehrani M.A., Davoudpour Y., Bhat A.H., Jawaid M. and Hassan A. (2013), Natural fiber reinforced poly(vinyl chloride) composites: A review, Journal of Reinforced Plastics and Composites, 32(5), pp. 330-356.

130. Abdulmajeeda A.A., Närhia T.O., Vallittu P.K. and Lassila L.V. (2011), The effect of high fiber fraction on some mechanical properties of unidirectional glass-fiber-reinforced composite, Dental materials, 27, pp. 313-321.

131. Garoushi S., Vallittu P.K. and Lassila L.V. (2007), Short glass fiber reinforced restorative composite resin with semi-inter penetrating polymer network matrix, Dental materials, 23, pp.1356-1362.

132. Karsli N.G. and Aytac A. (2013), Tensile and thermo-mechanical properties of short carbon fiber reinforced polyamide 6 composites, Composites Part B: Engineering, 51, pp. 270-275.

133. Oya N. and Hamada H. (1996), Effect of reinforcing fiber properties on various mechanical behaviour of unidirectional carbon/epoxy laminates, Science and Engineering of Composite Materials, 5, pp. 105-29.

134. Oya N. and Johnson D.J. (2001), Longitudinal compressive behavior and microstructure of PAN-based carbon fibers, Carbon, 39, pp. 635-45.

135. Shioya M. and Nakatani M. (2000), Compressive strengths of single carbon fibres and composite strands, Compo Sci Technol, 60, pp. 219-29.

136. Sudarisman and Davies I.J. (2008), Flexural failure of unidirectional hybrid fiber-reinforced polymer (FRP) composites containing different grades of glass fiber, Advanced Materials Research, 41-42, pp. 357-62.

137. Sudarisman and Davies I.J. (2008), Influence of compressive pressure, vacuum pressure,and holding temperature applied during autoclave curing on the microstructure of unidirectional CFRP composites, Advanced Materials Research, 41-42, pp. 323-328.

138. Manders P.W. and Bader M.G. (1981), The strength of hybrid glass/carbon fiber composites, Journal of Materials Science, 16, pp. 2233-45.

139. Zweben C. (1977), Tensile strength of hybrid composites, Journal of Materials Science, 12, pp. 1325-37.

140. Dong C. and Davies I.J. (2014), Flexural and tensile strengths of unidirectional hybrid epoxy composites reinforced by S-2 glass and T700S carbon fibres, Materials and Design, 54, pp. 955-966.

141. Encinas N., Lavat-Gil M., Dillingham R.G., Abenojar J. and Martínez M.A. (2014), Cold plasma effect on short glass fibre reinforced composites adhesion properties, International Journal of Adhesion and Adhesives, 48, pp.85-91.

142. Sridhar I., Adie P.P. and Ghista D.N. (2010), Optimal design of customized hip prosthesis using fiber reinforced polymer composites, Materials and Design, 31, pp. 2767-2775.

143. Kumar S., Murthy Reddy K.V.V.S., Kumar A. and Rohini Devi G. (2013), Development and characterization of polymer-ceramic continuous fiber reinforced functionally graded composites for aerospace application, Aerospace Science and Technology, 26, pp. 185-191.

144. Avci A., Arikan H. and Akdemir A. (2004), Fracture behavior of glass fiber reinforced polymer composite, Cement and Concrete Research, 34, pp. 429-434.

145. Shamsuddoha M.D., Islam M.D.M., Aravinthan T., Manalo A. and Lau K. (2013), Effectiveness of using fibre-reinforced polymer composites for underwater steel pipeline repairs, Composite Structures, 100, pp. 40-54.

146. Cercone L. and Lockwood J.D. (2005), Review of FRP composite materials for pipeline repair. Pipelines, pp. 1001-13.

147. Ramesh M., Palanikumar K. and Reddy Hemachandra K. (2013), Comparative Evaluation on Properties of Hybrid Glass Fiber- Sisal/Jute Reinforced Epoxy Composites, Procedia Engineering, 51, pp. 745-750.

148. Marom G., Fischer S., Tuler F.R. and Wagner H.D. (1978), Hybrid effects in composites: conditions for positive or negative effects versus rule-of-mixtures behavior, Journal of Materials Science, 13, pp. 1419-26.

149. Jang B.Z. (1994), Advanced Polymer composites: principles and applications, ASM International.

150. Fan L., Dang Z., Nan C-W. and Li M. (2002), Electrochimica Acta, 48(2), pp. 205-297.

151. Kim Y.D., Oh N.L., Oh S-T. and Moon I-H. (2001), Materials Letters, 51(5), pp. 420.

152. Gracia R., Evans R.E. and Palmer R.J. (1987), Toughened composites, STP 937, N.J.Johnson, Ed., ASTM. 397-412.

153 Liau J.Y., Jang B.Z., Hwang L.R., Wilcox R.C. (1988), Plast. Eng., Nov.

154. Bijwe J., Logani C.M. and Tewari U.S. (1990), Influence of fillers and fiber reinforcement on abrasive wear resistance of some polymeric composites, Wear, 138, pp. 77-92.

155. Wang J., Gu M., Songhao B. and Ge S. (2003), Investigation of the influence of MoS_2 filler on the tribological properties of carbon fiber reinforced nylon 1010 composites, Wear, 255, pp. 774-779.

156. Sarajaadevi M., Murugesan V., Rengaraj K. and Anamd P. (1998), Utilization of fly ash as filler for unsaturated polyester resin, J. Appl Polym. Sci, 69, pp. 1385-1391.

157. Chaowasakoo T. and Sombatsompop N. (2007), Mechanical and morphological properties of fly ash/epoxy composites using conventional thermal and microwave curing methods, Composites Science and Technology, 67, pp. 2282-229.

158. Raja R.S., Manisekar K. and Manikandan V. (2014), Study on mechanical properties of fly ash impregnated glass fiber reinforced polymer composites using mixture design analysis, Materials and Design, 55, pp. 499-508.

159. Srivastava V.K. and Pawar A.G. (2006), Solid particle erosion of glass fiber reinforced fly ash filled epoxy resin composites, Composite Science and Technology, 66, pp. 3021-3028.

160. Gu J., Wu G. and Zhang Q. (2007), Effect of porosity on the damping properties of modified epoxy composites filled with fly ash, Scripta Materialia, 57, pp. 529-532.

161. Patnaik A., Satapathy A., Mahapatra S.S. and Dash R.R. (2009), Modeling and prediction of erosion response of glass reinforced polyester-flyash composites, Journal of Reinforced Plastics and Composites, 28, pp. 513-536.

162. Patnaik A., Satapathy A., Mahapatra S.S. and Dash R.R. (2008), Erosive Wear Assesment of Glass Reinforced Polyester-Flyash Composites using Taguchi Method, International Polymer Processing, 13, pp. 192-199.

163. Patnaik A., Satapathy A., Dwivedy M. and Biswas S. (2009), Wear Behavior of Plant Fiber (Pine Bark) and Cement Kiln Dust Reinforced Polyester Composites Using Taguchi Experimental Model, Journal of Composite Materials, DOI: 10.1177/0021998309346547.

164. Asaad J.N. and Tawfik S.Y. (2011), Polymeric composites based on polystyrene and cement dust wastes, Materials and Design, 32, pp. 5113-5119.

165. Mahapatra S.S. (2010), Modelling and analysis of erosion wear behavior of hybrid composites using Taguchi experimental design, Proceedings of the Institution of Mechanical Engineers, Part J: Journal of Engineering Tribology, 224 (2), pp. 157-167.

166. Siddhartha V., Patnaik A. and Bhatt A.D. (2010), Friction and wear analysis of a cement kiln dust-reinforced epoxy-based functionally graded materials, Proceedings of the Institution of Mechanical Engineers, Part J: Journal of Engineering Tribology, 224(10), pp. 1103-1114.

167. Gangil B., Patnaik A., Kumar A. and Biswas S. (2012), Thermo-mechanical and sliding wear behaviour of vinylester-cement by-pass dust particulate-filled homogenous and their functionally graded composites, Proceedings of the Institution of Mechanical Engineers, Part J: Journal of Engineering Tribology, DOI: 1350650112460363.

168. Patel M., Padhi B.K., Vidyasagar P. and Pattnaik A.K. (1992), Extraction of titanium dioxide and production of building bricks from red mud, Research and Industry, 37**(**3), pp. 154-157.

169. Mahata T., Sharma B.P., Nair S.R. and Prakash D. (2000), Formation of aluminium titanate-mullite composite from bauxite red mud, Material and Mat. Trans. B, 318, pp. 551-553.

170. Zhang Y., Zhang A., Zhen Z., Lv F., Chu P.K. and Ji J. (2011), Red mud/polypropylene composite with mechanical and thermal properties, Journal of Composite Materials, DOI: 10.1177/0021998311401937.

171. Akinci A., Akbulut H. and Yimaz E. (2008), Mechanical Properties of Cost-Effective Polypropylene Composites Filled With Red-Mud Particles, Polymers and Polymer Composites, 16(7), pp. 439-446.

172. Bhat A.H., Khalil H.P.S.A., Bhat I.H. and Banthia A.K. (2012), Dielectric and Material Properties of Poly (Vinyl Alcohol): Based Modified Red Mud Polymer Nanocomposites, Journal of Polymers and The Environment, 20, pp.395-403.

173. Saradava B.J., Rachchh N.V., Misra R.K. and Roychowdhary D.G. (2012), Mechanical Characterization of Coir Fiber Reinforced Polymer Composite Using Red Mud as Filler, Journal of Information, Knowledge and Research In Mechanical Engineering.,02(02), ISSN 0975 - 668X.

174. Biswas A.K. and Davenport W.G. (2002), Extractive metallurgy of copper, Pergamon Press, pp. 518.

175. Biswas S. and Satapathy A. (2010), Use of copper slag in glass-epoxy composites for improved wear resistance, Waste Management and Research, 28(7), pp. 615-25.

176. Biswas S. and Satapathy A. (2009), Tribo-performance analysis of red mud filled glass-epoxy composites using Taguchi experimental design, Materials and Design, 30, pp. 2841-2853.

177. Biswas S., Patnaik A. and Kaundal R. (2012), Effect of Red Mud and Copper Slag Particles on Physical and Mechanical Properties of Bamboo-Fiber-Reinforced Epoxy Composites, Advances in Mechanical Engineering, doi.org/10.1155/2012/141248.

178. Padhi P.K. and Satapathy A. (2014), Processing and wear analysis of blast furnace slag filled polypropylene composites using Taguchi model and ANN, International Polymer Processing, 29 (2), pp. 233-244.

179. Padhi P.K. and Satapathy A. (2014), Solid particle erosion behaviour of BFS-filled epoxy-SGF composites using Taguchi's experimental design and ANN, Tribology Transactions, 57 (3), pp. 396-407.

180. Padhi P.K. and Satapathy A. (2012), Prediction and simulation of erosion wear behavior of glass-epoxy composites filled with blast furnace slag, Advanced Materials Research, 585, pp. 549-553.

181. Padhi P.K. and Satapathy A. (2013), Analysis of Sliding Wear Characteristics of BFS Filled Composites Using an Experimental Design Approach Integrated with ANN, Tribology Transactions, 56, pp. 789-796.

182. Biswas S. (2010), Processing, Characterization and wear response of Particulate Filled Epoxy Based Hybrid Composites, Ph.D. Thesis, NIT, Rourkela, India.

183. Organization for Economic Co-operation and Development. (1969), Research Group on Wear of Engineering Materials, Glossary of terms and definitions in the field of friction, wear and lubrication, Tribology, Paris, pp. 169.

184. Stolarski T.A. (1990), Tribology in Machine Design, Heinemann Newnes, UK.

185. Barkoula N.M. and Karger-Kocsis J. (2002), Review Processes and influencing parameters of the solid particle erosion of polymers and their composites, Journal of Material Science, 37 (18), pp. 3807-3820.

186. Burwell J.T. and Strang C.D. (1952), On the empirical law of adhesive wear, Journal of Applied Physics, 23 (1), pp. 18-28.

187. Burwell (Jr.) J.T. (1957/1958), Survey of Possible Wear Mechanisms, American-Standard Corporation, New York, U.S.A., Wear, 1, pp. 119-141.

188. Aquaro D. (2006), Erosion due to the impact of solid particles of materials resistant at high temperature, Meccanica, 41 (5), pp. 539-551.

189. Kulu P., Veinthal R. and Kaerdi H. (2007), Erosion due to the impact of solid particles of materials resistant at high temperature, Int. J. of Mat. And Prod. Tech., 28 (3-4), pp. 425-447.

190. Field J.E. and Hutchings I.M. (1984), Impact erosion processes, Presented at Mechanical Properties at High Rates of Strain, In: Proc. of the Third Conference, Oxford, England.

191. Pragatheeswaran A., Ananthapadmanabhan P.V., Chakravarthy Y., Bhandari S., Thiyagarajan T.K., Tiwari N., Saha T.K. and Ramachandran K. (2014), Plasma spray deposition and characterization of strontium zirconate coatings, Ceramics International, 40 (7B), pp. 10441-10446.

192. Garcia A., Cadenas M., Fernandez M.R. and Noriega A. (2013), Tribological effects of the geometrical properties of plasma spray coatings partially melted by laser, Wear, 305 (1-2), pp. 1-7.

193. Aruna S.T., Balaji N., Shedthi J. and William Grips V.K. (2012), Effect of critical plasma spray parameters on the microstructure, micro-hardness and wear and corrosion resistance of plasma sprayed alumina coatings, Surface and Coatings Technology, 208, pp. 92-100.

194. Sivakumar G., Dusane R.O. and Joshi S.V. (2013), A novel approach to process phase pure α-Al_2O_3 coatings by solution precursor plasma spraying, Journal of the European Ceramic Society, 33 (13-14), pp. 2823-2829.

195. Monica V., Bannier E., Moreno R., Salvador M.D. and Sanchez E. (2013), Atmospheric plasma spraying coatings from alumina-titania feedstock comprising bimodal particle size distributions, Journal of the European Ceramic Society, 33 (15-16), pp. 3313-3324.

196. Sadri E. and Ashrafizadeh F. (2013), Structural characterization and mechanical properties of plasma sprayed nanostructured Cr_2O_3-Ag composite coatings, Surface and Coatings Technology, 236, pp. 91-101.

197. Hawthorne H.M., Erickson L.C., Ross D., Tai H. and Troczynski T. (1997), The microstructure dependence of wear and indentation behaviour of some plasma sprayed alumina coatings, Wear, 203-204, pp. 709-714.

198. Tucker (Jr.) R.C. (1995), On the relationship between the microstructure and the wear characteristics of selected thermal spray coatings, In: Proceeding of ITSC, Kobe, Japan.

199. Erickson L.C., Troczynski T., Ross D., Tai H. and Hawthorne H.M. (1997), Processing dependent microstructure and wear related surface properties of plasma sprayed alumina coatings, Presented on World Tribology Congress, Londan, U. K.

200. Erickson L.C., Troczynski T., Hawthorne H.M., Tai H. and Ross D. (1998), Alumina coatings by plasma spraying of mono size sapphire powders, In: Proceeding of ITSC, Nice, France.

201. Ohmori A., Li C.J. and Arata Y. (1990), Influence of Plasma spray conditions on the structure of Al_2O_3 coatings, Transaction of Joining and Welding Research Institute, 19 (2), pp. 99-110.

202. Kulu P., Hussainova I. and Veinthal R. (2005), Solid particle erosion of thermal sprayed coatings, Wear, 258 (1-4), pp. 488-496.

203. Kulu P. (1989), The abrasive erosion resistance of powder coatings, Journal of Tribologia: Finnish J. Tribology, 8 (4), pp. 12-25.

204. Kulu P., Tumanok A. and Zimakov S. (1999), Treatment of recycled hard metals, In: Proceedings of 4th ASM International Conference and Exhibition on the Recycling of Metals, ASM International, Vienna, Austria, pp. 319-327.

205. Kulu P., Phil T. and Halling J. (1998), Wear-resistant WC-Co-NiCrSiB composite coatings, In (NORDTRIB'98): Proceedings of the 8th International Conference of Tribology, S.S. Eskilden, D.S. Larsen, H. Reitz, E.J. Bienk, and A. Straede, ed., DTI Tribology Centre, Aarhus, Denmark, pp. 809-817.

206. Wert J.J. and Oppliger S.J. (1992), Influence of composition and processing parameters on mechanical properties and erosion response of Ni0-TiB_2 coatings, Materials Science and Technology, 8, pp. 825-835.

207. Finnie I. (1995), Some reflections on the past and future of erosion, Wear, 186-187 (1), pp. 1-10.

208. Hamed A., Tabakoff W. and Wenglarz R. (2006), Erosion and deposition in turbo-machinery, J. Pro. Pow., 22 (2), pp. 350-360.

209. Finnie I. and McFadden D.H. (1978), On the velocity dependence of the erosion of ductile metals by solid particles at low angles of incidence, Wear, 48, pp. 181-190.

210. He C., Wang Y.S., Wallace J.S. and Hsu S.M. (1993), Effect of microstructure on the wear transition of zirconia-toughened alumina, Wear, 162-164 (1), pp. 314-321.

211. Ajayi O.O. and Ludema K.C. (1988), Surface damage of structural ceramics: Implications for wear modeling, Wear, 124 (2), pp. 237-257.

212. McPherson R. (1989), A review of microstructure and properties of plasma sprayed ceramic coatings, Surface and Coatings Technology, 39-40, pp. 173-181.

213. Wang B. (1996), Erosion-corrosion of thermal sprayed coatings in FBC boilers, Wear, 199 (1), pp. 24-32.

214. Zhang X.S., Clyne T.W. and Hutchings I.M. (1997), Relationship between microstructure and erosive wear resistance of plasma sprayed alumina coatings, Surface Engineering, 13 (5), pp. 393-401.

215. Branco J.R.T., Gansert R., Sampath S., Berndt C.C. and Herman H. (2004), Solid particle erosion of plasma sprayed ceramic coatings, Materials Research, 7 (1), pp. 147-153.

216. Mishra S.C., Sahu A., Das R., Satapathy A., Sen S., Ananthapadmanabhan P.V. and Sreekumar K.P. (2008), Microstructure, adhesion and erosion wear of plasma sprayed alumina-titania composite coatings, Journal of Reinforced Plastics And Composites, doi:10.1177/0731684407087758.

217. Ercenk E., Sen U. and Yilmaz S. (2012) The erosive wear behavior of basalt based glass and glass-ceramic coatings, Tribology International, 52, pp. 94-100.

218. Krishnamurthy N., Murali M.S., Venkataraman B. and Mukunda P.G. (2012), Characterization and solid particle erosion behavior of plasma sprayed alumina and calcia-stabilized zirconia coatings on Al-6061 substrate, Wear, 274-275, pp. 15-27.

219. Sahu S.P., Satapathy A., Mishra D., Patnaik A. and Sreekumar K.P. (2010), Tribo-performance analysis of fly ash-aluminum coatings using experimental design and ANN, Tribology Transactions, 53 (4), pp. 533-542.

220. Gupta G. and Satapathy A. (2014), Studies on erosion wear behavior of plasma sprayed coatings of glass microspheres premixed with Al_2O_3 particles, Advances in Tribology, DOI 10.1155/2014/763601.

221. Gupta G. and Satapathy A. (2014), Erosion Wear Response of Glass Microsphere Coatings: Parametric Appraisal and Prediction Using Taguchi Method and Neural Computation, Tribology Transactions, 57, pp. 899-907.

222. Finnie I. (1958), The mechanism of erosion of ductile metals, In: Proc. of 3rd US national congress of applied mechanics, pp. 527-532.

223. Nesic S. (1991), Computation of localized erosion-corrosion in disturbed two phase flow, PhD thesis, University of Saskatchewan, Saskatoon, Canada.

224. Bitter J.G.A. (1963), A study of erosion phenomena-Part I, Wear, 6, pp. 5- 21.

225. Glaeser W.A. and Dow A. (1977), Mechanisms of erosion in slurry pipelines, In: Proc. of the second Int. Conf. on Slurry Transportation, Las Vegas, NV: March 2-4, pp. 136-140.

226. Laitone J.A. (1979), Erosion prediction near a stagnation point resulting from aerodynamically entrained solid particles, J. Aircraft, 16 (12), pp. 809- 814.

227. Salama M.M. and Venkatesh E.S. (1983), Evaluation of erosion velocity limitations of offshore gas wells, In: 15th Annual OTC, Houston, TX: May 2-5, OTC no. 4485.

228. Bourgoyne A.T. (1989), Experimental study of erosion in diverter systems due to sand production, Presented at the SPE/IADC Drilling Conference, New Orleans, LA, SPE/IADC 18716, pp. 807-816.

229. Chase D.P., Rybicki E.F. and Shadley J.R. (1992), A model for the effect of velocity on erosion of N80 steel tubing due to the normal impingement of solid particles, Trans ASME, J. Ene. Resour. Tech., 114, pp. 54-64.

230. McLaury B.S. (1993), A model to predict solid particle erosion in oil field geometries, MS thesis, The University of Tulsa.

231. Svedeman S.J. and Arnold K.E. (1993), Criteria for sizing Multiphase flow lines for erosive/corrosive services, Paper presented at the 1993 SPE Conf., Houston SPE 265, pp. 69.

232. Jordan K. (1998), Erosion in multiphase production of oil and gas, Corrosion 98, Paper no. 58, NACE Int. Ann. Conf., San Antonio.

233. Engel P.A. (1976), Impact wear of materials, Elsevier, Amsterdam, New York, pp. 277-290.

234. Tilly G.P. (1979), Erosion caused by impact of solid particles, in Herman H. (ed.), Treatise on Materials Science and Technology, v13:D. Scott(ed), Wear, Academic Press: New York, pp. 287-320.

235. Rochester M.C. and Brunton J.H. (1979), In: J. E. Field (Ed.), 5th International Conference on Erosion by Liquid and Solid Impact, Cavendish Laboratory, Cambridge, U.K., Paper 6.

236. Lesser M.B. and Ezekoye O.A. (1987), Proceedings of 7th International Conference on Erosion by Liquid and Solid Impact (eds. Field J. E. and Dear J. P.), Cavendish Laboratory, Cambridge, U.K.

237. Evans A.G. (1979), Impact Damage Mechanism-Solid Projectile, in Herman H. (ed.), Treatise on Materials Science and Technology, Vol. 16: Preece C. M. (ed.), Materials Erosion, (Academic Press: New York, pp. 1-67.

238. Kosel T.H. (1992), Solid particle erosion, ASM Handbook, ASM International, 18, pp. 199-213. (T.H. Kosel. In: P. J. Blau, Editor, Friction, Lubrication and Wear Technology, ASM Handbook, 18, pp. 207).

239. Engel P.A. (1978), Percussive impact wear: A study of repetitively impacting solid components in engineering, Tribology International, 11 (3), pp. 169-176.

240. Preece C.M. and Macmillan N.H. (1977), Erosion, Annual Review of Materials Science, 7, pp. 95-121.

241. Hutchings I.M. (1981), A model for the erosion of metals by spherical particles at normal incidence, Wear, 70 (3), pp. 269-281.

242. Finnie I., Levy A. and McFadden D.H. (1979), The fundamental mechanisms of the erosion wear of ductile metals by solid particles, ASTM STP 664, Erosion: Prevention and Useful Applications, pp. 36-58.

243. Ruff A.W. and Wiederhorn S.M. (1979), Erosion by solid particle impact (Preece C. M., (Ed.) Treatise on Materials Science and Technology), Academic Press, New York, 16, pp. 65-70.

244. Shewmon P. and Sundararajan G. (1983), The erosion of metals, Annual Review of Materials Science, 13, pp. 301-318.

245. Sundararajan G. (1983), Solid particle erosion of metals and alloys, Transactions of the Indian Institute of Metals, 36 (6), pp. 474-495.

246. Levy A.V. (1995), Solid particle erosion and erosion-corrosion of materials, In: 2nd Ed., ASM International, Materials Park, Ohio, USA.

247. Guo D.Z., Li F.L., Wang Y. and Sun J.S. (1995), Effects of post-coating processing on structure and erosive wear characteristics off tame and plasma spray coatings, Surface and Coatings Technology, 73, pp. 73-78.

248. Hidalgo V.H., Varela F.J.B. and Fernandez R.E. (1997), Erosion wear and mechanical properties of plasma-sprayed nickel and iron-based coatings subjected to service conditions in boilers, Tribology International, 30 (9), pp. 641-649.

249. Mishra S.B., Chandra K. and Prakash S. (2013), Erosion-corrosion performance of NiCrAlY coating produced by plasma spray process in a coal-fired thermal power plant, Surface & Coatings Technology, 216, pp. 23-34.

250. Mishra S.B., Prakash S. and Chandra K. (2006), Studies on erosion behaviour of plasma sprayed coatings on a Ni-based super alloy, Wear, 260, pp. 422-432.

251. Perumal G., Geetha M., Asokamani R. and Alagumurthi N. (2014), Wear studies on plasma sprayed Al_2O_3-40 wt% 8YSZ composite ceramic coating on Ti-6Al-4V alloy used for biomedical applications, Wear, 311, pp. 101-113.

252. Proudhon H., Savkova J., Basseville S., Guipont V., Jeandin M. and Cailletaud G. (2014), Experimental and numerical wear studies of porous rweactive plasma sprayed Ti-6Al-4V/TiN composite coating, Wear, 311, pp. 159-166.

253. Yugeswaran S., Kobayashi A., Suresh K., Rao K.P. and Subramanian B. (2012), Wear behavior of gas tunnel type plasma sprayed Zr-based metallic glass composite coatings, Applied Surface Science, 258, pp. 8460-8468.

254. Singh V.P., Sil A. and Jayaganthan R. (2011), Study on sliding and erosive wear behaviour of atmospheric plasma sprayed conventional and nanostructured alumina coatings, Materials and Design, 32, pp. 584-591.

255. Ramachandrana C.S., Balasubramaniana V. and Ananthapadmanabhan P.V. (2013), Erosion of atmospheric plasma sprayed rare earth oxide coatings under air suspended corundum particles, Ceramics International, 39, pp. 649-672.

256. Hsiao W.T., Su C.Y., Huang S. and Liao W.H. (2013), Wear resistance and microstructural properties of Ni-Al/h-BN/WC-Co coatings deposited using plasma spraying, Materials Characterization, 79, pp. 84-92.

257. Sahab A.R.M., Saad N.H., Kasolang S. and Saedon J. (2012), Impact of Plasma Spray Variables Parameters on Mechanical and Wear Behaviour of Plasma Sprayed Al_2O_3 3% wt TiO_2 Coating in Abrasion and Erosion Application, Procedia Engineering, 41, pp. 1689-1695.

258. Alonso F., Fagoaga I. and Oregui P. (1991), Erosion Protection of carbon epoxy composites by plasma sprayed coatings, Surface and Coatings Technology, 49 (1-3), pp. 482-488.

259. Tabakoff W. and Shanov V. (1995), Erosion rate testing at high temperature for turbo machinery use, Surface and Coatings Technology, 76-77 (1), pp. 75-80.

260. Kulkarni S.M. and Kishore K. (2001), Influence of matrix modification on the solid particle erosion of glass/epoxy composites, Polymer Composites, 9, pp. 25-30.

261. Aglan H.A. and Chenock Jr. T.A. (1993), Erosion damage features of polyimide thermoset composites, SAMPEQ, 24, pp. 41-47.

262. Tewari U.S., Harsha A.P., Hager A.M. and Friedrich K. (2002), Solid particle erosion of unidirectional carbon fiber reinforced poly-ether ether ketone composites, Wear, 252, pp. 992-1000.

263. Häger A., Friedrich K., Dzenis Y.A. and Paipetis S.A. (1995), Study of erosion wear of advanced polymer composites In: Street K, Whistler BC, editors, Proceedings of the ICCM-10, Cambridge: Canada Wood Head Publishing Ltd., pp. 155-162.

264. Tilly G.P. and Sage W. (1970), The interaction of particle and material behaviour in erosion process, Wear, 16, pp. 447-465.

265. Thai C.M., Tsuda K. and Hojo H. (1981), Erosion behaviour of polystyrene, Journal of Testing and Evaluation, 9, pp. 359-365.

266. Walley S.M., Field J.E. and Yennadhiou P. (1984), Single solid particle impact erosion damage on polypropylene, Wear, 100 (1-3), pp. 263-280.

267. Friedrich K. (1986), Erosive wear of polymer surfaces by steel ball blasting, Journal of Materials Science, 21(9), pp. 3317-3332.

268. Rajesh J.J., Bijwe J., Tewari U.S. and Venkataraman B. (2001), Erosive wear of various polyamides, Wear, 249 (8), pp. 702-714.

269. Walley S.M and Field J.E. (1987), The erosion and deformation of polyethylene by solid particle impact, Philosophical Transactions of The Royal Society A, London, 321 (1558), pp. 277-303.

270. Wang Y.Q., Huang L.P., Liu W.L. and Li J. (1998), The blast erosion behavior of ultrahigh molecular weight polyethylene, Wear, 218 (1), pp. 128-133.

271. Walley S.M., Field J.E. and Greengrass M. (1987), An impact and erosion study of polyetheretherketone, Wear, 114 (1), pp. 59-72.

272. Rao P.V. and Buckley D.H. (1986), Angular particle impingement studies of thermoplastic materials at normal incidence, Tribology Transactions, 29 (3), pp. 283-298.

273. Brandstadter A., Goretta K.C, Routbort J.L, Groppi D.P and Karasek K.R. (1991), Solid particle erosion of bismaleimide polymers, Wear, 147 (1), pp. 155-164.

274. Hutchings I.M., Deuchar D.W.T and Muhr A.H. (1987), Erosion of unfilled elastomers by solid particle impact, Journal of Materials Science, 22 (11), pp. 407-4076.

275. Li J. and Hutchings I.M. (1990), Resistance of cast polyurethane elastomers to solid particle erosion, Wear, 135 (2), pp. 293-303.

276. Besztercey G, Karger-Kocsis J and Szaplonczay P. (1999), Solid particle erosion of electrically insulating silicone and EPDM rubber compounds, Polymer Bulletin, 42 (6), pp. 717-724.

277. Miyazaki N. and Takeda T. (1993), Solid particle erosion of fiber reinforced plastic, Journal of Composite Materials, 27, pp. 21-31.

278. Miyazaki N. and Hamao T. (1994). Solid particle erosion of thermoplastic resins reinforced by short fibers, Journal of Composite Materials, 28 (9), pp. 871-883.

279. Harsha A.P., Tewari U.S. and Venkataraman B. (2003), Solid particle erosion behaviour of various polyaryletherketone composites, Wear, 254 (7-8), pp. 693-712.

280. Barkoula N.M. and Karger-Kocsis J. (2002), Effects of fiber content and relative fiber-orientation on the solid particle erosion of GF/PP composites, Wear, 252 (1-2), pp. 80-87.

281. Tewari U.S., Harsha A.P., Hager A. M. and Friedrich K. (2003), Solid particle erosion of carbon fiber and glass fiber-epoxy composites, Composites Science and Technology, 63 (3), pp. 549-557.

282. Arjula S. and Harsha A.P. (2006), Study of erosion efficiency of polymers and polymer composites, Polymer Testing, 25 (2), pp. 188-196.

283. Patnaik A., Satapathy A., Mahapatra S.S. and Dash R.R., (2008), A Taguchi approach for investigation of erosion of glass fiber-polyester composites, Journal of Reinforced Plastics and Composites, 27 (8), pp. 871-888.

284. Patnaik A., Satapathy A., Mahapatra S.S. and Dash R.R. (2008), Parametric optimization of erosion wear of polyester-GF-alumina hybrid composites using Taguchi method, Journal of Reinforced Plastics and Composites, 27 (10), pp. 1039-1058.

285. Patnaik A., Satapathy A., Mahapatra S.S. and Dash R.R., (2008), Implementation of Taguchi design for erosion of fiber reinforced polyester composite systems with SiC filler, Journal of Reinforced Plastics and Composites, 27 (10), pp. 1093-1111.

286. Patnaik A., Satapathy A., Mahapatra S.S. and Dash R.R. (2008), A modeling approach for prediction of erosion behaviour of glass fiber-polyester composites, Journal of Polymer Research, 15 (2), pp. 147-160.

287. Patnaik A., Satapathy A., Mahapatra S.S. and Dash R.R., (2009), Tribo-performance of polyester hybrid composites: damage assessment and parameter optimization using Taguchi design, Materials and Design, 30 (1), pp. 57-67.

288. Patnaik A., Kaundal R., Satapathy A., Biswas S. and Kumar P. (2010), Solid particle erosion of particulate filled short glass fiber reinforced polyester resin composites, Advanced Materials Research, 123-125, pp. 213-216.

289. Patnaik A., Satapathy A., Chand N., Barkoula N.M. and Biswas S. (2010), Solid particle erosion wear characteristics of fiber and particulate filled polymer composites: A review, Wear, 268, pp. 249-263.

290. Panda P., Mantry S., Mohapatra S., Singh S.K. and Satapathy A. (2013), A study on erosive wear analysis of glass fiber-epoxy-AlN hybrid composites, Journal of Composite Materials, 48 (1),pp. 107-118.

291. Kaundal R. (2014), Role of process variables on the solid particle erosion of polymer composites: a critical review, Silicon, 6, pp. 5-20.

292. Bagci M. and Imrek H. (2013), Application of Taguchi method on optimization of testing parameters for erosion of glass fiber reinforced epoxy composite materials, Materials and Design, 46, pp. 706-712.

293. Zhao G., Hussainova I., Antonov M., Wang Q., Wang T. and Yung D.L. (2014), Effect of temperature on sliding and erosive wear of fiber reinforced polyimide hybrids, Tribology International, 82, pp. 525-533.

294. Zhang N., Yang F., Shen C., Castro J. and Lee L.J. (2013), Particle erosion on carbon nano fiber paper coated carbon fiber/epoxy composites, Composites Part B: Engineering, 54, pp. 209-214.

295. Mohapatra S., Mantry S. and Singh S.K. (2014), Performance Evaluation of Glass-Epoxy-TiC Hybrid Composites Using Design of Experiment, Journal of Composites, DOI: 10.1155/2014/670659.

296. Mohapatra S., Mantry S., Singh S.K. and Satapathy A. (2014), Solid particle erosion behavior of glass-epoxy composites filled with TiC derived from ilmenite, Int J Plast Technol, 18(1), pp. 75-87.

297. Tsuda K., Kubouchi M., Sakai T., Saputra A.H. and Mitomo N. (2006), General method for predicting the sand erosion rate of GFRP, Wear, 260, pp. 1045-52.

298. Rajesh J.J., Bijwe J., Venkataraman B. and Tewari U.S. (2004), Effect of impinging velocity on the erosive wear behaviour of polyamides, Tribology International, 37 (3), pp. 219-226.

299. Yang N. and Nayeb-Hashemi H. (2007), The effect of solid particle erosion on the mechanical properties and fatigue life of fiber-reinforced composites, Journal of Composite Materials, 41, pp. 559-74.

300. Harsha A.P. and Jha S.K. (2008), Erosive wear studies of epoxy-based composites at normal incidence, Wear, 265, pp. 1129-35.

301. Fernández J.E., Fernández M.D.R., Diaz R.V. and Navarro R.T. (2003), Abrasive wear analysis using factorial experiment design, Wear, 255(1-6), pp. 38-43.

302. Spuzic S., Zec M., Abhary K., Ghomashchi R. and Reid I. (1997), Fractional design of experiments applied to a wear simulation, Wear, 212(1), pp. 131-139.

303. Prasad B.K. (2002), Abrasive wear characteristics of a zinc-based alloy andzinc-alloy/SiC composite, Wear, 252(3-4), pp. 250-263.

304. Deuis R.L., Subramanian C. and Yellup J.M. (1998), Three-body abrasive wear of composite coatings in dry and wet environments, Wear, 214(1), pp. 112-130.

305. Banerji A., Prasad S.V., Surappa M.K. and Rohatgi P.K. (1982), Abrasive wear of cast aluminium alloy-zircon particle composites, Wear, 82(2), pp. 141-151.

306. Mondal D.P., Das S., Jha A.K. and Yegneswaran A.H. (1998), Abrasive wear of Al alloy-Al_2O_3 particle composite: a study on the combined effect of load and size of abrasive, Wear, 223(1-2), pp. 131-138.

307. Taguchi G. and Konishi S. (1987), Taguchi methods: orthogonal arrays and linear graphs: tools for quality engineering, American Supplier Institute Inc., Dearborn, MI.

308. Taguchi G. (1986), Introduction to quality engineering, Asian Productivity Organization, UNIPUB, White Plains, NY.

309. Pierlot C., Pawlowski L., Bigan M. and Chagnon P. (2008), Design of experiments in thermal spraying: A review, Surf. and Coat. Tech., 202, pp. 4483-4490.

310. Plackett R.L. and Burman J.P. (1946), The Design of Optimum Multifactorial Experiments, Biometrika, 33(4), pp. 305-325.

311. Steeper T.J., Varacalle Jr. D.J., Wilson G.C., Riggs W.L., Rotolico A.J. and Nerz J.E. (1992), A design of experimental study of plasma sprayed alumina-titania coatings, In: C.C. Berndt, Editor, Adv. in Coat. Tech., ASM Int., Materials Park, OH, USA, pp. 415-420.

312. Jaworski R., Pawlowski L., Roudet F., Kozerski S. and Le Maguer A. (2008), Influence of suspension plasma spraying process parameters on TiO_2 coating microstructure, J. Ther. Sp. Tech., 17(1), pp. 73-81.

313. Jaworski R., Pawlowski L., Roudet F., Kozerski S. and Petit F. (2008), Characterization of mechanical properties of suspension plasma sprayed TiO_2 coatings using scratch test, Surf. and Coat. Tech., 202(12), pp. 2644-2653.

314. Mohammadi Z., Moayyed A.A.Z. and Mesgar A.S.M. (2007), Grit blasting of Ti-6Al-4V alloy: optimization and its effect on adhesion strength of plasma sprayed hydroxyl-apatite coatings, J. of Mat. Proc. Tech., 194, pp. 15-23.

315. Pierlot C., Pawlowski L., Tomaszek R., Dyshlovenko S. and Bigan M. (2007), Interdependence of different properties of hydroxyapatite coatings and powders plasma sprayed into water, Chem. and Inte. Lab. Sys., 86(2), pp. 153-158.

316. Saravanan P., Selvarajan V., Srivastava M.P., Rao D.S., Joshi S.V. and Sundararajan G. (2000), Study of plasma and detonation gun-sprayed alumina coatings using taguchi experimental design, J. of Ther. Sp. Tech., 9(4), pp. 505-512.

317. Malinka J.G., Varacalle (Jr.) D.J. and Riggs W.L. (1992), Thermal Spray: International Advances in Coating Technology, ASM Int., Materials Park, Ohio, USA, pp. 87.

318. Phadke M.S. (1989), Quality engineering using robust design, Prentice Hall, Englewood Cliffs, NJ.

319. Wu Y. and Moore W.H. (1986), Quality engineering: product & process design optimization, American Supplier Institute Inc., Dearborn, MI.

320. Logothetis N. and Haigh A. (1987), The statistical flexibility of Taguchi method in the optimization of multi-response processes, Professional Statistician, 6 (7), pp. 10-16.

321. Logothetis N. and Haigh A. (1988), Characterizing and optimizing multi response processes by the Taguchi method, Quality and Reliability Engineering International, 4 (2), pp. 159-169.

322. Shoemaker A.C. and Kackar R.N. (1988), A methodology for planning experiments in robust product and process design, Quality and Reliability Engineering International, 4 (2), pp. 95-103.

323. Phadke M.S. and Dehnad K. (1988), Optimization of product and process design for quality and cost, Quality and Reliability Engineering International, 4 (2), pp. 105-112.

324. Mahapatra S.S. and Patnaik A. (2006), Optimization of parameter combinations in wire electrical discharge machining using Taguchi method, Indian Journal of Engineering and Materials Sciences, 13, pp. 493-502.

325. Mahapatra S.S. and Patnaik A. (2006), Optimization of wire electrical discharge machining (WEDM) process parameters using Taguchi method, The International Journal of Advanced Manufacturing Technology, 34 (9-10), pp. 911-925.

326. Mahapatra S.S. and Patnaik A. (2007), Parametric optimization of wire electrical discharge machining (WEDM) process using Taguchi method, Journal of the Brazilian Society of Mechanical Sciences and Engineering, 28 (4), pp. 423-430.

327. Mahapatra S.S. and Patnaik A. (2006), Determination of optimal parameters settings in wire electrical discharge machining (WEDM) process using Taguchi method, Journal of The Institution of Engineers (India), 87, pp. 16-24.

328. Patnaik A., Satapathy A., Mahapatra S.S. and Dash R.R. (2010), Modified erosion wear characteristics of glass-polyester composites by silicon carbide filling: a parametric study using Taguchi technique, International Journal of Materials and Product Technology, 38 (2-3), pp. 131-152.

329. Rubio J.C.C., Silva L.J.D., Leite W.D.O., Panzera T.H., Filho S.L.M.R. and Davim J.P. (2013), Investigations on the drilling process of unreinforced and reinforced polyamides using Taguchi method, Composites Part B: Engineering, 55, pp. 338-344.

330. Ramesh B.N. and Suresha B. (2014), Optimization of tribological parameters in abrasive wear mode of carbon-epoxy hybrid composites, Materials and Design, 59, pp. 38-49.

331. Vankanti V.K. and Ganta V. (2014), Optimization of process parameters in drilling of GFRP composite using Taguchi method, Journal of Materials Research and Technology, 3 (1), pp. 35-41.

332. Kartalopoulos S.V. (1996), Understanding neural networks and fuzzy logic: basic concepts and applications, IEEE Press, Piscataway, NJ.

333. Zhang Z. and Friedrich K. (2003), Artificial neural networks applied to polymer composites: a review, Composites Science and Technology, 63 (14), pp. 2029-2044.

334. Kadi H.E. (2006), Modeling the mechanical behavior of fiber-reinforced polymeric composite materials using artificial neural networks-A review, Composite Structures, 73 (1), pp. 1-23.

335. Jiang Z., Zhang Z. and Friedrich K. (2007), Prediction on wear properties of polymer composites with artificial neural network, Composites Science and Technology, 67, pp. 168-176.

336. Gyurova L.A., Minino-justel P. and Sclarb A.K. (2010), Modelling the sliding wear and friction properties of polyphenylene sulfide composites using artificial neural networks, Wear, 268 (5-6), pp. 708-714.

337. Abdelbary A., Abouelwafa M.N., El Fahham I.M. and Hamdy A.H. (2012), Modeling the wear of Polyamide 66 using artificial neural network, Materials and Design, 41, pp. 460-469.

338. Satapathy A., Tarkes D.P. and Nayak N.B. (2010), Wear response prediction of TiO_2-polyester composites using neural networks, International Journal of Plastics Technology, 14 (1), pp. 24-29.

339. Kranthi G. and Satapathy A. (2010), Evaluation and prediction of wear response of pine wood dust filled epoxy composites using neural computation, Computational material science, 49, pp. 609-614.

340. Gyurova L.A. (2010), Sliding friction and wear of polyphenylene sulfide matrix composites: experimental and artificial neural network approach, Ph.D. Thesis, Institut fur Verbundwerkstoffe GmbH: Kaiserslautern, Germany.

341. Satapathy A., Patnaik A. and Pradhan M.K. (2009), A study on processing, characterization and erosion behavior of fish (Labeo-rohita) scale filled epoxy matrix composites, Materials and Design, 30 (7), pp. 2359-2371.

342. Suresh A., Harsh A.P. and Ghosh M.K. (2009), Solid particle erosion studies on polyphenylene sulfide composites and prediction on erosion data using artificial neural networks, Wear, 266 (1-2), pp. 184-193.

343. Genel K., Kurnaz S.C. and Durman M. (2003), Modeling of tribological properties of alumina fiber reinforced zinc-aluminum composites using artificial neural network, Materials Science and Engineering: A, 363, pp. 203-210.

344. Zhang Z., Friedrich K. and Velten K. (2002), Prediction on tribological properties of short fibre composites using artificial neural networks, Wear, 252, pp. 668-675.

345. Barbero Ever J. (1999), Introduction to composite materials design, Taylor & Francis, Philadelphia, PA.

346. Chen H., Lee S.W., Du H., Ding C.X. and Cho C.H. (2004), Influence of feed stock and spraying parameters on the deposition efficiency and micro-hardness of plasma sprayed zirconia coatings, Materials Letters, 58 (7-8), pp. 1241-1245.

347. William, F.H, (2005). Mechanical Behavior of Materials, Cambridge University Press, UK.

348. Agarwal B.D. and Broutman L.J. (1990), Analysis and performance of fiber composites, Second edition, John Wiley & Sons, pp. 2-16.

349. Ruff A.W. and Ives L.K. (1975), Measurement of solid particle velocity in erosive wear, Wear, 35(1), pp.195-199.

350. Zeng P. (1998), Neural computing in mechanics, Applied Mechanics, 51 (2), pp. 173-197.

351. Haykin S. (1999), Neural Networks: a Comprehensive Foundation, Upper Saddle River, Prentice Hall, NJ, USA.

352. Rajasekaran S. and Vijayalakshmi Pai G.A. (2003), Neural networks, fuzzy logic and genetic algorithms-synthesis and applications, Prentice Hall of India, New Delhi.

353. Sobolev V.V., Guilemany J.M., Nutting J. and Miquel J.R. (1997), Development of substrate-coating adhesion in thermal spraying, International Materials Reviews, 42 (3), pp. 117-136.

354. Lima C.R.C. and Trevisan R.E. (1997), Graded Plasma Spraying of Premixed Metal Ceramic Powders on Metallic Substrates, Journal of Thermal Spray Technology, 62, pp. 199-204.

355. Lalleman G. and Tallaron (1996), Study of Microstructure and adhesion of spinelles coatings formed by plasma spraying, Ph. D. Thesis No. 96-58, E. C. Lyon, France.

356. Hansson C.M. (1992), Cavitation Erosion, In: ASM Handbook, Friction, Lubrication and Wear Technology, ASM International, USA, 18, pp. 214-220.

357. Sahu S.P. (2010), A study on solid particle erosion wear response of plasma sprayed fly ash coatings, Ph.D. Thesis, Sambalpur University, Burla, India.

358. Satapathy A., Mishra S.C., Ananthapadmanabhan P.V. and Sreekumar K.P. (2007), Development of ceramic coatings using red mud: a solid waste of alumina plants, Journal of Solid Waste Technology and Management, 33, pp. 48-53.

359. Sarikaya O. (2005), Effect of some parameters on microstructure and hardness of alumina coatings prepared by air plasma spraying process, Surface and Coatings Technology, 190, pp. 388-393.

360. Glen S.P. (1993), Taguchi Methods: A Hand on Approach, Addison-Wesley.

361. Mishra S.C., Das S., Satapathy A., Ananthapadmanabhan P.V. and Sreekumar K.P. (2009), Erosion wear analysis of plasma sprayed ceramic coating using the Taguchi technique, Tribology Transactions, 52, pp. 401-404.

362. Lindsley B.A. and Marder A.R. (1999), The effect of velocity on the solid particle erosion rate of alloys, Wear, 225-229, pp. 510-516.

363. Chen Q. and Li D.Y. (2003), Computer simulation of solid particle erosion, Wear, 254 (3-4), pp. 203-210.

364. Lopez D., Congote J.P., Cano J.R., Toro A. and Tschiptschin A.P. (2005), Effect of particle velocity and impact angle on the corrosion-erosion of AISI 304 and AISI 420 stainless steel, Wear, 25 (1-6), pp. 118-124.

365. Kretsis G. (1987), A review of the tensile, compressive, flexural and shear properties of hybrid fibre-reinforced plastics, Composites, 18 (1), pp. 13-23.

366. Singh B., Gupta M. and Verma A. (1995), Mechanical behavior of particulate hybrid composite laminates as potential building materials, Construction and Building Materials, 9, pp. 39-44.

367. Selzer R. and Friedrich K. (1997), Mechanical properties and failure behavior of carbon fibre-reinforced polymer composites under the influence of moisture, Composites: Part A, 28A, pp. 595-604.

368. Jawaid M., Khalil A. and Abu Baker A. (2011), Woven hybrid composites: tensile and flexural properties of oil-palm woven jute fiber based epoxy composites, Materials Science and Engineering A, 528, pp. 5190-5195.

369. Singh S., Mohanty A.K. and Misra M. (2010), Hybrid bio-composite from talc, wood fiber and bioplastic: fabrication and characterization, Composites: Part A, 41, pp. 304-312.

370. Liu S.P., Hwang S.S., Yeh J.M. and Hung C.C. (2011), Mechanical properties of polyamide-6/montmorillonite nanocomposites-prepared by the twin screw extruder mixed technique, International Communications in Heat And Mass Transfer, 38 (1), pp. 37-43.

371. Venkateshwaran N., Elayaperumal A., Sathiya G.K. (2011), Prediction of tensile properties of hybrid-natural fibre composites‖, Composites: Part B, 43, pp. 793-796.

*****

Appendices

Appendix **A1**

LIST OF PUBLICATIONS OUT OF THIS WORK

International Journals

1. **Pravat Ranjan Pati** and Alok Satapathy, "Development of wear resistant coatings using LD slag premixed with Al_2O_3", ***Journal of Material Cycles and Waste Management***, 17(1), 135-143, 2015.

2. **Pravat Ranjan Pati** and Alok Satapathy, "Tribo-performance Analysis of Coatings of LD slag premixed with TiO_2 Using Experimental Design and ANN", ***Tribology Transactions***, 58, 349-356, 2015.

3. **Pravat Ranjan Pati** and Alok Satapathy, "Prediction and simulation of wear response of Linz-Donawitz (LD) slag filled glass-epoxy composites using neural computation", ***Polymers for Advanced Technologies***, 26 (2), 121-127, 2015.

4. **Pravat Ranjan Pati** and Alok Satapathy, "Processing, characterization and erosion wear response of Linz-Donawitz (LD) slag filled polypropylene composites", ***Journal of Thermoplastic Composites Materials***, DOI: 10.1177/0892705714563122.

5. **Pravat Ranjan Pati** and Alok Satapathy, "A study on processing, characterization and erosion wear response of Linz-Donawitz slag filled epoxy composites", ***Advances in Polymer Technology***, DOI 10.1002/adv.21509.

International Conferences

1. **Pravat Ranjan Pati** and Alok Satapathy, "Parametric appraisal of erosion wear of epoxy composites filled with Linz-Donawitz slag", ***Proceedings of APM-2013, March 1-3, 2013, CIPET, Luckhnow***.

2. **Pravat Ranjan Pati** and Alok Satapathy, "Prediction and simulation of erosion wear response of Linz-Donawitz (LD) slag filled epoxy composites using ANN", ***International conference on Advance Engineering and Technology, 21st April 2013, Nagpur***.

3. **Pravat Ranjan Pati** and Alok Satapathy, "Processing and characterization of plasma sprayed coatings of LD slag premixed with micro-sized Al_2O_3 particles", ***4th Nirma University International Conference on Engineering, November 28-30, 2013, Nirma University, Ahmedabad***.

4. **Pravat Ranjan Pati** and Alok Satapathy, " A study on coatability of Linz-Donawitz (LD) slag by plasma spraying route" ***Proceedings of the ASME 2013 Gas Turbine India Conference, Dec 5-6, 2013, Bangalore, Karnataka, India***.

5. **Pravat Ranjan Pati** and Alok Satapathy, "Use of Linz-Donawitz slag in glass-epoxy composites for improved wear resistance", ***Proceedings of APM-2014, Feb 14-16, 2014, CIPET, Bhubaneswar***.

6. **Pravat Ranjan Pati** and Alok Satapathy, "Analysing erosion wear response of plasma sprayed coatings of LD slag premixed with TiO_2 using Taguchi experimental design", ***ICAT-2014, Feb 21-24, 2014, NIT, Calicut***.

7. **Pravat Ranjan Pati** and Alok Satapathy, "Processing and characterization of Glass-Epoxy composites filled with Linz-Donawitz (LD) slag", ***ISCEAS-2014, Aug 15-17, 2014, Singapore.***

8. Alok Satapathy and **Pravat Ranjan Pati**, "Utilization of waste LD slag of steel industries in developing wear resistant coatings for power plant applications", RESD-2015, June 15-17, 2015, Bhutan.

9. **Pravat Ranjan Pati** and Alok Satapathy, "Development of Plasma Spray Coatings using Linz-Donawitz (LD) Slag Particles" ***Proceedings of the ASME 2015 Gas Turbine India Conference, Dec 1-3, 2015, Hyderabad, India (Accepted)***.

*****

Appendix **A2**

Brief bio-data of the author

The author, **Pravat Ranjan Pati**, born on 06-05-1987 graduated in Mechanical Engineering from Ajay Binay Institute of Technology, Cuttack, India in the year 2008. He completed his Post-graduate study (M.Tech.) in Mechanical Engineering with specialization in Thermal Engineering from Institute of Technical Education & Research (ITER), Bhubaneswar, India in the year 2011. Immediately after the completion of his M.Tech. programme, he joined as an Institute Research Scholar in the Department of Mechanical Engineering at the National Institute of Technology, Rourkela.

The author is engaged in active research in the area of plasma spray coatings and polymer composites since 2012. He has 5 research papers to his credit which have been published in various international journals of repute. He has also presented 8 research papers in the area of coatings and composites at various national and international conferences held in India and abroad.

*****